Science

SPECIAL ISSUE

The End of PRIVACY

CONTENTS

477 & 534

Chicks, like people, count from left to right

SPECIAL SECTION
THE END OF PRIVACY

ON THE COVER

Data pour out of us and our devices every second of every day, and people no longer control their personal privacy. Understanding how these data streams can be used will help us to cope with the consequences. For a key to the data in the art on the cover and on page 490, search for an encrypted URL and decode it. *Image: William Duke*

NEWS

469

INSIGHTS

CONTENTS

551 & 555
How a disease mutation affects protein function

482

RESEARCH

459

Published by AAAS

Published by AAAS

Bridging the opinion gap

There is a wide opinion gap between scientists and the general public in the United States when it comes to their attitudes about the state of science and science-related policy. According to survey results released this week by the Pew Research Center, in collaboration with the American Association for the Advancement of Science (AAAS),* when asked whether U.S. scientific achievements are either the best or among the world's best, only 54% of the public said "yes," compared to 92% of the scientists. Such disparity is alarming because it ultimately affects both science policy and scientific progress. How can we bridge this gap? Forget the staged "town hall" meetings—studies show that they are not very effective. What does work is respectful bidirectional communication, where scientists truly listen, as well as speak, to the public.

What accounts for this large opinion gap? Hot topics such as the safety of eating genetically modified (GM) foods, the importance of using animals in scientific research, the reality of human-caused climate change, the safety of vaccinations, and human evolution are among the issues that cause substantial disquiet among the public. Most scientists (88%) said that eating GM foods is generally safe, for example, whereas a mere 37% of the public agreed. Similarly, the 2014 survey reports that the public's stance on climate change has become "increasingly contentious," as a greater percentage of the public (25% in 2014 versus 11% in 2009) believes that there is no solid evidence that Earth is getting warmer—a result that is inconsistent with the broad scientific consensus.

These findings should come as no real surprise, given increasing public attention to relatively rare events that, even though infrequent, undermine the public's trust of science, such as conflicts of interest, the failure to replicate certain results, or "silly-sounding" grant titles that imply wasteful spending. Among scientists, life is seen as being much more difficult than it appeared to be 5 years ago, when Pew Research conducted a similar survey. Only 52% of scientists say this is "a good time for science," down from 76% in 2009. This discouragement is not surprising either, given the long-standing threats to research and development funding and the resultant very low success rates for grant proposals. But complaining about these difficulties does nothing to improve respect or support for science among policy-makers or the public.

Speaking up for the importance of science to society is our only hope, and scientists must not shy away from engaging with the public, even on the most polarizing science-based topics. Scientists need to speak clearly with journalists, who provide a great vehicle for translating the nature and implications of their work. Scientists should also meet with members of the public and discuss what makes each side uncomfortable. In these situations, scientists must respond forthrightly to public concerns. In other words, there needs to be a conversation, not a lecture.

The public's perceptions of scientists' expertise and trustworthiness are very important, but they are not enough. Acceptance of scientific facts is not based solely on comprehension levels. It can be compromised whenever information confronts people's personal, religious, or political views, and whenever scientific facts provoke fear or make people feel that they have no control over a situation. The only recourse is to have genuine, respectful dialogues with people. Good venues are community clubs, science museums, science fairs, and religious institutions. Working with small groups is more effective than working with large groups. Fortunately, there is a growing science base to help guide more effective public engagement of this kind.†

The opinion gap must not be allowed to swell into an unbridgeable chasm. There is ample opportunity to do something about the situation now. Hopefully, a survey 5 years from now will bear better news.

– **Alan I. Leshner**

"Speaking up for the importance of science to society is our only hope..."
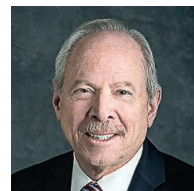
Alan I. Leshner is the Chief Executive Officer of AAAS and Executive Publisher of Science.
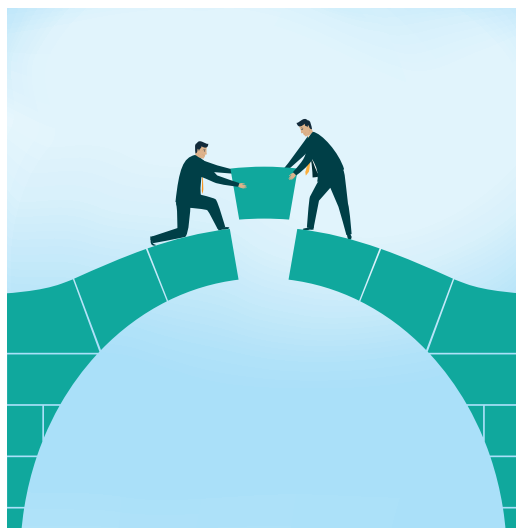
10.1126/science.aaa7477

IN BRIEF

Tug of war over Arctic oil

~ Brooks Range in Alaska's Arctic National Wildlife Refuge.

The Obama administration has announced several big moves on Arctic oil. On 27 January, the White House issued a long-term plan for offshore drilling that would put several areas in the Arctic's Chukchi and Beaufort seas off limits (while opening swathes of the Atlantic from Virginia to Georgia). On 25 January, officials announced they want to expand protections for 5 million hectares, including 600,000 in an oil- and gas-rich coastal plain, within Alaska's Arctic National Wildlife Refuge. Both plans are drawing criticism from politicians in Alaska, which depends heavily on the oil and gas industry for revenues. "We are going to fight back," vowed Senator Lisa Murkowski (R–AK), who heads the Senate's energy committee. The moves come on the heels of an executive order released last week by President Barack Obama aimed at improving coordination of U.S. policy in the Arctic as the United States prepares to assume the chairmanship of the multilateral Arctic Council later this year. The order creates an Arctic Executive Steering Committee to streamline agency policies and collaborate with state, local, tribal, and other groups.

AROUND THE WORLD

Senate: Climate change no hoax

WASHINGTON, D.C. | In a symbolic move, the U.S. Senate voted 98 to 1 on 21 January to approve a measure stating that climate change is real and "not a hoax." The measure, sponsored by Senator Sheldon Whitehouse (D–RI), was aimed at forcing Republican senators to take a stand on an issue that is sensitive with conservative voters. It also poked fun at Senator James Inhofe (R–OK), who has called climate change "a hoax." But Inhofe turned the tables at the last minute, endorsing the measure and redefining it: Only the idea that humans could affect climate is a hoax, he said. The switch gave Republicans political cover to vote for the measure, but 15 Republicans also supported a separate, ultimately unsuccessful, measure that said humans do contribute to climate change. http://scim.ag/climvote

No patent for hepatitis C drug

NEW DELHI | The Indian Patent Office this month rejected a patent on hepatitis C drug Sovaldi, produced by U.S.-based Gilead Sciences Inc. Sovaldi has transformed care for hepatitis C by dramatically cutting treatment time and side effects, but has also come under fire for its $84,000 price tag for a 12-week course. Gilead offered India a discount of 99%—still out of reach for most Indians. The patent rejection opens the door to sale of a generic form of Sovaldi in India; according to a 2014 study in *Clinical Infectious Diseases*, manufacturing a 12-week course of the generic would cost at most $136. Gilead has challenged the decision. In 2013, India rejected a patent on the leukemia drug Gleevec.

Ebola triggers WHO reforms

GENEVA, SWITZERLAND | The World Health Organization (WHO) has embarked on reforms to make it better able to deal with events like the Ebola epidemic in West Africa. At a special session on 25 January in Geneva, WHO's Executive Board adopted a resolution that calls for strengthening

The return of the tortoises

I n the mid-18th century, sailors who landed on the Galápagos island of Pinzón helped create an environmental catastrophe on the island: Rats stowed in their ships ran rampant, eating the eggs and hatchlings of the giant tortoises that lived there. Humans tried to right the wrong, first with a conservation project launched in the 1960s that collected the few unhatched eggs, incubated them on another island, and then transported the 5-year-old tortoises back. The eggs were still threatened by the rat populations, however—until, in 2012, biologists distributed a rat-specific poison on the island via helicopter, making the island rat-free. Now, more than a century since the last baby tortoise was seen on the island, researchers have spotted 10 new hatchlings—which, they say, likely means a hundred times more are in the wild.

A Pinzón Island tortoise hatchling at the Charles Darwin Research Station on Santa Cruz Island.

the agency's operational muscle, extending its global health workforce, and putting in place a contingency fund for future emergencies. The United Kingdom has already pledged $10 million to that fund, WHO Director-General Margaret Chan said on Sunday. The reforms, which must be approved by the World Health Assembly in May, come after WHO's acknowledgement that it bungled its response to Ebola last year. "The world, including WHO, was too slow to see what was unfolding before us," Chan told the board, which consists of representatives from 34 members states.

Research dog breeders sentenced

ROME | An Italian court has found three employees of Green Hill, a company that breeds beagles for animal studies, guilty of unjustified killing and mistreatment of dogs. The accusations against Green Hill

Volunteers from Legambiente holding beagle puppies rescued from Green Hill.

in Brescia, Italy, a subsidiary of U.S.-based Marshall BioResources and one of Europe's largest suppliers of dogs for research, were filed in June 2012 by the environmental organization Legambiente and the animal rights group Lega Anti Vivisezione. The complaint noted that the dogs were never outdoors, were exposed to artificial light night and day, and lived in spaces that weren't properly cleaned, among other charges. The European Animal Research Association strongly condemned the verdicts, calling them a "legal travesty" and part of a "campaign to end animal research in Italy." The court has to release a written motivation for the verdicts within 60 days. http://scim.ag/_GreenHill

Meetup with Neandertals?

WESTERN GALILEE, ISRAEL | Most Europeans and Asians have up to 2% Neandertal DNA in their genomes, but when and where did any love matches between Neandertals and modern humans take place? The discovery of a 55,000-year-old partial skull in Israel's Manot Cave, not far from previously excavated Neandertal fossils of similar age, shores up the suggestion from ancient DNA that these two human lineages engaged in at least some limited mating in the Middle East between about 50,000 and 60,000 years ago. Anthropologists agree that the new fossil, reported this week in *Nature*, is a member of *Homo sapiens*, the first to be found outside our African homeland during

BY THE NUMBERS

2

Treatment beds available for each suspected, probable, or confirmed case of Ebola in Sierra Leone, Liberia, and Guinea, according to the World Health Organization's Ebola situation report last week.

30%

Jump in tiger population from 2011 to 2014 in India (from 1706 to 2226), due to better conservation. India is home to 70% of the world's tigers.

$90
million

Cost of the roughly 3% of methane delivered to Boston that leaked into the air from 2012 to 2013, finds a study in the *Proceedings of the National Academy of Sciences*.

A 55,000-year-old modern human skull found in an Israeli cave.

this crucial time period. Researchers also think it could represent the population of modern humans that soon afterward swept across Europe and Asia.

Bill to revamp medical treatment

WASHINGTON, D.C. | A U.S. House of Representatives panel this week released a widely anticipated, bipartisan proposal for speeding the development of new medical treatments. The 393-page draft bill, dubbed the 21st Century Cures Act, has been under development by Fred Upton (R–MI) and Diana DeGette (D–CO) of the House Energy and Commerce Committee since April. The provisions aim to involve patients in drug development; speed clinical trials; streamline regulations; modernize manufacturing facilities; and encourage personalized treatments while also expanding support for young scientists at the National Institutes of Health. The bill is a discussion document, said Upton, who invited comments via the Twitter handle #Cures2015: "Some things may be dropped, some items may be added, but everything is on the table as we hope to trigger a thoughtful discussion toward a more polished product." http://scim.ag/21centcure

Corruption case snares scientist

A prominent cancer researcher has become entangled in a high-profile corruption case in New York state. **Robert Taub**, former director of the Columbia University Mesothelioma Center, has been named as the "Doctor-1" described in a criminal complaint that accuses Democratic state Representative Sheldon Silver, the speaker of the New York State Assembly, of arranging bribes and kickbacks that netted Silver millions of dollars. The complaint alleges that Silver steered $500,000 from a state health care research fund to Taub; in exchange, Taub referred patients suffering from asbestos-related disease to Silver's law firm, investigators allege. Doctor-1 is cooperating with federal investigators, according to the complaint, and will not be charged with any crime. However, Columbia University noted in a statement on 23 January that "Dr. Taub no longer serves as" the center's director. http://scim.ag/Taubcase

New head of NOAA research

Attorney **Craig McLean**, a veteran of the National Oceanic and Atmospheric Administration (NOAA), will be the new head of its research division, the agency announced on 21 January. A deputy chief of NOAA's Office of Oceanic and Atmospheric Research since 2006, McLean served as the first director of NOAA's Office of Ocean Exploration and Research. He's also been a top deputy at the National Ocean Service and the National Marine Sanctuaries Program and was a NOAA Corps officer for more than 2 decades. McLean "understands how to move ocean information out of the laboratory and into operations"—a transition that NOAA has struggled with, says Scott Rayder, a former chief of staff at NOAA and now a senior adviser at the University Corporation for Atmospheric Research in Boulder, Colorado. "He's a huge asset to the community. It's a clear signal that NOAA is placing a premium [on this]."

The National Synchrotron Radiation Research Center in Hsinchu.

Asia's newest synchrotron sees first light

Taiwan's scientists will shortly have a new research tool for use in biology, nanotechnology, and materials science in the new Taiwan Photon Source at the National Synchrotron Radiation Research Center (NSRRC) in Hsinchu. After nearly 5 years of construction and testing, the facility achieved first light on 31 December. The 518-meter-circumference storage ring is designed to accelerate electrons to 3 gigaelectronvolts. NSRRC claims it will be one of the world's brightest synchrotron x-ray sources. Envisioned uses include protein microcrystallography, studies of protein interactions with other biomolecules, and the development of new materials. Phase one of the project includes the construction of seven beamlines. The facility will become available to users by the end of this year.
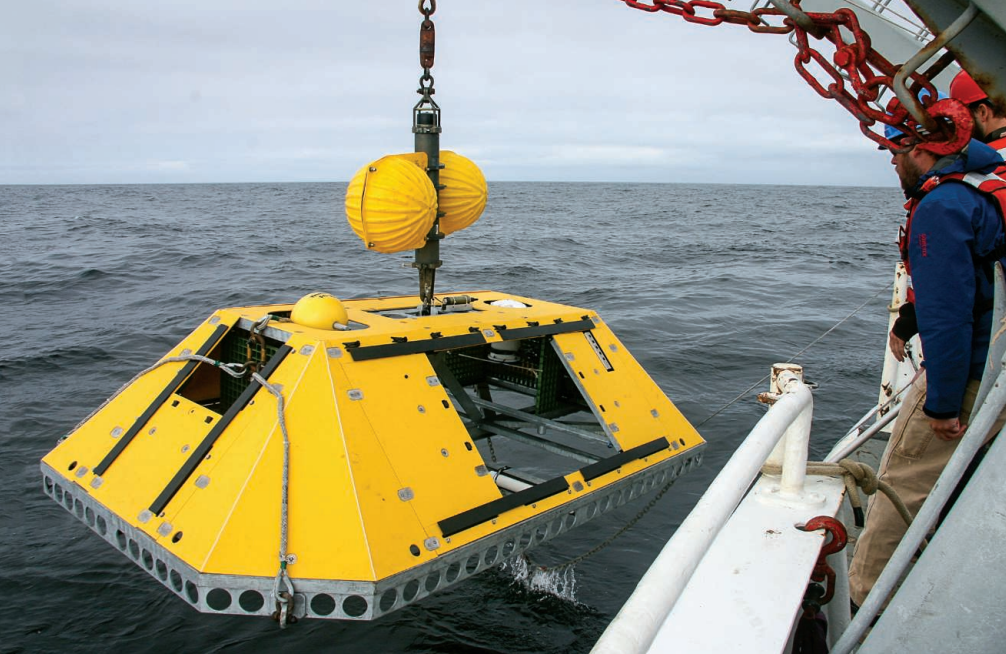
U.S. ocean observing network, which includes this seafloor platform, could face cuts.

OCEANOGRAPHY FUNDING

A moment of truth arrives for U.S. ocean science

Report urges infrastructure cuts to boost research

By **Eli Kintisch**

For years, U.S. marine scientists have fretted about the future of their field, watching as federal funding stagnated and the cost of seafloor observatories and other infrastructure steadily eroded the money available for research. But there's been little agreement on how to respond.

That changed last week, as an unprecedented, 2-year effort to set priorities for the beleaguered field unveiled some hard-edged recommendations. The National Science Foundation (NSF) should immediately cut funding for several major hardware programs in order to divert some $40 million a year back to science, concluded a 20-member panel organized by the National Research Council. Its 23 January report calls for a 20% cut to the Ocean Observatories Initiative (OOI), a $386 million network of seafloor instruments and buoys set to start operating in March; a 10% reduction in ocean drilling programs; and a 5% trim to spending on the NSF-funded fleet of research vessels, now 20 strong. The ultimate goal: to restore a balance between science and infrastructure in NSF's $350 million ocean research portfolio, which currently allocates nearly 60% to hardware (see graph, below).

Such cuts are "the only way to recover funding for core science," concluded the panel, which was led by marine scientist Shirley Pomponi of the Harbor Branch Oceanographic Institution in Fort Pierce, Florida, and retired Adm. David Titley of Pennsylvania State University, University Park.

Researchers are cautiously welcoming the advice. The current situation is "unsustainable" and "a rebalancing of funding is essential," says oceanographer Ken Johnson of the Monterey Bay Aquarium Research Institute in Moss Landing, California. Titley says he's gotten e-mails "congratulating us for finally writing a report that makes the tough calls, but I'm sure some people are less happy."

Physicists and astronomers have long used similar forward-looking surveys to set priorities, but oceanographers had never undertaken one. NSF asked for the survey 2 years ago, after the funding crunch became clear. In 2000, 62% of NSF's oceans budget went to research grants; the share is now about 45% and sinking.

Several factors drove the shift, says oceanographer David Conover of Stony Brook University in New York, who led NSF's oceans division from 2010 to 2013. A decade ago, as NSF planned OOI and other infrastructure, many believed Congress would double the agency's budget in the coming years. Instead, the budget remained relatively flat, even as infrastructure operating costs grew.

In formulating its priorities, the committee conducted town halls and combed through 402 comments. The result is a 134-page tome that identifies eight high-priority research areas—including studying the rate and impact of sea level change and characterizing the environment beneath deep sea floors. It also lays out the funding shifts needed to make the science happen.

The bottom line: NSF should reallocate one-fifth of the $189 million it now spends annually on infrastructure to research grants. The OOI, for instance, could save money by abandoning instrumented moorings after they fail. The Integrated Ocean Drilling Program, which is co-led by NSF and Japan, could cut costs by charging partners more to work on the *JOIDES Resolution*, the U.S. drilling ship. And NSF might consider cutting one of three planned mid-sized vessels for the academic fleet. "Such reductions are not easy and will cause disruptions," the panel acknowledges. But they could result in about 230 new grants to individual scientists annually, at the current average grant size of $170,000 per year.

The report is "excellent," says NSF ocean science chief Richard Murray, although he declined to comment on the specifics. And Conover thinks it could help the agency make "a much stronger case" to Congress for eventually increasing NSF's ocean budget. That discussion will begin next week, after the White House presents Congress with its 2016 budget proposal. ■

Science sinks as hardware rises

As the NSF budget for ocean research has stagnated, spending on infrastructure has, for the first time, exceeded spending on science.

Total
Science
Infrastructure
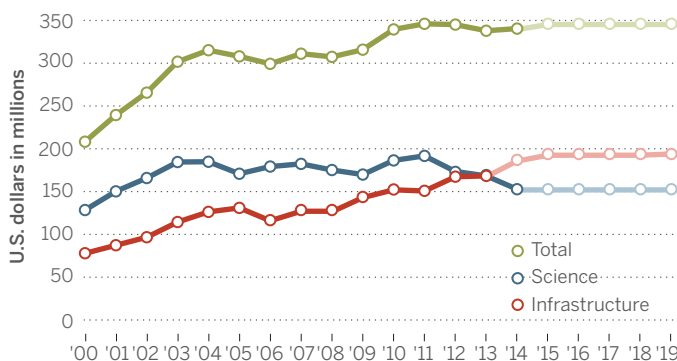
PARTICLE PHYSICS

India's costly neutrino gamble

The country splurges on a bid to regain leadership in neutrino physics

By **Richard Stone** *and* **Pallava Bagla**

Naba Mondal began his career 37 years ago snaring elusive subatomic particles called neutrinos in the depths of a gold mine in southern India. Now Mondal, a physicist at the Tata Institute of Fundamental Research (TIFR) in Mumbai, India, expects to go back underground in a subterranean laboratory of his own design to answer the next big question in neutrino physics.

India's central government this month approved plans to build the India-based Neutrino Observatory (INO), a $244 million facility 1200 meters under a mountain in southern India. Its goal—to determine which of the three types of neutrinos is heaviest and which is lightest—may seem esoteric. But it could help answer other fundamental questions in physics, including how neutrinos acquire mass, whether they are their own antiparticles, and why the universe has so much more matter than antimatter.

INO is competing for the neutrino mass hierarchy with new facilities in other countries (*Science*, 7 February 2014, p. 590). "India has not lost the race," says Alessandro Bettini, director of the Canfranc Underground Laboratory in Paseo de los Ayerbe, Spain. But INO is getting a late start after years of battling environmental concerns, unfounded radiation fears, and bureaucratic snags.

Even if India falls short, INO—India's most expensive basic science facility ever—will have a profound impact on the nation's science. Its opening in 2020 would mark a homecoming for India's particle physicists, many of whom dispersed overseas over the last quarter-century. And the INO team is laying plans to propel the facility beyond neutrinos into other areas, such as the hunt for dark matter. INO will "transform physics of

this kind in India and will make a global impact," says K. VijayRaghavan, secretary of India's Department of Science and Technology.

Neutrinos are produced in stars, nuclear reactors, and particle accelerators, and when cosmic rays smash into the upper atmosphere. They interact with other matter only through the weak nuclear force, making them difficult to detect. And because cosmic rays swamp any neutrino signal at Earth's surface, physicists have to go underground to study the particles, which easily slip through kilometers of solid rock.

India was once at the forefront of neutrino research. In 1964, a TIFR team working in a mineshaft in southern India's Kolar Gold Fields was the first to detect neutrinos created in the atmosphere. After the mine closed in 1992, India's tiny community of high-energy physicists—fewer than two dozen at the time—sought havens abroad, for example at Fermi National Accelerator Laboratory (Fermilab) in Illinois and

A subterranean neutrino snare

Deep under a mountain in southern India. INO will house the biggest iron calorimeter ever built and have room to spare for other experiments.
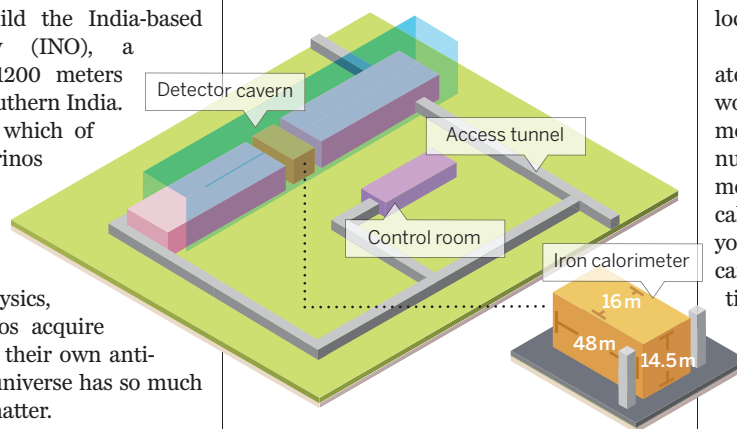
CERN, the European laboratory for particle physics near Geneva, Switzerland.

Mondal and his fellow exiles plotted a return to India. Around 2001, he says, "we started thinking about where we could make an impact." They opted to return to their roots by building a supersized version of the Kolar detector: an iron calorimeter, which detects charged particles called muons generated when muon neutrinos—one of the three neutrino types—tangle with nuclei in the iron.

If they can count muon neutrinos generated in the atmosphere precisely enough, INO physicists should be able to pin down the hierarchy of neutrino masses. Neutrinos can morph from one type to another

through a process called neutrino oscillation that depends on the differences in their masses. From such oscillations, physicists know that two of the neutrinos are close in mass and the other is different—but they don't know whether there are two heavier neutrinos and one lighter one or the other way around. By comparing the morphing of muon neutrinos and muon antineutrinos as they zip through the earth, INO physicists hope to resolve the puzzle.

But it will take a very large detector. At 50,000 tons and 48 meters long, INO's calorimeter will be the largest of its kind ever built. Sandwiched between 140 iron plates will be more than 30,000 thin glass resistive plate chambers that will detect muons and measure their properties. Far too bulky to fit in the shaft of an existing mine, the device requires a purpose-built cavern.

The Geological Survey of India recommended that the INO team burrow into a granite mountain in Tamil Nadu state. But local forestry officials opposed the idea, because the mountain is at the edge of a tiger reserve (*Science*, 9 January 2009, p. 197). After a long standoff, the INO team in 2009 retreated and the geological survey pointed them to their current site, also in Tamil Nadu, where they encountered even fiercer local opposition.

Villagers feared that INO would generate "artificial neutrinos" whose radioactivity would sicken people and livestock. Then a rumor arose that the government would dump nuclear waste at INO, Mondal says. His team mounted an outreach campaign, targeting local professors and high school students. "If you can convey the concepts to students, they can talk to their parents," he says. The scientists also dangled a sweetener: Construction crews would be mainly local.

After winning hearts in Tamil Nadu, the physicists still had to seal the deal in Delhi. Once the central government signed off in 2011, it became a matter of slotting the big-ticket item into India's budgetary cycle, which revolves around 5-year plans.

Mondal's team originally hoped to have INO up and running by 2012. The 8-year delay has left the door open to other facilities aiming to work out the mass hierarchy, including China's Jiangmen Underground Neutrino Observatory, which will study neutrinos from a reactor, and the U.S.-Japanese NOvA experiment, which will watch for neutrinos from a Fermilab accelerator. But no matter what happens, Mondal insists, India will win: "Just having a big science project will get young people excited about science." ∎

With reporting by Adrian Cho.

ARTIFICIAL INTELLIGENCE

DARPA sets out to automate research

Crash program aims to teach computers to read journals and hatch new ideas

By **Jia You**

The physics Nobel laureate Frank Wilczek has famously predicted that in 100 years, the best physicist will be a machine. Now the U.S. Defense Advanced Research Projects Agency (DARPA) is working toward that vision in a different arena: cancer research. Last summer, the agency launched a $45 million program called Big Mechanism, aimed at developing computer systems that will read research papers, integrate the information into a computer model of cancer mechanisms, and frame new hypotheses for flesh-and-blood scientists (or even other robots) to test—all by the end of 2017.

Last week, 12 teams of computer scientists and biologists met in Washington, D.C., to take stock of progress on the challenge. Although some outside researchers question Big Mechanism's methodology, others applaud it—including artificial intelligence researcher Oren Etzioni of the Allen Institute for Artificial Intelligence in Seattle, Washington, who calls it "an outstanding program."

The program's manager, artificial intelligence researcher Paul Cohen, says its goal is to help scientists cope with complexity at a time when most read more and more narrowly. "Just when we need to understand highly connected systems as systems, our research methods force us to focus on little parts," Cohen says.

Big Mechanism, if it succeeds, could aid researchers studying complicated systems from climate science to military operations and poverty. But for now it focuses on cancer driven by mutations in the Ras gene family, which underlie about a third of all human cancers. Cancer biologists have established a rough road map of Ras-driven cancer pathways: sequences of interactions among proteins affecting cell replication and death. But they amount to what Cohen calls a "hairball" of intertwining causal relations. "We all recognize the need for a better system of organizing this tremendous amount of information, visualizing it, and representing it in a way that's accessible," says Frank McCormick, who directs the Ras initiative at the U.S. National Institutes of Health.

The Big Mechanism program will tackle the problem in three stages. First, machines will read literature on the cancer pathways and convert useful information into formal representations that they can understand. Then, they will integrate the pieces of knowledge into computational models of the cancer pathways. Finally, the system will produce explanations and predictions that can be tested with experiments. The teams are developing four systems capable of all three tasks.

The evaluation meeting focused on the first step, machine reading. Pharmaceutical companies already text-mine papers to glean information on interactions between genes and proteins for drug development, but Big Mechanism seeks to develop machines that read a paper more as scientists do: judging how it contributes to existing knowledge.

The teams worked on different pieces of this "deep reading" challenge. One team, led by computer scientist Ed Hovy of Carnegie Mellon University in Pittsburgh, Pennsylvania, focused on extracting details on experimental procedures and assigning different certainty values to statements such as "we demonstrate" and "we suggest." Another, led by computational linguist James Allen of the Florida Institute for Human and Machine Cognition, built systems for mapping the meaning of sentences and their relationships to one another.

The evaluation started small: Participating teams were given a rudimentary model of Ras cancer pathways and six paragraph-long passages. Their systems had to extract information from the texts, determine how the passages related to the model, and suggest appropriate revisions based on their reading.

Two teams came close to fully automating the process. The best performing machine-reading system extracted 40% of all the relevant information from the passages and correctly determined how each passage related to the model—an excellent start, Cohen says. The systems will face a more comprehensive evaluation in July, he says.

Also coming this summer, Cohen says, is a hackathon in which programmers will build a single reference model of Ras-driven cancer pathways to replace the multiple models the teams are now using. A coherent model, including details about where and how proteins in the Ras pathways interact, is key to enabling the computer to generate hypotheses, Cohen says.

Building a system that actually produces scientific insight will not be easy, says computational biologist Larry Hunter of Smart Information Flow Technologies in Minneapolis, Minnesota, a co–principal investigator of one of the teams. The artificial intelligence community doesn't have a strong track record at building systems that can develop useful causal hypotheses, he says. But molecular biology is a good place to try, he says, because it's an area in which common sense plays a minor role; most of the knowledge is technical and available in textbooks and papers.

Other researchers question whether Big Mechanism takes the right approach to studying complex systems. "The Big Mechanism program is trying to map microscopic mechanisms, but complex systems are characterized by collective behaviors," says complex system researcher Yaneer Bar-Yam of the New England Complex Systems Institute in Cambridge, Massachusetts, who was not involved with the project. "The expectation that the accumulation of details will tell us what we want to know is not well justified."

Cohen is confident that the program will pay off, one way or another. "DARPA seeks revolutionary technology," he says. "Sometimes those technologies are turned into practice. Sometimes, they show the world what is possible." ∎

> *"Just when we need to understand highly connected systems as systems, our research methods force us to focus on little parts."*
>
> **Paul Cohen**, DARPA

Representative Tom Cole listens to physicist Michael Santos in his University of Oklahoma lab.

U.S. SCIENCE POLICY

Meet two new science spending cardinals in Congress

Representatives Cole, Culberson share enthusiasm for research, but differ in approach

By **Jeffrey Mervis**

The November elections have meant new federal lawmakers overseeing federal research spending. This year sees two key changes in the House of Representatives: Representative Tom Cole (R–OK) will lead the subcommittee that oversees the budget of the National Institutes of Health (NIH), and Representative John Culberson (R–TX) will head the panel responsible for NASA and the National Science Foundation (NSF). *Science* met recently with the two appropriations "cardinals" to discuss their new roles in crafting a budget for the 2016 fiscal year that starts in October. (Go to http://scim.ag/Budget2016 for expanded versions.)

A dealmaker …

Combine the analytical mind of a Ph.D. historian with the savvy of a longtime political operative, add a genial personality, and throw in the requisite dose of political conservatism. House Republican leaders hope against hope that the recipe will allow Tom Cole to produce a spending bill covering NIH and other agencies.

Cole's subcommittee, known as Labor-H, is traditionally the most contentious of the 12 spending panels that fund the government. Hot-button issues such as Obamacare, family planning, student loans, and work-place regulations come with its territory, which includes the federal departments of Health and Human Services, Education, and Labor. The committee hasn't agreed on a stand-alone version of its spending bill since 2009.

House Speaker John Boehner (R–OH) and other Republican leaders asked Cole, who was first elected in 2002, to take the job because Cole has kept open the lines of communication with the party's unruly right wing. Despite Cole's impeccable credentials as a conservative, Democrats say he's also willing to listen to other viewpoints.

"He has a strong partisan background, but he does not lean over backward to put politics over substance," says former Representative David Obey (D–WI), who retired in 2010 after 42 years in Congress and who once ran both Labor-H and the overall Appropriations Committee. "I think he tries to see that people behave as adults."

The 65-year-old Cole entered politics after his mother lost her 1976 race for the Oklahoma legislature. Then a graduate student at the University of Oklahoma, Cole was in England on a Fulbright scholarship during the campaign and blamed himself. "I told her that, if she decided to run again, I would learn how to run her campaign," Cole recalls. He did, and she won. "So I thought, 'This is kinda cool.'"

He helped her win several more times and also ran other local and national campaigns. But he still cared enough about British history to complete his dissertation on the evolution of a working-class village in London's East End.

Cole's academic experience has shaped his views of at least one contentious research issue: an effort by Republicans on the House science committee to alter peer review and restrict social science research at NSF. Researchers have vigorously resisted the moves, and Cole says: "I'd have to come down more on the side of the scientists on this one."

In making his case, Cole cites a prominent Marxist historian, E. P. Thompson, who analyzed everyday phenomena like the diets of the working class in 19th century England to obtain fresh insights into world events. "Now, Thompson is not a guy I'd agree with philosophically," Cole says, "but it was great social analysis and a groundbreaking piece of work. That may not sound like real history to someone who thinks all history should be about politicians and wars," he continues. "But historians have a pretty good sense of what type of research should be pursued. And I don't think that people who aren't historians should be deciding whether that type of research should be done."

On funding issues, Cole says he can't promise a healthy increase for NIH or even to keep the $30 billion agency on pace with inflation. Until Congress and the Obama administration "come to an agreement on the appropriate balance and sources of revenue and entitlement reform," he says, "we'll always be scrambling to maintain the programs we think are important, at the expense of those of lesser importance."

Cole's own list starts with maintaining a strong military and protecting the National

Weather Service's Weather Forecast Office in Norman, Oklahoma—his nearby hometown of Moore has been hit by several devastating tornadoes. He's a strong advocate for the Indian Health Service. (As a Chickasaw, he's one of two Native Americans in Congress, and his rural district has a sizable Native American population.) He's also a fan of NIH's Institutional Development Award program, which steers research funds to states like Oklahoma that get relatively little federal science funding.

But sometimes party and state loyalties take precedence over his personal views. Although he relied on U.K. census data for his thesis and believes such data are important, he voted in 2012 to eliminate funding for the annual American Community Survey, a perennial target of some conservatives who feel its questions are intrusive. "It's very seldom that I will split with a colleague from my own state," he explains about his support for the spending amendment, offered by Senator James Lankford, then a representative. (The proposed cut was never enacted.)

As Labor-H chair, he says he plans to hold numerous committee hearings so that members can thrash out their differences. "I'm not coming here with some big vision," he says. "But what I'm really good at is finding areas of cooperation in a very polarized situation."

… and an enthusiast

Probably no House member is more excited about becoming a cardinal than John Culberson. Being chair of the Commerce, Justice, Science (CJS), and Related Agencies appropriations subcommittee, which includes NASA and NSF, "is my dream job. … It is pure joy," says Culberson, who since 2001 has represented a staunchly conservative district in west Houston.

A longtime astronomy buff, Culberson has been an ardent supporter of planetary exploration, in particular, a proposed multibillion-dollar NASA mission to Jupiter's moon Europa in search of extraterrestrial life. But many researchers are likely to be troubled by his views on climate change and social science research, as well as his definition of wasteful research spending. Some may also balk at Culberson's overall political philosophy, which he ascribes to Thomas Jefferson.

"Government is a necessary evil," Culberson says. "It should give us the freedom and ability to do what God meant us to do, and stay away from my wallet, my gun case, my home, my kids, my church. Just leave me alone."

Culberson, 58, grew up in a family that was "fiscally conservative, devoted to the Constitution, and believed the American republic is a special inheritance." Despite his fascination with science—he still uses the classic Celestron 8 telescope he bought himself as a high school graduation present—he took no science courses in college and eventually headed to law school.

He was elected to the Texas legislature in

Representative John Culberson (*left*) and Bill Nye pose with Earth and Europa.

1986 as a second-year law student, and in 2000 he beat a crowded field to succeed retiring Representative Bill Archer. Two years later, then–Majority Leader Tom DeLay, another influential Texas Republican, offered him a seat on the Appropriations Committee. Culberson says he got the post after telling DeLay: "I'm going to say no to everything except science and national defense."

A member of the Tea Party Caucus, Culberson doesn't hide his scorn for President Barack Obama or his administration's policies. "I hope I never get in a picture with Obama," he said at a 2013 district town meeting, asserting later that "health insurance is none of the federal government's business, and Obamacare is proving it."

His predecessor as CJS chair, retired Representative Frank Wolf (R-VA), praises Culberson for "his knowledge, his enthusiasm, and his passion." He respects passion in others despite political differences, says the panel's top Democrat, Representative Chaka Fattah (D-PA). "Neuroscience is my No. 1 priority, and he's offered to do an entire hearing on the topic," Fattah says.

Culberson takes credit for lifting NASA's 2015 budget for planetary science to within $65 million of a $1.5 billion annual target set by the Planetary Society, a nonprofit that lobbies for space exploration. Bill Nye, the society's CEO, praises the legislator's support for the Europa mission. "He believes that a higher power has put life on other worlds, and he wants us to find it on his watch," Nye says.

Culberson also wants to hold NASA to the recommendations in the 2011 decadal survey of planetary science by the National Academies. He vows to continue to require NASA "to fund and fly" the survey's priority missions, a list topped by a trip to collect, and eventually return, samples from Mars.

Yet like most House Republicans, Culberson questions the need for government-funded climate change studies. He cites "scientific evidence of dramatically higher temperatures [in the distant past] that are completely unrelated to human activity." Culberson also believes "there's a tremendous amount of data out there that are still in conflict."

The White House deserves much of the blame, he adds. "The whole thrust of President Obama's climate program and the liberal obsession with climate change is driven by their desire to raise more money for the government."

On NSF's process of deciding what research to fund, Culberson sides with the Republicans on the House science committee. "I'd encourage [NSF] to avoid funding studies like shrimp on a treadmill or alcoholism among prostitutes in Thailand," he counsels, referring to two grants targeted by conservatives. "Instead of pursuing obscure and obtuse social science research, NSF should be focused on the great mysteries of the universe, like what is dark energy."

NASA's mission is grander still, he believes. "It's the only agency that can truly uplift the human heart and inspire the human spirit," he says. "I want to see NASA blaze a trail to Alpha Centauri and beyond." ∎

PHOTO: COURTESY OF THE OFFICE OF REPRESENTATIVE JOHN CULBERSON

PRIVACY

Credit card study blows holes in anonymity

Attack suggests need for new data safeguards

By **John Bohannon**

For social scientists, the age of big data carries big promises: a chance to mine demographic, financial, medical, and other vast data sets in fine detail to learn how we lead our lives. For privacy advocates, however, the prospect is alarming. They worry that the people represented in such data may not stay anonymous for long. A study of credit card data in this week's issue of *Science* (p. 536) bears out those fears, showing that it takes only a tiny amount of personal information to de-anonymize people.

The result, coming on top of earlier demonstrations that personal identities are easy to pry from anonymized data sets, indicates that such troves need new safeguards. "In light of the results, data custodians should carefully limit access to data," says Arvind Narayanan, a computer scientist at Princeton University who was not involved with the study. Or as the study's lead author, Yves-Alexandre de Montjoye, an applied mathematician at the Massachusetts Institute of Technology (MIT) in Cambridge, puts it: When it comes to sensitive personal information, "the open sharing of raw data sets is not the future."

De Montjoye's team analyzed 3 months of credit card transactions, chronicling the spending of 1.1 million people in 10,000 shops in a single country. (The team is tightlipped about the data's source—a "major bank," de Montjoye says—and it has not disclosed which country.) The bank stripped away names, credit card numbers, shop addresses, and even the exact times of the transactions. All that remained were the metadata: amounts spent, shop type—restaurant, gym, or grocery store, for example—and a code representing each person.

But because each individual's spending pattern is unique, the data have a very high "unicity." That makes them ripe for what de Montjoye calls a "correlation attack." To reveal a person's identity, you just need to correlate the metadata with information about the person from an outside source.

One correlation attack became famous last year when the New York City Taxi and Limousine Commission released a data set of the times, routes, and cab fares for 173 million rides. Passenger names were not included. But armed with time-stamped photos of celebrities getting in and out of taxis—there are websites devoted to celebrity spotting—bloggers, after deciphering taxi driver medallion numbers, easily figured out

"*The open sharing of raw data sets is not the future.*"

Yves-Alexandre de Montjoye, MIT

which celebrities paid which fares.

Stealing a page from the taxi data hack, de Montjoye's team simulated a correlation attack on the credit card metadata. They armed their computers with a collection of random observations about each individual in the data: information equivalent to a single time-stamped photo. (These clues were simulated, but people generate the real-world equivalent of this information day in and day out, for example through geolocated tweets or mobile phone apps that log location.) The computer used those clues to identify some of the anonymous spenders. The researchers then fed a different piece of outside information into the algorithm and tried again, and so on until every person was de-anonymized.

Just knowing an individual's location on four occasions was enough to fingerprint 90% of the spenders. And knowing

the amount spent on those occasions—the equivalent of a few receipts from someone's trash—made it possible to de-anonymize nearly everyone and trace their entire transaction history with just three pieces of information per person. The findings echo the results of a 2013 *Scientific Reports* study in which de Montjoye and colleagues started with a trove of mobile phone metadata on subscribers' movements and showed that knowing a person's location on four occasions was enough to identify them.

One way to protect against correlation attacks is to blur the data by binning certain variables. For example, rather than revealing the exact day or price of a transaction, the public version of the data set might reveal only the week in which it occurred or a price range within which it fell. Binning did not thwart de Montjoye's correlation attack; instead, it only increased the amount of information needed to de-anonymize each person to the equivalent of a dozen receipts.

These studies needn't be the death knell for social science research using big data. "We need to bring the computation to the data, not the other way around," de Montjoye says. Big data with sensitive information could live "in the cloud," protected by gatekeeper software, he says. The gatekeeper would not allow access to individual records, thwarting correlation attacks, but would still let researchers ask statistical questions about the data.

The mathematics needed to run such a system, a set of standards and algorithms known as differential privacy, is one of the hottest topics in data science. "It works best when you have a large amount of data," says Cynthia Dwork, a computer scientist at Microsoft Research in Mountain View, California, who is one of the pioneers of the technique. She admits that it is a stark departure from the traditional academic practice of open data sharing, and many scientists are resistant.

But without such safeguards, rich databases could remain off limits. Take, for example, the data MIT has accumulated from its massive open online courses. It's an information trove that education researchers dream of having: a record of the entire arc of the learning process for millions of students, says Salil Vadhan, a computer scientist at Harvard University. But the data are under lock and key, partly out of fears of a prospective privacy breach. "If we can provide data for research without endangering privacy," Vadhan says, "it will do a lot of good." ∎

A NEW DRUG WAR

As a growing wave of designer drugs hits
the streets, researchers try to forecast which will
prove most popular—and dangerous

By **Emily Underwood**

Roughly 2 years ago, just before her 24th birthday, Tessa Shlaer went with a friend to the back aisles of an adult superstore in Gwinnett County, Georgia, and bought three clear jars, each containing an ounce of a cloudy white substance. The jars bore different brand names—"Meow Meow," "Bolivian MDPV," and "Miami Ice"—and the contents of one resembled crumbling lumps of sugar; another, shards of glass; the third, white powder. Later, at a hotel room a few hours' drive away, Shlaer and her friend lit the white crystals from one jar in a methamphetamine pipe. The smoke, she recalls, had a sickly odor that lodged in her nose—a combination of scorched rubber and vanilla hand soap. "There was a sweetness, a chemical smell, like something that's not supposed to be burned."

Shadowy figures soon appeared in her

peripheral vision and urged her to do violent and self-destructive things. As the hours, then days, marched on in that hotel room, Shlaer and her friend binge-smoked, injected, and snorted nearly all the contents of the jars. She fantasized about tearing human flesh with her teeth and scraped her face and body with her nails in violent fits.

Shlaer is a recovering cocaine addict and had used methamphetamine before, but she always thought she could tell the difference between her own mind and her mind on drugs. In that hotel room, she couldn't. "For the first time, I felt evil," says Shlaer, who was studying to become a paramedic when drug use derailed her academic plans.

The jars Shlaer bought most likely contained a mix of powerful stimulants called synthetic cathinones. Often referred to as "bath salts," "research chemicals," or "plant food," these compounds belong to a rapidly

Often looking like cocaine, the designer drugs known as "bath salts" can be up to 10 times as potent.

expanding array of substances that mimic or increase the effects of an illegal drug. Yet they mostly slip past law enforcement, their formulas tweaked just enough to skirt existing regulations or to go undetected in a drug test.

Evaluating the addictiveness of those drugs, deciphering how they work in the brain, and predicting which are likely to become a major threat is the job of a small lab at the National Institute on Drug Abuse (NIDA) in Baltimore, Maryland, headed by neuroscientist Michael Baumann. Set up in 2012, the four-person lab only takes on drugs that have at least 1000 mentions in the National Forensic Laboratory Information System, a U.S. drug surveillance program run by the Drug Enforcement Administration (DEA). Still, the team sometimes screens as

many as 12 new compounds per day to keep up with requests from forensics labs within the United States and abroad.

Baumann is part of a small but growing fraternity of researchers worldwide fighting back against science that has broken bad. Designer drug labs, Baumann notes, operate much like pharmaceutical companies, mining the existing scientific literature to find a new blockbuster. Rather than hunting for therapies, however, chemists in designer drug labs often seek out compounds that were abandoned because they were too dangerous or habit-forming, he explains. "They're looking for the things that will be most addictive." Baumann's task is to sound the alarm when he believes they have succeeded.

MOST DESIGNER DRUGS are not produced in a mobile home trailer like the one where methamphetamine is brewed in the TV series *Breaking Bad*, notes Jim Hall of Nova Southeastern University, Fort Lauderdale, in Florida, who studies the epidemiology of drug outbreaks. Instead, Hall says, they come from large-scale manufacturers in China, India, and Pakistan, often operating out of former chemical or perfume plants. Dealers order many of the compounds, including synthetic cathinones, in bulk, then put the raw product into empty pill capsules or sell it in baggies or jars, giving it a popular or local brand name.

> ## "I could not stop thinking about and researching bath salts."
>
> **Tessa Shlaer**, recovering addict

Historically, Europe has led the world in designer drug consumption and surveillance. According to the European Monitoring Centre for Drugs and Drug Addiction, 73 previously unknown psychoactive substances hit European markets in 2012 alone. In the United Kingdom, the problem is so extreme that researchers have started diving for data in latrines: Just last year, they discovered 13 unknown new psychoactive drugs over the course of 6 months by sampling urine from central London's portable toilets.

In recent years, however, the number of new designer drugs appearing first in the United States—rather than migrating from Europe—has skyrocketed, says Jill Head, a supervisory chemist at DEA. Since 2009, Head and her colleagues, whose job is to analyze seized compounds and determine their chemical structure, have identified more than 300 new drugs, she says. In response to the crisis, NIDA last year launched a 5-year project called the National Drug Early Warning System, or NDEWS, which aims to create a network of scientists, public health experts, and law enforcement representatives for sharing information and assisting with local drug research.

The largest percentage of new chemicals found in U.S. drug busts are synthetic cannabinoids—drugs marketed as marijuana mimics that don't show up in standard drug tests (see sidebar, p. 473). Synthetic cathinones come in second; as of late 2010, Head and her colleagues had found 70 new, synthetic permutations of the cathinone molecule, which is made by the khat plant *Catha edulis*. People have chewed khat for its mild stimulant qualities for hundreds of years, and safe, modern-day versions of the compound can be found in drugs as widely prescribed as the antidepressant Wellbutrin.

But tinker with the molecule's structure in key places—a methyl group here, a few oxygens there—and you can produce many psychoactive compounds, including powerful stimulants and hallucinogens (see chart, p. 472). "The sheer number of possibilities can be staggering," Head says.

Shlaer's first experience with bath salts came a few weeks before her visit to the Georgia superstore—and it was inadvertent. She injected methamphetamine that hospital blood tests later showed had been cut with two synthetic cathinones, methylone and MDPV. The consequences were dramatic: intense euphoria, heightened interest in everything, and the desire to be in constant motion, followed by nightmarish visions and suicidal despair. As soon as the drugs began to wear off, however, Shlaer became consumed with the desire to try them again. "I could not stop thinking about and researching bath salts," she says.

Shlaer had experienced two of the first synthetic cathinones to hit the United States. By the time she tried them, they were already illegal. Starting around late 2010, alarming reports of fatal overdoses, as well as a rash of grisly shootings and other violent crimes linked to the drugs, were pouring in from around the country. In 2011, DEA placed a 2-year emergency ban on methylone, MDPV, and a third substance called mephedrone, and began working with the agencies of the Department of Health and Human Services to determine whether the ban should be permanent.

Once a drug has been banned, obtaining samples for study becomes difficult for many scientists. They must possess or apply for a special DEA license in order to work with even minuscule amounts. But NIDA

Long after a bath salts overdose, Tessa Shlaer still experiences symptoms of withdrawal and hallucinations.

holds an institutional license to work on illegal drugs, and it has an annual budget devoted to studying designer drugs, which in-house chemists can synthesize to order. As a result, Baumann and colleagues are uniquely equipped to act quickly when a new drug hits the street.

After getting samples of the cathinones—in this case, from a colleague at the University of Wisconsin—Baumann sent them to John Partilla, a research chemist with an appropriate nickname: the Gatekeeper. One of Partilla's roles is to determine which drugs have the potential to be addictive or otherwise dangerous and which the lab can safely ignore.

In the case of the psychostimulants found in bath salts, the answer to that question lies in how they interact with key pieces of neuronal machinery called monoamine transporter proteins. When a neuron fires a signal to its neighbors, it releases a burst of neurotransmitter molecules into the gap between the cells, called the synapse. The neurotransmitters bind to receptors on adjacent neurons, transmitting the chemical signal, but then quickly drop off. The first cell, which sent the signal, uses the transporter proteins to vacuum up the neurotransmitter, removing it from the synapse. If that does not happen, the lingering neurotransmitter molecules will continue to bind with receptors on the neighboring cells, sending and resending an aberrant, repetitive message.

Psychostimulants act on the transporter for the neurotransmitter dopamine, a key pleasure molecule in the brain, boosting its levels in the synapse. Methamphetamine, for example, slips through the transporter to trick the cell into releasing more dopamine, "essentially throwing the vacuum cleaner into reverse," Baumann says. Cocaine acts more like a rolled up sock in a vacuum hose, he explains. It blocks the transporter from vacuuming dopamine out of the synapse. In either case, as excess dopamine builds up in the synapse, it stimulates neuronal activity in regions that are involved with feelings of pleasure and its anticipation, generating an intense high that addicts come to crave.

To determine how MDPV, methylone, and mephedrone affect the dopamine transporter, Partilla delicately ground up rat brain tissue with a mortar and pestle, then put the tissue into a test tube and spun it in a centrifuge to separate its component parts. He collected assemblies of membranes and proteins, called synaptosomes, which include the transporters. When in solution, the cell membranes and their proteins will obligingly reassemble themselves into round, miniature nerve endings, Baumann

Designed to be addictive

A small sample of synthetic cathinones seized by DEA in recent years; as of 2010, the agency had found 70 new variations on the cathinone molecule (center).

not directly advise DEA, but the agency often uses such information to decide how to "schedule" a new drug according to a five-level ranking system, with Schedule I drugs considered the most addictive and dangerous, says DEA spokeswoman Barbara Carreno. In 2012, DEA permanently listed all three synthetic cathinones as Schedule I substances.

WHY MDPV'S CHEMICAL STRUCTURE is so much more potent at blocking the dopamine transporter than cocaine or any other cathinone-based molecule remained unclear. The question is not merely academic, says Louis De Felice, a biophysicist at Virginia Commonwealth University in Richmond. If scientists can determine precisely how a drug binds to its target in the brain, they can sometimes devise an antidote that dislodges the compound or counteracts it. The drug naloxone, for example, binds to the same neuronal receptors as heroin and can stop and even reverse an overdose by blocking heroin's effects. In the United States, naxolone has been responsible for reversing the effects of a heroin or other opioid overdose in more than 10,000 people since 1996, according to a 2010 survey by the Centers for Disease Control and Prevention.

In hopes of finding a similar antidote for MDPV and related designer drugs, Baumann, De Felice, and a handful of other researchers have begun to deconstruct the molecule piece by piece, as well as the dopamine transporter protein to which it binds. In December 2012, De Felice and one of his Ph.D. students, Krasnodara Cameron, made a bet over which parts of MDPV's chemical structure made it so potent. Was it the three-carbon propyl hook attached to the body of the molecule like a zigzagging arm? Or was it the molecule's pentagonal head, called a pyrrolidine ring?

Cameron bet on the head, De Felice on the hook. The stakes were high: a batch of homemade cookies, winner's choice. "Sweeties," De Felice calls sugary treats. After all, he says, "we're all driven by dopamine."

Renata Kolanos, a synthetic chemist in De Felice's lab at the time, systematically created MDPV derivatives missing different parts of the molecule, which the team tested in experiments similar to those used in Baumann's lab to screen new drugs. The ring and the hook both turned out to be vital to MDPV's ability to jam the dopamine

says: "They basically form with the proteins all oriented in the proper direction."

Next, Partilla loaded the synaptosomes with radioactive dopamine, allowing him to precisely trace how much of the neurotransmitter escaped the miniature nerve endings when they were exposed to one of his drug samples. Both methylone and mephedrone slipped through the dopamine transporters into the droplets and immediately triggered a burst of neurotransmitter release, which mimics the mechanism of methamphetamine and means they are likely addictive.

The MDPV story was more complicated. It didn't slip through the transporter. So Partilla performed a second experiment to see whether MDPV instead jammed the do-

pamine transporter, like cocaine. It did—and the synthetic compound turned out to be 10 times more potent than cocaine at blocking dopamine uptake. When other members in Baumann's lab injected rats with the drug, it produced large, long-lasting dopamine spikes in their brains, comparable to those triggered by much higher doses of cocaine.

The rats' behavior on the drug was also extreme, Baumann says: They jumped and reared and often bobbed their heads and sniffed uncontrollably—an animal model of psychosis in humans. They avidly self-administered injections of the drug by pressing a lever. Taken together, Baumann recalls, the evidence added up to "red alert"—indicating MDPV's risk for abuse and addictiveness. Baumann's lab does

Alarm over synthetic cannabinoids

By **Emily Underwood**

Grisly media reports of cannibalism and shooting sprees prompted by synthetic cathinones (see main story, p. 469) have given them an especially bad reputation, but there's another class of designer drugs worrying drug enforcement and public health officials: synthetic cannabinoids, humanmade chemicals designed to mimic THC, the key psychoactive ingredient in marijuana.

The drugs are typically sprayed onto dried plant material so they can be smoked. They are billed as providing marijuanalike highs while eluding drug tests. Sold since the early 2000s under brand names such as K2 and Spice, they act on the same brain receptors as THC but are up to 100 times more potent, leading to dangerous side effects such as heart attack, kidney failure, psychosis, and sometimes death. Many people underestimate the risk of synthetic cannabinoids because they see marijuana as benign, says Marilyn Huestis, a toxicologist at the U.S. National Institute on Drug Abuse (NIDA) who is developing tests for the drugs in blood, saliva, urine, and breath. "People are less afraid of a joint than they are of a white powder."

Since the Drug Enforcement Administration banned the first synthetic cannabinoids in 2011, more than 250 new compounds have arisen to take their place. In a recent study of 20,017 samples of urine collected from U.S. military service members worldwide between July 2011 and June 2012, Huestis and her colleagues found traces of the compounds in 290 of them. And according to a 2012 NIDA-funded survey, one in nine 12th graders in the United States reported using synthetic cannabinoids in the past year. ∎

transporter, De Felice says. (Cameron still made him peanut butter cookies.)

Baumann, De Felice, and their colleagues then went a step further, dismantling the alkyl chain that forms the hook piece by piece and testing the resulting molecules in rodents. The shorter it got, the less potent the drug became. Such painstaking work "provides a high level of predictive power" for researchers examining a new designer drug, Baumann says. "We can now look at a drug on a cathinone scaffold and say we know how this drug will affect transporter function and influence behavior."

In the meantime, a new crop of potent synthetic cathinones is already wreaking havoc in U.S. communities. Although reports of MDPV dropped precipitously after it was banned in 2011, designer drug–makers were far ahead of the curve. At almost the same time, DEA surveillance reports of a drug called α-PVP, widely known as "gravel" in the Northeast, shot up from a total of roughly 20 to more than 3000. When α-PVP first hit the streets, Baumann suspected it would have psychological and physical effects similar to those of MDPV, based on the compounds' structural similarity. In 2013, he ordered samples of the compound and ran it through the same tests he had applied to MDPV. He found that it did act almost exactly like the banned drug—a finding that supported DEA's decision to outlaw α-PVP in 2014.

WEEKS AFTER her hotel room binge, Shlaer says her paranoid hallucinations remained so vivid that she called the police, convinced that she was facing a conspiracy. Family members took her to the emergency room, where she crawled on the floor and tables, snarling like an animal, she says. Now, a year and a half into her recovery at a residential treatment center in North Carolina, Shlaer still experiences hallucinations, occasional cravings for bath salts, and sudden bouts of rage, she says. Last winter, desperate for more information, she remembered a name she had read while researching the drugs: Louis De Felice.

"I am not really sure how appropriate it is for me to be emailing you," Shlaer wrote him. Apologizing for her scattered state, she added, "no one here has ever dealt with bath salts' long term effects before. Do you know of anyone I could talk to or with whom I could correspond?"

Although De Felice gets many such letters from addicts, Shlaer's message, which described her experiences in articulate detail, stood out, he says. He wrote back immediately: "You don't sound scattered, you sound rational, sincere and in trouble."

De Felice told Shlaer that evil intentions, hallucinations, and rage are all common symptoms of bath salts overdose. And he invited Shlaer to come to his university to see the lab and talk to some of his students about her experiences. The trip last spring was "incredible," Shlaer notes. The undergraduates she spoke to "were actually interested in what I had to say, from a human and a scientific perspective." She is now considering a career in biomedical research, which De Felice says he will help her pursue. And she is resuming her training to become a paramedic. Although drugs are never far from her mind, she says, "now, my thoughts are of a more clinical nature." ∎

Research chemist John Partilla screens emerging designer drugs at the National Institute on Drug Abuse, looking for those likely to be most addictive.
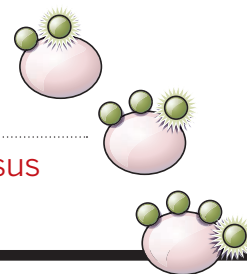
PERSPECTIVES
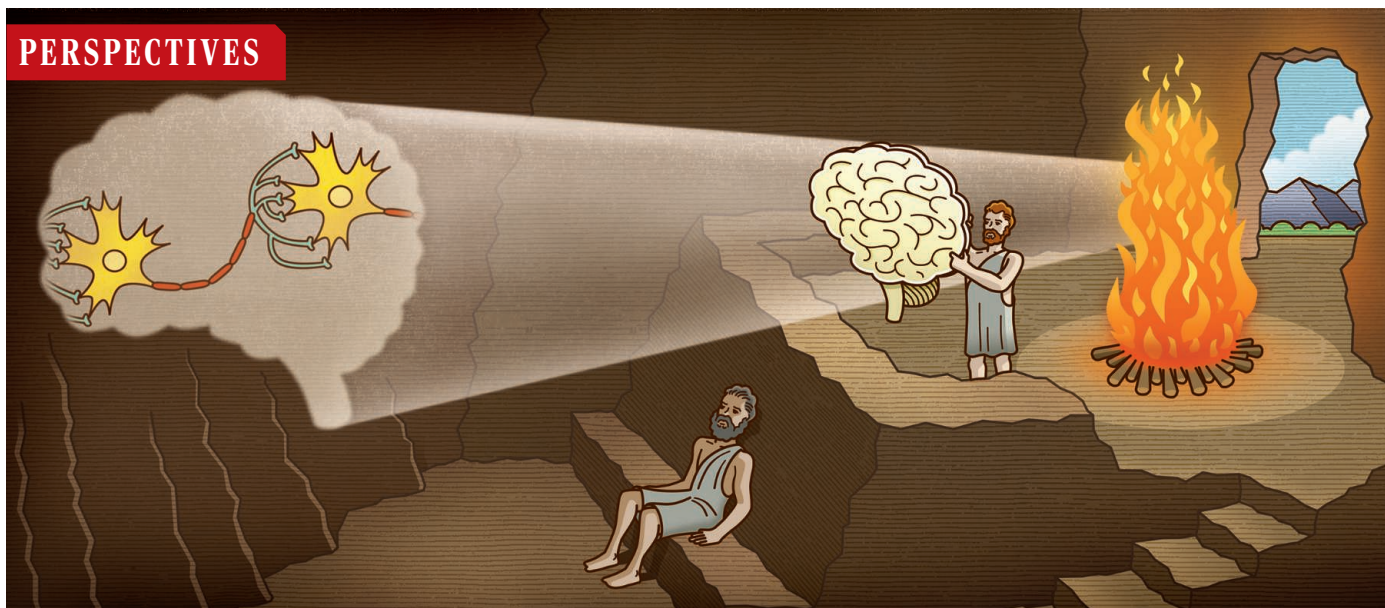
Like Plato's cave. In the Greek philosopher's allegory, a man sits in a cave and observes on the wall the shadows of ideas, which he takes for the real world. In expansion microscopy, today's neuroscientist can observe the enlarged shadows of neurons in brains.

MICROSCOPY

The superresolved brain

Physically enlarged neurons can be observed at high resolution with light microscopy

By **Hans-Ulrich Dodt**

I n the past decade, important advances have been made to increase the resolution of the light microscope, as acknowledged by last year's Nobel Prize for superresolved fluorescence microscopy (*1*, *2*). This progress is fascinating but comes at the price of high illumination intensities or long recording times, and expensive instruments. As reported on page 543 of this issue, Chen *et al.* (*3*) have cleverly turned the problem around by asking: What if we leave the microscope as it is, and increase the object instead?

Numerous methods have been developed to make mouse brains transparent for imaging, with the aim of visualizing the neuronal network in three dimensions (*4*–*9*).

Vienna University of Technology, 1040 Vienna, Austria, and Medical University of Vienna, 1090 Vienna, Austria. E-mail: dodt@tuwien.ac.at

Most groups struggled with swelling of the brain that was induced by such methods. Two years ago, an approach was described that basically transforms the mouse brain into an acrylamide gel (*10*). The process involves synthesizing a polymer within a formalin-fixed brain by perfusing the specimen with chemicals. Such polymer gels can excessively swell if put in distilled water. However, to take advantage of this, the brain expansion would have to be isotropic.

Chen *et al.* have solved this problem by digesting the mouse brain away after transforming it into a polymer gel but before inducing matrix expansion. But how can one study a brain in which all the neurons are gone? Here, a second idea came into play: For some questions, it would be enough to study a "shadow" of the brain in the polymer matrix. This was realized by first marking molecules of interest in neurons with antibodies. The antibodies then were labeled with fluorescent markers that bind both to

the antibodies and the matrix. The brain was then digested away and the matrix expanded. The fluorescent neuronal shadows also expanded and could be studied in "superresolution." Chen *et al.* could thus increase specimen size by about a factor of 5 while preserving general morphology, and could visualize cultured neurons and brain slices at 70-nm resolution. This allowed them to observe proteins localized to synapses. The resolution does not compare badly to that of superresolution microscopy techniques (*1*, *2*), which enable a resolution of 20 to 70 nm. The additional advantage of expansion microscopy is that it depends on conventional microscopes; hence, data can be acquired quickly.

The study of just the shadows of neurons reminds one of Plato's philosophy of ideas. Plato postulated that ideas (rather than material things) possess the highest kind of reality. Things we perceive and take for real are only the shadows of ideas. He illustrated this

sciencemag.org **SCIENCE**

with an allegory: We are like a man sitting in a cave looking at the wall, a fire burning behind him. If objects (i.e., ideas) are carried before the fire, the man sees only their enlarged shadows on the wall, and he will take them as the real world. Today's neuroscientist also can view "shadows" of the real world. The enlarged shadows of neurons, dendritic spines, and synapses can now be seen through expansion microscopy and attempts can be made to put together a super-resolved model of the brain (see the figure).

Expanded brains have the great advantage that the heavy absorption of water makes them completely transparent. Thus, they are ideal objects for light sheet microscopy, which requires transparent specimens. In light sheet microscopy, an object is illuminated from the side with a thin sheet of light to create optical sectioning, whereas in traditional microscopy, the light comes from below or above. Since the demonstration 8 years ago (4) that neuronal networks in cleared mouse brains can be visualized with light sheet microscopy, the application of this approach has grown rapidly. In retrospect, it is puzzling that light sheet microscopy was not taken up sooner to study the brain, as the technique is 100 years old. Technically, it is easier to implement than confocal microscopy, in which a light beam is used to take images through serial planes of a sample and their subsequent stacking creates a three-dimensional (3D) image. But light sheet microscopy still needed clearing technology to have sufficient impact. Today's clearing technology not only aims at perfect transparency but also now provides, with the method of Chen *et al.*, a way to circumvent Abbe's resolution limit.

One might imagine that in the future, a whole mouse brain could be expanded 10 times to the size of a small orange, with all neurons and synapses of interest labeled in various colors. Light sheet microscopy may well adopt superresolving stimulated emission depletion (STED) technology to scan such a sample with extremely thin sheets of light in all three dimensions. For the thousands of exabytes then generated to create 3D images, supercomputers for "the human brain project" will be desperately needed. ∎

REFERENCES

1. T. A. Klar, S. Jakobs, M. Dyba, A. Egner, S. W. Hell, *Proc. Natl. Acad. Sci. U.S.A.* **97**, 8206 (2000).
2. E. Betzig *et al.*, *Science* **313**, 1642 (2006).
3. F. Chen *et al.*, *Science* **347**, 543 (2015).
4. H.-U. Dodt *et al.*, *Nat. Methods* **4**, 331 (2007).
5. H. Hama *et al.*, *Nat. Neurosci.* **14**, 1481 (2011).
6. K. Becker *et al.*, *PLOS ONE* **7**, e33916 (2012).
7. A. Ertürk *et al.*, *Nat. Protoc.* **7**, 1983 (2012).
8. T. Kuwajima *et al.*, *Development* **140**, 1364 (2013).
9. M. T. Ke, S. Fujimoto, T. Imai, *Nat. Neurosci.* **16**, 1154 (2013).
10. K. Chung *et al.*, *Nature* **497**, 332 (2013).

The global engine that could

How do hydrological processes affect Earth's heat engine?

By **Olivier M. Pauluis**

It has been widely accepted since Carnot's seminal work (*1*) that the atmosphere acts as a thermodynamic heat engine: Air motions redistribute the energy gained from the Sun in the warm part of the globe to colder regions where it is lost through the emission of infrared radiation to space. Through this process, some internal energy is converted into the kinetic energy needed to maintain the atmospheric circulation against dissipation. The analogy to a heat engine has been applied to explain work produced by a heat engine compared to a Carnot cycle. In particular, when the energy source of the Carnot cycle is replaced by evaporation, the mechanical work of the cycle is reduced and strongly depends on the relative humidity (*7*).

Idealized cycles such as the Carnot cycle are useful theoretical models for understanding how much wind can be sustained around the globe. However, the atmosphere is highly turbulent, and extracting a single cycle from the complex motions that make up the global circulation is not straightforward. Thermodynamic studies of the climate system have
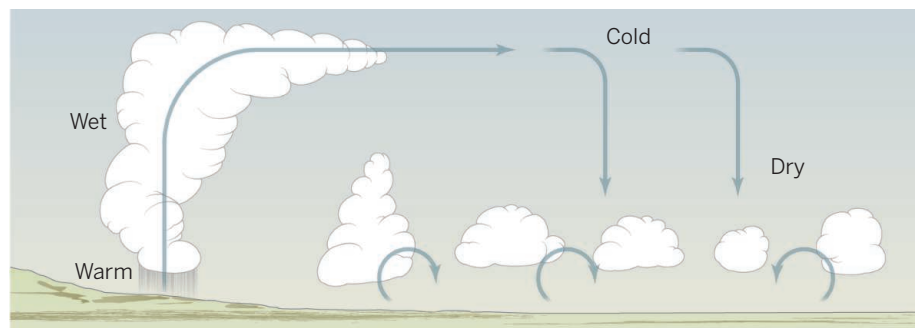
Fine weather machine. Nice, sunny weather occurs when dry air from the upper troposphere sinks and is mixed with moist air near Earth's surface. Laliberté *et al*. show that such mixing weakens the atmospheric heat engine.

various atmospheric phenomena, such as the global circulation (*2*), hurricanes (*3*), and dust devils (*4*). On page 540 of this issue, Laliberté *et al.* (*5*) show that the hydrological cycle reduces the efficiency of the global atmospheric heat engine.

Although the atmosphere acts overall as a heat engine, it may not be a very efficient one. The distribution of energy sources and sinks around Earth implies a maximum work of ~10 W·m^{-2} when averaged globally, yet estimates for the rate of kinetic energy production by atmospheric motions are about half this figure. The difference is very likely due to Earth's hydrological cycle, which reduces the production of kinetic energy in two ways. First, as rain droplets, hail pellets, or snowflakes fall through the atmosphere, they generate microphysical shear zones in which a substantial amount of dissipation occurs. Satellite data yield an estimated dissipation rate from precipitation of ~1.2 W·m^{-2} in the tropics (*6*). Second, water mostly evaporates in unsaturated air, and this evaporation is thus thermodynamically irreversible. Such irreversibility reduces the

typically required detailed knowledge of all thermodynamic transformations and have involved a complex analysis of numerical simulations (*8*–*10*). These intensive data requirements explain why there have been relatively few thermodynamic studies of the global climate.

Laliberté *et al.* offer an elegant way to address this problem. Meteorologists have studied air flow on surfaces of constant entropy since the 1930s. Atmospheric scientists and oceanographers have extended this approach to study how air and water move around the planet on various thermodynamic surfaces, such as surfaces of constant temperature or salinity (*11*, *12*). Laliberté *et al.* push this idea even further by averaging the circulation in a three-dimensional thermodynamic space (pressure, entropy, and water content). Dalton's law, however, states that all thermodynamic properties of moist air can be determined from the knowledge of these three state variables. This means that the circula-

Center for Atmosphere Ocean Science, New York University, New York, NY 10012, USA. E-mail: pauluis@cims.nyu.edu

tion computed by Laliberte *et al.* can be used to infer all thermodynamic transformations in the atmosphere, based solely on standard meteorological measurements.

The authors apply their methodology to the global thermodynamic cycle using data from meteorological reanalysis and from a global climate model. The results confirm that the hydrological cycle reduces the amount of kinetic energy generated by the large-scale atmospheric flow by about one-third. As much as we may associate the hydrological cycle with severe weather and heavy precipitation, it is also responsible for nice, sunny weather, which occurs when air masses gradually regain some of the water vapor lost during an earlier rainfall (see the figure). The hydrological cycle reduces the average intensity of the winds around Earth mostly by generating pleasant weather around large portions of the globe.

The study by Laliberté *et al.* offers a blueprint for the systematic analysis of the thermodynamic transformations in the climate system. The method can be applied based solely on the standard output of numerical models and can easily be used to compare the thermodynamic cycles simulated by different global climate models. It also opens up two important questions.

First, what are the contributions of convection and other atmospheric motions at small scales in the atmospheric heat engine? The approach presented by Laliberté *et al.* is limited to motions resolved by their data set, which excludes anything with a horizontal scale of less than 100 km. Yet, many thermodynamic transformations occur within clouds, at scales that are not typically resolved in an atmospheric or climate model. Second, how are the thermodynamic processes affected by climate change? As Earth's climate warms, the air will be able to contain more water vapor on average. Laliberté *et al.* indicate that this would lead to a slight reduction in the work done by the atmospheric circulation. This result, if confirmed, could offer important insights into what Earth's global engine could do in the future. ∎

REFERENCES

1. S. Carnot, *Reflexions sur la puissance motrice du feu et sur les machines propres a développer cette puissance* (Gauthier-Villars, Paris, 1824).
2. E. Lorenz, *Tellus* **7**, 157 (1955).
3. K. A. Emanuel, *Nature* **326**, 483 (1987).
4. N. O. Renno, *Tellus* **60**, 688 (2008).
5. F. Laliberté *et al.*, *Science* **347**, 540 (2015).
6. O. Pauluis, J. Dias, *Science* **335**, 953 (2012).
7. O. Pauluis, *J. Atmos. Sci.* **68**, 91 (2011).
8. O. Pauluis, I. M. Held, *J. Atmos. Sci.* **59**, 140 (2002).
9. V. Lucarini, *Phys. Rev. E Stat. Nonlin. Soft Matter Phys.* **80**, 021118 (2009).
10. S. Pascale *et al.*, *Clim. Dyn.* **36**, 1189 (2011).
11. J. D. Zika *et al.*, *J. Phys. Oceanogr.* **42**, 708 (2012).
12. J. Kjellsson *et al.*, *J. Atmos. Sci.* **71**, 916 (2014).

When the circadian clock becomes blind

The conceptual model of circadian oscillator function may need revision

By **Achim Kramer**

Your alarm clock rings in the morning —it's time to get up, but you feel like it's the middle of the night. If this is happening regularly, your circadian clock may not be adjusted to your social life. Circadian clocks are endogenous oscillators that coordinate not only our sleep-wake behavior with the environmental 24-hour light-dark cycle but also a myriad of rhythmic physiological and metabolic processes. A set of so-called clock genes comprises a regulatory network that generates self-sustained molecular ~24-hour rhythms of gene expression. For eukaryotic clocks, the prevailing conceptual model proposes a negative transcriptional-translational feedback loop (*1*). On page 518 of this issue, Larrondo *et al.* (*2*) challenge the molecular basis of this view.

In the course of 1 day, a negative element (a clock protein) is synthesized, progressively phosphorylated and, after a delay of several hours, shuts down its synthesis by acting negatively on its own transcription. Once the negative element is degraded and cleared from the cell, the transcriptional

Laboratory of Chronobiology, Charité Universitätsmedizin Berlin, Germany E-mail: achim.kramer@charite.de

inhibition is relieved and a new cycle can start. The key finding of Larrondo *et al.* is that the circadian cycle is not one of synthesis and destruction as the prevailing model reflects, but instead, a cycle of synthesis and progressive posttranslational modifications. In other words, degradation of the negative element does not seem to be required for generating circadian rhythmicity. Rather, progressive and sequential phosphorylation of negative elements occurs in a characteristic temporal pattern, thereby controlling the negative element's activity and clock speed. According to their model, the circadian loop is closed by phosphorylation-induced inactivation of the negative element rather than by its degradation (see the figure).

Larrondo *et al.* base their model primarily on observations made in the filamentous fungus *Neurospora crassa*, a well-established genetic model of eukaryotic clocks. A protein called Frequency (FRQ) is the key circadian negative element of *Neurospora*. FRQ expression is rhythmic and controlled by the transcriptional activator White Collar Complex (WCC). FRQ represses WCC by bringing along casein kinase 1a (CK1a) that—with other protein-phosphorylating enzymes—phosphorylates and inactivates WCC. FRQ itself is progressively phosphorylated at over 100 sites, and hyperphosphory-

Progressive phosphorylation determines circadian clock speed

Hyperphosphorylation

Proteasomal degradation

FRQ

WCC

Rhythmic expression of genes, synthesis of FRQ
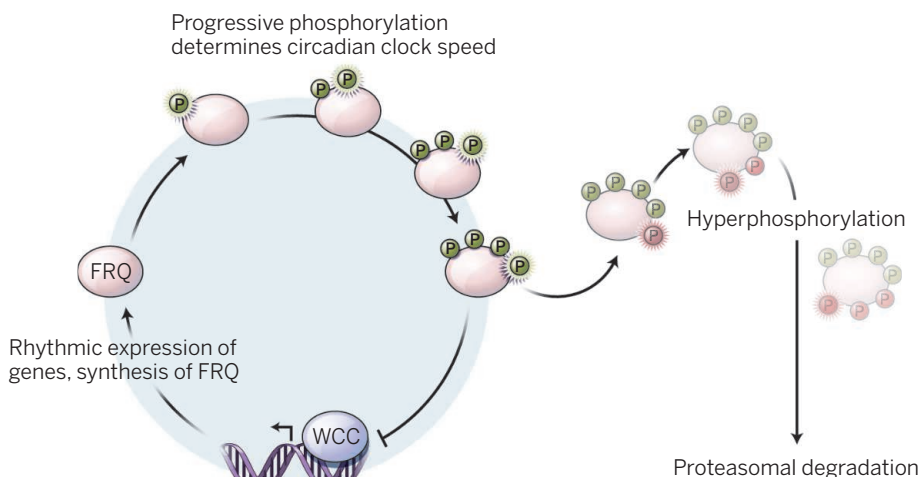
Closing the loop. Clock speed is determined by progressive phosphorylation (green) of the negative element (FRQ for *N. crassa*) rather than by its degradation rate. A second class of phosphorylation (red) inactivates FRQ, to which the circadian clock then becomes blind.

lation of FRQ promotes its rapid degradation through its association with a protein called F-box and WD40 repeat–containing protein 1 (FWD-1). FWD-1 is the substrate-recruiting subunit of an E3-ubiquitin ligase that supports FRQ ubiquitination and proteasomal degradation. If degradation of FRQ is an essential step for its inactivation (as the prevailing model predicts), circadian rhythms should be lost in *Neurospora* strains lacking FWD-1. At first glance, this indeed seems to be the case: In a mutant strain lacking FWD-1, degradation of FRQ is severely impaired and circadian rhythms of asexual spore formation (a convenient readout of the *Neurospora* clock) are absent. However, Larrondo *et al.* looked more closely at the molecular clockwork using sensitive bioluminescence-based reporters and detected, surprisingly, rather normal rhythms of FRQ expression. Thus, negative element turnover does not seem to be a critical step for circadian rhythm generation.

Why was degradation of the negative element thought to be required for circadian rhythm generation? Probably because previous studies reported that the degree of FRQ phosphorylation determines FRQ stability, and FRQ stability determines circadian period. For example, in strains with long-period *frq* alleles (thus making the length of a circadian cycle more than 24 hours), FRQ protein is more stable, whereas in short-period strains, FRQ is less stable. Larrondo *et al.* suggest that these are not cause-and-effect relations but just correlations. The authors could (pharmacologically) manipulate the degree of FRQ phosphorylation without affecting FRQ stability. In addition, more stable FRQ does not always affect the circadian period. New FRQ can be synthesized while old, hyperphosphorylated FRQ is still around (*3*). It seems that the (phosphorylation) quality of FRQ rather than its quantity is important; it does not matter whether the degradation of hyperphosphorylated FRQ takes place because the circadian oscillator becomes blind toward old FRQ. This is consistent with the inability of hyperphosphorylated FRQ to recruit CK1a (*4*) as well as its weak binding to WCC (*5*), conditions that make it an inefficient transcriptional repressor.

Can this circadian model be generalized to other species? Indeed, several findings from the fruit fly *Drosophila melanogaster* and mammals hint at a less important role of negative element destruction than previously assumed. In *Drosophila*, mutations in the negative element Period (PER) that interfere with binding to the E3-ligase subunit Slimb (and thereby with PER degradation) lead to hyperphosphorylated PER even at times when new hypophosphorylated PER is

already synthesized (*6*). Moreover, constitutive overexpression of Cryptochrome (CRY), the strongest negative element of the mammalian oscillator, does not lead to long periods (although it does dampen the strength of the rhythms) (*7*). Also, mice deficient for the F-box/LRR-repeat protein 3 (FBXL3), an E3-ligase subunit that is necessary for CRY protein degradation, display normal circadian periods yet large amounts of CRY, but only when a second clock gene (the nuclear hormone receptor REV-ERBα, the inactivation of which results in a rather normal period) is also deleted (*8*).

Nevertheless, it is probably premature to revise the prevailing clock model—at least for animal clocks. Much evidence indicates that perturbing the degradation of negative elements PER and CRY leads to drastic period changes (*1*). Whether this is just a correlation rather than cause-and-effect relation, as Larrondo *et al.* suggest, needs to be carefully investigated. For example, it will be necessary to unambiguously tease apart which phosphorylation events regulate clock speed and which events just target negative elements for degradation without affecting circadian period. This is likely a difficult endeavor given the dozens of phosphorylation sites (and clusters) in FRQ, PER, and CRY proteins (*5*, *9*).

Our understanding of the circadian clock appears to be moving toward a mechanism of less evolved organisms—that is, posttranslationally controlled oscillators—but with questions about the role of (theoretically dispensable) degradation in its operation. In cyanobacteria, a pure phosphorylation-based mechanism (a "phoscillator") is at the heart of the clock (*10*), and in mammals, transcription-independent posttranslational oscillators have been proposed (*11*). Individuals with extremely early chronotypes can experience a 4- to 6-hour phase advance in sleep-wake behavior, attributed to the mutation of a single phosphorylation site in a clock constituent (*9*, *12*). It may be that a phosphorylation defect in a clock protein is what keeps you tired in the morning. ■

REFERENCES

1. S. A. Brown, E. Kowalska, R. Dallmann, *Dev. Cell* **22**, 477 (2012).
2. L. F. Larrondo, C. Olivares-Yañez, C. L. Baker, J. J. Loros, J. C. Dunlap, *Science* **347**, 1257277 (2015).
3. J. Cha, H. Yuan, Y. Liu, *J. Biol. Chem.* **286**, 11469 (2011).
4. L. Lauinger, A. Diernfellner, S. Falk, M. Brunner, *Nat. Commun.* **5**, 3598 (2014).
5. C. L. Baker *et al. Mol. Cell* **34**, 354 (2009).
6. J. C. Chiu *et al.*, *Genes Dev.* **22**, 1758 (2008).
7. H. R. Ueda *et al.*, *Nat. Genet.* **37**, 187 (2005).
8. G. Shi *et al.*, *Proc. Natl. Acad. Sci. U.S.A.* **110**, 4750 (2013).
9. K. Vanselow *et al.*, *Genes Dev.* **20**, 2660 (2006).
10. M. Nakajima *et al.*, *Science* **308**, 414 (2005).
11. J. S. O'Neill, A. B. Reddy, *Nature* **469**, 498 (2011).
12. K. L. Toh *et al.*, *Science* **291**, 1040 (2001).
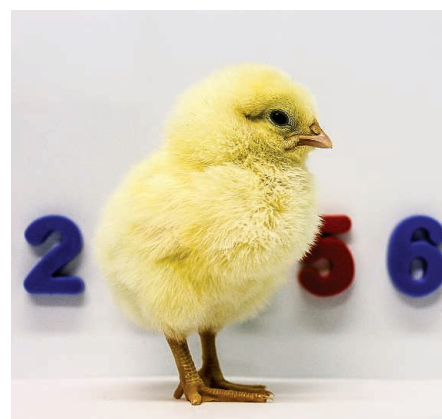
Far from bird-brained. Rugani *et al.* report elegant experiments investigating the sense of numerical order in 3-day-old domestic chicks.

ANIMAL BEHAVIOR

Chicks with a number sense

Chicks and humans map numbers to space in a similar way

By **Peter Brugger**

Regardless of cultural background and mathematical training, all humans have an intuitive sense of numerical magnitude (numerosity). We share with various nonhuman animals the ability to discriminate among different sets of quantities (*1*), but one aspect of number processing is commonly assumed to be uniquely human (*2*): the consistent mapping of increasing quantities along the horizontal extension of space—that is, the construction of a mental number line. On page 534 of this issue, Rugani *et al.* (*3*) show that 3-day-old domestic chicks (see the photo) associate small numerosities with the left side, and large ones with the right side, of a given space (see the figure, panel A). The results show that newborn chicks can understand both relative and absolute quantities. They also suggest that the brain may be prewired in how it relates numbers to space.

The authors first trained the chicks to find food behind a central panel marked with five dots. In the next test phase, the birds were placed before two laterally placed panels. When each panel showed two elements, the birds searched behind the left of the two panels; when each panel showed eight elements, they searched behind the right. In
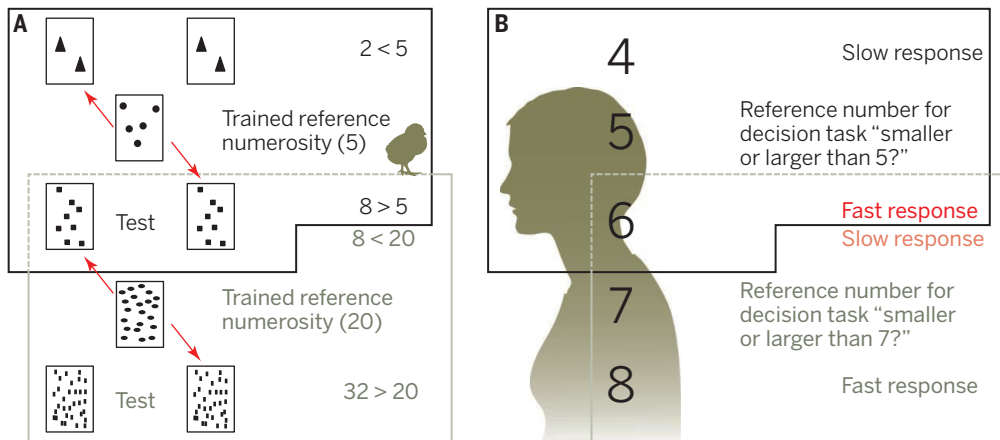
Of chicks and humans. (**A**) Rugani *et al.* show that chicks trained to find food behind a panel representing an abstract number (dots differed in color and shape but were matched for area and circumference) expect food behind the left of two panels representing a smaller number, but behind the right for a larger number. In the example, the numerosity representing 8 is smaller than that experienced during training with 20 and thus associated with the left side of space. After exposure to a training numerosity of 5, the same numerosity of 8 is associated with the right side of space. (**B**) In humans, patients who neglect the left side of space after right hemisphere damage are slow in classifying 6 as smaller or larger than 7, but fast if the reference number is 5 (*11*). The representation of increasing quantities from left to right may be the biological default, modulated (but not caused) by situational demands or cultural habits.

contrast, after training with a numerosity of 20, eight elements initiated a leftward search (see the figure, panel A). These findings suggest the existence of a mental number line in the chick's mind. Small numbers are represented to the left of larger numbers, but whether a quantity is deemed small or large depends on the situation.

The work casts doubt on the importance of language and symbolic thought for the ability to represent discrete quantities larger than 3 and to develop a sense of numerical order and counting routines. Field studies of avian behavior have previously documented this ability in adult birds. A particularly revealing model system is that of brood parasites such as cowbirds. Females of this species must locate, observe, and remember the exact location of host nests (*4*). They must also synchronize their own egg laying with that of the host by keeping track of the daily increase in host clutch sizes (*5*). The cowbirds' reproductive success thus depends on their ability to accurately judge magnitudes in space, time, and number. Whereas the observations in cowbirds involved adult individuals, Rugani *et al.*'s experiments with 3-day-old domestic chicks support the view that a general magnitude system may be functional at birth. Recent experiments with newborn humans are compatible with this notion; de Hevia *et al.* have shown that infants aged 8 hours to 3 days systematically related increases in numerical magnitude with increases in spatial extent and temporal duration (*6*).

Neuropsychology Unit, Department of Neurology, University Hospital Zürich, CH-8091 Zürich, Switzerland. E-mail: peter. brugger@usz.ch

A more specific insight from Rugani *et al.*'s study is that a chick's sense of numerical order is tightly coupled with its sense of space: "More than" is equivalent to "to the right of." This leads to a left-to-right directionality in the mapping of numbers to space—a finding that puts several previous proposals for the origin of mental number lines into perspective. One reason why researchers have assumed that this kind of numerical mapping is an invention of the human mind is its cultural modification. In cultures with a left-to-right reading and writing direction, the number line expands from left to right, but cultures with an opposite directional handling of script align numbers from right to left (*2*). Obviously, reading/writing direction cannot be the ultimate cause of directionality, nor can finger-counting habits (*7*). Presumably, the predominant role of the right hemisphere for numerical ordering (*8*) biases initial attention to the left side of both physical and number space. Together with a preference for increasing over decreasing order—already apparent in 4-month-old human infants (*9*, *10*)—the biological default of a number line would point from left to right.

The chicks' positioning of a numerosity to either the left or the right side of space depending on a given standard gives testimony to a flexibility that is far from bird-brained. Such flexible assignment is in direct analogy to the relativity of number-space associations in the human brain. Neurological patients who neglect the left side of space are also impaired in processing numerals located to the left of a given standard (see the figure, panel B) (*11*). It is the flexible

classification of extents, amounts, and magnitudes as left-sided or right-sided that may have allowed situational and possibly cultural variations in the directionality of number lines to arise.

Rugani *et al.* offer a key lesson in how informative a simple but elegantly designed behavioral experiment with a precocious species can be for the interpretation of number-space associations in the human mind. They provide a provocative set of hypotheses to be tested in future research. What is the role of emotions in the spatialization of magnitudes? In both natural environments and laboratory situations, "more" is commonly equivalent to "better." Chicks, like other animals, prefer more over less food and prefer to follow many rather than few companions (*12*). In animals and humans, the left cerebral hemisphere is specialized for the processing of positive emotions, the right hemisphere for negative emotions (*13*). If more feels better, could the left hemisphere's positivity bias favor an association of larger magnitudes with the right side of space, which it primarily controls? With respect to human number-space associations, what environmental or epigenetic factors have contributed to the development of a right-to-left orientation in only a minority of cultures with a horizontally organized script? Such questions need to be tackled by many disciplines jointly, including behavioral ecology, developmental psychology, comparative linguistics, and culture-sensitive neuroscience (*14*). ∎

REFERENCES

1. S. Dehaene, *The Number Sense* (Oxford Univ. Press, New York, 2011)
2. S. M. Göbel, S. Shaki, M. H. Fischer, *J. Cross Cult. Psychol.* **42**, 543 (2011).
3. R. Rugani, G. Vallortigara, K. Priftis, L. Regolin, *Science* **347**, 534 (2015).
4. D. J. White, L. Ho, G. Freed-Brown, *Psychol. Sci.* **20**, 1140 (2009).
5. J. Low, K. C. Burns, M. E. Hauber, *Int. J. Avian Sci.* **151**, 775 (2009).
6. M. D. de Hevia, V. Izard, A. Coubart, E. S. Spelke, A. Streri, *Proc. Natl. Acad. Sci. U.S.A.* **111**, 4809 (2014).
7. M. H. Fischer, P. Brugger, *Front. Psychol.* **2**, 260 (2011).
8. A. Knops, K. Willmes, *Neuroimage* **84**, 786 (2014).
9. V. Macchi Cassia, M. Picozzi, L. Girelli, M. D. de Hevia, *Cognition* **124**, 183 (2012).
10. M. D. de Hevia, L. Girelli, M. Addabbo, V. Macchi Cassia, *PLOS ONE* **9**, e96412 (2014).
11. P. Vuilleumier, S. Ortigue, P. Brugger, *Cortex* **40**, 399 (2004).
12. R. Rugan *et al.*, *Front. Psychol.* **5**, 150 (2014).
13. L. J. Rogers, G. Vallortigara, R. J. Andrew, *Divided Brains: The Biology and Behavior of Brain Asymmetries* (Cambridge Univ. Press, New York, 2013).
14. S. Kazandjian, S. Chokron, *Nat. Rev. Neurosci.* **9**, 965 (2008).

ILLUSTRATION: ADAPTED BY P. HUEY/*SCIENCE*

Balancing privacy versus accuracy in research protocols

Restricting data at collection, processing, or release

By **Daniel L. Goroff***

Designing protocols for research using personal data entails trade-offs between accuracy and privacy. Any suggestion that would make empirical work less precise, open, representative, or replicable seems contrary to the needs and values of science. A careful reexamination has begun of what "accuracy" or "privacy" should mean and how research plans can balance these objectives.

Attitudes toward research that analyzes personal data should depend both on how well the protocol generates valuable statistics and on how well it protects confidential details. There is always some risk of a leak, so it hardly makes sense to support a study incapable of producing valid and robust results. It would also be reassuring to know that the same or better scientific reliability could not be obtained via some other protocol that provides more privacy protection.

POLICY

PARSING PROTOCOLS. A given research plan can be assessed by comparing it along accuracy and privacy dimensions with other potential protocols. Many purport to deliver more than they do on either score. Research on even a simple population statistic—say, average salary—involves collecting, processing, and releasing data. Various protocols can introduce obfuscation, or not, at any combination of these three stages. Eight examples follow, starting with traditional methods whose strengths and shortcomings motivate more recent approaches.

Open data. Suppose a researcher wishes to study faculty wages. Some U.S. states publish names, salaries, and other information about public university employees. There are no restrictions on data collecting and sampling, linking and analysis, or release and reuse. This is the ideal supported by "open data" advocates. It facilitates accuracy but not confidentiality. People who care about keeping their pay private need to be aware of such policies before they decide to take a position.

Vice President and Program Director, Alfred P. Sloan Foundation, New York, NY 10111, USA. E-mail: goroff@sloan. org. *Opinions or errors are the author's own rather than those of the foundation or its grantees.

Data enclaves for federal data. Suppose a researcher wishes to study U.S. wage and employment trends more broadly. Academics can apply for access to Research Data Centers run by the U.S. Census Bureau (*1*). Approved researchers are subject to prosecution for misuse of private information under the same terms as government officials. Computations typically take place in a data enclave disconnected from the rest of the world. Papers must be reviewed by the Census Bureau before they can be released, mainly to ensure that information is aggregated or obfuscated enough to protect individuals' privacy. This is akin to how pixelating the photo of an unfamiliar face renders it unidentifiable (see image). Federal enclaves have produced no known security breaches and are becoming less cumbersome to use, but replication is problematic.

Nondisclosure agreements for online business data. Suppose a researcher wishes to study the relation between salary and other behaviors. Online companies often ask or draw inferences about users' income, usually for unstated purposes. Researchers who seek such data rarely gain access without signing a nondisclosure agreement (NDA) that gives the company control over what details may be released. Arrangements like this usually protect proprietary interests of businesses rather than privacy interests of customers. NDAs can also preclude replication of results or reuse of data (*2*).

Anonymization of administrative data. Suppose a researcher wishes to study earnings of cab drivers. New York City recently released "anonymized" data about every taxi trip taken in 2013. These data were reidentified by exploiting weak encoding and by linking with other publicly available data sets. Not only is it possible to track earnings of each cabbie by name, one can also map GPS coordinates on either end of each ride and even deduce the trip times, fares, and tips of certain celebrities (*3*).

This joins many other examples of data

Aggregation and averaging, as in the pixelated image, can hide identities. Linkage with other information, like the familiar portrait of President Lincoln on U.S. currency, can undermine obfuscation. Image from (*16*).

sets that were released with assurances that they had been scrubbed of any personally identifiable information but were easily linked with other public information to yield private confidences, including health records of Governor Weld (*4*) and movie rental histories of Netflix users (*5*). Sweeney even suggests that a vast majority of Americans can be uniquely identified using only zip code, sex, and birthday data (*6*). So anonymization can reduce accuracy while failing to protect private information against "linkage attacks." In other words, "sanitizing data doesn't" and "deidentified data isn't" (*7*).

Randomized response in survey data. A researcher may want to estimate what percentage of a group lives in poverty and so gives each person a coin to flip, together with these instructions: "If it lands heads, truthfully answer yes or no to the question 'Is your income below the poverty line?' If it lands tails, flip again. If the second toss is a head, answer truthfully, but if the second toss is a tail, then lie by giving the answer opposite to what is true." Twice the fraction of yes responses minus one-half provides a good estimate of the actual fraction sought (*8*).

Even if you know who answered what, that does not tell you who is impoverished. The usefulness of this technique depends on having lots of participants, all of whom follow instructions. There are privacy-preserving variants that provide more efficient estimators, but some accuracy is sacrificed in any case.

Multiparty computation for reporting sensitive data. Suppose a researcher would like to calculate the average salary of a group, but without anyone ever communicating her own. Say there are three people. Each generates two random numbers and gives one to each of the other two participants. Everyone then adds the two random numbers she generated to her own salary, subtracts the two numbers she was given, and reports the result. All the random numbers cancel when these three results are added, so their sum equals the sum of the salaries. Dividing by three gives the average. Special and more convoluted computations can secretly carry out operations beyond just taking averages (*9*).

Although no individual's salary was communicated, this protocol does not necessarily keep participants from finding out one another's personal information. If, for example, all but one collude by using the same
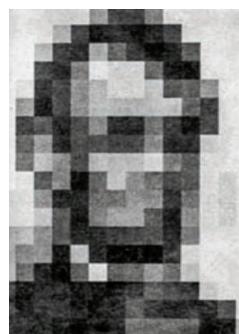
method to compute their average salary, that group could deduce what the salary was of their original colleague. The protocol delivers completely accurate results but can also endanger privacy.

Fully homomorphic encryption of cloud data. Suppose a researcher wishes to study salaries using bank data. People routinely and confidently send such information encrypted over the Internet. Financial institutions decrypt the messages and perform calculations. But what if the bank or other data receiver not only could perform calculations without ever decrypting the private information but also could return encrypted answers that only the sender could decode? Long thought to be impossible, "fully homomorphic encryption" methods have recently been devised (*10*) to do just that. Most algorithms are still too slow for practical applications. Proposed protocols could, however, analyze a population's encrypted data but only allow statistics to be decrypted if participants verify that calculations have been done to their satisfaction (*11*).

By giving control over their data to potential subjects rather than to researchers, such techniques jeopardize plans for replicability and reuse, as well as for representative or even adequate sampling. Supposing there are results to release, it may still be possible for a researcher to violate the privacy of individuals who participate in the study. Any protocol that allows exact counts of subpopulations is vulnerable to a "differencing attack," for example. To find out whether the CEO of a company earns more than $1 million, just make two simple inquiries: how many employees earn over $1 million in salary, and how many who are not the CEO earn over $1 million. It may seem straightforward to rule out lines of questioning like this. Provably, however, no algorithm can reliably determine whether a given set of questions that seem to ask only about statistical aggregates would nevertheless have answers that, taken together, reveal private information (*12*).

Differential privacy for curated data. Consider a data set D that contains my personal information and another data set D' that is missing my data but otherwise the same. A research protocol would be privacy-preserving if it could not distinguish between D and an adjacent D'. It also would not be very useful. But what if the protocol could barely and rarely make such a distinction? Consider the probabilities that a certain methodology generates a given answer to a given question when applied to D as compared with D'. The ratio of those

two probabilities should be as close to one as possible. The log of that ratio measures the loss of privacy incurred when the protocol answers the given question. If the log is always less than ε for any adjacent data sets, the protocol provides ε-differential privacy.

Dwork, McSherry, Nissim, and Smith formulated this definition, showed it captures basic intuitions about privacy, and devised research protocols that provide ε-differential privacy (*13*). Data are held by a trusted curator who only accepts certain questions from the investigator. The curator performs

Privacy is breached when "secure" data can be linked with publicly available data.

calculations behind a firewall but only returns answers after adding a small amount of carefully chosen noise. It suffices, for example, to draw noise from a Laplace distribution with parameter $1/\varepsilon$ when responding to a counting query. There are limits on the type and number of questions allowed, as each could deplete a privacy budget by as much as ε.

Choosing ε for a differentially private protocol determines how the research will trade accuracy against privacy. The smaller ε is, the less leakage of information but at the cost of more noise. One promising application is the Census Bureau's OnTheMap Project (*14*). Payroll records in each state have been carefully perturbed and aggregated to create a "synthetic database." The public can query that database to receive approximate, but quite accurate, answers to a large class of counting and geographic questions (*15*).

PICKING PROTOCOLS. Setting aside administrative, financial, legal, or institutional factors that do not bear directly on accuracy and privacy, some basic suggestions for comparing protocols are clear. Potential subjects considering participation in a study should ask if there is another protocol that would yield at least as reliable scientific results while offering better privacy protection. Researchers designing studies should ask if the protocols will actually deliver the levels of accuracy and privacy anticipated.

Funders or others deciding on whether a research plan moves forward should also ask about the broader incentive effects of using a particular methodology. Accuracy and privacy achieved by a protocol are public goods and, hence, subject to free-rider problems. To increase chances of curing a disease, say, every patient wants accurate research but preferably using other people's data rather than their own. To decrease chances of linkage or other attacks, every researcher wants all other projects held to high thresholds of privacy protection but preferably not their own.

Policy-makers reviewing U.S. legislation should also ask about laws like FERPA, HIPAA, or the Privacy Act of 1974 that govern data collection and use by educators, health care providers, or federal officials, respectively (*17*). Do these actually promote accuracy and privacy, or are they based on outmoded ideas about anonymization and identifiability, for example? Unlike other countries, the United States has no legislation specifically regulating or facilitating the use of personal information by academic researchers.

Critically, society as a whole must also ask about promising and threatening aspects of new information technologies. How well society balances the accuracy and privacy of research protocols will determine the extent to which "big data" either allows everyone to benefit from advances in empirical science or only those private interests who hold enormous and growing stores of sensitive information about us all. ∎

REFERENCES AND NOTES

1. RDC Research Opportunities, Center for Economic Studies (CES), https://www.census.gov/ces/rdcresearch/.
2. L. Einav, J. Levin, *Science* **346**, 1243089 (2014).
3. Riding with the Stars, Passenger Privacy in the NYC Taxicab Dataset; http://research.neustar.biz/2014/09/15/.
4. L. Sweeney, *J. Law Med. Econ.* **25**, 98 (1997).
5. A. Narayanan, V. Shmatikov, *Proc. of IEEE Symp. on Security and Privacy* (IEEE, 2008), pp. 111–125.
6. How Unique are You? http://aboutmyinfo.org/.
7. C. Dwork, in *Privacy, Big Data, and the Public Good*, J. Lane et al., Eds. (Cambridge Univ. Press, Cambridge, 2014), pp. 296–322.
8. $E(r) = p/2 + p/4 + (1 - p)/4$, where r is the fraction reporting "yes" and p is the true proportion.
9. M. Prabhakaran, A. Sahai, *Secure Multi-party Computation* (IOS Press, Amsterdam, 2013).
10. C. Gentry, *STOC '09: Proc. of the 41st ACM Symp. on Theory of Computing* (ACM, New York, 2009), pp. 169–178.
11. A. López-Alt, E. Tromer, V. Vaikuntanathan, *STOC '12: Proc. of the 44th ACM Symp. on Theory of Computing* (ACM, New York, 2012), pp. 1219–1234.
12. C. Dwork, in *Automata, Languages and Programming* (Springer, New York, 2006), pp. 1–2.
13. C. Dwork, F. McSherry, K. Nissim, A. Smith, *Proc. 3rd Theory of Cryptography Conference (TCC)* (Springer, New York, 2006), pp. 265–284.
14. A. Machanavajjhala, D. Kifer, J. Abowd, J. Gehrke, L. Vilhuber, *Proc. 24th IEEE International Conf. on Data Engineering (ICDE)* (IEEE, 2008), pp. 277–286.
15. On the Map, http://onthemap.ces.census.gov.
16. L. D. Harmon, B. Julesz, *Science* **180**, 1194 (1973).
17. The Family Educational Rights and Privacy Act (FERPA) and the Health Insurance Portability and Accountability Act (HIPAA).

PHOTO: DIBROVA/THINKSTOCK

PRIVACY

Connecting the dots

When it comes to the data that can make or break us, who holds the power?

By **Viktor Mayer-Schönberger**

For years, people like Scott McNealy, long-time CEO of the now defunct computer company SUN Microsystems, have said that privacy is dead. After Edward Snowden's revelations about the prevalence of covert digital surveillance and countless reports of data breaches at large corporations, many may agree. And yet, surveys find that a large majority of people in the United States and elsewhere treasure information privacy and want it protected. This tension has led to a proliferation of books arguing the importance of privacy, lamenting its demise, and advocating for its resurrection. But the story is getting stale.

In contrast, *The Black Box Society,* by Frank Pasquale, offers a good dose of fresh thinking and may advance our debates over privacy. It also helps greatly that it is a good read, not just for those who are curious about privacy but also for those who are already familiar with the privacy literature.

Pasquale's main argument is that power has become concentrated in the hands of a few players in three key sectors: reputation, search, and finance. Reputation and search, he says, cover how we are perceived and how we perceive. The aim of the financial sector is price discovery, providing information that allows people to make economic decisions.

Actors in these sectors have amassed gigantic piles of personal data about all of us.

But Pasquale, a law professor and privacy expert, points out that information about how these actors operate, how they use the troves of personal data they have, and how they design the algorithms that drive their decision-making has ebbed to a historic low. Credit scoring, a reputational device, is shockingly opaque. The algorithm used by Google to rank search results is a highly protected trade secret, inaccessible to anyone outside of the company. The recent financial crisis has revealed shockingly complex legal constructs deliberately established by banks to obfuscate ownership and to hide risks.

Pasquale also argues that the private sector is now sharing its troves of personal data with government agencies, leading to even more powerful, as well as impenetrable, data uses. He is right when one just looks at the past few decades, but the early information privacy debates in the late 1960s were fueled by precisely the same concerns, as governments and corporations began planning huge data centers to combine and share their data holdings. Massive public backlash stopped these projects then, but more recently, a growing preference for safety over privacy—fueled by the trauma of 9/11—has done much to silence public concern.

Early privacy experts highlighted the importance of informational power and how heavy power imbalances often lead to suboptimal (and unethical) outcomes for society. However, the classic remedy has been to require informed consent from the individual. As long as someone is told how their data will be used, and as long as they consent, the idea goes, privacy is maintained.
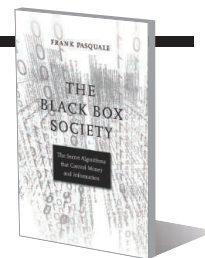
Pasquale suggests that this approach is no longer effective (if it ever was). "Notice and consent," he claims, has degenerated to a formalistic farce, in which most of us consent to terms we have neither the time nor the expertise to decipher. Current privacy protection, as Pasquale aptly notes, at best works for the rich, who can afford pricy lawyers and "reputation managers" to enforce their privacy rights. "Big Data"—the ability to gain novel insights from the collection and analysis of a large number of data points—with its emphasis on reuse and the combination of diverse data sets, will only exacerbate the current system's shortcomings.

In contrast, Pasquale argues for a fundamental shift in privacy protection, from a focus on notice and consent at the time of data collection to stringent regulation of the actual use of data by corporations and government agencies. His reasoning is sensible, and he is not alone; a growing number of privacy advocates are in favor of data use regulation. If such regulations were to be put in place, it would represent an epic change in how we aim to protect privacy in our society.

There is a second valuable and important idea in *The Black Box Society*. It is the implicit red thread throughout the book but emerges clearly in the last chapter. Many of the information tussles that arise in reputation, search, and finance can be framed as privacy challenges, but they are, Pasquale suggests, more than that. They reflect how much of our lives is now affected by information and how this has created an urgent need for a framework of information governance, as well as a need to define what role the public sector ought to play. Perhaps we need a public agency offering credit scores, not just private corporations. Perhaps the Library of Congress ought to scan books, much like Google does, and permit us to search them. Perhaps, Pasquale boldly suggests, there is even a public role in finance—for instance, to provide mortgages and loans to underserved communities. He is right. As data-driven decision-making becomes commonplace, our ethical and legal frameworks need to broaden. This is precisely the debate that we need to have.

10.1126/science.aaa5358

The reviewer is at the Oxford Internet Institute, University of Oxford, Oxford OX1 3JS, UK. E-mail: viktor.ms@oii.ox.ac.uk

POLITICAL PSYCHOLOGY

The selfish voter

A closer look at the factors that influence our political preferences

By **John R. Hibbing**

Seventy years ago, the prevailing view of American voting behavior was that individuals who were Catholic, urban, and poor voted Democratic; those who were Protestant, rural, and rich voted Republican; and people with mixtures of these traits split their tickets or abstained (*1*). This somewhat deterministic interpretation of voting patterns quickly fell out of favor as scholarly tastes shifted toward psychologically based approaches that took into consideration factors such as party identification, campaign effects, and ideology. In *The Hidden Agenda of the Political Mind*, psychologists Jason Weeden and Robert Kurzban reject psychological embellishments in order to resurrect the claim that voting patterns are really quite simple: people vote according to their self-interest. Their thesis is boldly stated, entertainingly developed, and ultimately flawed.

To their credit, the authors help to correct several common misperceptions about the factors that influence individual voting behavior. First, they effectively argue that self-interest extends well beyond economics and demography. As such, it is possible for Kansas farmers to vote for subsidy-cutting Republican candidates and still be acting in their own self-interest (*2*). After all, if voting for Democrats who support abortion rights is believed to lead to eternal damnation, it is easy to see how voting Republican could be considered to be in a person's self-interest. Second, they point out that individuals typically are incorrect in their assumptions about the reasons they hold the political attitudes they do. People are convinced that reflection and rationality are the foundations of their beliefs when the real influences often are nonconscious and emotive. Third, they correctly note that

The reviewer is coauthor of Predisposed: Liberals, Conservatives, and the Biology of Political Differences *(Routledge, New York, 2013). E-mail: jhibbing@unl.edu*

"psychological" studies of voting behavior often become nearly tautological, generating unstimulating conclusions, such as that individuals who identify as Democrats frequently vote for Democratic candidates.

The trouble is that in the process of correcting these misperceptions, new ones are introduced. The pattern of the book is to take a policy and then demonstrate how positions on that policy are shaped by self-interest, broadly defined. For example, readers are informed that non–gun owners are more likely than gun owners to support enhanced gun control; that proponents of marijuana legalization are disproportionately individuals the authors categorize as "freewheelers" (those who tend to be, among other things, unmarried and who engage in recreational alcohol and drug use) as opposed to "ring-bearers" (those who are married and settled); and that people who

Can self-interest explain our voting behavior?

oppose school prayer and support gay marriage are more likely to be "heathens," the authors' shorthand for "people who are either lesbian/gay/bisexual or not Christian". These kinds of conclusions, however, are examples of the very circular reasoning that the authors rightly decry. Providing evidence that religious people support school prayer and that drug users want marijuana to be legalized seems unlikely to advance our understanding of the human condition. Expanding the list of factors that constitute self-interest beyond gender, age, occupation, and race is useful and even necessary, but if it is not done carefully, the line between these factors and whatever they are intended to explain becomes blurred.

With no explanation, the book conceptualizes religious beliefs and lifestyle choices as part of the "self" but treats political orientations as mere manifestations of self-interest. Recent research, however, increasingly concludes that political orientations run every bit as deep as religious beliefs and lifestyle choices (*3*). A more accurate interpretation, it would seem, is
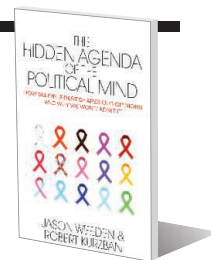
that individuals possess deep physiological and psychological predispositions that then influence all the choices they make and preferences they register, from personality tendencies to religious beliefs and from leisure pursuits to political opinions.

I agree that political preferences mostly bubble up from within each individual, but the internal milieu from which these preferences arise is more than a motley collection of ill-defined interests. If we accept the author's argument, the real question becomes, why do people have the interests they do? Why are some freewheelers? Why are some gun owners? Why are some religious traditionalists? Economists have long preferred to define away these questions by taking individual preferences as a given, but such an approach is sterile, defeatist, unhelpful, and increasingly unnecessary.

As the authors wisely, though tellingly, admit, self-interest cannot explain why people register the (often strong) preferences they do on issues seemingly remote from them (e.g., birth control in Africa). Moreover, people with identical backgrounds and demographics often report vastly different political preferences. Still other people simply go against what would seem to be their self-interest (for instance, white parents who support racial affirmative action in college admissions).

Weeden and Kurzban begin their commendable and thought-provoking journey on the right track by acknowledging that, when asked to describe the sources of their political beliefs, people offer little more than post hoc rationalizations. However, those looking for real guidance in identifying the underlying factors that influence political preferences are unlikely to be satisfied with blithe attributions to self-interest.

REFERENCES

1. P. F. Lazersfeld, B. Berelson, H. Gaudet, *The People's Choice* (Duell, Sloan, Pearce, New York, 1944).
2. T. Frank, *What's the Matter with Kansas?* (Macmillan, New York, 2007).
3. J. R. Hibbing, K. B. Smith, J. R. Alford, *Behav. Brain Sci.* **37**, 297 (2014).

Edited by **Jennifer Sills**

Rough waters for native Chinese fish

IN THE POLICY FORUM "China's aquaculture and the world's wild fisheries" (9 January, p. 133), L. Cao *et al.* identify the increasing growth of aquaculture in China as potentially placing considerable pressure on global marine stocks. The impact of aquaculture on wild fisheries will also be felt much closer to home, particularly in China's freshwaters.

Aquaculture in Asia is increasingly reliant on the farming of alien species, whether stocked from other countries or intentionally translocated from remote water basins within the same nation (*1*). Recent estimates suggest that more than 100 alien species of freshwater finfish are farmed in China (*2*). Many of these species have become widely established in the wild either as a result of escape from aquaculture ponds or through deliberate introductions into lakes and freshwaters to enrich wild fisheries. Unfortunately, the consequences have usually been disastrous. Several alien finfish

Bighead carp threaten native species in China.

threaten native species through predation (*3*), competition (*4*), the spread of pathogens (*5*), and hybridization (*6*). The end result is often the decline in native finfish and associated wild fisheries. For example, following the introduction of bighead and silver carp in Lake Xingyun for aquaculture, the proportion of the endemic barbless carp in the total fish yield declined from 50% to less than 1% within a few decades (*7*).

China is recognized as a major center for global freshwater fish diversity with a high level of endemism, attributable to its major river systems that have been isolated for millennia (*8*). Thus, while the economic

value of alien aquaculture species provides a strong incentive to their introduction, the loss of wild fisheries and the extinction of endemic species as well as the reduced resilience of freshwater ecosystems should be taken into account in regulations regarding stocking practices (*9*). In the absence of effective regulation of species introductions and translocations to support aquaculture development in China, progressive reductions in the size and sustainability of wild freshwater fisheries are to be expected.

Philip E. Hulme

The Bio-Protection Research Centre, Lincoln University, Canterbury, 7647, New Zealand. E-mail: philip.hulme@lincoln.ac.nz

REFERENCES

1. S. S. De Silva, T. T. T. Nguyen, N. W. Abery, U. S. Amarasinghe, *Aquac. Res.* **37**, 1 (2006).
2. P. Jia, W. Zhang, Q. Liu, *Fish. Res.* **140**, 66 (2013).
3. M. Luo *et al.*, *Acta Hydrobiol. Sin.* **36**, 932 (2012).
4. J. Qin, J. Xu, P. Xie, *J. Freshw. Ecol.* **22**, 365 (2007).
5. K. V. Radhakrishnan, Z. J. Lan, J. Zhao, N. Qing, X. L. Huang, *Biol. Invasions* **13**, 1723 (2011).
6. W. Tang, Y. Chen, *Zool. Sci.* **29**, 311 (2012).
7. P. Xie, Y. Y. Chen, *Science* **294**, 999 (2001).
8. B. Kang, *et al.*, *Fish Fish.* **15**, 209 (2014).
9. P. E. Hulme, P. Pysek, W. Nentwig, M. Vila, *Science* **324**, 1015 (2009).

The value of audiovisual archives

FOR CENTURIES, HUMANS have collected specimens and deposited them in scientific collections housed in zoological or natural history museums. Such documentation is essential for the recognition and classification of our extinct and extant biodiversity. As technology improved, we created DNA databases that have helped us to understand the evolutionary relationships between organisms. Both genetic archives and museum specimens are well recognized as important biodiversity repositories, and scientific literature routinely refers to them.

Equally important, but often overlooked, are audiovisual archives, which allow us to record complementary information that could not be recovered from dead specimens or DNA sequences. Sound archives are particularly interesting, as they capture behavior with great accuracy and are often involved in conspecific recognition. These digital archives are relatively inexpensive to store and curate, and are usually obtained with no harm to the focal species and no need for collection.

Unfortunately, audiovisual archives are being neglected; voucher numbers, which provide access to the files and the possibility of replication, are often not available in articles. Furthermore, the files are not always georeferenced, despite the importance

of verifying the presence of certain taxa in a specific space and time. To raise the standards of documentation, we call for all scientific journals to require authors to deposit their audiovisual recordings in scientific collections or online repositories, just as they do for specimens, DNA sequences, and even raw data.

Luís Felipe Toledo,[1]* Cheryl Tipp,[2] Rafael Márquez[3]

[1]Fonoteca Neotropical Jacques Vielliard, Unicamp, Campinas, 13083-970, Brazil. [2]British Library, London, NW1 2DB, UK. [3]Fonozoo, Museo Nacional de Ciencias Naturales-CSIC, Madrid, 28006, Spain.

*Corresponding author. E-mail: toledolf2@yahoo.com

Tyranny of trees in grassy biomes

TREE PLANTING, FIRE suppression, and exclusion of megafaunal herbivores (native or domestic) are ecologically reasonable restoration strategies in deforested landscapes, but similar interventions can be catastrophic when applied to grassy biomes such as grasslands, savannas, and open-canopy woodlands (*1*). As hopes grow that carbon payment schemes will finance forest restoration (*2*), we must clearly distinguish between "reforestation"—planting trees on deforested land—and "afforestation"—converting historically nonforest lands to forests or tree plantations (*3*). Afforestation of grassy biomes can severely compromise ecosystem services, including hydrology (*4*) and soil nutrient cycles (*5*), and markedly reduce biodiversity (*6*).

Despite these high environmental costs, grassy biomes, particularly those with seasonally dry tropical climates, are prime targets for carbon sequestration programs that emphasize tree planting (*1, 7*). Threats of afforestation and agricultural conversion are exacerbated because the grassy biomes are not formally recognized by the United

Highland grassland in Brazil is considered a forest landscape restoration opportunity

Nations (UN) Framework Convention on Climate Change, the program for Reducing Emissions from Deforestation and Forest Degradation (REDD+), or the UN Food and Agriculture Organization. This lack of recognition reflects fundamental misperceptions about the ecology, conservation values, locations, and antiquity of the grassy biomes.

The World Resources Institute's (WRI's) map of "Forest and Landscape Restoration Opportunities" (2) serves as an example of these misperceptions. The map identifies 23 million km[2] of the terrestrial biosphere as highly suitable for tree planting. Yet much of the area targeted for "forest restoration" corresponds to the world's ancient grassy biomes. The WRI erroneously assumes that nonforest areas where climate could theoretically permit forest development are "deforested," an assumption rooted in outdated ideas about potential vegetation and the roles of fire and herbivores in natural systems (8). This map is intended as a tool to help meet the Bonn Challenge to "restore 150 million hectares of the world's deforested and degraded lands by 2020." Although many ecosystems within the grassy biomes might benefit from ecological restoration, the restoration strategies proposed by WRI (2) are incompatible with grassland biodiversity.

Meanwhile, among the landscapes correctly identified as deforested by the WRI map, extensive areas of agriculture are not considered restoration opportunities (2). Clearly, the economic output of agricultural lands makes them expensive to reforest. But attempts to offset agricultural deforestation through afforestation of the grassy biomes will simply worsen biodiversity losses and further compromise ecosystem services.

The "Forest and Landscape Restoration Opportunities" map was produced and presumably vetted by influential scientific and environmental organizations, which lends it legitimacy. WRI (2) collaborated with and/or was supported by the International Union for the Conservation of Nature, the Global Partnership on Forest and Landscape Restoration, the Program on Forests, the University of Maryland, South Dakota State University, the German Ministry for the Environment, and the Forestry Commission of Great Britain. The producers of the map also acknowledge receiving review comments from the UN Environment Programme–World Conservation Monitoring Center.

That such a scientifically flawed analysis is poised to promote misinformed tree planting is emblematic of deep misunderstandings about the grassy biomes, as well as their devaluation relative to forests. We worry that so long as tree planting is viewed as innately good and the grassy biomes are assumed to be the result of deforestation, afforestation projects will face limited public resistance and analyses such as this WRI map will escape scientific scrutiny. Deforestation and forest degradation are critical problems that must be addressed, but with due consideration of the value of the many naturally nonforest biomes that also face tremendous pressure from human-caused environmental change.

Joseph W. Veldman,[1]* Gerhard E. Overbeck,[2] Daniel Negreiros,[3] Gregory Mahy,[4] Soizig Le Stradic,[4] G. Wilson Fernandes,[3,5] Giselda Durigan,[6] Elise Buisson,[7] Francis E. Putz,[8] William J. Bond[9]

[1]Department of Ecology, Evolution, and Organismal Biology, Iowa State University, Ames, IA 50011, USA. [2]Department of Botany, Universidade Federal do Rio Grande do Sul, Porto Alegre, RS, 91501-970, Brazil. [3]Ecologia Evolutiva e Biodiversidade, Universidade Federal de Minas Gerais, Belo Horizonte, MG, 30161-901, Brazil. [4]Gembloux Agro-Bio Tech, Biodiversity and Landscape unit, University of Liege, Gembloux, 5030, Belgium. [5]Department of Biology, Stanford University, Stanford, CA 94305, USA. [6]Laboratório de Ecologia e Hidrologia Florestal, Floresta Estadual de Assis, Instituto Florestal, Assis, SP, 19802-970, Brazil. [7]Institut Méditerranéen de Biodiversité et d'Ecologie marine et continentale (IMBE), Université d'Avignon et des Pays de Vaucluse, Avignon, 84911, France. [8]Department of Biology, University of Florida, Gainesville, FL 32611, USA. [9]Department of Biological Sciences, University of Cape Town and South African Environmental Observation Network, NRF, Rondebosch, 7701, South Africa.

*Corresponding author. E-mail: jveldman@iastate.edu

REFERENCES

1. C. L. Parr *et al.*, *Trends Ecol. Evol.* **29**, 205 (2014).
2. WRI, "Atlas of Forest and Landscape Restoration Opportunities" (World Resources Institute, Washington, DC, 2014); www.wri.org/resources/maps/atlas-forest-and-landscape-restoration-opportunities/.
3. F. E. Putz, K. H. Redford, *Glob. Environ. Change* **19**, 400 (2009).
4. R. B. Jackson *et al.*, *Science* **310**, 1944 (2005).
5. S. T. Berthrong, E. G. Jobbagy, R. B. Jackson, *Ecol. Appl.* **19**, 2228 (2009).
6. L. L. Bremer, K. A. Farley, *Biodivers. Conserv.* **19**, 3893 (2010).
7. United Nations Framework Convention on Climate Change, CDM Methodology Booklet, 6th Edition (UNFCCC, 2014); https://cdm.unfccc.int/methodologies/documentation/.
8. W. J. Bond, F. I. Woodward, G. F. Midgley, *New Phytol.* **165**, 525 (2005).

Investing in technology that turns tidal energy into clean power has paid off for the state of Maine.

States lean in on R&D

As federal spending remains tight, AAAS is helping some states make the most of their own R&D programs.

By **Kathy Wren**

At the mouth of the Bay of Fundy, just off the coast of Maine, a tidal power system built and operated by the Ocean Renewable Power Company (ORPC) draws energy from currents created as 100 billion tons of water flow into and out of the bay. The system was the first commercial, grid-connected tidal power system in the United States, and ORPC expects to expand in the coming years to provide electricity to roughly 2000 homes and businesses.

The company, which estimates that it has pumped more than $25 million into the Maine economy, attributes much of its early success to the $1.75 million in loans and grants it received from the Maine Technology Institute (MTI). This publicly funded nonprofit offers early-stage capital and commercialization assistance for the development of technologies that create new products, services, and jobs in Maine. Other state legislatures have also created similar funding programs to boost their high-tech sectors and attract top talent and investment.

While local support for these programs is strong and in some cases growing, the organizations must be strategic with their resources. To ensure that these dollars are going to projects based on the soundest, most promising science, MTI and other organizations rely on AAAS's Research Competitiveness Program (RCP), which uses its nationwide network of expert reviewers to evaluate funding proposals for state-level funders in Maine, Connecticut, Rhode Island, North Carolina, and South Dakota.

Some of these programs are expanding their activities, with new funding opportunities rolling out and voters or legislators approving new financing mechanisms. This is happening despite, or in some cases because of, belt-tightening in Washington; federal R&D funding as a percentage of GDP is at its lowest levels in several decades, according to the AAAS R&D Budget and Policy Program. AAAS is active in a number of efforts to encourage lawmakers to turn this trend around and close the "innovation deficit." In the meantime, states are doing what they can to support innovation within their own borders.

When designing their funding competitions, "states play to their strengths," said Rieko Yajima, RCP's associate director. "They are targeting their research dollars to areas where they feel they have the best competitive edge." RCP staff then draw from their nationwide network of reviewers whose areas of expertise match the proposals.

If reviewers do not reach consensus on a proposal, RCP staff facilitate a discussion to help them arrive at a final decision that includes suggestions to applicants for strengthening their proposals. "Going through those different opinions and coming to an agreement strengthens the review in the end. You have an opinion that is backed up by all the reviewers," Yajima said.

Representatives from MTI and other funding programs agreed that it would be nearly impossible for them to develop a similar peer-review system on their own. They also said the confidential process provides objectivity that, along with AAAS's strong reputation, can assure voters that their dollars are being spent fairly.

This credibility has long-term benefits for awardees. Those that have received MTI

funding often report that they are then able to attract further funding, said Joe Migliaccio, director of business development at MTI. Migliaccio's program at MTI invests $4 to 5.5 million per year in loans, grants, and equity to support R&D of new products or services in Maine's key technology sectors. Since 2007, MTI has also awarded $53 million in bond-backed grants through its Maine Technology Asset Fund, said Martha Bentley, the fund's program manager.

"Voters are continuing to support R&D as an economic engine in Maine," Bentley said. For example, a 2014 referendum approved additional bonds in support of biomedical and marine research.

Another state-based funder, Connecticut Innovations, has responded directly to national trends with its Connecticut Bioscience Innovation Fund (CBIF), which opened its doors in 2014 and has awarded approximately $4.5 million to five universities and four companies, with AAAS overseeing the scientific review of applications.

"The key opinion leaders in our state saw a couple of factors coming together," when they created the CBIF, said Margaret Cartiera, director of bioscience initiatives at Connecticut Innovations. The state has a strong concentration of pharmaceutical and medical device companies, but many were downsizing or closing their R&D units. And state officials were concerned that decreased federal funding to Connecticut universities would make them less attractive to top faculty and slow technology transfer, according to Cartiera, which is why the fund is open to universities and nonprofits as well as commercial establishments.

A funding initiative is also newly launched in North Carolina, where in 2014 the general assembly created a $3 million annual fund for "game-changing" research in several key areas at the University of North Carolina (UNC). The money will be distributed via UNC's Research Opportunities Initiative, which has contracted with AAAS to administer the peer review of the research proposals, and the first set of recipients will be announced in the coming weeks.

Christopher Brown, vice president for research and graduate education at the University of North Carolina, noted that UNC continues to pull in research dollars from federal agencies. But, he said that the new initiative reflects legislators' growing appreciation of the importance of R&D to the state's economic growth, and understanding that supporting UNC researchers will help position them to attract other federal or industry funding. ∎

PHOTO: AAAS/CARLA SCHAFFER

Former congressman Holt joins AAAS as new CEO

By **Ginger Pinholster**

Retired Congressman Rush D. Holt, Ph.D., has agreed to join AAAS as the 18th chief executive officer and executive publisher of the *Science* family of journals. He will succeed Alan I. Leshner at the Association's 12 to 16 February Annual Meeting in San Jose, California.

Holt, 66, represented Central New Jersey (12th District) in Congress from 1999 to 2015. His science- and education-related roles in Congress have included service with the Committee on Education and the Workforce, the Committee on Natural Resources, and the National Commission on Mathematics and Science Teaching for the 21st Century. Over the course of his career, Holt also has held positions as a teacher and as an arms control expert at the U.S. State Department. From 1989 until 1998, he served as assistant director of the Princeton Plasma Physics Laboratory, the largest research facility of Princeton University.

On Capitol Hill, Holt established a long track record of advocacy for federal investment and private-sector support for research and development, science education, and innovation. He has also broadly promoted the value of science communication, particularly for conveying information about climate change, and he has said that "thinking like a scientist" can benefit the policy-making process.

AAAS Board member Laura H. Greene, the Swanlund Professor of Physics at the University of Illinois at Urbana-Champaign, described Holt as an effective advocate for the importance of science to society: "Rush Holt has long been a champion of a broad spectrum of scientific research areas, and of education," she said. "He very effectively communicates with the public and policymakers, and he brings exciting new ideas to the table. Those abilities will help AAAS to achieve an even greater role in supporting international scientific collaborations and advances."

In 1982-83, while he was teaching physics and public policy at Swarthmore College, Holt was selected by the American Physical Society to receive a highly competitive AAAS Science & Technology Policy Fellowship. Holt has said that his AAAS S&T Policy Fellowship was "life changing," and served as a springboard to his role in Congress.

"AAAS, as one of the world's most respected nonprofit, nonpartisan organizations and publisher of the leading *Science* family of journals, helps to promote scientific progress and to improve human welfare," Holt said regarding his acceptance of the leadership role at AAAS. "I look forward to supporting the Association's mission to advance science, engineering, and innovation throughout the world, for the benefit of all people." ∎

Rush Holt (right) and Alan Leshner.

Call for nomination of 2015 Fellows

Fellows who are current members of AAAS are invited to nominate members for election as Fellows. A member whose efforts on behalf of the advancement of science or its applications are scientifically or socially distinguished, and who has been a continuous member for the 4-year period leading up to the year of nomination, may by virtue of such meritorious contribution be elected a Fellow by the AAAS Council.

A nomination must be sponsored by three previously elected AAAS Fellows (who are current in their membership), two of whom must have no affiliation with the nominee's institution.

Nominations undergo review by the steering groups of the Association's sections (the chair, chair-elect, retiring chair, secretary, and four members-at-large of each section). Each steering group reviews only those nominations designated for its section.

Names of Fellow nominees who are approved by the steering groups are presented to the Council in the fall for election.

Nominations with complete documentation must be received by 22 April 2015. Nominations received after that date or nominations that are incomplete as of the deadline will not move forward.

Complete instructions and a copy of the nomination form are available at www.aaas.org/current-nomination-cycle. Questions may be directed to fellownomination@aaas.org.

Results of the 2014 election of AAAS officers

Following are the results of the 2014 election. Terms begin on 17 February 2015.

GENERAL ELECTION

President-Elect: Barbara A. Schaal, Washington Univ. in St. Louis

Board of Directors: Michael S. Gazzaniga, Univ. of California, Santa Barbara; Mercedes Pascual, Univ. of Michigan

Committee on Nominations: Peter C. Agre, Johns Hopkins Malaria Research Institute; Frances H. Arnold, California Institute of Technology; Michael A. Marletta, Scripps Research Institute; Marc Tessier-Lavigne, Rockefeller Univ.

SECTION ELECTIONS

Agriculture, Food, and Renewable Resources

Chair Elect: Steven C. Huber, Univ. of Illinois at Urbana-Champaign

Member-at-Large: Johanna Schmitt, Univ. of California, Davis

Electorate Nominating Committee: Amanda D. Rodewald, Cornell Univ.; Roger Philip Wise, USDA-ARS/Iowa State Univ.

Council Delegate: Jim Giovannoni, USDA-ARS/Cornell Univ.

Anthropology

Chair Elect: Dennis H. O'Rourke, Univ. of Utah

Member-at-Large: Joanna E. Lambert, Univ. of Texas at San Antonio

Electorate Nominating Committee: Yolanda T. Moses, Univ. of California, Riverside; Anne C. Stone, Arizona State Univ.

Astronomy

Chair Elect: Debra Meloy Elmegreen, Vassar College

Member-at-Large: Henry C. Ferguson, Space Telescope Science Institute

Electorate Nominating Committee: Harriet L. Dinerstein, Univ. of Texas at Austin Nancy A. Levenson, Gemini Observatory

Atmospheric and Hydrospheric Sciences

Chair Elect: Jack A. Kaye, NASA

Member-at-Large: Carol Arnosti, Univ. of North Carolina at Chapel Hill

Electorate Nominating Committee: Chris E. Forest, Pennsylvania State Univ.; James M. Russell, Brown Univ.

Biological Sciences

Chair Elect: Pamela C. Ronald, Univ. of California, Davis

Member-at-Large: Sarah M. (Sally) Assmann, Pennsylvania State Univ.

Electorate Nominating Committee: David A. Baum, Univ. of Wisconsin-Madison; N. Louise Glass, Univ. of California, Berkeley

Chemistry

Chair Elect: Carol J. Burns, Los Alamos National Laboratory

Member-at-Large: Michael P. Doyle, Univ. of Maryland, College Park

Electorate Nominating Committee: Joanna Aizenberg, Harvard Univ.; Stephanie L. Brock, Wayne State Univ.

Dentistry and Oral Health Sciences

Chair Elect: Susan Reisine, Univ. of Connecticut

Member-at-Large: Matthew P. Hoffman, NIDCR/NIH

Electorate Nominating Committee: Laurie K. McCauley, Univ. of Michigan; James E. Melvin, NIDCR/NIH

Education

Chair Elect: Cathy Middlecamp, Univ. of Wisconsin-Madison

Member-at-Large: Tammy M. Long, Michigan State Univ.

Electorate Nominating Committee: Claire A. Hemingway, National Science Foundation; M. Patricia Morse, Northeastern Univ.

Engineering

Chair Elect: Larry V. McIntire, Georgia Tech

Member-at-Large: Lance Collins, Cornell Univ

Electorate Nominating Committee: Carol K. Hall, North Carolina State Univ.; Rebecca Richards-Kortum, Rice Univ.

Council Delegate: Molly Sandra Shoichet, Univ. of Toronto (Canada); Stuart L. Cooper, Ohio State Univ.

General Interest in Science and Engineering

Chair Elect: Cristine Russell, Harvard Univ.

Member-at-Large: David F. Salisbury, Vanderbilt Univ.

Electorate Nominating Committee: Sharon Dunwoody, Univ. of Wisconsin-Madison; Ginger Pinholster, AAAS

Geology and Geography

Chair Elect: Philip D. Gingerich, Univ. of Michigan

Member-at-Large: Paul H. Glaser, Univ. of Minnesota

Electorate Nominating Committee: Mary L. Droser, Univ. of California, Riverside; Sarah L. Shafer, U.S. Geological Survey

History and Philosophy of Science

Chair Elect: Janet Browne, Harvard Univ.

Member-at-Large: Hanne Andersen, Aarhus Univ. (Denmark)

Electorate Nominating Committee: Michael A. Osborne, Oregon State Univ.; James Woodward, Univ. of Pittsburgh

Council Delegate: Frederick Grinnell, Univ. of Texas Southwestern Medical Center

Industrial Science and Technology

Chair Elect: Katharine Blodgett Gebbie, National Institute of Standards and Technology

Member-at-Large: William D. Provine, DuPont

Electorate Nominating Committee: Laura Privalle, Bayer CropScience; Proctor Reid, National Academy of Engineering

Council Delegate: Frances M. Ross, IBM Research

Information, Computing, and Communication

Chair Elect: Jeannette Wing, Microsoft/ Carnegie Mellon Univ.

Member-at-Large: Nancy Amato, Texas A&M Univ.

Electorate Nominating Committee: Jeffrey Dean, Google, Inc.; Manuela M. Veloso, Carnegie Mellon Univ.

Linguistics and Language Science

Chair Elect: Jennifer Cole, Univ. of Illinois at Urbana-Champaign

Member-at-Large: Maria Polinsky, Harvard Univ.

Electorate Nominating Committee: Dan Jurafsky, Stanford Univ.; Angelika Kratzer, Univ. of Massachusetts Amherst

Mathematics

Chair Elect: Eric M. Friedlander, Univ. of Southern California

Member-at-Large: Jack Xin, Univ. of California, Irvine

Electorate Nominating Committee: L. Pamela (Pam) Cook, Univ. of Delaware; Joceline Lega, Univ. of Arizona

Medical Sciences

Chair Elect: Harry B. Greenberg, Stanford Univ. School of Medicine

Member-at-Large: Barbara J. McNeil, Brigham and Women's Hospital/Harvard Medical School

Electorate Nominating Committee: Nancy C. Andrews, Duke Univ.; Mary E. Klotman, Duke University School of Medicine

Council Delegate: Anna Di Gregorio, Weill Cornell Medical College; Jeffrey S. Chamberlain, Univ. of Washington; Garrett A. FitzGerald, Univ. of Pennsylvania School of Medicine; Charles M. Rice, Rockefeller Univ.

Neuroscience

Chair Elect: Don W. Cleveland, UC San Diego/ Ludwig Inst. for Cancer Research

Member-at-Large: Diane Lipscombe, Brown Univ.

Electorate Nominating Committee: Leslie C. Griffith, Brandeis Univ.; Lori L. Isom, Univ. of Michigan Medical School

Pharmaceutical Sciences

Chair Elect: Peter Wipf, Univ. of Pittsburgh

Member-at-Large: Gunda I. Georg, Univ. of Minnesota

Electorate Nominating Committee: Jeffrey Aubé, Univ. of Kansas; Amy M. Barrios, Univ. of Utah

Physics

Chair Elect: Greg Boebinger, Florida State Univ./ Univ. of Florida

Member-at-Large: Lynn R. Cominsky, Sonoma State Univ.

Electorate Nominating Committee: Gail G. Hanson, Univ. of California, Riverside; M. Cristina Marchetti, Syracuse Univ.

Psychology

Chair Elect: Barbara Landau, Johns Hopkins Univ.

Member-at-Large: Randi C. Martin, Rice Univ.

Electorate Nominating Committee: Susan A. Gelman, Univ. of Michigan; Dedre Gentner, Northwestern Univ.

Council Delegate: David A. Rosenbaum, Pennsylvania State Univ.

Social, Economic, and Political Sciences

Chair Elect: Ann Bostrom, Univ. of Washington

Member-at-Large: Guillermina Jasso, New York Univ.

Electorate Nominating Committee: Stanley Presser, Univ. of Maryland, College Park; Gary Sandefur, Oklahoma State Univ.

Council Delegate: Paula Stephan, Georgia State Univ.

Societal Impacts of Science and Engineering

Chair Elect: Jane Maienschein, Arizona State Univ.

Member-at-Large: Anne Fitzpatrick, U.S. Department of Energy

Electorate Nominating Committee: Anne-Marie Carroll Mazza, National Academy of Sciences; Julia A. Moore, Pew Charitable Trusts

Statistics

Chair Elect: Nicholas P. Jewell, Univ. of California, Berkeley

Member-at-Large: Charmaine Dean, Univ. of Western Ontario (Canada)

Electorate Nominating Committee: Sastry G. Pantula, Oregon State Univ.; Simon Tavaré, Univ. of Cambridge (UK)
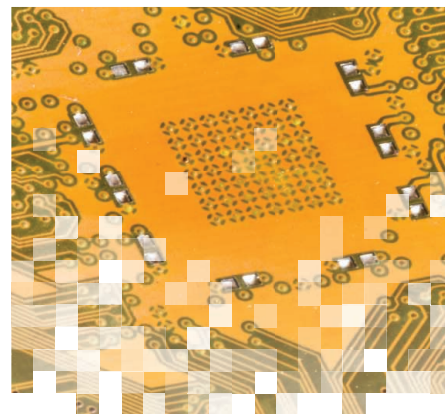
AAAS 2015 Annual Meeting

This year's theme: innovations, information, and imaging

Information and imaging technologies are helping scientists from particle physicists to oceanographers organize and visualize their work in new ways. These innovative technologies also have made science open and accessible to the public at an unprecedented level, with the potential for truly global collaborations. In February 2015, thousands of scientists, journalists, students, and others will convene in San Jose, California, to show how this data revolution can be used to benefit society and inspire new avenues of research. Visit the 2015 Annual Meeting Web site at www.aaas.org/meetings to see the full program of scientific symposia, lectures, career workshops, and free public events.

The 181st Annual Meeting will convene in San Jose for the first time in the association's 167-year history and may draw as many as 8000 attendees from 60 countries. Sessions will include cutting-edge research on topics such as lessons learned from the 2014 Ebola outbreak, the pros and cons of electronic cigarettes, earthquakes related to energy extraction, and new technology to combat childhood deafness. For 2015, two free Family Science Days—14 and 15 February—at the San Jose Convention Center will feature hands-on science-learning activities and stage shows for children, teenagers, and young adults, along with a "Meet the Scientists" speaker series designed especially for middle- and high-school students. ■

The End of
PRIVACY

From big data to ubiquitous Internet connections,
technology empowers researchers and the public—but makes
traditional notions of privacy obsolete

By **Martin Enserink** *and* **Gilbert Chin**

At birth, your data trail began. You were given a name, your height and weight were recorded, and probably a few pictures were taken. A few years later, you were enrolled in day care, you received your first birthday party invitation, and you were recorded in a census. Today, you have a Social Security or national ID number, bank accounts and credit cards, and a smart phone that always knows where you are. Perhaps you post family pictures on Facebook; tweet about politics; and reveal your changing interests, worries, and desires in thousands of Google searches. Sometimes you share data intentionally, with friends, strangers, companies, and governments. But vast amounts of information about you are collected with only perfunctory consent—or none at all. Soon, your entire genome may be sequenced and shared by researchers around the world along with your medical records, flying cameras may hover over your neighborhood, and sophisticated software may recognize your face as you enter a store or an airport.

For scientists, the vast amounts of data that people shed every day offer great new opportunities but new dilemmas as well. New computational techniques can identify people or trace their behavior by combining just a few snippets of data. There are ways to protect the private information hidden in big data files, but they limit what scientists can learn; a balance must be struck. Some medical researchers acknowledge that keeping patient data private is becoming almost impossible; instead, they're testing new ways to gain patients' trust and collaboration. Meanwhile, how we think and feel about privacy isn't static. Already, younger people reveal much more about their lives on the Web than older people do, and our preferences about what we want to keep private can change depending on the context, the moment, or how we're nudged. Privacy as we have known it is ending, and we're only beginning to fathom the consequences.

This special issue was also edited by Brad Wible and Barbara Jasny.

For a key to the data in the art here and on the cover, search for an encrypted URL and decode it.

IMAGE: WILLIAM DUKE

UNMASKED

Facial recognition software could soon ID you in any photo *By* **John Bohannon**

A ppear in a photo taken at a protest march, a gay bar, or an abortion clinic, and your friends might recognize you. But a machine probably won't—at least for now. Unless a computer has been tasked to look for you, has trained on dozens of photos of your face, and has high-quality images to examine, your anonymity is safe. Nor is it yet possible for a computer to scour the Internet and find you in random, uncaptioned photos. But within the walled garden of Facebook, which contains by far the largest collection of personal photographs in the world, the technology for doing all that is beginning to blossom.

Catapulting the California-based company beyond other corporate players in the field, Facebook's DeepFace system is now as accurate as a human being at a few constrained facial recognition tasks. The intention is not to invade the privacy of Facebook's more than 1.3 billion active users, insists Yann LeCun, a computer scientist at New York University in New York City who directs Facebook's artificial intelligence research, but rather to protect it. Once DeepFace identifies your face in one of the 400 million new photos that users upload every day, "you will get an alert from Facebook telling you that you appear in the picture," he explains. "You can then choose to blur out your face from the picture to protect your privacy." Many people, however, are troubled by the prospect of being identified at all—especially in strangers' photographs. Facebook is already using the system, although its face-tagging system only reveals to you the identities of your "friends."

DeepFace isn't the only horse in the race. The U.S. government has poured funding into university-based facial recognition research. And in the private sector, Google and other companies are pursuing their own projects to automatically identify people who appear in photos and videos.

Exactly how automated facial recognition will be used—and how the law may limit it—is unclear. But once the technology matures, it is bound to create as many privacy problems as it solves. "The genie

is, or soon will be, out of the bottle," says Brian Mennecke, an information systems researcher at Iowa State University in Ames who studies privacy. "There will be no going back."

SIMPLY DETECTING FACES is easy for a computer, at least compared with detecting common objects like flowers, blankets, and lamps. Nearly all faces have the same features—eyes, ears, nose, and mouth—in the same relative positions. This consistency provides such an efficient computational shortcut that "we've been able to detect faces in images for about 2 decades," LeCun says. Even the puny computers in cheap consumer cameras have long been able to detect and focus on faces.

But "identifying a face is a much harder problem than detecting it," LeCun says. Your face uniquely identifies you. But unlike your fingerprints, it is constantly changing. Just smile and your face is transformed. The corners of your eyes wrinkle, your nostrils flare, and your teeth show. Throw your head back with laughter and the apparent shape of your face contorts. Even when you wear the same expression, your hair varies from photo to photo, all the more so after a visit to the hairdresser. And yet most people can spot you effortlessly in a series of photos, even if they've seen you in just one.

In terms of perceiving the world around us, facial recognition may be "the single most impressive thing that the human brain can do," says Erik Learned-Miller, a computer scientist at the University of Massachusetts, Amherst. By contrast, computers struggle with what researchers call the problem of A-PIE: aging, pose, illumination, and expression. These sources of noise drown out the subtle differences that distinguish one person's face from another.

Thanks to an approach called deep learning, computers are gaining ground fast. Like all machine learning techniques, deep learning begins with a set of training data—in this case, massive data sets of labeled faces, ideally including multiple photos of each person. Learned-Miller helped create one such library, called Labeled Faces in the Wild (LFW), which is like the ultimate tabloid magazine: 13,000 photographs scraped from the

Web containing the faces of 5749 celebrities, some appearing in just a few photos and others in dozens. Because it is online and free to use, LFW has become the most popular benchmark for machine vision researchers honing facial recognition algorithms.

To a computer, faces are nothing more than collections of lighter and darker pixels. The training of a deep learning system begins by letting the system compare faces and discover features on its own: eyes and noses, for instance, as well as statistical features that make no intuitive sense to humans. "You let the machine and data speak," says Yaniv Taigman, DeepFace's lead engineer, who's based at Facebook's Menlo Park headquarters. The system first clusters the pixels of a face into elements such as edges that define contours. Subsequent layers of processing combine elements into nonintuitive, statistical features that faces have in common but are different enough to discriminate them.

This is the "deep" in deep learning: The input for each processing layer is the output of the layer beneath. The end result of the training is a representational model of the human face: a statistical machine that compares images of faces and guesses whether they belong to the same person. The more faces the system trains on, the more accurate the guesses.

Is that really you?

Just glance at these photos and it is immediately obvious that you're looking at the same person (computer scientist Erik Learned-Miller). To a computer, however, almost every parameter that can be measured varies from image to image, stymieing its ability to identify a face. A technique called deep learning squelches noise to reveal statistical features that these visages have in common, allowing a computer to predict correctly that they all belong to the same individual.

The DeepFace team created a buzz in the machine vision community when they described their creation in a paper published last March on Facebook's website. One benchmark for facial recognition is identifying whether faces in two photographs from the LFW data set belong to the same celebrity. Humans get it right about 98% of the time. The DeepFace team reported an accuracy of 97.35%—a full 27% better than the rest of the field.

Some of DeepFace's advantages are from its clever programming. For example, it overcomes part of the A-PIE problem by accounting for a face's 3D shape. If photos show people from the side, the program uses what it can see of the faces to reconstruct the likely face-forward visage. This "alignment" step makes DeepFace far more efficient, Taigman says. "We're able to focus most of the [system's] capacity on the subtle differences."

"The method runs in a fraction of a second on a single [computer] core," Taigman says. That's efficient enough for DeepFace to work on a smart phone. And it's lean, representing each face as a string of code called a 256-bit hash. That unique representation is as compact as this very sentence. In principle, a database of the facial identities of 1 billion people could fit on a thumb drive.

But DeepFace's greatest advantage—and the aspect of the project that has sparked the most rancor—is its training data. The DeepFace paper breezily mentions the existence of a data set called SFC, for Social Face Classification, a library of 4.4 million labeled faces harvested from the Facebook pages of 4030 users. Although users give Facebook permission to use their personal data when they sign up for the website, the DeepFace research paper makes no mention of the consent of the photos' owners.

"JUST AS CREEPY as it sounds," blared the headline of an article in *The Huffington Post* describing DeepFace a week after it came out. Commenting on *The Huffington Post*'s piece, one reader wrote: "It is obvious that police and other law enforcement authorities will use this technology and search through our photos without us even knowing." Facebook has confirmed that it provides law enforcement with access

to user data when it is compelled by a judge's order.

"People are very scared," Learned-Miller says. But he believes the fears are misplaced. "If a company like Facebook really oversteps the bounds of what is ruled as acceptable by society ... they could go out of business. If they break laws, then they can be shut down and people can be arrested." He says that the suspicion stems from the lack of transparency. Whereas academic researchers must obtain explicit consent from people to use private data for research, those who click "agree" on Facebook's end-user license agreement (EULA) grant the company permission to use their data with few strings attached. Such online contracts "are the antithesis of transparency," Learned-Miller says. "No one really knows what they're getting into." Last year, the company introduced a friendly looking dinosaur cartoon that pops up on the screen and occasionally reminds users of their privacy settings, and it boiled down the EULA language from 9000 words to 2700.

THE PRIVACY ARMS RACE

When your voice betrays you

By **David Shultz**

"My voice is my password." You may soon find yourself saying that—or perhaps you already do—when you call your bank or credit card company. Like a fingerprint or an iris scan, every voice is unique, and security companies have embraced voice recognition as a convenient new layer of authentication. But experts worry that voiceprints could be used to identify speakers without their consent, infringing on their privacy and freedom of speech.

Voiceprints are created by recording a segment of speech and analyzing the frequencies at which the sound is concentrated. Physical traits like the length of a speaker's vocal tract or a missing tooth leave their mark on a voice, creating a unique spectral signature.

Unlike a fingerprint, a voiceprint incorporates behavioral elements as well; traits like cadence, dialect, and accent easily distinguish, say, Christopher Walken from Morgan Freeman. Speech recognition systems, which aim to understand what is being said, minimize these differences, normalizing pitch and overlooking pauses and accents. But for identifying a unique individual, the disparities are crucial.

Because voiceprint systems typically have the user repeat a standard phrase, identity thieves could theoretically record such phrases and play them back to fool the technology. The systems are designed to detect recordings or synthesized speech, however. An even safer alternative is to ask the customer to repeat a randomly chosen bit of text. "The system will prompt the user, 'Now say this phrase,'" says Vlad Sejnoha, the chief technology officer at Nuance Communications Inc. in Burlington, Massachusetts, an industry leader in voice recognition technology. "It's hard to come prepared with all possible recordings." Some systems require no pass phrase at all but rather analyze a person's voice by listening in the background—for instance, as they talk to a sales representative—and compare it with a stored voiceprint.

Demand for voiceprint authentication is skyrocketing. Nuance Director Brett Beranek says the company has logged more than 35 million unique voiceprints in the past 24 months, compared with only 10 million over the previous 10 years. But massive voiceprint databases could make anonymity a scarcer commodity.

"Like other biometrics, voiceprint technology does raise privacy issues, because it gives companies and the government the ability to identify people even without their knowledge," says Jennifer Lynch, an attorney at the Electronic Frontier Foundation in San Francisco, California, specializing in biometrics. "That does create a challenge to anonymous speech protection" as enshrined in the United States' First Amendment, she says.

How and when voiceprints can be captured legally is murky at best. Many countries have legislation regulating wiretapping, but voice recognition adds a major new dimension that most lawmakers have yet to consider, Lynch says. If the past is any guide, companies have massive financial incentives to track consumers' movements and habits. Recognizing someone as soon as they pick up the phone or approach a cashier will open up marketing opportunities—as well as ease transactions for the consumer. As with many new authentication technologies, the balance between convenience and privacy has yet to be struck. ∎

There is already a bustling trade in private data—some legal, others not—and facial identity will become another hot commodity, Iowa State's Mennecke predicts. For example, facial IDs could allow advertisers to follow and profile you wherever there's a camera—enabling them to cater to your preferences or even offer different prices depending on what they know about your shopping habits or demographics. But what "freaks people out," Mennecke says, "is the idea that some stranger on the street can pick you out of a crowd. ... [You] can't realistically evade facial recognition." FacialNetwork, a U.S. company, is using its own deep learning system to develop an app called NameTag that identifies faces with a smart phone or a wearable device like Google Glass. NameTag reveals not only a person's name, but also whatever else can be discovered from social media, dating websites, and criminal databases. Facebook moved fast to contain the scandal; it sent FacialNetwork a cease and desist letter to stop it from harvesting user information. "We don't provide this kind of information to other companies, and we don't have any plans to do so in the future," a Facebook representative told *Science* by e-mail.

The potential commercial applications of better facial recognition are "troublesome," Learned-Miller says, but he worries more about how governments could abuse the technology. "I'm 100% pro–Edward Snowden," Learned-Miller says, referring to the former National Security Agency contractor who in 2013 divulged the U.S. government's massive surveillance of e-mail and phone records of U.S. citizens (see p. 495). "We have to be vigilant," he says.

Learned-Miller's sentiment is striking, considering that he is funded in part by the U.S. Intelligence Advanced Research Projects Activity to develop a classified facial recognition project called Janus. Perhaps that's all the more reason to take his warning seriously. ∎

BREACH OF TRUST

After the Snowden revelations, U.S. mathematicians are questioning their long-standing ties with the secretive National Security Agency *By* **John Bohannon**

Each year, recruiters from the National Security Agency (NSA), said to be the largest employer of mathematicians in the United States, visit a few dozen universities across the country in search of new talent. It used to be an easy sell. "One of the appealing aspects that they pitch is that you'll be working on incredibly hard and interesting puzzles all day," says one mathematician who requested anonymity. In the wake of the terrorist attacks of 11 September 2001, he adds, "I felt that if there was any way I could use my mathematical ability to prevent such a thing from ever happening again, I was morally obligated to do it." Several times over the past decade, he has set aside his university research to work for the agency.

Lately, however, that sense of moral clarity has clouded for some mathematicians, and the recruiters' task has become more complicated. In 2013, former NSA contractor Edward Snowden began releasing documents revealing, among other things, that the agency has been harvesting e-mail and phone records from ordinary American citizens on a massive scale. NSA may have also purposefully compromised a mathematical standard used widely for securing personal computers the world over.

The revelations unsettled the anonymous mathematician. "For people who share my motivations," he says, "the ethics of the NSA's mission matter a great deal." The news has also roiled the mathematics community and led some to question its long, symbiotic relationship with the spy agency, which nurtures budding mathematicians in school, supports the field with research and training grants, and offers academic mathematicians the chance to take part in the murky world of spy craft. Mathematician David Vogan of the Massachusetts Institute of Technology in Cambridge, who finishes his term as president of the American Mathematical Society (AMS) this week, has urged the society to rethink its long-running, close-knit ties with the agency—though he won little support from other AMS officials.

In a sign of the difficulty of convincing the most talented mathematicians and computer scientists to work for the agency, NSA Director Admiral Michael Rogers has hit the road himself to make the pitch. "Many of you are potential future employees that I want to compete for," he told an audience at Stanford University in Palo Alto, California, last November. "The biggest challenge for us … is getting people in the door in this environment." A student in the audience asked

what NSA offers to researchers who may be "disillusioned by the U.S. government." In a reply that may not have helped, Rogers listed both the chance to "serve the nation" and "the opportunity to do some neat stuff that you can't legally do anywhere else."

"THE NSA NEEDS MATHEMATICIANS like a papermaker needs trees," Vogan says. The number of mathematicians employed by the agency cannot be verified. But its total staff is known to be in the tens of thousands, and its official mission—to design cryptologic systems for protecting U.S. information while exploiting weaknesses in the information systems of foreign countries—is deeply mathematical. Since NSA was established in 1952, it has engaged in a mathematical arms race, with ever more sophisticated code-making and code breaking. As NSA has long affirmed, it has a vested interest in maintaining a healthy domestic mathematics community.

Like the rest of its activities, the full extent of NSA's involvement with academia is secret. "We do not release specific budgets for programs," the agency's public affairs office said in response to e-mail queries from *Science*. Even the total annual budget that Congress provides the agency is classified information; estimates have ranged from $8 billion to $25 billion.

Only one line item in the NSA budget is publicly reported each year, and only because it involves a grants program for which AMS provides peer review. Through its Mathematical Sciences Program, the agency will spend $4 million this year on research grants, summer internships for undergraduates, sabbaticals for university professors to work at NSA, and mathematical conferences. It's a pittance compared with the more than $400 million that mathematicians receive each year from other federal agencies. But for a handful of areas that benefit, such as number theory and probability, "it's not a trivial amount of money," Vogan says.

The fruits of NSA support are readily found in academic journals. "It is expected that you will acknowledge the funding in your papers," says Egon Schulte of Northeastern University in Boston, whose research in combinatorics is supported by an NSA grant. That makes it possible to directly track the academic output of NSA funding.

An analysis by *Science* of academic papers indexed on Google Scholar (see graph, below) shows that NSA-supported research output grew steadily through the Cold War and the fall of the Soviet Union, dropped briefly between 1999 and 2002, then mushroomed in the wake of the 9/11 terrorist attacks. In 2013, more than 500 papers acknowledged NSA support.

But direct grants for individual researchers are only a tiny portion of NSA's support for mathematics. Documents that the agency shared with *Science* describe a broad range of academic programs, from STEM (science, technology, engineering, and mathematics) education in schools to research labs at universities. NSA experts give classroom talks and judge science fairs. A small competitive grants program supports science summer camps and high school math clubs and computer labs. And an NSA program called Gen-Cyber brings some of the most talented high school students and their teachers to universities to focus on "cyber-related education and careers" with help from NSA experts.

The outreach helps the agency develop a close relationship with the brightest mathematicians at the start of their careers. "What we found is that the sooner you get in contact with students, the better chance you have to employ them," NSA's then-director of human resources, Harvey Davis, told Congress in a 2002 hearing. Davis also pointed to the agency's cozy ties with higher education. "We are locked in with key professors who make decisions at the universities as well as the math community throughout the country."

At the 55 universities designated by NSA as Centers of Academic Excellence, a full-time NSA "representative" is embedded on campus. According to the documents provided to *Science*, they serve as the "gateway" for the agency to "influence research and research partnerships that will impact the cyber world and workforce in the future." NSA's target campuses include well-known private institutions such as Princeton University, New York University, and Carnegie Mellon University, as well as many public ones such as North Carolina State University, Pennsylvania State University, and the University of California, Davis.
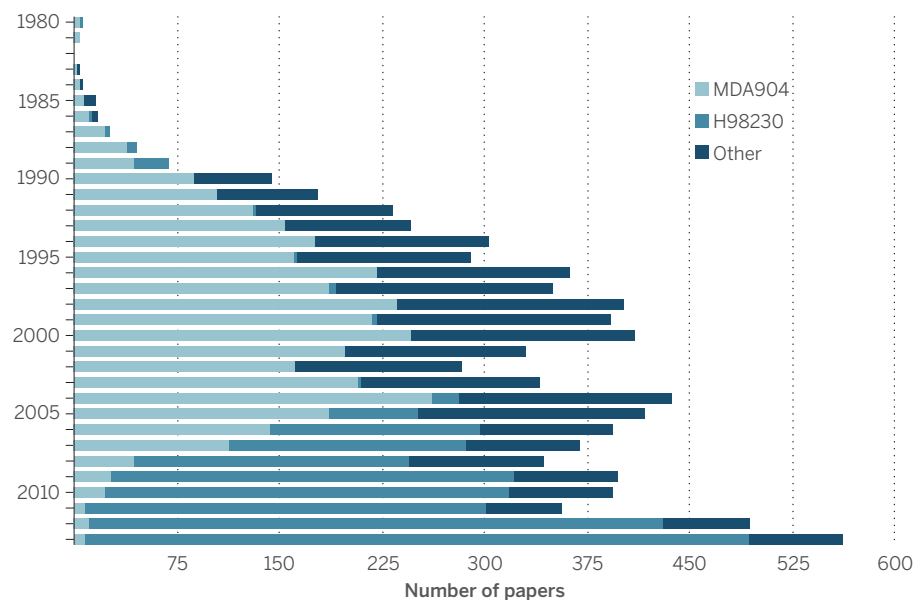
Some universities also receive significant funding from NSA to support research and training. For example, NSA is creating what it calls lablets, research groups within academic departments focused on cybersecurity. According to press releases from the universities, each has received between $2.5 million and $4.5 million so far, but again, the total budgets are unclear.

This close relationship with academia stirred little controversy until recently, says Thomas Hales, a mathematician at the University of Pittsburgh in Pennsylvania. "Everyone knows colleagues who have worked for the NSA." After stints at the agency, "they seem to get amnesia about what they were working on," he quips, but with few exceptions, "no one really cared." That changed in 2013, when mathematicians got a glimpse of how the agency was using some of their work.

IN THE WAKE of the Snowden revelations, most of the media attention has focused on NSA's large-scale harvesting of data from U.S. citizens. But it is a more obscure exploit

Follow the money

The number of research papers indexed by Google Scholar that acknowledge NSA support was falling at the time of the 11 September 2001 terrorist attacks, then rebounded strongly. *Science* performed this analysis using an open-source program called scholar.py created by Christian Kreibich of the International Computer Science Institute. The two main NSA grant codes that emerge are MDA904 and H98230.

Legend: MDA904, H98230, Other

X-axis: Number of papers (75, 150, 225, 300, 375, 450, 525, 600)
Y-axis: 1980, 1985, 1990, 1995, 2000, 2005, 2010

that concerns Hales and many other mathematicians: what they see as an attack on the very heart of modern Internet security.

When you check your bank account online, for example, the information is encrypted using a series of large numbers generated by both the bank server and your own computer. Generating random numbers that are truly unpredictable requires physical tricks, such as measurements from a quantum experiment. Instead, the computers use mathematical algorithms to generate pseudorandom numbers. Although such numbers are not fundamentally unpredictable, guessing them can require more than the world's entire computing power. As long as those pseudorandom numbers are kept secret, the encoded information can safely travel across the Internet, protected from eavesdroppers—including NSA.

But the agency appears to have created its own back door into encrypted communications. The computer industry, both in the United States and abroad, routinely adopts security standards approved by the National Institute of Standards and Technology (NIST). But in 2006, NIST put its seal of approval on one pseudorandom number generator—the Dual Elliptic Curve Deterministic Random Bit Generator, or DUAL_EC_DRBG—that was flawed. The potential for a flaw was first identified in 2007 by Microsoft computer security experts. But it received little attention until internal NSA memos made public by Snowden revealed that NSA was the sole author of the flawed algorithm and that the agency worked hard behind the scenes to make sure it was adopted by NIST.

"[A]n algorithm that has been designed by NSA with a clear mathematical structure giving them exclusive back door access is no accident," Hales wrote in an open letter published by AMS in February 2014. He tells *Science* that since then, "my conclusions have been reinforced by other sources." For example, a July 2014 NIST report suggested that NIST was all but following orders from the intelligence agency. "NSA's vastly superior expertise on elliptic curves led NIST to defer to NSA regarding DUAL_EC," the report said. Research by academic mathematicians has also revealed that the flaw is easier to exploit if the targeted computer uses other security products that were designed at the request of NSA. NIST dropped its support for the faulty standard in April last year. NSA has not made a public statement about it.

Some defended the agency. In an open letter in AMS's online journal, *Notices of the American Mathematical Society*, Richard George, who describes himself as a mathematician who worked for NSA for 41 years, declared that his NSA colleagues "would not dream of violating U.S. citizens' rights,"

although "there may be a few bad apples in any set of people." As for NSA's engineering of a back door into personal computers, George wrote: "I have never heard of any proven weakness in a cryptographic algorithm that's linked to NSA; just innuendo."

In the pages of *Notices*, the revelations triggered a sharp debate about whether the society should cut its ties with the agency. Alexander Beilinson, a mathematician at the University of Chicago in Illinois who helped spur the discussion, argued that the society should completely wash its hands of NSA. The scale of the domestic spying and software tampering makes the United States seem like "a bloated version of the Soviet Union of the time of my youth," he says. Vogan, AMS's president, was outraged as well. "The NSA may have deliberately broken

commercial encryption software," he says. "I see this activity as parallel to falsification of medical research for profit: as an individual wrong action, which damages permanently the position of science in the world."

But after all was said and done, no action was taken. Vogan describes a meeting about the matter last year with an AMS governing committee as "terrible," revealing little interest among the rest of the society's leadership in making a public statement about NSA's ethics, let alone cutting ties. Ordinary AMS members, by and large, feel the same way, adds Vogan, who this week is handing over the presidency to Robert Bryant, a mathematician at Duke University in Durham, North Carolina. For now, U.S. mathematicians aren't willing to disown their shadowy but steadfast benefactor. ∎

Game of drones

By **David Shultz**

Lately, drones seem to be everywhere. They're monitoring endangered wildlife, launching missiles, mapping rainforests, and filming athletes. They can fly high above a neighborhood or just hover outside a bedroom window. The Defense Advanced Research Projects Agency has already built robotic fliers not much larger than an insect; once batteries become small enough, they may become quite literally a fly on the wall. The opportunities—and potential violations of privacy— seem endless. But current and new laws may offer some protection.

In the United States, the Supreme Court has concluded that nobody owns the airways and anyone can take pictures in public. As a result, citizens have been convicted of growing marijuana in their own backyards based on naked-eye observations made from planes flying overhead in "public navigable airspace." On the other hand, a newly proposed law in California would make it illegal for paparazzi to use drones to snap pictures of celebrities on their own property.

Existing laws also ban a peeping Tom from setting up in a tree at the edge of

your property and peering into your bathroom window with binoculars; the same laws are likely to extend to flying a drone outside the same window. The Fourth Amendment, which protects citizens inside their homes from unreasonable searches and seizures without a warrant, may shield Americans from miniature government drones searching for illicit substances. But the extent of the protection will likely hinge on the finer points of the law.

The Federal Aviation Administration is now producing new regulations for unmanned aircraft systems that will limit when and where commercial drones can fly; these may also help protect privacy in some cases. Many other countries, too, are debating how to balance privacy and freedom as drones proliferate.

Creepy as it is to be watched from aircraft controlled by others, drones are hardly privacy worry No. 1, says John Villasenor, a policy analyst at the Brookings Institution in Washington, D.C., because there are ways to collect far more information easily. "Drone privacy is a legitimate concern," Villasenor says. "But there are other technologies, such as mobile phones and the use of data gathered by mobile apps running on those phones, that, for me at least, raise far more pressing privacy issues." ∎

RISK OF EXPOSURE

When new or dangerous infectious diseases strike, public health often trumps personal privacy *By* **Martin Enserink**

Few things can make you famous—or notorious—as fast as an encounter with the Ebola virus. New York physician Craig Spencer saw his daily life dissected by the media, which noted an evening at a Brooklyn bowling alley, a meal at the Meatball Shop, and rides on the 1, A, and L subway trains. Kaci Hickox, a nurse from Maine, was publicly attacked for defying a quarantine that scientists agreed made little sense. *The Daily Mail*, a British tabloid, delved into the past of freelance cameraman and Ebola patient Ashoka Mukpo and dug up salacious details about his parents' love life.

Protecting medical information is tricky enough, but when you fall ill during an outbreak of a new or particularly scary disease, everything appears to become fair game. It's not just reporters who pore over your life. Doctors and public health officials, too, want to know where you have been, what you have done, and with whom. The more widely they share any of that information, the greater the risk to your privacy.

A rise in the number of new and re-emerging diseases in the past 2 decades—including SARS, MERS, and several influenza subtypes—has brought such problems painfully into focus, and the advent of social media and cell phone cameras has increased the pressure. When ambulance workers clad in white protective suits picked up a man at his home in the Dutch city of Maastricht on 26 October 2014, for instance, "it was on Twitter in 20 minutes," says George Haringhuizen, a lawyer at the National Institute for Public Health and the Environment in Bilthoven, the Netherlands. Regional health officials were quick to deny claims that Ebola was involved.

Reining in bloggers and Twitter users may not be easy. But even professional efforts to track outbreaks pose new threats to privacy. Information about specific patients—although anonymized—is now shared worldwide on public e-mail lists for emerging diseases such as ProMED, which often recirculates newspaper stories from around the world. Although it always redacts patient names, says ProMED Editor Larry Madoff, a simple Google search is enough to find the original story with those names.

There is a growing need for global ethical standards for governmental disease surveillance, akin to what the Declaration of Helsinki provides for medical research, says Amy Fairchild, a historian at Columbia University who studies public health policy. Fairchild co-chairs a group of ethicists and public health experts assembled by the World Health Organization (WHO) to make recommendations on the subject; privacy will be a key issue, she says.

UNTIL THE 1960S, major U.S. newspapers routinely printed the names and addresses of people with infectious diseases such as polio, Fairchild says. It wasn't until the 1970s, when governments and other organizations began storing large amounts of electronic data on citizens, including medical records, that privacy emerged as a political issue. Heart-wrenching cases of stigmatization and discrimination against AIDS patients in the 1980s—which led many to hide their HIV status—galvanized support for the protection of medical privacy.

Many countries now have complex laws and regulations governing how and when medical information can be shared, such as the Privacy Rule of the U.S. Health Insurance Portability and Accountability Act, passed in 1996. Yet there still is a "huge tension" between the worlds of clinical care—where doctors try to protect individual patients—and public health, which tries to protect communities, says bioethicist Arthur Caplan of New York University's Langone Medical Center in New York City—especially during disease outbreaks. "Privacy doesn't fit well in the mindset of people in public health," he says. "For them, the question is: How much can I get away with without privacy going completely out of the window?"

Disease detectives at the U.S. Centers for Disease Control and Prevention, for instance, can't track down a mysterious outbreak without having as much information about the patients as possible. At the same time, governments can't know if public health policies work without gathering detailed data about disease incidence.

But because of privacy concerns, doctors sometimes don't comply with requirements to notify health authorities when they diagnose a patient with a reportable disease, of which there are about a hundred in the United States. A qualitative study conducted in Canada at the height of the 2009 influenza pandemic showed that some doctors were surprisingly reluctant to report patients with flulike symptoms, as they were supposed to. "I think the bottom line for most family physicians is we will not share names, addresses, or phone numbers, period, without individual patient consent," one said in a focus group.

There are debates about how reported data can be used as well. New York state, for example, requires doctors not only to report HIV diagnoses, but also to forward lab results such as viral loads and CD4 cell counts. When such reports stop coming in for a given patient, researchers say, it's a sign they may have dropped out of treatment, which could help the virus rebound and put sex partners at risk. A 2013 study showed that of 409 dropouts, 57% were brought back into care after they had been traced and contacted—but some believe that's crossing a line.

EVEN WHEN DOCTORS or government agencies treat health data discreetly, patient identities often become known—in their neighborhoods, towns, or in the press. When federal agents go around the block to trace the contacts of an Ebola patient, it's usually not hard to find out who the patient is. Europe's very first AIDS patient, who died in 1976, was long known as "the Norwegian sailor," and later by an anagram of his real name, used in Edward Hooper's book *The River*—until journalists revealed his name around a decade ago. (The man is believed to have picked up HIV in West Africa in the early 1960s; his wife and one

Could your pacemaker be hackable?

By **Daniel Clery**

In a 2012 episode of the TV series *Homeland*, Vice President William Walden is assassinated by a terrorist who hacks into his Internet-enabled heart pacemaker and accelerates his heartbeat until he has a heart attack. A flight of fancy? Not everyone thinks so.

Internet security experts have been warning for years that such devices are open to both data theft and remote control by a hacker. In 2007, Vice President Dick Cheney's cardiologist disabled the wireless functionality of his pacemaker because of just that risk. "It seemed to me to be a bad idea for the vice president to have a device that maybe somebody on a rope line or in the next hotel room or downstairs might be able to get into—hack into,"

said the cardiologist, Jonathan Reiner of George Washington University Hospital in Washington, D.C., in a TV interview last year.

Medical devices such as insulin pumps, continuous glucose monitors, and pacemakers or defibrillators have become increasingly small and wearable in recent years. They often connect with a hand-held controller over short distances using Bluetooth. Often, either the controller or the device itself is connected to the Internet by means of Wi-Fi so that data can be sent directly to clinicians. But security experts have demonstrated that with easily available hardware, a user manual, and the device's PIN number, they can take control of a device or monitor the data it sends.

Medical devices don't get regular security updates, like smart phones and computers, because changes to their

software could require recertification by regulators like the U.S. Food and Drug Administration (FDA). And FDA has focused on reliability, user safety, and ease of use—not on protecting against malicious attacks. In a Safety Communication in 2013, the agency said that it "is not aware of any patient injuries or deaths associated with these incidents nor do we have any indication that any specific devices or systems in clinical use have been purposely targeted at this time."

FDA does say that it "expects medical device manufacturers to take appropriate steps" to protect devices. Manufacturers are starting to wake up to the issue and are employing security experts to tighten up their systems. But unless such steps become compulsory, it may take a fatal attack on a prominent person for the security gap to be closed. ■
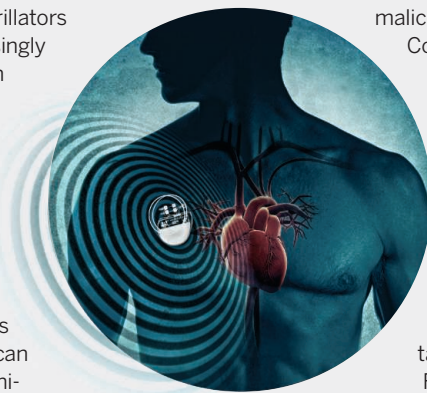
of his two daughters succumbed to AIDS as well.) The case still upsets Stig Frøland, a researcher at the Rikshospitalet in Oslo who published about the family and says he tried hard to protect their identity. Still, Frøland isn't surprised, "in view of my experience with the very aggressive attitude from national and international media through the years."

Craig Spencer's identity was revealed by the press, too. (A Twitter search suggests the *New York Post* identified Spencer first, 8 hours after his hospitalization, simply citing "sources," followed shortly after by the New York *Daily News*.) The details that the health department subsequently made public about Spencer's movements before he fell ill were a clear invasion of his privacy, Fairchild says—and an unwarranted one, because he didn't have symptoms at the time and wasn't infectious. (Spencer, who asked the media to respect his right to privacy after he recovered, did not respond to requests for comment.)

Mukpo, by contrast, agreed that his name could be released after he got Ebola, in part hoping it might help get him repatriated from Liberia, where he became infected. "Honestly, though," he adds, "me remaining anonymous would never have been a realistic option," given that he worked for NBC and knew many journalists.

The upcoming WHO report, expected in 2016, will come up with recommendations for disease surveillance in general, not just for infectious diseases. But the panel may well borrow some pages from a similar WHO report, published in 2013, on the ethics of HIV surveillance, which remains an extremely sensitive issue today. That document recommended that the names of HIV patients be reported only for public health purposes—not for discrimination or criminalization—and only when confidentiality of the data is assured. It also said that people's right not to participate in surveillance should be respected as much as possible.

The tension between privacy and public health will always remain, Caplan says, but preventing stigmatization and other negative consequences could help relieve some of the worries. "If you're not going to lose your job, lose your house, lose your mate, there's less reason to worry about your privacy," he says. And eventually, he says, people may care less than they do today about whether officials track their movements and contacts. Young people already share massive amounts of information online—including where they are, what they're doing, and who they're with. ("When I ask them if they aren't worried about their privacy, I get a condescending look," Caplan says.) Medical privacy, too, will become a "quaint notion," Caplan predicts.

For Mukpo—who noted the irony when *Science* e-mailed him to ask questions about his privacy—the exposure was actually a mixed experience. Although it was "very disconcerting to become such a public figure so quickly," he did use the media spotlight to raise awareness about the Ebola situation in Africa. What's more, "the publicity also was an opportunity to see just how many amazing people I have in my life," he adds. "The outpouring of concern was humbling." ∎

THE PRIVACY ARMS RACE

Hiding in plain sight

By **Jia You**

Whether they're looking for nearby restaurants, wondering what to wear, or finding the fastest route, most people allow their smart phones to send their GPS locations to Yelp, AccuWeather, or Google Maps without a second thought. But these data can be shared with advertisers and other third parties that profile users' movement patterns, often without their knowledge.

Even anonymizing people's location data doesn't necessarily protect their privacy. When New York City released anonymized data on more than 173 million taxi trips in response to a Freedom of Information Act request in March, researchers quickly combined the data with known reference points— addresses, for example—to pinpoint celebrities' cab trips and identify who frequented local strip clubs.

Computer scientists are devising countermeasures. CacheCloak, a system developed by researchers at Duke University in Durham, North Carolina, throws off tracking efforts by hiding users' actual location data. When you want to find, say, nearby restaurants, CacheCloak doesn't send Yelp or Google your exact GPS coordinates, but an entire path that it predicts you will take. That path is made to intersect with predicted paths from other users, so that the service sees requests from a series of interweaving paths where a driver can go either way at each crossing, and cannot track any single user. But consumers can still receive relatively accurate results.

A slightly different camouflage strategy is to send dummy locations along with a user's real location. Researchers at Microsoft, for instance, have built an algorithm that can generate realistic car trips in Seattle based on real GPS data on 16,000 drives taken by about 250 volunteer drivers in the area. The dummy trips have plausible start and end points—no stopping in the middle of a highway—adhere to speed limits, and deliberately follow slightly non-optimal routes, so that a filter can't easily pick out the false trips from the real ones. A mobile phone would draw on the library of routes to send both the user's actual location and points from many dummy trips to a cloud-based location service like Google Maps. The app responds—say, to a request for traffic warnings—for all locations, but users can use the answers they need and disregard the rest.

The downside of the strategy is that such dummy searches can result in embarrassment, says computer scientist Michael Herrmann of the University of Leuven in Belgium. For example, many people might not want their trip to the library masked as a visit to an HIV testing site.

In a third strategy, algorithms can simply send imprecise location data to services, cloaking a user's whereabouts in 1-kilometer squares rather than revealing precise GPS coordinates. But that has the obvious drawback of decreasing the quality of an online service, Herrmann says. For a weather app, your exact location may not matter, but if you're on foot and need to find a nearby ATM, precision is crucial.

In the end, human movements are often so predictable that they are hard to conceal. Location-hiding techniques are most valuable when you want to hide one-off trips, Herrmann says. But when it comes to protecting the location of your home and workplace, you might as well give up on privacy. ∎
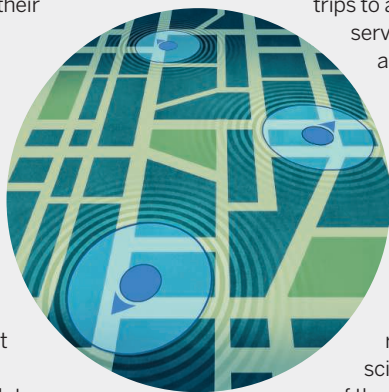
TRUST ME,
I'M A MEDICAL RESEARCHER

Scientists can no longer guarantee patients' privacy.
They're looking for new ways to build trust *By* **Jennifer Couzin-Frankel**

n an Oxford, U.K., suburb, a short distance from the track where Roger Bannister ran the world's first 4-minute mile, a quiet revolution is under way. One hundred and twenty-six people and counting, all suffering from a rare rheumatologic disease or the parent of an affected child, are involved in a research project on the disorders. But rather than donating a few samples, filling out a questionnaire, and hoping something useful will come of it one day, these subjects are

deeply invested in the research. They are contributors with a voice.

One is Elaine Rush, a 53-year-old from outside Southampton. She was born with the brittle bone disease osteogenesis imperfecta and has had, in her words, "only around 25 fractures in all—quite low compared to many." Once not expected to live past the age of 5, Rush uses a wheelchair and has battled heart and lung problems associated with the disease. An eager partner in the quest to advance science, she now di-

als in to Skype calls every other month with one or more researchers and offers advice. When they were struggling with recruitment, Rush advocated posting on Facebook, where patients find each other. The study leaders are looking to follow her suggestion.

RUDY, as this project to study rare diseases of the bones, joints, and muscles is called, represents a new kind of bargain between researchers and subjects in response to dwindling expectations of privacy. Until quite recently, a volunteer might have

offered DNA or tissue to a single research group at a nearby university. Today many samples are banked, sequenced, and shared with potentially thousands of researchers. That allows for bigger studies with more statistical muscle, but it also makes it more difficult to keep patients' data private. It's now widely accepted that if someone can read your DNA, they might figure out who you are, either now or in the future, as technology marches ahead. The promise long made to participants—that their identity is stored in an unbreakable vault—no longer holds.

"Patients are scared about access to 'my data,' " says one of RUDY's leaders, Kassim Javaid, a balding, bespectacled University of Oxford rheumatologist based at the university's Nuffield Orthopaedic Centre. Offering them many layers of control, as RUDY does, "is a possible solution," he believes.

Rush and other participants in RUDY—which is co-funded by the United Kingdom's National Institute for Health Research—can decide whether their blood, their scans, and their medical histories can be shared with researchers at, say, a lab elsewhere in Europe or in the United States. They will be able to log on to a clinical trial Web page to learn whether one of their tissue samples has been flagged—an indication that a researcher somewhere is studying it.

Throughout biomedical research, the advent of large repositories of DNA and tissue samples has forced researchers and ethicists to rethink their relationship with the volunteers who make their work possible. "Twenty years ago, people consented to do experiments based on trust and a handshake," says Jamie Heywood, the co-founder of PatientsLikeMe in Cambridge, Massachusetts, a company that provides a platform for people with different diseases to share their health data. Now, patients shake hands with faceless others around the world. And in return for sharing their DNA far and wide—and potentially shelving their privacy—participants want a louder voice in research, and transparency about how it's conducted.

THAT THE END OF GENOMIC PRIVACY has arrived became clear 2 years ago, when a young human geneticist now at Columbia University, Yaniv Erlich, published a startling paper in *Science* (18 January 2013, p. 321) that confirmed the worries of many in the field. Erlich and his colleagues showed that it was possible to identify a man based on a partial DNA sequence of his Y chromosome, his age, and his U.S. state of residence—the type of basic information that researchers commonly

post in DNA databases widely accessible to their community. By combining these snippets of information with what he found for others in the same family on popular genealogy databases—where more than 100,000 people have already posted DNA markers—Erlich could not only identify the donors of the DNA, but also their family members as far as second cousins once removed. "I don't even know my second cousins," he says.

Erlich hastens to point out that DNA can be anonymized, for instance by scrambling

or deleting nucleotides containing sensitive information. That technique can render the information largely useless for research, however, and doesn't even always protect the donor. When James Watson, a co-discoverer of DNA's double helix, had his genome sequenced and published in *Nature* in 2008, he requested that his *APOE* gene—which can reveal a predisposition to Alzheimer's disease—be left out. But as three geneticists politely pointed out later that year in the *European Journal of Human Genetics*,

---

Camouflaging searches in a sea of fake queries

By **Jia You**

From health questions to shopping habits, your Web search history contains some of the most personal information that you reveal online. Search engine giants such as Google and Bing carefully log these data and save them in databases, where they might be shared with advertisers and the government.

Privacy-conscious users can switch to anonymous search engines such as DuckDuckGo, which doesn't log a user's IP address, identifying information, or search history. DuckDuckGo alone processes about 7 million direct queries a day; traffic spiked after the 2013 revelations about the National Security Agency's snooping. But these services don't match the speed and convenience that Google offers. For consumers who want to continue using their favorite search services but with added protection, researchers at New York University in New York City have developed a browser extension that produces dummy search requests that drown out a user's real queries, thwarting any attempt to profile them.

The software, known as TrackMeNot—which can be downloaded as a Firefox or Chrome extension—creates the fake search queries by harvesting phrases from RSS feeds from popular websites

such as *The New York Times*. Dummies such as "George Clooney" and "Amtrak" are sent to a search engine in the background while consumers use their browsers as usual. You can customize the RSS feed to control the content of the decoys and pick which search engines to target. To make the dummies more believable, the algorithm automatically updates the search terms and even simulates clicks on links displayed on the results pages. It can also schedule fake queries primarily when users are actually searching.

There's no guarantee that search engines wouldn't be able to separate the fake searches from the real ones, but it could cost them considerable resources to do so, says privacy expert Helen Nissenbaum, who co-developed the software. She hopes the project will serve as a proof of concept and garner sufficient users—it has more than 60,000 so far—to pressure search engine companies into meaningful dialogues on their privacy policies.

The software may not be much help to users who look up sensitive terms monitored by governments—those related to political opposition, for instance—as it doesn't hide a user's real queries. For those users, computer scientists at Purdue University have developed an algorithm that not only sends out fake queries, but also hides a user's real interests by substituting real queries with phrases related to the same topics. The downside: The results become less relevant, forcing users to go through multiple pages of results to find the link they need. ∎
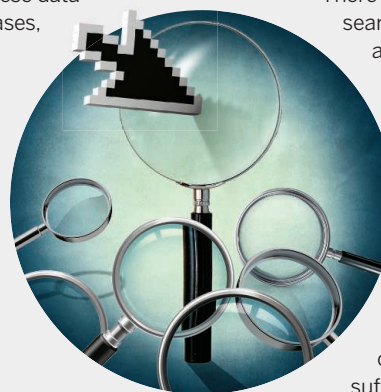
genetic knowledge had advanced sufficiently to impute Watson's *APOE* status based on patterns in nearby DNA.

Cryptographers are still exploring how to better protect DNA, and many agree it's important to continue that work. But Erlich's energies have shifted elsewhere. About a year ago, he and about 30 others convened at Cold Spring Harbor Laboratory to consider alternatives to privacy in research. They came back to that decades-old handshake and contemplated how to adapt it for 21st century science.

Erlich was inspired in part by recent Internet phenomena where trust is a guiding force, such as Uber, which runs an online car-sharing service that matches drivers with passengers. "Uber takes two individuals that don't know each other," he says. "I'm getting into someone else's car; he could chop me to pieces." Airbnb, where people offer a room or their entire home for rent to complete strangers, is another example. These websites hold users accountable with reviews, profiles, and extensive documentation. This openness appears to build trust, Erlich says, and he thinks the same strategy can be applied to genetics and biomedical research.

Research volunteers have always valued trust and transparency. In 2007, Alan Westin, a legal scholar who studied privacy and who died in 2013, conducted a survey of almost 2400 people for the Institute of Medicine. He found that respondents were less preoccupied with whether researchers knew who they were than with knowing what was happening to their medical information. Among those surveyed, 81% were not happy to have researchers parsing even so-called de-identified health data without their consent.

"They are not hung up on privacy so much as autonomy," says Mark Rothstein, a law professor at the University of Louisville in Kentucky. "Let's assume that you've de-identified, anonymized, and nobody can figure out who it is—but if people think you've used that information without their permission, they're still going to be very angry."

U.S. regulation is adapting to that sentiment. In August, the National Institutes of Health announced that, starting this month, it expects researchers to obtain informed consent from participants if their DNA, cell lines, tissue, or any other de-identified biological material will be used for research at any point in the future. "Part of governance is transparency," says Bartha Maria Knoppers, who studies law and genetics at McGill University in Montreal, Canada, and is a member of a consortium called the Global Alliance for Genomics and Health, which is looking

for new methods to share data more openly and responsibly. "You put in place a process of oversight and a mechanism to ensure that what you tell me is going to happen to my data is what is going to happen to my data."

Knoppers and many others point out that patients often want to share their DNA in the name of advancing research—and that fears of being identified through DNA may be overblown. Some databases ban researchers from re-identifying volunteers. There have been no breaches yet—or at least none that anyone knows about. Gail Jarvik, a medical geneticist at the University of Washington, Seattle, believes that most scientists don't care who handed over a blood or tissue sample. "Why identify them?" she asks.

A HANDFUL OF EXPERIMENTS are now testing how to better inform volunteers about what's happening to their data. PatientsLikeMe has recruited 300,000 people with more than 2300 different diseases. Participants share their health data, analyze how they're faring in clinical trials, support each other, and help researchers and drug companies answer existing scientific questions and pose new ones. Heywood founded the nonprofit in 2004 while his younger brother Stephen was suffering from amyotrophic lateral sclerosis. (Stephen died 2 years later.) Jamie Heywood's philosophy is that if people are "understanding and enthu-

> ## "I personally don't feel that there's anything I need to hide."
> **Elaine Rush**, trial participant

siastic participants," they will agree that sharing widely will maximize the value of their DNA and other health information to the community—even if this offers them less privacy. The company keeps in touch with participants with a blog, social media, and regular e-mails.

The Personal Genome Project (PGP) at Harvard Medical School in Boston, founded by geneticist George Church, goes even further: It asks participants to share their DNA sequences and health histories online for everyone to see. Almost 4000 have signed up so far; last month, PGP launched a "real name" option, whereby they can post their identity. "Many participants do mention altruistic reasons: sharing data publicly in order to promote our collective knowledge," says Jeantine Lunshof, a Harvard ethicist on the project. "That seems to outweigh potential drawbacks." To make sure participants understand its ramifications, PGP asks a series of hard questions. One example, says Heywood, who participates in PGP but flunked the test the first time: "If I commit a crime, could the DNA in this bank

be used to identify me?" (The answer is yes.)

Javaid of RUDY hopes that his strategy, called dynamic consent because consent is a continual process, will change how patients think about research. Patients can choose which portions of the study to complete—questionnaires, or the sharing of scans, for example—and also whether to restrict their data to RUDY investigators or allow them to be more broadly distributed. If someone says, "don't use my DNA, don't use my blood … we archive the samples so no one else can use them," Javaid says, but they're preserved in case the patient changes his or her mind.

Rush, the participant with brittle bone disease, has given broad consent, along with nearly all of RUDY's early adopters. "I personally don't feel that there's anything I need to hide," Rush says, but she recognizes that not everyone feels the same way. She has also reached out to fellow patients. "The fact that they can opt out of some things" has helped her explain the study to those who might hesitate to sign on.

As for Erlich, he's ready to borrow more ideas from Uber and Airbnb. In November, he and nine other attendees at the Cold Spring Harbor meeting published a paper in *PLOS Biology* outlining a "trust-centric framework … that rewards good behavior, deters malicious behavior, and punishes noncompliance." Like people griping online about a driver's body odor or praising the free coffee and snacks in their vacation home, patients could write reviews about the researchers they have worked with. The system could include trusted mediators to engage both researchers and participants, and automated auditing of how study data are used. Perhaps, Erlich speculates, the visibility of researchers and their reputation would climb when they received accolades from peers or high marks from patients for returning results and raw data.

Of course, trust is difficult to build and easy to squander. Last year, Uber itself received a failing grade from the Better Business Bureau after a deluge of customer complaints, and the company has been accused of exaggerating how carefully it vets its drivers. A similar breakdown could transpire in scientific projects.

RUDY has won Rush's trust. "The RUDY researchers are reputable," she says. "They wouldn't be sharing with [just] anyone." As the study plods on in the months and years ahead, its success will depend on upholding that confidence. ∎

PERSPECTIVE

Control use of data to protect privacy

Susan Landau*

Massive data collection by businesses and governments calls into question traditional methods for protecting privacy, underpinned by two core principles: (i) notice, that there should be no data collection system whose existence is secret, and (ii) consent, that data collected for one purpose not be used for another without user permission. But notice, designated as a fundamental privacy principle in a different era, makes little sense in situations where collection consists of lots and lots of small amounts of information, whereas consent is no longer realistic, given the complexity and number of decisions that must be made. Thus, efforts to protect privacy by controlling use of data are gaining more attention. I discuss relevant technology, policy, and law, as well as some examples that can illuminate the way.

We live in an era of an explosion of data. For a variety of reasons, including massive collection by both the private sector and governments, as well as the ease of computing correlations—from which information can be derived even about people whose data are not in the set—the old methods for protecting privacy no longer work. An old protection made new, managing use, now seems the most appropriate way to secure privacy. Controlling use is complex, but combining technology, policy, and law is the best way to control incursions from businesses and governments.

The principles governing data protection are 40 years old. The Fair Information Practices (FIPs) were developed in response to the rise in the 1960s of computerized data systems. Coming originally from a report from the U.S. Department of Health, Education, and Welfare (*1*), the FIPs were revised by the Organization of Economic Cooperation and Development (OECD) (*2*). The more expansive OECD privacy principles have been the basis for many national and international privacy regulations.

Notice, consent, context

User control sits at the heart of the FIPs. Transparency and/or notice says that there should be no data collection system whose existence is secret; access, that there should be a way for the data subject to find out what information is in her record and how it is used; consent—sometimes called choice—that data collected for one purpose not be used for another without user permission; redress, that the data subject must have the ability to correct inaccuracies; and integrity and security, that the data collector keeps reliable records and protects them. In 1998, the U.S. Federal Trade Commission (FTC) identified these as the "five core principles of privacy protection" and noted that notice was fundamental, calling choice or consent the "second widely accepted core principle" (*3*).

Whereas the U.S. and Europe have taken different routes to protecting privacy—the U.S. using

Worcester Polytechnic Institute, Worcester, MA 01609, USA.
*Corresponding author. E-mail: susan.landau@privacyink.org

sector-specific protections (financial data, banking information, health records), Europe pursuing broader data-protection schemes—both emphasized notice and consent. But, although the FIPs made sense when an individual could discern and react to a data-collection event, this is no longer true.

Consider data collection from a smart phone. The combination of information from the user

> *"Controlling use is complex, but combining technology, policy, and law is the best way to control incursions from businesses and governments."*

and aggregated data from others can improve her experience. For companies, such data promotes faster, more-targeted services (and advertising), ties the consumer more strongly to the business, and boosts profits. For researchers, massive data illuminates connections that might not have been apparent and may uncover correlations that are actually causations.

Because data collection involves compilation of massive amounts of small bits of data, notice and consent are difficult for users to manage. Should collection of phone location data increase when a traffic accident blocks a popular route? What if the user is on a private assignation that day? That a service that provides up-to-date route information also collects up-to-date location data is not something all users realize (although they should). Frequent queries about permission for collection create a situation in which the user inattentively clicks "Yes"—not exactly a win for privacy.

Notice simply doesn't make much sense in a situation where collection consists of lots and lots of small amounts of information (Fig. 1). Written to cover all contingencies, privacy notices are not designed for human use. A 2008 study

showed that the average reader would need 244 hours simply to read the privacy policies for all websites she accessed in a year (*4*).

Consent is often not an option. Almost a decade ago, Fred Cate noted, "If consent is required as a condition for opening an account or obtaining a service, a high response rate can always be obtained" (*5*), whereas a 2014 President's Advisory Committee on Science and Technology (PCAST) report on big data and privacy observed, "Only in some fantasy world do users actually read these notices and understand their implications before clicking their consent." (*6*).

Sometimes the user is not even given a choice about consent. Because of overwhelming complexity, Google, whose Android platform dominates the consumer smart phone market (*7*), decided to put permissions for information access into groups. Thus, a user lacks the ability to conduct fine-grained decisions on which information to permit apps to access (*8*). The user moves on, rarely examining—or withdrawing—consent afterward.

A fundamental problem is that seemingly innocuous data may trigger a privacy incident. Using the history of buying patterns of other customers, Target predicted a teenager's pregnancy from her vitamin purchases (*9*), and the ride-share firm Uber claimed to be able to discern one-night stands from the usage patterns of rider pick-up and drop-off data (*10*). Solon Barocas and Helen Nissenbaum noted, "The willingness of a few individuals to disclose information about themselves may implicate others who happen to share the more easily observable traits that correlate with the traits disclosed." (*11*).

Context matters in privacy. That idea first espoused by Nissenbaum a decade ago (*12*) is gaining support in policy circles, including in the White House Consumer Bill of Rights (*13*) and a recent FTC report (*14*). Massive amounts of data create such personal and societal benefits that collection is unlikely to stop.

Controlling use

The FIPs protected privacy through notice and consent, but for reasons of complexity (too many tiny collections, too many repurposings), those are no longer effective. Nonetheless, notice and consent provide benefits: notice, for transparency, and consent, for certain types of data or use, as well as for controlling context (*15*). But the value of big data means we must directly control use rather than using notice and consent as proxies (*6*). That is true no matter who the collector is.

This is easier said than done. Big data provides the patterns that allow us to use resources efficiently. Determining how to continue to collect and use big data, but control its use, is complex. The tools are technology, policy, and law, and there are some examples that can illuminate the way.

Once the most solitary of activities, reading is losing the privacy between the reader and the page. Amazon and other purveyors of e-books have discovered multiple ways of tracking activity: where readers start, what they reread, whether they mark a passage, if they finish the text (*16*).

There are other approaches that make tracking user reading more difficult, rather than less so.

One such is Shibboleth, software that enables a user at one participating institution, say, the University of Michigan, to access electronic resources at another, say, the University of Illinois. A user authenticates on the University of Michigan. The user, however, is identified to the University of Illinois not by personal identifier such as name or e-mail address but by her right to the resource. This could be because she is a member of the University of Michigan community (student or staff), a participant in a particular course, or one of a set of users authorized to access particular resources. Unless the information is specifically needed, the University of Illinois does not learn the user's actual online identity. The Family Educational Rights and Privacy Act, which protects the privacy of student educational records, and the fact that librarians view reader privacy as fundamental motivated this privacy-protective architecture.

A potentially powerful approach to controlling data usage is "accountable http," a variant of the http protocol. Proposed by MIT researchers Oshani Seneviratne and Lalana Kagal, httpa creates a system to track information usage (*17*). The system consists of a user who wishes to access data that have usage restrictions (e.g., no sharing, no sharing without informing the data owner, etc.); a data provider using an httpa server; and a Provenance Tracking Network (PTN). The PTN is a network of servers that log each data access and usage, either from the original data provider or any user downstream.

The magic behind the system is httpa, a protocol that conveys usage restrictions between the data providers and data users, creating a log in the PTN for each time a protected resource is accessed. These logs do not enforce compliance but can be used to determine it. This general approach to controlling data usage has only been tested in a small-scale effort; whether it can scale to the Internet is unclear. But it might be valuable in limited settings, such as patient health data, where a motivator might be the Health Insurance Affordability and Accountability Act (HIPAA), the U.S. law that restricts the sharing of patient medical data.

Online identities are used ubiquitously across the Internet to access restricted resources (e.g., pay-for-use subscriptions or library memberships confined to a university community), to post comments in restricted settings such as YouTube, and to conduct business at a bank or online broker. Although the need for secure, interoperable, and easy-to-use credentials for online identities was clear, development and adoption of such tools was slow.

The U.S. federal government stepped in, creating the National Strategy for Trusted Identities in Cyberspace (NSTIC) to provide funding for pilot programs and standards efforts that would provide both privacy and security. Using access to federal government sites as a lever, NSTIC requires that private-sector identity providers protect the privacy of information regarding user activities on federal sites (*18*).

Tracking when a user goes on a .gov website can reveal their private information, e.g., interest in HIV/AIDs or in penalties for unpaid taxes. Federal rules prevent identity providers from using tracking information from federal sites
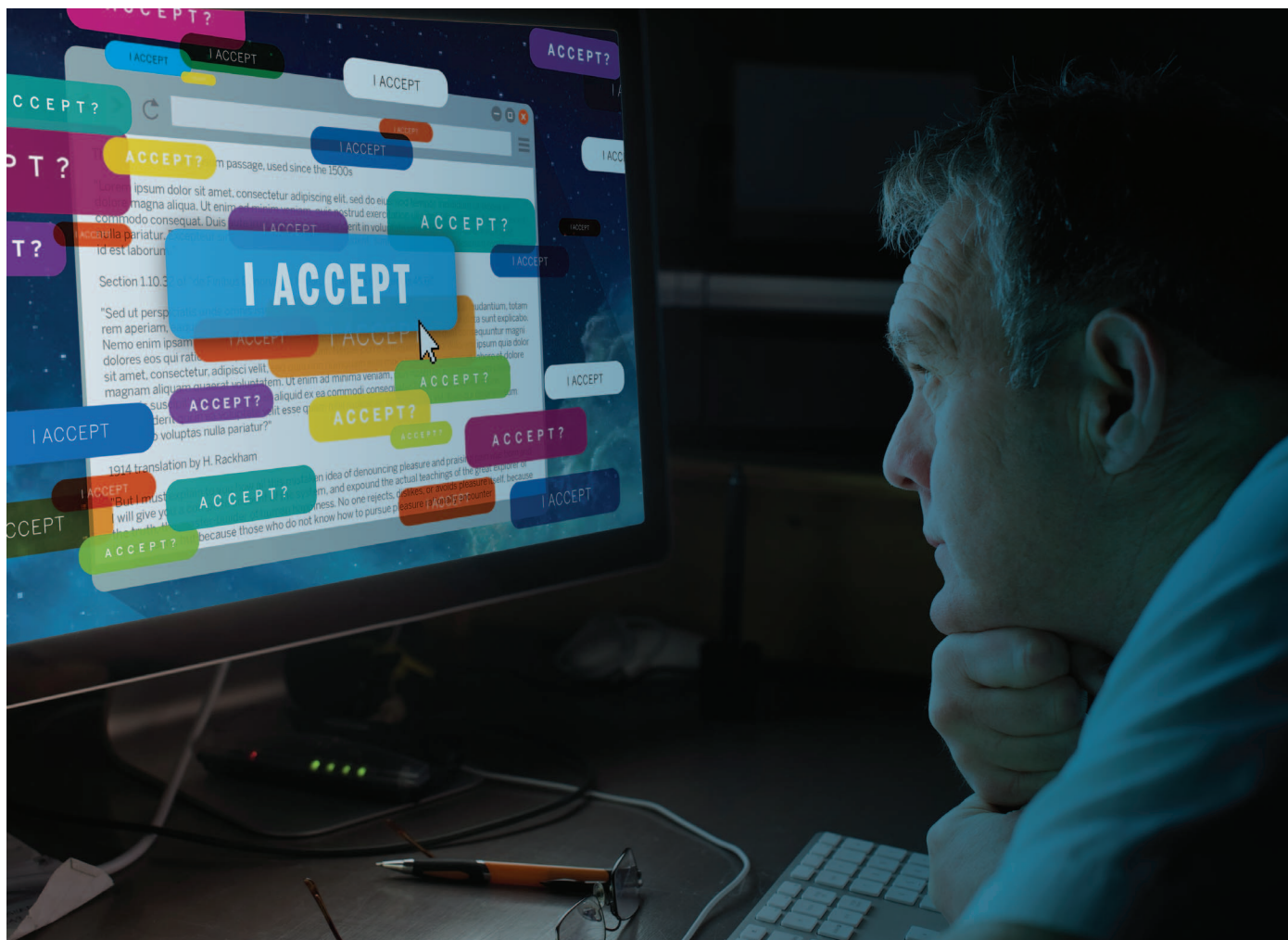
Fig. 1. Permission to run software has become complicated. In signing "I accept"—typically necessary to use an application—the user agrees to collection and use of information present on their device. Such data may not only be revelatory, it may also have been collected without the user's knowledge or understanding of what can be discovered from this information.

for anything but authentication, audit, or complying with the law (*19*). In other words, no ads, no sharing the information with a third party, and no using the information to promote the identity provider's products. A signed-on user has greater privacy protections when visiting the National Cancer Institute website than when visiting the American Cancer Society site. Policy controls data usage and is then manifested in technical design.

Laws can provide shields against inappropriate data usage. The 1970 U.S. Fair Credit Reporting Act (FCRA), which predates the FIPs, does not control collection. Instead the FCRA strictly limits the circumstances under which a person's credit information can be accessed (essentially for credit, employment, and in response to court orders) (*20*).

A different example of control is the Genome Information Nondiscrimination Act (GINA) of 2008, which protects against discrimination in health insurance and employment based on genetic data. But GINA, too, has its limits. If a woman discovers through genetic testing that she is BRAC1- or BRAC2-positive, with a 55 to 65% or 45% chance, respectively, of developing breast cancer by age 70, GINA protects her ability to obtain health insurance and employability but says nothing about her ability to obtain disability, long-term care, or life insurance in the face of the BRAC1 and BRAC2 data.

There are other examples of how technology, policy, and law combine to control use. A well-known one is in medical research. The HIPAA privacy rule governs how researchers within health care organizations handle the health information of individuals; it also governs researchers who interact with such data (*21*). There are a number of ways this is done: through the law itself; its implementation in regulations (*21*); and Institutional Review Boards, which examine researchers' access and use of patient data, as well as by social controls. A researcher who is careless about the privacy of health records will find future access to such records very difficult.

Privacy and national security

An example that doesn't tend to appear when discussing privacy and big data is national-security collection. Yet the Snowden leaks disclosed massive collection both domestically and abroad. These disclosures started a national discussion on collection and use, although not, for obvious reasons, on notice and consent, which have little role in national-security collection.

I recently participated in a National Academies study on software alternatives to bulk signals intelligence collection (*22*). Bulk collection, specifically of telephony metadata—NSA receives daily downloads of telephony metadata (to, from, time, data, and length of call data) from major service providers—has generated much consternation. Metadata are data about the call, not its content, but mobile phones and the fact that cell phones are usually associated with a single individual mean that metadata themselves are remarkably revelatory (*23*, *24*). Both a presiden-

tially appointed review group on intelligence and communications technologies and the Privacy and Civil Liberties Oversight Board, an executive-branch oversight board, recommended ending the government telephony metadata program (*25*, *26*).

Our charge was somewhat different—technical alternatives to the collection—and our conclusion was also somewhat different. Because the program provides information that cannot be found in other ways, we believe there are no alternatives providing the same information (*22*). In particular, if past events become interesting in the present—a non-nuclear nation is discovered to be pursuing nuclear weapons or a new target is identified as a terrorist—past history may present new leads (*22*). Such past history will be available, in general, only if there were bulk collection in the past.

We made no judgment on whether the bulk collection program should continue; that is a policy decision, not a technical analysis, and out of scope for the study. We observed that the only way to protect privacy in the face of bulk collection is to control use—the same solution as the one to the private-sector big data collection issue.

We had no evidence that NSA was inappropriately using bulk data that were being collected. Nonetheless, we found that there were possible improvements for controlling use. We recommended increased utilization of automated controls and auditing, noting that manual controls and auditing will also always be necessary (*22*). Automating controls on data usage means data usage rules must be stated with great precision. That has its own advantages, including preventing inconsistencies (one such, on the meaning of archive, resulted in inappropriate access to the database) (*22*). Automated controls on data usage will also provide transparency. We also proposed research into privacy-protective methods of auditing by outsiders (*22*).

Controls on use

Our point was that "Controls on use … offer an alternative to controls on collection as a way of protecting privacy." The same is true outside the national-security domain. Privacy intrusions are everywhere. The technologies—smart phones and their apps; the ubiquity of Google, which performs 68% of searches in the United States (*27*) and over 90% in Europe (*28*); and Internet-connected sensors in automobiles, bridges, cargo trucks, and so forth—are novel, but the fact that technologies and changing social morés create privacy intrusions is not. In 1890, a similar situation—yellow journalism and hand-held cameras—induced Samuel Warren and Louis Brandeis to write "The right to privacy," which laid a foundation for U.S. privacy protections. Warren and Brandeis observed that, "it has been found necessary from time to time to define anew the exact nature and extent of such protection" (*29*). Today is such a time. The nature and extent of redefinition will be of control on use, and determining the right controls, and the right ways to exercise them, will be challenging—but that is what we must do.

REFERENCES

1. Secretary's Advisory Committee on Automated Personal Data Systems, U.S. Department of Health, Education, and Welfare, *Records, Computers and the Rights of Citizens* (HEW, Washington, DC, 1973).
2. OECD, *OECD Guidelines on the Protection of Privacy and Transborder Flows of Personal Data* (OECD, Brussels, 1980).
3. FTC, *Privacy Online: A Report to Congress* (FTC, Washington, DC, 1998).
4. A. M. McDonald, L. F. Cranor, *ISJLP* **4**, 540–565 (2008).
5. F. H. Cate, in *Consumer Protection in the Age of the 'Information Economy,'* J. K. Winn, Ed. (Ashgate Publishing, Burlington, VT, 2006), pp. 341–378.
6. PCAST, *Big Data and Privacy: A Technological Perspective* (White House, Washington, DC, 2014).
7. International Data Corporation, Smartphone OS Market Share, Q2, 2014; www.idc.com/prodserv/smartphone-os-market-share.jsp.
8. Google, Review App Permissions; https://support.google.com/googleplay/answer/6014972?hl=en.
9. C. Duhigg, *New York Times Sunday Magazine,* 19 February 2012, pp. MM30.
10. B. Voytek, Rides of Glory, Uber [blog] (2012); https://web.archive.org/web/20140827195715/http://blog.uber.com/ridesofglory.
11. S. Barocas, H. Nissenbaum, *Commun. ACM* **57**, 11 (2014).
12. H. Nissenbaum, *Wash. L. Rev.* **79**, 119–157 (2004).
13. White House, *Consumer Data Privacy in a Networked World: A Framework for Protecting Privacy and Promoting Innovation in the Global Digital Economy* (White House, Washington, DC, 2012).
14. FTC, *Protecting Consumer Privacy in an Era of Rapid Change: Recommendations for Businesses and Policymakers* (FTC, Washington, DC, 2012).
15. F. H. Cate, V. Mayer-Schonberger, *Int. Data Privacy L.* **3**, 67–73 (2013).
16. A. Alter, *Wall Street Journal*, 19 July 2012; http://on.wsj.com/1KsLM1K.
17. O. Seneviratne, L. Kagal, *IEEE International Symposium on Policies for Distributed Systems and Networks* (IEEE, 2011), pp. 141–144.
18. National Institute for Standards and Technology, National Strategy for Trusted Identities in Cyberspace (NSTIC); www.nist.gov/nstic/.
19. Georgia Tech Research Institute, GTRI NSTIC Trustmark Pilot (2014); https://trustmark.gtri.gatech.edu/operational-pilot/trustmark-definitions/ficam-privacy-activity-tracking-requirements-for-csps-and-bae-responders/1.0/.
20. Fair Credit Reporting Act, 15 USC §1681.
21. Centers for Disease Control, HIPPA Privacy Rule and Public Health; www.cdc.gov/Mmwr/Preview/Mmwrhtml/M2e411a1.Htm.
22. Committee on Responding to Section 5(d) of Presidential Policy Directive 28: The Feasibility of Software to Provide Alternatives to Bulk Signals Intelligence Collection, National Research Council, *Bulk Collection of Signals Intelligence: Technical Options* (National Academy of Sciences, Washington, DC, 2014); www.nap.edu/catalog/19414/bulk-collection-of-signals-intelligence-technical-options.
23. S. Landau, *Surveillance or Security? The Risks Posed by New Wiretapping Technologies* (MIT Press, Cambridge, MA, 2011).
24. J. Mayer, P. Mutchler "Metaphone: The sensitivity of telephone metadata" (2014); http://webpolicy.org/2014/03/12/metaphone-the-sensitivity-of-telephone-metadata/.
25. President's Review Committee on Intelligence and Communications Technologies, *Liberty and Security in a Changing World* (White House, Washington, DC, 2013).
26. Privacy and Civil Liberties Oversight Board, *Report on the Telephone Records Program Conducted Under Section 215 of the USA PATRIOT Act and on the Operations of the Foreign Intelligence Surveillance Court* (White House, Washington, DC, 2014).
27. comScore Releases March 2014 U.S. Search Engine Rankings; https://www.comscore.com/Insights/Press-Releases/2014/4/comScore-Releases-March-2014-U.S.-Search-Engine-Rankings.
28. J. Kanter, *New York Times*, 4 September 2014; http://nyti.ms/1tTrIX9.
29. S. Warren, L. Brandeis, *Harv. Law Rev.* **4**, 193 (1890).

What the "right to be forgotten" means for privacy in a digital age

Abraham L. Newman*

Despite the attention the right has received, we should not forget that it is just one innovative piece of a comprehensive privacy framework that must be implemented locally and enforced globally.

Has Europe upended Internet privacy and free speech with its decision to create a "right to be forgotten"? In May 2014, the European Court of Justice ruled that European citizens have the right to request that search engines delink results to items that are considered inaccurate, irrelevant, or excessive (*1*). In the specific case, a Spanish citizen asked that Google remove a link to a newspaper account of his home foreclosure, a debt he had subsequently paid. In essence, this right acknowledges the stickiness of digital footprints. Photos, court records, and letters that used to get lost in file cabinets are neatly organized and accessible from our laptops. A childhood foible can haunt someone for a lifetime. The right reasserts our human instinct for redemption and forgiveness in the digital age (*2*).

This debate matters not only for how individuals use the right to be forgotten but also as a window into privacy protection more generally. In this essay, I review the controversies surrounding the European decision, describe where the right fits into a broader privacy protection framework, and discuss several implications of the debate. In particular, I argue that the right to be forgotten highlights differences in privacy protection across the globe, marks the emergence of distributed regulatory approaches, and underscores the importance of the international context for successful privacy policy.

Critics of the ruling claim that it will bring the demise of everything from Internet search to free speech (*3*). Search firms will be saddled with the excessive costs associated with processing requests to remove links, and individuals who exercise the right will disrupt free expression by altering search results. In the first five months since the ruling, Google has processed roughly 180,000 requests of which it accepted 40% (*4*). Although review requests are no doubt cumbersome for search firms, they do not appear to pose an insurmountable technical or financial burden. Google's stock in December 2014 is close to its 5-year high and enjoys a market capitalization at over $360 billion. Search firms from Google to DuckDuckGo must be prepared to respond to takedown requests ranging from libel and defa-

Associate Professor in the Edmund A. Walsh School of Foreign Service at Georgetown University, Washington, DC 20057, USA.
*Corresponding author. E-mail: aln24@georgetown.edu

mation to copyright, which far outpace the right to be forgotten. In the week of 1 December 2014, for example, Google received copyright takedown requests concerning more than 9 million links (*4*).

In terms of free speech, the European Court decision did not create a right that trumps all others but explicitly called for a balance between the right to be forgotten and other interests. Moreover, the effect of the decision on speech is limited as it does not require the deletion of the original content but rather the delinking of that content from search results. It takes us back to a world where people might have to go to a city hall or library to research past debts rather than instantly downloading them.

The stakes of data correction for consumers can be high. A 2012 study by the Federal Trade Commission in the United States estimates that one in four individuals have an error in their credit report that could affect their credit score (*5*). A 2014 lawsuit filed by the State of Mississippi against Experian, one of the largest credit reporting agencies in the United States, suggests that Experian produces reports with errors and that consumers have considerable difficulty correcting them (*6*). These errors affect the ability of millions of Americans to get competitive interest rates for home and auto loans, obtain security clearances, or pass rental applications.

When considering a privacy framework, however, rules about data correction and erasure are just one piece of the puzzle. Equally vital, if not more important, are rules that govern how data can be collected and then used by other parties that were not involved in the original data collection. Can a company like Uber (the app-based transportation network and taxi company) collect and store location data from individuals as they use their services; can those data be used for purposes other than securing transportation; can it then share that data with other companies or the government; and can it store data even after a customer has cancelled an account? The right to be forgotten is just one piece of a comprehensive data privacy framework that would include rules surrounding data collection and how data are then used, analyzed, shared, and secured (*7*).

Privacy is not dead

The right to be forgotten is a potent reminder that Europe has developed such a comprehensive approach and stands in sharp contrast to U.S.

privacy policies. The European Court of Justice's decision builds upon a coherent and robust privacy framework in both the European Union and its member countries that includes rules concerning the collection, use, and storage of personal data in the public and private sector. These rules are overseen by independent national regulatory agencies known as data privacy authorities. Originally, the regulations were based in national laws dating back to the 1970s, but the European Union has taken on a greater role in this domain since the passage of the Data Privacy Directive in 1995 (*8*). In this system, big players like eBay or IBM work closely with regulators and implement internal data privacy policies in order to prevent data privacy scandals (*9*).

In contrast to the European system, the United States has a fragmented, patchwork approach to privacy regulation. With the passage of the Privacy Act in 1973, the United States focused privacy rules on data collection by the federal government along with a limited number of regulations covering a varied and idiosyncratic set of private-sector activities. The United States is notorious for having stronger privacy protections for video rentals than online marketing. Moreover, as the lines between sectors such as telecommunications, marketing, and finance merge, such divisions become less and less tenable. Equally important, there is no single regulator dedicated to overseeing the implementation and enforcement of disparate regulations (*10*).

The different approaches to privacy in Europe and the United States shape how governments and firms process and share personal information. In the United States, for example, nearly 100% of the population has a private-sector credit report, including "positive" information ranging from income to purchasing patterns. These types of data are routinely used to construct predictive scores such as the Consumer Profitability Score or the Individual Health Risk Score (*11*). In France, roughly 3% of the population has a credit report, which details "negative" information, such as defaults or missed payments, and as a result, there are far fewer predictive scores (*12*). European privacy rules are not a panacea for the immense challenges posed by digital technologies, but they offer a strikingly different set of ground rules from which to begin the debate.

Distributed regulation

The right to be forgotten is part of a trend in privacy protection toward distributed regulation, in which regulators rely on individuals and firms to monitor and implement regulations. Such legislation leverages the large number of consumers across the economy to be part of the regulatory process. Transparency, accountability, and class-action remedies encourage consumer advocacy groups to organize and hold firms and governments accountable to the rules.

At the same time as consumer groups press for action (*13*), private firms increasingly carry out remedies. Companies, such as Google or Microsoft, have been deputized (in consultation with data privacy authorities) to evaluate and implement

delinking requests. Whereas involving companies in the solutions has the benefit of distributing the task of enforcement, it raises the real risk of delegating sensitive issues like free speech regulation to corporations.

The right to be forgotten's emphasis on distributed regulation is similar to data breach laws that emerged from state-level experimentation in the United States. These laws require firms to notify customers when their personal data have been lost or stolen. California was among the first jurisdictions to adopt such rules in 2002, which have now spread to all U.S. states except Alabama, New Mexico, and South Dakota. Europe adopted similar rules in 2013 for telecommunications and Internet service providers and will pass more encompassing rules as part of the General Data Protection Regulation, which will be adopted in 2015 (*14*). These laws have had a number of important impacts. Firms that encrypt their data are exempt from notification requirements, and so they have increased the use of encryptions. And although critics have argued that consumers may become fatigued by notices, data breach rules have raised the salience of the issue to a top-level executive concern that might have previously been squirreled away in an information technology department. Finally, they put firms in the position of providing an important remedy by making credit report checks available to affected customers (*15*). These distributed regulatory policies do not eliminate more traditional forms of regulation, such as direct oversight or sanction, but expand the toolbox.

Privacy goes global

Describing the European and U.S. approaches to privacy separately misses the important ways in which data protection is increasingly international. In today's digital world, information flows routinely cross borders, and such data flows are carried out by a handful of large technology and telecommunications firms. Citizens from Germany to Brazil must trust largely American companies like Google or Cisco to protect their privacy rights.

The right to be forgotten demonstrates the limits of national data privacy systems in a world of transnational data flows. In the wake of the European Court of Justice decision, once a delinking request has been approved, Google removes the link in the national domain name environment (for example, google.de, in Germany), while maintaining the link in other domains (such as the global google.com). Critics have argued that this negates the right as the offending information is still available on other domain name platforms. In November 2014, European privacy regulators made this concern official by recommending that companies respect such right-to-be-forgotten decisions globally (*16*) (Fig. 1).

The mismatch between regulatory jurisdiction and the transnational flow of information is a much more general phenomenon that plagues privacy protection. As revealed by the recent scandal involving the U.S. National Security Agency (NSA), personal data are often transmitted across networks that span countries. As companies employ

Fig. 1. How long will digital shadows remain? Shadows of members of a panel are seen on a wall before a meeting about the "right to be forgotten," in Madrid, 9 September 2014. [REUTERS/ANDREA COMAS]

more sophisticated surveillance techniques such as Super Cookies (*17*), these concerns are not limited to covert government activity. Data havens could emerge similar to tax havens, in which firms store data in jurisdictions with weak privacy rules.

To address these challenges, Europe has attempted to extend its jurisdiction beyond its borders (*8*). An important component of the European privacy system is that it limits data transfers to jurisdictions like the United States that do not have "adequate" protections in place. This has led many major information technology firms, such as Amazon and Google, to quarantine data about European citizens within European data centers. The NSA scandal has accelerated this trend, with U.S.-based cloud computing firms, for example, expecting to lose 20% of their business in foreign markets (*18*). In other words, the regulation of U.S. information technology companies is increasingly being set in Berlin or Brussels.

The right to be forgotten has energized a debate concerning privacy on the Internet. In particular, it has the potential to mobilize consumers to become involved in the process and to provide a new way to minimize the harms associated with the publicity of inaccurate or outdated information. At the same time, it needs to be kept in context of a broader privacy framework that considers how personal information is collected, shared, used, and secured. The European model offers one such approach. And that approach has been widely adopted outside of the United States in countries ranging from Canada to Argentina (*8*). National or regional privacy solutions, however, will face considerable difficulties if other countries, like the United States, maintain weak privacy systems that give safe haven to data brokers. Distributed regulatory tools, such as the right to be forgotten, as well as the broader comprehensive privacy framework's success will depend in large part on Europe's commitment to defending its system globally even if that means enforcing its rules across borders and periodically taking U.S. firms to task.

REFERENCES

1. European Commission, "Factsheet on the 'right to be forgotten' ruling" (C-131/12, EC, Brussels, 2014); http://ec.europa.eu/justice/data-protection/files/factsheets/factsheet_data_protection_en.pdf
2. V. Mayer-Schonberger, *Delete: The Virtues of Forgetting in the Digital Age* (Princeton Univ. Press, Princeton, NJ, 2011).
3. Editors, *New York Times*, 14 May 2014, p. A26; http://nyti.ms/1tOQdiJ.
4. Google, Transparency Report: European Privacy Requests for Search Removals (Google, 2014); https://www.google.com/transparencyreport/removals/europeprivacy/?hl=en.
5. Federal Trade Commission, "Report to Congress under section 319 of the Fair and Accurate Credit Transaction Act of 2003" (FTC, Washington, DC, 2012).
6. J. Horwitz, *Columbus Dispatch*, 17 June 2014; http://bit.ly/1yAX1Bt.
7. D. Solove, P. Schwartz, *Information Privacy Law* (Wolters Kluwer, New York, 2014).
8. A. Newman, *Protectors of Privacy: Regulating Personal Data in the Global Economy* (Cornell Univ. Press, Ithaca, NY, 2008).
9. F. Bignami, *Am. J. Comp. Law* **59**, 411–461 (2011).
10. P. Regan, *Legislating Privacy: Technology, Social Values, and Public Policy* (Univ. of North Carolina Press, Raleigh, 1995).
11. P. Dixon, R. Gellman, "The scoring of America: How secret consumer scores threaten your privacy and your future" (World Privacy Forum, San Diego, CA, 2014).
12. N. Jentzsch, *Financial Privacy: An International Comparison of Credit Reporting Systems* (Springer, Berlin, 2007).
13. C. Bennett, *Privacy Advocates: Resisting the Spread of Surveillance* (MIT Press, Cambridge, MA, 2008).
14. European Commission, Commission proposes comprehensive reform of data protection rules [news release] (EC, Brussels, 2012); http://ec.europa.eu/justice/newsroom/data-protection/news/120125_en.htm.
15. Experian, "Data breach industry forecasts" (Experian, Costa Mesa, CA, 2015); www.experian.com/assets/data-breach/white-papers/2015-industry-forecast-experian.pdf?_ga=1.172114915.1943093614.1418003182.
16. S. Schechner, F. Robinson, *Wall Street Journal*, 26 November 2014; http://on.wsj.com/1xFhvI4.
17. C. Timberg, *Washington Post*, 3 November 2014; http://wapo.st/1FnxzmQ.
18. C. Miller, *New York Times*, 22 March 2014), p. A1; http://nyti.ms/141KBEY.

Privacy and human behavior in the age of information

Alessandro Acquisti,[1]* Laura Brandimarte,[1] George Loewenstein[2]

This Review summarizes and draws connections between diverse streams of empirical research on privacy behavior. We use three themes to connect insights from social and behavioral sciences: people's uncertainty about the consequences of privacy-related behaviors and their own preferences over those consequences; the context-dependence of people's concern, or lack thereof, about privacy; and the degree to which privacy concerns are malleable—manipulable by commercial and governmental interests. Organizing our discussion by these themes, we offer observations concerning the role of public policy in the protection of privacy in the information age.

I f this is the age of information, then privacy is the issue of our times. Activities that were once private or shared with the few now leave trails of data that expose our interests, traits, beliefs, and intentions. We communicate using e-mails, texts, and social media; find partners on dating sites; learn via online courses; seek responses to mundane and sensitive questions using search engines; read news and books in the cloud; navigate streets with geotracking systems; and celebrate our newborns, and mourn our dead, on social media profiles. Through these and other activities, we reveal information—both knowingly and unwittingly—to one another, to commercial entities, and to our governments. The monitoring of personal information is ubiquitous; its storage is so durable as to render one's past undeletable (1)—a modern digital skeleton in the closet. Accompanying the acceleration in data collection are steady advancements in the ability to aggregate, analyze, and draw sensitive inferences from individuals' data (2).

Both firms and individuals can benefit from the sharing of once hidden data and from the application of increasingly sophisticated analytics to larger and more interconnected databases (3). So too can society as a whole—for instance, when electronic medical records are combined to observe novel drug interactions (4). On the other hand, the potential for personal data to be abused—for economic and social discrimination, hidden influence and manipulation, coercion, or censorship—is alarming. The erosion of privacy can threaten our autonomy, not merely as consumers but as citizens (5). Sharing more personal data does not necessarily always translate into more progress, efficiency, or equality (6).

Because of the seismic nature of these developments, there has been considerable debate about individuals' ability to navigate a rapidly evolving privacy landscape, and about what, if anything, should be done about privacy at a policy level. Some trust people's ability to make self-interested

decisions about information disclosing and withholding. Those holding this view tend to see regulatory protection of privacy as interfering with the fundamentally benign trajectory of information technologies and the benefits such technologies may unlock (7). Others are concerned about the ability of individuals to manage privacy amid increasingly complex trade-offs. Traditional tools for privacy decision-making such as choice and consent, according to this perspective, no longer provide adequate protection (8). Instead of individual responsibility, regulatory intervention may be needed to balance the interests of the subjects of data against the power of commercial entities and governments holding that data.

Are individuals up to the challenge of navigating privacy in the information age? To address this question, we review diverse streams of empirical privacy research from the social and behavioral sciences. We highlight factors that influence decisions to protect or surrender privacy and how, in turn, privacy protections or violations affect people's behavior. Information technologies have progressively encroached on every aspect of our personal and professional lives. Thus, the problem of control over personal data has become inextricably linked to problems of personal choice, autonomy, and socioeconomic power. Accordingly, this Review focuses on the concept of, and literature around, informational privacy (that is, privacy of personal data) but also touches on other conceptions of privacy, such as anonymity or seclusion. Such notions all ultimately relate to the permeable yet pivotal boundaries between public and private (9).

We use three themes to organize and draw connections between streams of privacy research that, in many cases, have unfolded independently. The first theme is people's uncertainty about the nature of privacy trade-offs, and their own preferences over them. The second is the powerful context-dependence of privacy preferences: The same person can in some situations be oblivious to, but in other situations be acutely concerned about, issues of privacy. The third theme is the malleability of privacy preferences, by which we mean that privacy preferences are subject to

influence by those possessing greater insight into their determinants. Although most individuals are probably unaware of the diverse influences on their concern about privacy, entities whose interests depend on information revelation by others are not. The manipulation of subtle factors that activate or suppress privacy concern can be seen in myriad realms—such as the choice of sharing defaults on social networks, or the provision of greater control on social media—which creates an illusion of safety and encourages greater sharing.

Uncertainty, context-dependence, and malleability are closely connected. Context-dependence is amplified by uncertainty. Because people are often "at sea" when it comes to the consequences of, and their feelings about, privacy, they cast around for cues to guide their behavior. Privacy preferences and behaviors are, in turn, malleable and subject to influence in large part because they are context-dependent and because those with an interest in information divulgence are able to manipulate context to their advantage.

Uncertainty

Individuals manage the boundaries between their private and public spheres in numerous ways: via separateness, reserve, or anonymity (10); by protecting personal information; but also through deception and dissimulation (11). People establish such boundaries for many reasons, including the need for intimacy and psychological respite and the desire for protection from social influence and control (12). Sometimes, these motivations are so visceral and primal that privacy-seeking behavior emerges swiftly and naturally. This is often the case when physical privacy is intruded—such as when a stranger encroaches in one's personal space (13–15) or demonstratively eavesdrops on a conversation. However, at other times (often including when informational privacy is at stake) people experience considerable uncertainty about whether, and to what degree, they should be concerned about privacy.

A first and most obvious source of privacy uncertainty arises from incomplete and asymmetric information. Advancements in information technology have made the collection and usage of personal data often invisible. As a result, individuals rarely have clear knowledge of what information other people, firms, and governments have about them or how that information is used and with what consequences. To the extent that people lack such information, or are aware of their ignorance, they are likely to be uncertain about how much information to share.

Two factors exacerbate the difficulty of ascertaining the potential consequences of privacy behavior. First, whereas some privacy harms are tangible, such as the financial costs associated with identity theft, many others, such as having strangers become aware of one's life history, are intangible. Second, privacy is rarely an unalloyed good; it typically involves trade-offs (16). For example, ensuring the privacy of a consumer's

[1]H. John Heinz III College, Carnegie Mellon University, Pittsburgh, PA, USA. [2]Dietrich College, Social and Decision Sciences, Carnegie Mellon University, Pittsburgh, PA, USA.
*Corresponding author. E-mail: acquisti@andrew.cmu.edu

purchases may protect her from price discrimination but also deny her the potential benefits of targeted offers and advertisements.

Elements that mitigate one or both of these exacerbating factors, by either increasing the tangibility of privacy harms or making trade-offs explicit and simple to understand, will generally affect privacy-related decisions. This is illustrated by one laboratory experiment in which participants were asked to use a specially designed search engine to find online merchants and purchase from them, with their own credit cards, either a set of batteries or a sex toy (*17*). When the search engine only provided links to the merchants' sites and a comparison of the products' prices from the different sellers, a majority of participants did not pay any attention to the merchants' privacy policies; they purchased from those offering the lowest price. However, when the search engine also provided participants with salient, easily accessible information about the differences in privacy protection afforded by the various merchants, a majority of participants paid a roughly 5% premium to buy products from (and share their credit card information with) more privacy-protecting merchants.

A second source of privacy uncertainty relates to preferences. Even when aware of the consequences of privacy decisions, people are still likely to be uncertain about their own privacy preferences. Research on preference uncertainty (*18*) shows that individuals often have little sense of how much they like goods, services, or other people. Privacy does not seem to be an exception. This can be illustrated by research in which people were asked sensitive and potentially incriminating questions either point-blank, or followed by credible assurances of confidentiality (*19*). Although logically such assurances should lead to greater divulgence, they often had the opposite effect because they elevated respondents' privacy concerns, which without assurances would have remained dormant.

The remarkable uncertainty of privacy preferences comes into play in efforts to measure individual and group differences in preference for privacy (*20*). For example, Westin (*21*) famously used broad (that is, not contextually specific) privacy questions in surveys to cluster individuals into privacy segments: privacy fundamentalists, pragmatists, and unconcerned. When asked directly, many people fall in the first segment: They profess to care a lot about privacy and express particular concern over losing control of their personal information or others gaining unauthorized access to it (*22, 23*). However, doubts about the power of attitudinal scales to predict actual privacy behavior arose early in the literature (*24*). This discrepancy between attitudes and behaviors has become known as the "privacy paradox."

In one early study illustrating the paradox, participants were first classified into categories of privacy concern inspired by Westin's categorization based on their responses to a survey dealing with attitudes toward sharing data (*25*). Next, they were presented with products

to purchase at a discount with the assistance of an anthropomorphic shopping agent. Few, regardless of the group they were categorized in, exhibited much reluctance to answering the increasingly sensitive questions the agent plied them with.

Why do people who claim to care about privacy often show little concern about it in their daily behavior? One possibility is that the paradox is illusory—that privacy attitudes, which are defined broadly, and intentions and behaviors, which are defined narrowly, should not be expected to be closely related (*26, 27*). Thus, one might care deeply about privacy in general but, depending on the costs and benefits prevailing in a specific situation, seek or not seek privacy protection (*28*).

This explanation for the privacy paradox, however, is not entirely satisfactory for two reasons. The first is that it fails to account for situations in which attitude-behavior dichotomies arise under high correspondence between expressed concerns and behavioral actions. For example, one study compared attitudinal survey answers to actual social media behavior (*29*). Even within the subset of participants who expressed the highest degree of concern over strangers being able to easily find out their sexual orientation, political views, and partners' names, 48% did in fact publicly reveal their sexual orientation online, 47% revealed their political orientation, and 21% revealed their current partner's name. The second reason is that privacy decision-making is only in part the result of a rational "calculus" of costs and benefits (*16, 28*); it is also affected by misperceptions of those costs and benefits, as well as social norms, emotions, and heuristics. Any of these factors may affect behavior differently from how they affect attitudes. For instance, present-bias can cause even the privacy-conscious to engage in risky revelations of information, if the immediate gratification from disclosure trumps the delayed, and hence discounted, future consequences (*30*).

Preference uncertainty is evident not only in studies that compare stated attitudes with behaviors, but also in those that estimate monetary valuations of privacy. "Explicit" investigations ask people to make direct trade-offs, typically between privacy of data and money. For instance, in a study conducted both in Singapore and the United States, students made a series of hypothetical choices about sharing information with websites that differed in protection of personal information and prices for accessing services (*31*). Using conjoint analysis, the authors concluded that subjects valued protection against errors, improper access, and secondary use of personal information between $30.49 and $44.62. Similar to direct questions about attitudes and intentions, such explicit investigations of privacy valuation spotlight privacy as an issue that respondents should take account of and, as a result, increase the weight they place on privacy in their responses.

Implicit investigations, in contrast, infer valuations of privacy from day-to-day decisions in

which privacy is only one of many considerations and is typically not highlighted. Individuals engage in privacy-related transactions all the time, even when the privacy trade-offs may be intangible or when the exchange of personal data may not be a visible or primary component of a transaction. For instance, completing a query on a search engine is akin to selling personal data (one's preferences and contextual interests) to the engine in exchange for a service (search results). "Revealed preference" economic arguments would then conclude that because technologies for information sharing have been enormously successful, whereas technologies for information protection have not, individuals hold overall low valuations of privacy. However, that is not always the case: Although individuals at times give up personal data for small benefits or discounts, at other times they voluntarily incur substantial costs to protect their privacy. Context, as further discussed in the next section, matters.

In fact, attempts to pinpoint exact valuations that people assign to privacy may be misguided, as suggested by research calling into question the stability, and hence validity, of privacy estimates. In one field experiment inspired by the literature on endowment effects (*32*), shoppers at a mall were offered gift cards for participating in a non-sensitive survey. The cards could be used online or in stores, just like debit cards. Participants were given either a $10 "anonymous" gift card (transactions done with that card would not be traceable to the subject) or a $12 trackable card (transactions done with that card would be linked to the name of the subject). Initially, half of the participants were given one type of card, and half the other. Then, they were all offered the opportunity to switch. Some shoppers, for example, were given the anonymous $10 card and were asked whether they would accept $2 to "allow my name to be linked to transactions done with the card"; other subjects were asked whether they would accept a card with $2 less value to "prevent my name from being linked to transactions done with the card." Of the subjects who originally held the less valuable but anonymous card, five times as many (52.1%) chose it and kept it over the other card than did those who originally held the more valuable card (9.7%). This suggests that people value privacy more when they have it than when they do not.

The consistency of preferences for privacy is also complicated by the existence of a powerful countervailing motivation: the desire to be public, share, and disclose. Humans are social animals, and information sharing is a central feature of human connection. Social penetration theory (*33*) suggests that progressively increasing levels of self-disclosure are an essential feature of the natural and desirable evolution of interpersonal relationships from superficial to intimate. Such a progression is only possible when people begin social interactions with a baseline level of privacy. Paradoxically, therefore, privacy provides an essential foundation for intimate disclosure. Similar to privacy, self-disclosure confers numerous objective and subjective benefits, including psychological

and physical health (*34, 35*). The desire for interaction, socialization, disclosure, and recognition or fame (and, conversely, the fear of anonymous unimportance) are human motives no less fundamental than the need for privacy. The electronic media of the current age provide unprecedented opportunities for acting on them. Through social media, disclosures can build social capital, increase self-esteem (*36*), and fulfill ego needs (*37*). In a series of functional magnetic resonance imaging experiments, self-disclosure was even found to engage neural mechanisms associated with reward; people highly value the ability to share thoughts and feelings with others. Indeed, subjects in one of the experiments were willing to forgo money in order to disclose about themselves (*38*).

Context-dependence

Much evidence suggests that privacy is a universal human need (Box 1) (*39*). However, when people are uncertain about their preferences they often search for cues in their environment to provide guidance. And because cues are a function of context, behavior is as well. Applied to privacy, context-dependence means that individuals can, depending on the situation, exhibit anything ranging from extreme concern to apathy about privacy. Adopting the terminology of Westin, we are all privacy pragmatists, privacy fundamentalists, or privacy unconcerned, depending on time and place (*40*).

The way we construe and negotiate public and private spheres is context-dependent because the boundaries between the two are murky (*41*): The rules people follow for managing privacy vary by situation, are learned over time, and are based on cultural, motivational, and purely situational criteria. For instance, usually we may be more comfortable sharing secrets with friends, but at times we may reveal surprisingly personal information to a stranger on a plane (*42*). The theory of contextual "integrity" posits that social expectations affect our beliefs regarding what is private and what is public, and that such expectations vary with specific contexts (*43*). Thus, seeking privacy in public is not a contradiction; individuals can manage privacy even while sharing information, and even on social media (*44*). For instance, a longitudinal study of actual disclosure behavior of online social network users highlighted that over time, many users increased the amount of personal information revealed to their friends (those connected to them on the network) while simultaneously decreasing the amounts revealed to strangers (those unconnected to them) (Fig. 1) (*45*).

The cues that people use to judge the importance of privacy sometimes result in sensible behavior. For instance, the presence of government regulation has been shown to reduce consumer concern and increase trust; it is a cue that people use to infer the existence of some degree of privacy protection (*46*). In other situations, however, cues can be unrelated, or even negatively related,

to normative bases of decision-making. For example, in one online experiment (*47*) individuals were more likely to reveal personal and even incriminating information on a website with an unprofessional and casual design with the banner "How Bad R U" than on a site with a formal interface—even though the site with the formal interface was judged by other respondents to be much safer (Fig. 2). Yet in other situations, it is the physical environment that influences privacy concern and associated behavior (*48*), sometimes even unconsciously. For instance, all else being equal, intimacy of self-disclosure is higher in warm, comfortable rooms, with soft lighting, than in cold rooms with bare cement and overhead fluorescent lighting (*49*).

Some of the cues that influence perceptions of privacy are one's culture and the behavior of other people, either through the mechanism of descriptive norms (imitation) or via reciprocity (*50*). Observing other people reveal information increases the likelihood that one will reveal it oneself (*51*). In one study, survey-takers were asked a series of sensitive personal questions regarding their engagement in illegal or ethically questionable behaviors. After answering each question, participants were provided with information, manipulated unbeknownst to them, about the percentage of other participants who in the same survey had admitted to having engaged in a given behavior. Being provided with information that suggested that a majority of survey takers had admitted a certain questionable behavior increased participants' willingness to disclose their engagement in other, also sensitive, behaviors. Other studies have found that the tendency to reciprocate information disclosure is so ingrained that people will reveal more information even to a computer agent that provides information about itself (*52*). Findings such as this may help to explain the escalating amounts of self-disclosure we witness online: If others are doing it, people seem to reason unconsciously, doing so oneself must be desirable or safe.

Other people's behavior affects privacy concerns in other ways, too. Sharing personal information with others makes them "co-owners" of that information (*53*) and, as such, responsible for its protection. Mismanagement of shared information by one or more co-owners causes "turbulence" of the privacy boundaries and, consequently, negative reactions, including anger or mistrust. In a study of undergraduate Facebook users (*54*), for instance, turbulence of privacy boundaries, as a result of having one's profile exposed to unintended audiences, dramatically increased the odds that a user would restrict profile visibility to friends-only.

Likewise, privacy concerns are often a function of past experiences. When something in an environment changes, such as the introduction of a camera or other monitoring devices, privacy concern is likely to be activated. For instance, surveillance can produce discomfort (*55*) and negatively affect worker productivity (*56*). However, privacy concern, like other motivations, is adaptive; people get used to levels of intrusion that do not

Fig. 1. Endogenous privacy behavior and exogenous shocks. Privacy behavior is affected both by endogenous motivations (for instance, subjective preferences) and exogenous factors (for instance, changes in user interfaces). Over time, the percentage of members in the Carnegie Mellon University Facebook network who chose to publicly reveal personal information decreased dramatically. For instance, over 80% of profiles publicly revealed their birthday in 2005, but less than 20% in 2011. The decreasing trend is not uniform, however. After decreasing for several years, the percentage of profiles that publicly revealed their high school roughly doubled between 2009 and 2010—after Facebook changed the default visibility settings for various fields on its profiles, including high school (bottom), but not birthday (top) (*45*).

Disclosure behavior in online social media

Percentage of profiles publicly revealing information over time (2005-2011)

Shares **birthday** publicly on profile

Shares **high school** publicly on profile

change over time. In an experiment conducted in Helsinki (57), the installation of sensing and monitoring technology in households led family members initially to change their behavior, particularly in relation to conversations, nudity, and sex. And yet, if they accidentally performed an activity, such as walking naked into the kitchen in front of the sensors, it seemed to have the effect of "breaking the ice"; participants then showed less concern about repeating the behavior. More generally, participants became inured to the presence of the technology over time.

The context-dependence of privacy concern has major implications for the risks associated with modern information and communication technology (58). With online interactions, we no longer have a clear sense of the spatial boundaries of our listeners. Who is reading our blog post? Who is looking at our photos online? Adding complexity to privacy decision-making, boundaries between public and private become even less defined in the online world (59) where we become social media friends with our coworkers and post pictures to an indistinct flock of followers. With different social groups mixing on the Internet, separating online and offline identities and meeting our and others' expectations regarding privacy becomes more difficult and consequential (60).

Malleability and influence

Whereas individuals are often unaware of the diverse factors that determine their concern about privacy in a particular situation, entities whose prosperity depends on information revelation by others are much more sophisticated. With the emergence of the information age, growing institutional and economic interests have developed around disclosure of personal information, from online social networks to behavioral advertising. It is not surprising, therefore, that some entities have an interest in, and have developed expertise in, exploiting behavioral and psychological processes to promote disclosure (61). Such efforts play on the malleability of privacy preferences, a term we use to refer to the observation that various, sometimes subtle, factors can be used to activate or suppress privacy concerns, which in turn affect behavior.

Default settings are an important tool used by different entities to affect information disclosure. A large body of research has shown that default settings matter for decisions as important as organ donation and retirement saving (62). Sticking to default settings is convenient, and people often interpret default settings as implicit recommendations (63). Thus, it is not surprising that default settings for one's profile's visibility on social networks (64), or the existence of opt-in or opt-out privacy policies on websites (65), affect individuals' privacy behavior (Fig. 3).

In addition to default settings, websites can also use design features that frustrate or even confuse users into disclosing personal information (66), a practice that has been referred to as "malicious interface design" (67). Another obvious strategy that commercial entities can use to avoid raising privacy concerns is not to "ring alarm bells"

when it comes to data collection. When companies do ring them—for example, by using overly fine-tuned personalized advertisements—consumers are alerted (68) and can respond with negative "reactance" (69).

Various so-called "antecedents" (70) affect privacy concerns and can be used to influence privacy behavior. For instance, trust in the entity receiving one's personal data soothes concerns. Moreover, because some interventions that are intended to protect privacy can establish trust, con-

cerns can be muted by the very interventions intended to protect privacy. Perversely, 62% of respondents to a survey believed (incorrectly) that the existence of a privacy policy implied that a site could not share their personal information without permission (40), which suggests that simply posting a policy that consumers do not read may lead to misplaced feelings of being protected.

Control is another feature that can inculcate trust and produce paradoxical effects. Perhaps because of its lack of controversiality, control has

---

Box 1. Privacy: A modern invention?

Is privacy a modern, bourgeois, and distinctly Western invention? Or are privacy needs a universal feature of human societies? Although access to privacy is certainly affected by socioeconomic factors (87) [some have referred to privacy as a "luxury good" (15)], and privacy norms greatly differ across cultures (65, 85), the need for privacy seems to be a universal human trait. Scholars have uncovered evidence of privacy-seeking behaviors across peoples and cultures separated by time and space: from ancient Rome and Greece (39, 88) to preindustrialized Javanese, Balinese, and Tuareg societies (89, 90). Privacy, as Altman (91) noted, appears to be simultaneously culturally specific and culturally universal. Cues of a common human quest for privacy are also found in the texts of ancient religions: The Quran (49:12) instructs against spying on one another (92); the Talmud (Bava Batra 60a) advises home-builders to position windows so that they do not directly face those of one's neighbors (93); the Bible (Genesis, 3:7) relates how Adam and Eve discovered their nakedness after eating the fruit of knowledge and covered themselves in shame from the prying eyes of God (94) [a discussion of privacy in Confucian and Taoist cultures is available in (95)]. Implicit in this heterogeneous selection of historical examples is the observation that there exist multiple notions of privacy. Although contemporary attention focuses on informational privacy, privacy has been also construed as territorial and physical, and linked to concepts as diverse as surveillance, exposure, intrusion, insecurity, appropriation, as well as secrecy, protection, anonymity, dignity, or even freedom [a taxonomy is provided in (9)].

Fig. 2. The impact of cues on disclosure behavior. A measure of privacy behavior often used in empirical studies is a subject's willingness to answer personal, sometimes sensitive questions— for instance, by admitting or denying having engaged in questionable behaviors. In an online experiment (47), individuals were asked a series of intrusive questions about their behaviors, such as "Have you ever tried to peek at someone else's e-mail without them knowing?" Across conditions, the interface of the questionnaire was manipulated to look more or less professional. The y axis captures the mean affirmative admission rates (AARs) to questions that were rated as intrusive (the proportion of questions answered affirmatively) normed, question by question, on the overall average AAR for the question. Subjects revealed more personal and even incriminating information on the website with a more casual design, even though the site with the formal interface was judged by other respondents to be much safer. The study illustrates how cues can influence privacy behavior in a fashion that is unrelated, or even negatively related, to normative bases of decision-making.

A measure of privacy behavior

Relative admission rates in an experiment testing the impact of different survey interfaces on willingness to answer questions about various sensitive behaviors

$F_{2,196} = 6.8$, $P = 0.001$
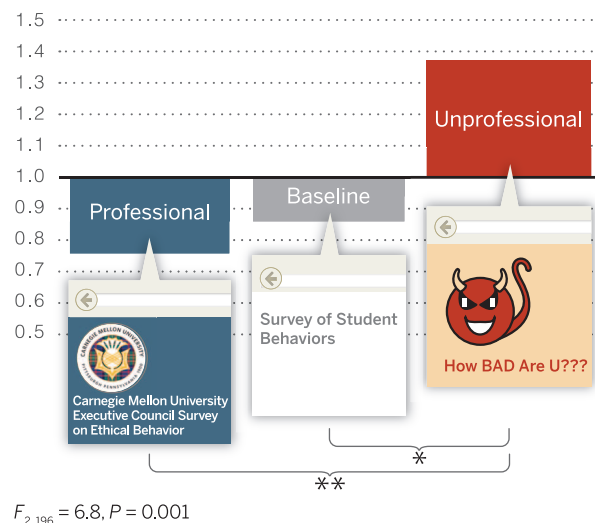
Fig. 3. Changes in Facebook default profile visibility settings over time (2005–2014).
Over time, Facebook profiles included an increasing amount of fields and, therefore, types of data. In addition, default visibility settings became more revelatory between 2005 (top) and 2014 (bottom), disclosing more personal information to larger audiences, unless the user manually overrode the defaults (fields such as "Likes" and "Extended Profile Data" did not exist in 2005). "Basic profile data" includes hometown, current city, high school, school (status, concentration, secondary concentration), interested in, relationship, workplace, about you, and quotes. Examples of "Extended profile data" include life events such as new job, new school, engagement, expecting a baby, moved, bought a home, and so forth. "Picture" refers to the main profile image. "Photos" refers to the additional images that users might have shared in their account. "Names" refers to the real name, the username, and the user ID. This figure is based on the authors' data and the original visualization created by M. McKeon, available at http://mattmckeon.com/facebook-privacy.

Default visibility settings in social media over time
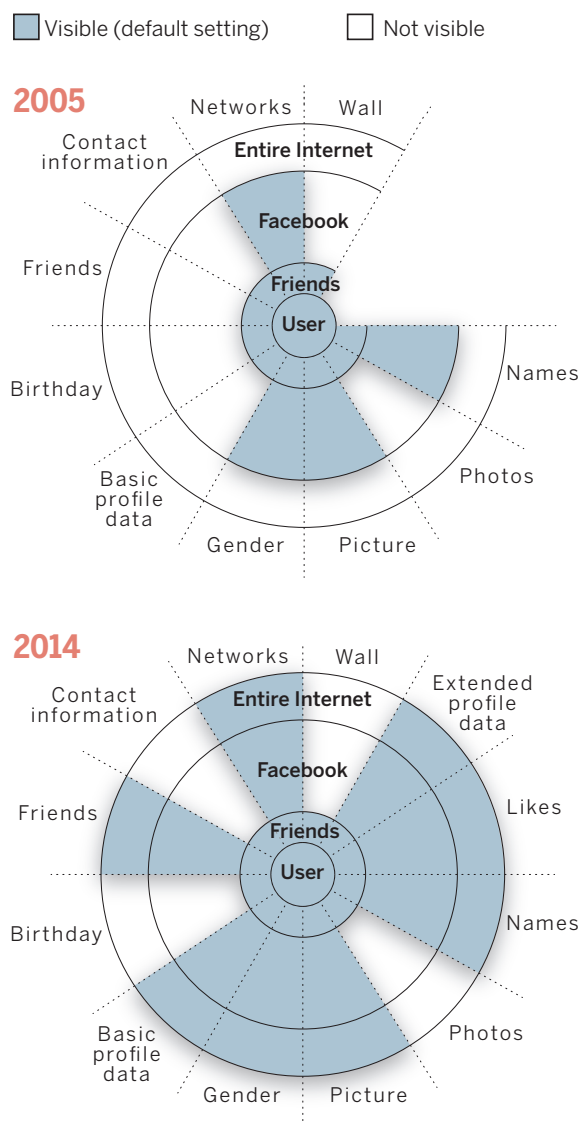
been one of the capstones of the focus of both industry and policy-makers in attempts to balance privacy needs against the value of sharing. Control over personal information is often perceived as a critical feature of privacy protection (39). In principle, it does provide users with the means to manage access to their personal information. Research, however, shows that control can reduce privacy concern (46), which in turn can have unintended effects. For instance, one study found that participants who were provided with greater explicit control over whether and how much of their personal information researchers could publish ended up sharing more sensitive information with a broader audience—the opposite of the ostensible purpose of providing such control (71).

Similar to the normative perspective on control, increasing the transparency of firms' data practices would seem to be desirable. However, transparency mechanisms can be easily rendered ineffective. Research has highlighted not only that an overwhelming majority of Internet users do not read privacy policies (72), but also that few users would benefit from doing so; nearly half of a sample of online privacy policies were found to be written in language beyond the grasp of most Internet users (73). Indeed, and somewhat amusingly, it has been estimated that the aggregate opportunity cost if U.S. consumers actually read the privacy policies of the sites they visit would be $781 billion/year (74).

Although uncertainty and context-dependence lead naturally to malleability and manipulation, not all malleability is necessarily sinister. Consider monitoring. Although monitoring can cause discomfort and reduce productivity, the feeling of being observed and accountable can induce people to engage in prosocial behaviors or (for better or for worse) adhere to social norms (75). Prosocial behavior can be heightened by monitoring cues as simple as three dots in a stylized face configuration (76). By the same token, the depersonalization induced by computer-mediated interaction (77), either in the form of lack of identifiability or of visual anonymity (78), can have beneficial effects, such as increasing truthful responses to sensitive surveys (79, 80). Whether elevating or suppressing privacy concerns is socially beneficial critically depends, yet again, on context [a meta-analysis of the impact of de-identification on behavior is provided in (81)]. For example, perceptions of anonymity can alternatively lead to dishonest or prosocial behavior. Illusory anonymity induced by darkness caused participants in an experiment (82) to cheat in order to gain more money. This can be interpreted as a form of disinhibition effect (83), by which perceived anonymity licenses people to act in ways that they would otherwise not even consider. In other circumstances, though, anonymity leads to prosocial behavior—for instance, higher willingness to share money in a dictator game, when coupled with priming of religiosity (84).

Conclusions

Norms and behaviors regarding private and public realms greatly differ across cultures (85). Americans, for example, are reputed to be more open about sexual matters than are the Chinese, whereas the latter are more open about financial matters (such as income, cost of home, and possessions). And even within cultures, people differ substantially in how much they care about privacy and what information they treat as private. And as we have sought to highlight in this Review, privacy concerns can vary dramatically for the same individual, and for societies, over time.

If privacy behaviors are culture- and context-dependent, however, the dilemma of what to share and what to keep private is universal across societies and over human history. The task of navigating those boundaries, and the consequences of mismanaging them, have grown increasingly complex and fateful in the information age, to the point that our natural instincts seem not nearly adequate.

In this Review, we used three themes to organize and draw connections between the social and behavioral science literatures on privacy and behavior. We end the Review with a brief discussion of the reviewed literature's relevance to privacy policy.

Uncertainty and context-dependence imply that people cannot always be counted on to navigate the complex trade-offs involving privacy in a self-interested fashion. People are often unaware of the information they are sharing, unaware of how it can be used, and even in the rare situations when they have full knowledge of the consequences of sharing, uncertain about their own preferences. Malleability, in turn, implies that people are easily influenced in what and how much they disclose. Moreover, what they share can be used to influence their emotions, thoughts, and behaviors in many aspects of their lives, as individuals, consumers, and citizens. Although such influence is not always or necessarily malevolent or dangerous, relinquishing control over one's personal data and over one's privacy alters the

balance of power between those holding the data and those who are the subjects of that data.

Insights from the social and behavioral empirical research on privacy reviewed here suggest that policy approaches that rely exclusively on informing or "empowering" the individual are unlikely to provide adequate protection against the risks posed by recent information technologies. Consider transparency and control, two principles conceived as necessary conditions for privacy protection. The research we highlighted shows that they may provide insufficient protections and even backfire when used apart from other principles of privacy protection.

The research reviewed here suggests that if the goal of policy is to adequately protect privacy (as we believe it should be), then we need policies that protect individuals with minimal requirement of informed and rational decision-making—policies that include a baseline framework of protection, such as the principles embedded in the so-called fair information practices (86). People need assistance and even protection to aid in navigating what is otherwise a very uneven playing field. As highlighted by our discussion, a goal of public policy should be to achieve a more even equity of power between individuals, consumers, and citizens on the one hand and, on the other, the data holders such as governments and corporations that currently have the upper hand. To be effective, privacy policy should protect real people—who are naïve, uncertain, and vulnerable—and should be sufficiently flexible to evolve with the emerging unpredictable complexities of the information age.

REFERENCES AND NOTES

1. V. Mayer-Schönberger, *Delete: The Virtue of Forgetting In the Digital Age* (Princeton Univ. Press, Princeton, 2011).
2. L. Sweeney, *Int. J. Uncert. Fuzziness Knowl. Based Syst.* **10**, 557–570 (2002).
3. A. McAfee, E. Brynjolfsson, *Harv. Bus. Rev.* **90**, 60–66, 68, 128 (2012).
4. N. P. Tatonetti, P. P. Ye, R. Daneshjou, R. B. Altman, *Sci. Transl. Med.* **4**, 125ra31 (2012).
5. J. E. Cohen, *Stanford Law Rev.* **52**, 1373–1438 (2000).
6. K. Crawford, K. Miltner, M. L. Gray, *Int. J. Commun.* **8**, 1663–1672 (2014).
7. R. A. Posner, *Am. Econ. Rev.* **71**, 405–409 (1981).
8. D. J. Solove, *Harv. Law Rev.* **126**, 1880–1903 (2013).
9. D. J. Solove, *Univ. Penn. L. Rev.* **154**, 477–564 (2006).
10. F. Schoeman, Ed., *Philosophical dimensions of privacy—An anthology* (Cambridge Univ. Press, New York, 1984).
11. B. M. DePaulo, C. Wetzel, R. Weylin Sternglanz, M. J. W. Wilson, *J. Soc. Issues* **59**, 391–410 (2003).
12. S. T. Margulis, *J. Soc. Issues* **59**, 243–261 (2003).
13. E. Goffman, *Relations in Public: Microstudies of the Public Order* (Harper & Row, New York, 1971).
14. E. Sundstrom, I. Altman, *Hum. Ecol.* **4**, 47–67 (1976).
15. B. Schwartz, *Am. J. Sociol.* **73**, 741–752 (1968).
16. R. S. Laufer, M. Wolfe, *J. Soc. Issues* **33**, 22–42 (1977).
17. J. Y. Tsai, S. Egelman, L. Cranor, A. Acquisti, *Inf. Syst. Res.* **22**, 254–268 (2011).
18. P. Slovic, *Am. Psychol.* **50**, 364–371 (1995).
19. E. Singer, H. Hippler, N. Schwarz, *Int. J. Public Opin. Res.* **4**, 256–268 (1992).
20. V. P. Skotko, D. Langmeyer, *Sociometry* **40**, 178–182 (1977).
21. A. Westin, Harris Louis & Associates, Harris-Equifax Consumer Privacy Survey (Tech. rep. 1991).
22. M. J. Culnan, P. K. Armstrong, *Organ. Sci.* **10**, 104–115 (1999).
23. H. J. Smith, S. J. Milberg, S. J. Burke, *Manage. Inf. Syst. Q.* **20**, 167–196 (1996).
24. B. Lubin, R. L. Harrison, *Psychol. Rep.* **15**, 77–78 (1964).
25. S. Spiekermann, J. Grossklags, B. Berendt, *E-Privacy in 2nd Generation E-Commerce: Privacy Preferences versus Actual Behavior* (Third ACM Conference on Electronic Commerce, Tampa, 2001), pp. 38–47.
26. P. A. Norberg, D. R. Horne, D. A. Horne, *J. Consum. Aff.* **41**, 100–126 (2007).
27. I. Ajzen, M. Fishbein, *Psychol. Bull.* **84**, 888–918 (1977).
28. P. H. Klopfer, D. I. Rubenstein, *J. Soc. Issues* **33**, 52–65 (1977).
29. A. Acquisti, R. Gross, in *Privacy Enhancing Technologies*, G. Danezis, P. Golle Eds. (Springer, New York, 2006), pp. 36–58.
30. A. Acquisti, *Privacy in Electronic Commerce and the Economics of Immediate Gratification* (Fifth ACM Conference on Electronic Commerce, New York, 2004), pp. 21–29.
31. I. Hann, K. Hui, S. T. Lee, I. P. L. Png, *J. Manage. Inf. Syst.* **24**, 13–42 (2007).
32. A. Acquisti, L. K. John, G. Loewenstein, *J. Legal Stud.* **42**, 249–274 (2013).
33. I. Altman, D. Taylor, *Social Penetration: The Development of Interpersonal Relationships* (Holt, Rinehart & Winston, New York, 1973).
34. J. Frattaroli, *Psychol. Bull.* **132**, 823–865 (2006).
35. J. W. Pennebaker, *Behav. Res. Ther.* **31**, 539–548 (1993).
36. C. Steinfield, N. B. Ellison, C. Lampe, *J. Appl. Dev. Psychol.* **29**, 434–445 (2008).
37. C. L. Toma, J. T. Hancock, *Pers. Soc. Psychol. Bull.* **39**, 321–331 (2013).
38. D. I. Tamir, J. P. Mitchell, *Proc. Natl. Acad. Sci. U.S.A.* **109**, 8038–8043 (2012).
39. A. Westin, *Privacy and Freedom* (Athenäum, New York, 1967).
40. C. J. Hoofnagle, J. M. Urban, *Wake Forest Law Rev.* **49**, 261–321 (2014).
41. G. Marx, *Ethics Inf. Technol.* **3**, 157–169 (2001).
42. J. W. Thibaut, H. H. Kelley, *The Social Psychology Of Groups* (Wiley, Oxford, 1959).
43. H. Nissenbaum, *Privacy in Context: Technology, Policy, and the Integrity of Social Life* (Stanford Univ. Press, Redwood City, 2009).
44. d. boyd, *It's Complicated: The Social Lives of Networked Teens* (Yale Univ. Press, New Haven, 2014).
45. F. Stutzman, R. Gross, A. Acquisti, *J. Priv. Confidential.* **4**, 7–41 (2013).
46. H. Xu, H. H. Teo, B. C. Tan, R. Agarwal, *J. Manage. Inf. Syst.* **26**, 135–174 (2009).
47. L. K. John, A. Acquisti, G. Loewenstein, *J. Consum. Res.* **37**, 858–873 (2011).
48. I. Altman, *The Environment and Social Behavior: Privacy, Personal Space, Territory, and Crowding* (Cole, Monterey, 1975).
49. A. L. Chaikin, V. J. Derlega, S. J. Miller, *J. Couns. Psychol.* **23**, 479–481 (1976).
50. V. J. Derlega, A. L. Chaikin, *J. Soc. Issues* **33**, 102–115 (1977).
51. A. Acquisti, L. K. John, G. Loewenstein, *J. Mark. Res.* **49**, 160–174 (2012).
52. Y. Moon, *J. Consum. Res.* **26**, 323–339 (2000).
53. S. Petronio, *Boundaries of Privacy: Dialectics of Disclosure* (SUNY Press, Albany, 2002).
54. F. Stutzman, J. Kramer-Duffield, *Friends Only: Examining a Privacy-Enhancing Behavior in Facebook* (SIGCHI Conference on Human Factors in Computing Systems, ACM, Atlanta, 2010), pp. 1553–1562.
55. T. Honess, E. Charman, *Closed Circuit Television in Public Places: Its Acceptability and Perceived Effectiveness* (Police Research Group, London, 1992).
56. M. Gagné, E. L. Deci, *J. Organ. Behav.* **26**, 331–362 (2005).
57. A. Oulasvirta *et al.*, *Long-Term Effects of Ubiquitous Surveillance in the Home* (ACM Conference on Ubiquitous Computing, Pittsburgh, 2012), pp. 41–50.
58. L. Palen, P. Dourish, *Unpacking "Privacy" For A Networked World* (SIGCHI Conference on Human Factors in Computing Systems, ACM, Fort Lauderdale, 2003), pp. 129–136.
59. Z. Tufekci, *Bull. Sci. Technol. Soc.* **28**, 20–36 (2008).
60. J. A. Bargh, K. Y. A. McKenna, G. M. Fitzsimons, *J. Soc. Issues* **58**, 33–48 (2002).
61. R. Calo, *Geo. Wash. L. Rev.* **82**, 995–1304 (2014).
62. E. J. Johnson, D. Goldstein, *Science* **302**, 1338–1339 (2003).
63. C. R. McKenzie, M. J. Liersch, S. R. Finkelstein, *Psychol. Sci.* **17**, 414–420 (2006).
64. R. Gross, A. Acquisti, *Information Revelation and Privacy in Online Social Networks* (ACM Workshop–Privacy in the Electronic Society, New York, 2005), pp. 71–80.
65. E. J. Johnson, S. Bellman, G. L. Lohse, *Mark. Lett.* **13**, 5–15 (2002).
66. W. Hartzog, *Am. Univ. L. Rev.* **60**, 1635–1671 (2010).
67. G. Conti, E. Sobiesk, *Malicious Interface Design: Exploiting the User* (19th International Conference on World Wide Web, ACM, Raleigh, 2010), pp. 271–280.
68. A. Goldfarb, C. Tucker, *Mark. Sci.* **30**, 389–404 (2011).
69. T. B. White, D. L. Zahay, H. Thorbjørnsen, S. Shavitt, *Mark. Lett.* **19**, 39–50 (2008).
70. H. J. Smith, T. Dinev, H. Xu, *Manage. Inf. Syst. Q.* **35**, 989–1016 (2011).
71. L. Brandimarte, A. Acquisti, G. Loewenstein, *Soc. Psychol. Personal. Sci.* **4**, 340–347 (2013).
72. C. Jensen, C. Potts, C. Jensen, *Int. J. Hum. Comput. Stud.* **63**, 203–227 (2005).
73. C. Jensen, C. Potts, *Privacy Policies as Decision-Making Tools: An Evaluation of Online Privacy Notices* (SIGCHI Conference on Human factors in computing systems, ACM, Vienna, 2004), pp. 471–478.
74. A. M. McDonald, L. F. Cranor, *I/S: J. L. Policy Inf. Society.* **4**, 540–565 (2008).
75. C. Wedekind, M. Milinski, *Science* **288**, 850–852 (2000).
76. M. Rigdon, K. Ishii, M. Watabe, S. Kitayama, *J. Econ. Psychol.* **30**, 358–367 (2009).
77. S. Kiesler, J. Siegel, T. W. McGuire, *Am. Psychol.* **39**, 1123–1134 (1984).
78. A. N. Joinson, *Eur. J. Soc. Psychol.* **31**, 177–192 (2001).
79. S. Weisband, S. Kiesler, *Self Disclosure On Computer Forms: Meta-Analysis And Implications* (SIGCHI Conference Conference on Human Factors in Computing Systems, ACM, Vancouver, 1996), pp. 3–10.
80. R. Tourangeau, T. Yan, *Psychol. Bull.* **133**, 859–883 (2007).
81. T. Postmes, R. Spears, *Psychol. Bull.* **123**, 238–259 (1998).
82. C. B. Zhong, V. K. Bohns, F. Gino, *Psychol. Sci.* **21**, 311–314 (2010).
83. J. Suler, *Cyberpsychol. Behav.* **7**, 321–326 (2004).
84. A. F. Shariff, A. Norenzayan, *Psychol. Sci.* **18**, 803–809 (2007).
85. B. Moore, *Privacy: Studies in Social and Cultural History* (Armonk, New York, 1984).
86. *Records, Computers and the Rights of Citizens* (Secretary's Advisory Committee, U.S. Dept. of Health, Education and Welfare, Washington, DC, 1973).
87. E. Hargittai, in *Social Stratification*, D. Grusky Ed. (Westview, Boulder, 2008), pp. 936-113.
88. P. Ariès, G. Duby (Eds.), *A History of Private Life: From Pagan Rome to Byzantium* (Harvard Univ. Press, Cambridge, 1992).
89. R. F. Murphy, *Am. Anthropol.* **66**, 1257–1274 (1964).
90. A. Westin, in *Philosophical Dimensions of Privacy: An Anthology*, F.D. Schoeman Ed. (Cambridge Univ. Press, Cambridge, UK, 1984), pp. 56–74.
91. I. Altman, *J. Soc. Issues* **33**, 66–84 (1977).
92. M. A. Hayat, *Inf. Comm. Tech. L.* **16**, 137–148 (2007).
93. A. Enkin, "Privacy," www.torahmusings.com/2012/07/privacy (2014).
94. J. Rykwert, *Soc. Res. (New York)* **68**, 29–40 (2001).
95. C. B. Whitman, in *Individualism and Holism: Studies in Confucian and Taoist Values*, D. J. Munro, Ed. (Center for Chinese Studies, Univ. Michigan, Ann Arbor, 1985), pp. 85–100.

RESEARCH

Edited by **Stella Hurtley**

SUPERNOVAE

Burbling explosions blow metallic bubbles

Stars more than about eight times the mass of the Sun don't go out quietly. Asymmetric explosions are kicked off by the collapse of their iron cores when no more fusion energy can sustain them. Exactly how this stellar catastrophe proceeds is difficult to probe. Milisavljevic *et al.* have now peered into the supernova remnant Cas A in the near-infrared and present a three-dimensional map of its interior unshocked ejecta. The bubble-like structure points to turbulent mixing, which may help us understand other supernova remnants whose structure cannot be seen in such detail. — MMM

Science, this issue p. 526

PROTEIN STRUCTURE

Structural clues to protein function

Translocator protein (TSPO) is a mitochondrial membrane protein thought to transport cholesterol and porphyrins. Its detailed function remains unclear, but interest in it is high because TSPO is involved in a variety of human diseases. Two papers now present crystal structures of bacterial TSPOs. Li *et al.* show that a mutant that mimics a human single polymorphism associated with psychiatric disorders has structural changes in a region implicated in cholesterol binding. Guo *et al.* suggest that TSPO may be more than a transporter. They show how it catalyzes the degradation of porphyrins, a function that could be important in protection against oxidative stress. — VV

Science, this issue p. 555, p. 551

OPTICAL IMAGING

Overcoming the limits of the microscope

The resolution of a light microscope is limited. Physicists have long since worked out what these limits are and which parameters determine the spatial resolution. Many groups have nevertheless made numerous attempts to overcome these resolution limits. Rather than improving the power and quality of the microscope, Chen *et al.* instead expanded the biological specimens under study (see the Perspective by Dodt). They introduced a polymer gel into fixed cells and tissues and chemically induced swelling of the polymer by almost two orders of magnitude. They could then produce much higher-resolution images of their samples, which included the mouse hippocampus. — PRS

Science, this issue p. 543; see also p. 474
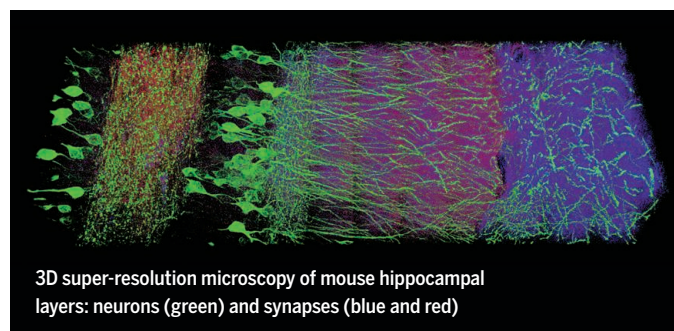
3D super-resolution microscopy of mouse hippocampal layers: neurons (green) and synapses (blue and red)

REACTION DYNAMICS
Deuterium fluoride gets born shivering

Modern spectroscopic techniques can analyze collisions between gas phase molecules in exquisite detail, highlighting exactly which vibrations and rotations come into play. However, much chemistry of interest takes place in solution, where it's harder to tease out what happens. Dunning *et al.* applied infrared spectroscopy to study solution-phase formation of deuterium fluoride (DF) from F atoms, a longstanding test bed of gas phase dynamics. The DF product vibrated for a surprisingly long time before dissipating its energy to the surrounding solvent molecules. — JSY

Science, this issue p. 530

ANIMAL COGNITION
Even chicks may count from left to right

For the most part, humans represent numbers across a mental number line, with smaller numbers on the left and larger numbers on the right. Some have argued that this is due to culture rather than being innate. Rugani *et al.*, however, show that 3-day-old chicks share this representation of numbers, consistently seeking lower numbers to the left of a target and larger numbers to the right (see the Perspective by Brugger). These results suggest that there may be an innate spatial representation of numerical values that we share with other animals. — SNV

Science, this issue p. 534; see also p. 477

IDENTITY AND PRIVACY
Where and when you spend reveals who you are

How do you ensure individual privacy when analyzing bulk information? De Montjoye *et al.* used 3 months of data on financial traces of 1.1 million people to determine the privacy bounds of credit card metadata. The risk of re-identification from financial data sets was high: Four spatiotemporal observations, (of the shop and the day the transaction took place) were enough to re-identify 90% of the individuals. Knowing the approximate price of a transaction increased the likelihood of re-identification. — BJ

Science, this issue p. 536

ATMOSPHERIC DYNAMICS
Because the rain falls and the wind blows

Global warming is expected to intensify the hydrological cycle, but it might also make the atmosphere less energetic. Laliberté *et al.* modeled the atmosphere as a classical heat engine in order to evaluate how much energy it contains and how much work it can do (see the Perspective by Pauluis). They then used a global climate model to project how that might change as climate warms. Although the hydrological cycle may increase in intensity, it does so at the expense of its ability to do work, such as powering large-scale atmospheric circulation or fueling more very intense storms. — HJS

Science, this issue p. 540; see also p. 475

INFLAMMATION
Preventing sepsis in type 1 diabetics

Patients with type 1 diabetes have chronic systemic inflammation and are more prone to developing sepsis. Filgueiras *et al.* found that mice that are a model for type 1 diabetes had higher amounts of leukotriene B_4, a proinflammatory lipid, and of 5-lipoxygenase, the enzyme that produces leukotriene B_4. Model mice treated with an inhibitor of 5-lipoxygenase survived sepsis and had decreased markers of inflammation. Thus, targeting 5-lipoxygenase to prevent the production of leukotriene B_4 could potentially decrease the susceptibility of diabetic patients to sepsis. — WW

Sci. Signal. **8**, ra10 (2015).

Edited by **Kristen Mueller** *and* **Jesse Smith**

The Fraser River in British Columbia, Canada

ECOLOGY
Healthy rivers need diversity, too

Savvy financial investors know that a diverse portfolio generates stability due to a balance of ups and downs across investments. A similar hypothesis posits that larger river systems offer similar stability to their ecosystems. Moore *et al.* tested this hypothesis in one of the few remaining free-flowing river systems in North America, the Fraser River watershed. They found that larger watersheds were more stable in terms of water temperature and flow, and produced salmon more consistently. This shows that greater biological diversity can buffer ecosystems against environmental variability and may enhance long-term stability. — SNV

Ecol. Soc. Am. 10.1890/14-0326.1 (2014).

CLIMATE CHANGE
Another cause of climate change is developing

The continuing increase in greenhouse gas concentrations is not the only thing driving global warming; changing land use, such as the conversion of forests to farmland, is adding to the problem, too. Because increasing population and rising affluence will require more land be farmed in order to supply food to the world, our climate will experience even more disruption in the coming decades. Ward *et al.* calculate the climate forcing due to land use and land cover change and find that it is contributing nearly

ALSO IN *SCIENCE* JOURNALS

Edited by **Stella Hurtley**

CIRCADIAN RHYTHMS
Defining necessary circadian clock elements

The circadian clock in organisms as diverse as fungi and humans have a rather similar structure: Timing depends on daily cycles of transcription in circuits in which feedback loops control the timing of oscillations. A critical role has been ascribed to negative elements, which lead to inhibition of their own transcription, and to degradation of these elements, which is signaled by phosphorylation events. However, Larrando *et al*. show that in the fungus *Neurospora*, after manipulations that prevent phosphorylation-signaled degradation of the negative element FREQUENCY (FRQ), rhythms still persist (see the Perspective by Kramer). They suggest a model in which other phosphorylation events on Frq (of which there are over 100) must have critical roles in controlling the clock, independent of negative element degradation. — LBR

Science, this issue p. 518; see also p. 476

SOLAR CELLS
Large-crystal perovskite films

The performance of organic-inorganic hybrid perovskite planar solar cells has steadily improved. One outstanding issue is that grain boundaries and defects in polycrystalline films degrade their output. Now, two studies report the growth of millimeter-scale single crystals. Nie *et al.* grew continuous, pin-hole-free, thin iodochloride films with a hot-casting technique and report device efficiencies of 18%. Shi *et al.* used antisolvent vapor-assisted crystallization to grow millimeter-scale bromide and iodide cubic crystals with charge-carrier diffusion lengths exceeding 10 mm. — PDS

Science, this issue p. 522, p. 519

MITOCHONDRIAL BIOLOGY
Switching transcription and replication

Because mitochondrial DNA is circular, the transcription and replication machinery might be expected to collide. A single mitochondrial RNA polymerase (mtRNAP) transcribes the mitochondrial DNA and also generates primers for replication. Agaronyan *et al*. now show that transcription and replication are kept separate in human mito-chondria, with the mitochondrial transcription elongation factor TEFM serving as a key player in the switch. In the absence of TEFM, mtRNAP terminates downstream from the promoter, forming primers to promote repli-cation. In the presence of TEFM, the primers are not formed, and the overall processivity of mtRNAP elongation complexes is enhanced, promoting genome transcription. These mutually exclusive mechanisms allow the processes to proceed indepen-dently as needed by the cell. — BAP

Science, this issue p. 548

BIOMATERIALS
Location, location, location

When buying a house, we research neighborhoods and carefully choose an environment that works for us. So why does a "one-material-fits-all" mentality dominate when choosing a biomaterial for various clini-cal scenarios? Now, Oliva *et al*. attempt to shift that mind-set by defining the molecular properties of diseased-tissue microenvironments and then tuning a dendrimer:dextran–based material to thrive differentially under selected clinical conditions. The authors measured tissue modifications and material performance in two gut diseases and under varying degrees of severity. The context affected the compatibility between a biomaterial and its neighborhood. A resulting pre-dictive paradigm could match a material with its model home, which may one day translate into improved clinical outcomes. — KL

Sci. Transl. Med. **7**, 272ra11 (2015).

REACTION DYNAMICS
Deuterium fluoride gets born shivering

Modern spectroscopic techniques can analyze collisions between gas phase molecules in exquisite detail, highlighting exactly which vibrations and rotations come into play. However, much chemistry of interest takes place in solution, where it's harder to tease out what happens. Dunning *et al.* applied infrared spectroscopy to study solution-phase formation of deuterium fluoride (DF) from F atoms, a longstanding test bed of gas phase dynamics. The DF product vibrated for a surprisingly long time before dissipating its energy to the surrounding solvent molecules. — JSY

Science, this issue p. 530

ANIMAL COGNITION
Even chicks may count from left to right

For the most part, humans represent numbers across a mental number line, with smaller numbers on the left and larger numbers on the right. Some have argued that this is due to culture rather than being innate. Rugani *et al.*, however, show that 3-day-old chicks share this representation of numbers, consistently seeking lower numbers to the left of a target and larger numbers to the right (see the Perspective by Brugger). These results suggest that there may be an innate spatial representation of numerical values that we share with other animals. — SNV

Science, this issue p. 534; see also p. 477

IDENTITY AND PRIVACY
Where and when you spend reveals who you are

How do you ensure individual privacy when analyzing bulk information? De Montjoye *et al.* used 3 months of data on financial traces of 1.1 million people to determine the privacy bounds of credit card metadata. The risk of re-identification from financial data sets was high: Four spatiotemporal observations, (of the shop and the day the transaction took place) were enough to re-identify 90% of the individuals. Knowing the approximate price of a transaction increased the likelihood of re-identification. — BJ

Science, this issue p. 536

ATMOSPHERIC DYNAMICS
Because the rain falls and the wind blows

Global warming is expected to intensify the hydrological cycle, but it might also make the atmosphere less energetic. Laliberté *et al.* modeled the atmosphere as a classical heat engine in order to evaluate how much energy it contains and how much work it can do (see the Perspective by Pauluis). They then used a global climate model to project how that might change as climate warms. Although the hydrological cycle may increase in intensity, it does so at the expense of its ability to do work, such as powering large-scale atmospheric circulation or fueling more very intense storms. — HJS

Science, this issue p. 540; see also p. 475

INFLAMMATION
Preventing sepsis in type 1 diabetics

Patients with type 1 diabetes have chronic systemic inflammation and are more prone to developing sepsis. Filgueiras *et al.* found that mice that are a model for type 1 diabetes had higher amounts of leukotriene B_4, a proinflammatory lipid, and of 5-lipoxygenase, the enzyme that produces leukotriene B_4. Model mice treated with an inhibitor of 5-lipoxygenase survived sepsis and had decreased markers of inflammation. Thus, targeting 5-lipoxygenase to prevent the production of leukotriene B_4 could potentially decrease the susceptibility of diabetic patients to sepsis. — WW

Sci. Signal. **8**, ra10 (2015).

The Fraser River in British Columbia, Canada

IN OTHER JOURNALS
Edited by **Kristen Mueller** *and* **Jesse Smith**

ECOLOGY
Healthy rivers need diversity, too

Savvy financial investors know that a diverse portfolio generates stability due to a balance of ups and downs across investments. A similar hypothesis posits that larger river systems offer similar stability to their ecosystems. Moore *et al.* tested this hypothesis in one of the few remaining free-flowing river systems in North America, the Fraser River watershed. They found that larger watersheds were more stable in terms of water temperature and flow, and produced salmon more consistently. This shows that greater biological diversity can buffer ecosystems against environmental variability and may enhance long-term stability. — SNV

Ecol. Soc. Am. 10.1890/14-0326.1 (2014).

CLIMATE CHANGE
Another cause of climate change is developing

The continuing increase in greenhouse gas concentrations is not the only thing driving global warming; changing land use, such as the conversion of forests to farmland, is adding to the problem, too. Because increasing population and rising affluence will require more land be farmed in order to supply food to the world, our climate will experience even more disruption in the coming decades. Ward *et al.* calculate the climate forcing due to land use and land cover change and find that it is contributing nearly

half as much as anthropogenic greenhouse gas emissions, and that could grow in the future. Their work shows how important land policy will be in efforts to minimize continued climate warming. — HJS

Atmos. Chem. Phys. 10.5194/acp-14-12701-2014 (2014).

CANCER BIOLOGY
Engineering cancer cell metastasis

Cancer cell metastasis is not random. Breast cancer, for example, tends to metastasize to bone. To explore what underlies this selectivity, Jeon *et al.* took an engineering approach: They built in vitro microfluidic models that allowed them to compare how different tissue microenvironments affect the ability of breast cancer cells to exit blood vessels (extravasate) and enter surrounding tissue. They found that a bone-mimicking microenvironment was particularly potent in inducing extravasation. Adding a protein called adenosine to the system, which binds to breast cancer cells, reduced their extravasation, suggesting that this model might be a valuable way to screen for drugs that block metastasis. — PAK

Proc. Natl. Acad. Sci. U.S.A. **112**, 214 (2015).

AGING
The downside of living a longer life

Over the years, scientists have identified many factors that increase longevity in animal models. But do these interventions also let animals stay healthy longer, giving them an extended "healthspan"? To find out, Bansal *et al.* measured a range of physiological parameters over the lifetime of worms with mutations that extended their lifespans. The effect of these mutations on healthspan was variable. In fact, control worms had the greatest healthspan when calculated as a percentage of total lifespan. Extending the period of ill health

of an increasingly aged human population could be devastating, suggesting that researchers should focus on optimizing healthspan rather than lifespan. — LBR

Proc. Natl. Acad. Sci. U.S.A. 10.1073/pnas.1412192112 (2015).

SOLID-STATE PHYSICS
Engineering a copper oxide look-alike

Many discoveries of spectacular material properties are serendipitous. Scientists can make the discovery process more predictable if they design materials from the "bottom up" to behave in a certain way. Disa *et al.* fabricated heterostructures consisting of alternating layers of $LaTiO_3$, $LaNiO_3$, and $LaAlO_3$, with the aim of making a material in which the top two valence orbitals are filled

with electrons to very different degrees. This property can lead to exotic effects and may be useful for making high temperature copper oxide superconductors. The authors used x-ray absorption spectroscopy to verify the properties of the heterostructure. Their theoretical calculations showed that replacing $LaAlO_3$ with a different material can lead to further improvements. — JS

Phys. Rev. Lett. 10.1103/PhysRevLett.114.026801 (2015).

ORGANIC CHEMISTRY
Olefins from seed oils at industrial scales

Linear-chain olefins with terminal double bonds (linear α-olefins, or LAOs) are essential building blocks for both commodity

products, such as lubricants and thermoplastics, and fine chemicals and drugs. Many fatty acids derived from seed oils have a linear tail containing a central double bond, and exchanging this tail with ethylene (ethenolysis) would provide a renewable source of LAOs. However, most catalysts for this reaction deactivate after thousands of reaction cycles (turnovers) and require unacceptable amounts of catalyst. Marx *et al.* now report a ruthenium ethenolysis catalyst bearing a cyclic alkyl amino carbene ligand that achieves more than 100,000 turnovers at a catalyst loading of only three parts per million. — PDS

Angew. Chem. Int. Ed. 10.1002/anie.201410797 (2014).
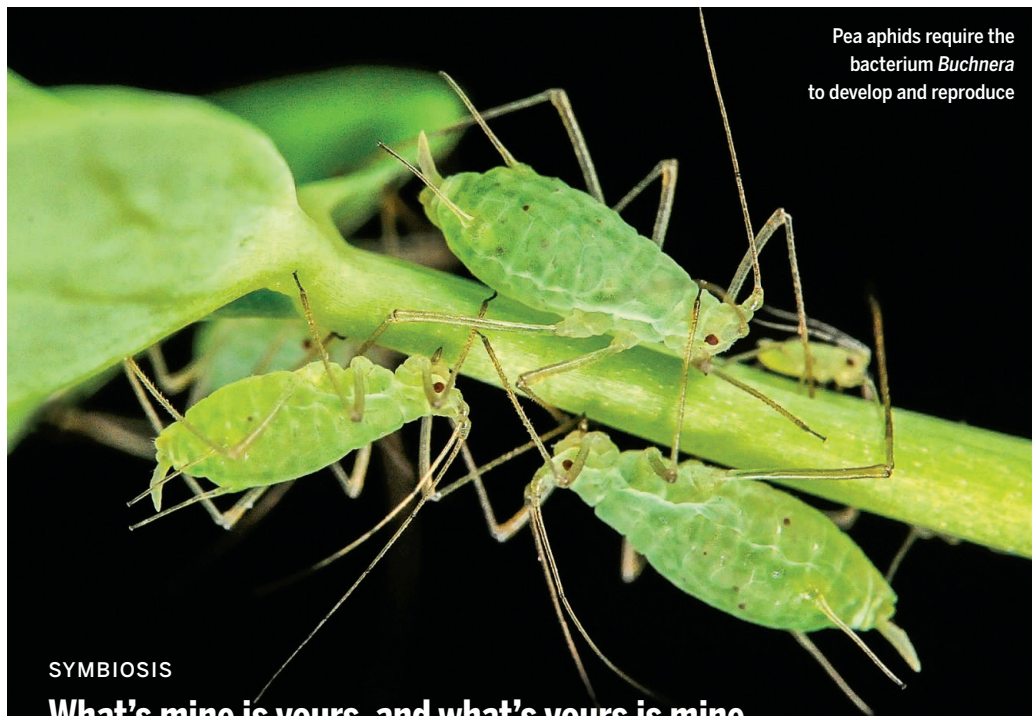
Pea aphids require the bacterium *Buchnera* to develop and reproduce

SYMBIOSIS
What's mine is yours, and what's yours is mine

Many invertebrates harbor symbiotic bacteria. Because these relationships have evolved over millions of years, dissecting whether a particular feature of an organism results from the host's or the symbiont's genes is a challenge. Moran and Yun discovered how to manipulate an obligatory symbiosis between a bacterium and its aphid host. They did this by exploiting a natural mutation in the bacteria that causes them to die at high temperatures. They then replaced the dead bacteria by injecting heat-tolerant bacteria. Evidence of success came when not just the symbionts but also the recipient aphids developed a striking tolerance to high temperatures. — CA

Proc. Natl. Acad. Sci. U.S.A. 10.1073/pnas.1420037112 (2015).

RESEARCH ARTICLE SUMMARY

CIRCADIAN RHYTHMS

Decoupling circadian clock protein turnover from circadian period determination

Luis F. Larrondo,* Consuelo Olivares-Yañez, Christopher L. Baker, Jennifer J. Loros, Jay C. Dunlap*

INTRODUCTION: Circadian oscillators allow individual organisms to coordinate metabolism with day/night cycles and to anticipate such changes. Such oscillators in fungi and animals share a common regulatory architecture centered on transcription and translation-based negative feedback loops. Within such oscillators, extensive coordinated and progressive phosphorylation of negative element proteins leads to their proteasome-mediated degradation. Current clock models posit that this turnover event is the final essential step in the loop and that the time taken to achieve phosphorylation and turnover determines the speed of the circadian clock. The clock in *Neurospora* exemplifies such oscillators: FREQUENCY (FRQ) is a negative element, and its half-life is well correlated with circadian period length. Surprisingly, however, using real-time reporters in cells with compromised proteasomal turnover, we unveiled an unexpected uncoupling between negative element half-life and circadian period determination.

RATIONALE: We followed FRQ dynamics as well as transcriptional activity of the *frq* promoter in vivo using luciferase-based reporters. FRQ turnover was tracked through Western blotting, and kinase inhibitors helped to test the correlation between phosphorylation and period length. Strains bearing *frq* alleles causing abnormal period lengths were used, as were strains with diminished FRQ turnover, including knockouts of both the F-box protein FWD-1 (a ubiquitin ligase that mediates FRQ proteasomal degradation) and individual components of the COP9 signalosome.

RESULTS: Without FWD-1, FRQ turnover is severely compromised and circadian regulation of development is lost; however, in such Δ*fwd-1* cells, the amount of FRQ still oscillated, the result of cyclic transcription of *frq* and reinitiation of FRQ synthesis. The circadian nature of these rhythms was confirmed by examining well-established *frq* mutants having altered periods. Analyses of additional strains bearing knockouts of individual COP9

signalosome components further confirmed circadian oscillations in FRQ amounts, despite compromised FRQ turnover. Broadly accepted oscillator models posit that negative element stability determines clock period length; thus, Δ*fwd-1* strains with long FRQ half-lives are predicted to have extremely long periods. This, however, is not seen: Period is mainly determined by the characteristics of the *frq* allele irrespective of the half-life of this negative element. Partial inhibition of overall phosphorylation provided additional evidence that clock protein phosphorylation events, not the resulting stability changes, provide key information in determining period length.

DISCUSSION: The long-standing and assumed causal loop uniting clock protein phosphorylation, stability, and period determination should be revisited. Data indicate that qualities of FRQ—in particular, its phosphorylation status rather than its quantity—are crucial for determining when the circadian feedback loop is completed and can be restarted. Previously described strong correlations between clock protein phosphorylation and half-life and between half-life and period length are, in fact, just correlations that do not always imply cause and effect. Although degradation is the final outcome of FRQ posttranslational modifications, phosphorylation and its effects of secondary, tertiary, and quaternary protein structure may actually be the key elements determining clock speed. Although it may be premature to broadly generalize these findings to all circadian oscillators, diverse data from several animal circadian systems are not inconsistent with this revised model. ∎
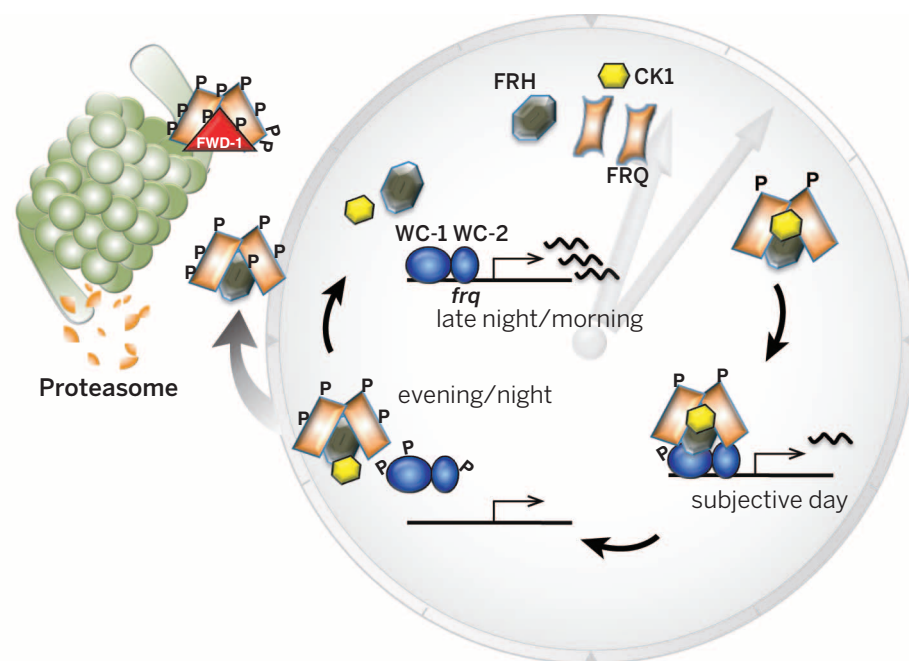
Distinct roles for FRQ phosphorylation and degradation in the clock. White Collar-1 and -2 (WC-1 and WC-2) activate *frq* expression and FRQ (with FRH and CK1) later inhibit expression. FRQ phosphorylation affects interactions with WC-1/WC-2, reducing inhibition. By influencing these key interactions, FRQ phosphorylations determine the rate at which core clock events, those within the clock face, occur. After key phosphorylations close the loop, degradation-related events need not affect circadian period.

CIRCADIAN RHYTHMS

Decoupling circadian clock protein turnover from circadian period determination

Luis F. Larrondo,[1,2]* Consuelo Olivares-Yañez,[1] Christopher L. Baker,[2]†
Jennifer J. Loros,[2,3] Jay C. Dunlap[2]*

The mechanistic basis of eukaryotic circadian oscillators in model systems as diverse as *Neurospora*, *Drosophila*, and mammalian cells is thought to be a transcription-and-translation–based negative feedback loop, wherein progressive and controlled phosphorylation of one or more negative elements ultimately elicits their own proteasome-mediated degradation, thereby releasing negative feedback and determining circadian period length. The *Neurospora crassa* circadian negative element FREQUENCY (FRQ) exemplifies such proteins; it is progressively phosphorylated at more than 100 sites, and strains bearing alleles of *frq* with anomalous phosphorylation display abnormal stability of FRQ that is well correlated with altered periods or apparent arrhythmicity. Unexpectedly, we unveiled normal circadian oscillations that reflect the allelic state of *frq* but that persist in the absence of typical degradation of FRQ. This manifest uncoupling of negative element turnover from circadian period length determination is not consistent with the consensus eukaryotic circadian model.

C ircadian clocks provide individuals with the ability to anticipate daily changes associated with the transition of day to night (*1*, *2*). In organisms as diverse as humans, mice, fungi, insects, cyanobacteria, and plants, the molecular components of the circadian clocks have been identified in molecular detail (*1*, *3–6*). In eukaryotes, the circadian oscillator underlying these subcellular clocks is generally viewed as comprising transcription and translation-based negative feedback loops (TTFLs) with interconnected feedback loops (*1*). Although posttranslational oscillators have been described (*7*, *8*), their generalizability is still being tested. Thus, in the circadian paradigm for fungi and animals, (Per-Arnt-Sim) domain–containing transcription factors drive the expression of genes [e.g., *frequency (frq)*, *period (per)*] whose products lead to the inhibition of their own transcription; only after degradation of these products can reinitiation of the cycle begin, and period length is thus obligately coupled to turnover kinetics of clock proteins (*9–13*). In the case of *Neurospora crassa,* transcription of the *frq* gene encoding the negative element FRQ is controlled by the White-Collar complex (WCC, the

positive element), a heterodimer of PAS-containing GATA transcription factors White Collar-1 (WC-1) and White Collar-2 (WC-2). Beginning shortly after its synthesis, FREQUENCY (FRQ) is progressively phosphorylated, finally reaching a multiphosphorylated (hyperphosphorylated) state that leads to its proteasome-mediated degradation (*14*, *15*). Such changes, including timely turnover, are thought to underlie the daily rhythms in negative element abundance and phosphorylation that characterize eukaryotic circadian oscillators (*13*, *16*).

More specifically, data supporting the importance of phosphorylation dynamics to clock protein turnover and period determination come from animals (*10*) and *Neurospora* (*14*, *17*, *18*) in which precise spatiotemporal arrangement of phosphorylation events dictates period and controls negative element stability. A key aspect in FRQ degradation is the association of its hyperphosphorylated isoforms with FWD-1, the substrate-recruiting subunit of an SCF (SKP/Cullin/F-box)–type ubiquitin ligase that facilitates FRQ ubiquitination and presentation to the proteasome (*17–21*). FWD-1 is the ortholog of mammalian β-TrCP (*22*) and *Drosophila* Slimb (*23*, *24*), which have similar roles in those circadian systems. That FRQ stability is a determinant of period length has been supported by the fact that strains bearing long-period *frq* alleles display a more stable FRQ, whereas this protein exhibits decreased half-life in strains with shorter periods (*9*, *14*, *17*, *18*). Consistent with this, mutant strains in which ubiquitin-dependent proteasomal degradation of FRQ is severely altered show neither overt rhythms nor molecular circadian rhythmic-

ity in FRQ abundance, as detected by Western blotting (*15*, *19*, *25*, *26*). Also consistent with this model, mutations of genes encoding *Neurospora* COP9 signalosome components lead to destabilization of FWD-1, impairment of FRQ degradation, and apparent loss of both overt and molecular rhythmicity (*25–27*).

Results

Circadian rhythms in the absence of proper FRQ degradation

Overt circadianly regulated developmental rhythms (daily spore production) are reported to be lost in Δ*fwd-1* mutants (*19*). Codon-optimized luciferase developed for *Neurospora* can report in vivo, and with high precision, *frq* expression dynamics or changes in abundance of FRQ, by the use of transcriptional (an ectopic construct in which the *frq* promoter controls luciferase expression) or translational (luciferase fused to the C terminus of the FRQ protein, *frq^luc*) reporters (*6*, *28–30*). We therefore crossed *Neurospora frq^luc* to a Δ*fwd-1* strain to assess whether, under free-running conditions, FRQ protein displayed residual regulation. We confirmed the absence of overt developmental rhythms (Fig. 1A). But, to our surprise, dynamic analysis of bioluminescence revealed oscillations in LUC activity—a direct measurement of FRQ-LUC synthesis given the short in vivo half-life of LUC (*28*)—in Δ*fwd*-1 cells (Fig. 1, B to D, and movie S1), this despite the presence of high amounts of hyperphosphorylated FRQ and attenuated turnover (fig. S1 and Fig. 2A). This suggests that complete or even substantial daily turnover of the negative element in the circadian clock, here FRQ, was not required to relieve the negative arm of the feedback loop in order to reinitiate new cycles of FRQ synthesis. We explicitly tested this possibility, confirming biochemically that, as described (*19*), abundance of FRQ in liquid cultures does not display detectable cycling in strains lacking FWD-1 (Fig. 2, A and B). Nevertheless, if synthesis of FRQ-LUC was dynamically tracked in vivo by measuring bioluminescence in 96-well plates, rhythms were evident in the Δ*fwd-1* strain (Fig. 2C). To further validate that the Δ*fwd-1* strain behaved as reported (*19*), we confirmed its genotype by polymerase chain reaction (PCR) and examined FRQ abundance by Western blot and by luciferase activity after blocking protein synthesis (fig. S1). In the absence of FWD-1, FRQ degradation was reduced and amounts appear elevated, consistent with previous work (*19*, *31*). Our results, therefore, are incompatible with the current TTFL paradigm as applied to *Neurospora* and, taken at face value, compel a revised model in which FRQ stability as measured by its degradation rate is not a period determinant.

FRQ-LUC oscillations correspond to bona fide circadian rhythms

To confirm that rhythms in abundance of FRQ-LUC rely on a functional FRQ-WCC circadian oscillator, we tested this reporter in a strain carrying a point mutation in FRQ-interacting RNA helicase (*frh*) that leads to a clock-null phenotype

[1]Millennium Nucleus for Fungal Integrative and Synthetic Biology, Departamento de Genética Molecular y Microbiología, Facultad de Ciencias Biológicas, Pontificia Universidad Católica de Chile, Casilla 114-D, Santiago, Chile. [2]Department of Genetics, Geisel School of Medicine at Dartmouth, Hanover, NH 03755, USA. [3]Department of Biochemistry, Geisel School of Medicine at Dartmouth, Hanover, NH 03755, USA.
*Corresponding author. E-mail: jay.c.dunlap@dartmouth.edu (J.C.D.); llarrondo@bio.puc.cl (L.F.L.) †Present address: Jackson Laboratory, Bar Harbor, ME, USA.

(*6*, *32*). In this strain, LUC levels were erratic, with no hints of rhythms, validating a central role for FRH (*32*, *33*) in the FRQ-WCC oscillator (fig. S2). In addition, when examined in a WCC-deficient strain, amounts of FRQ-LUC were extremely low and arrhythmic (fig. S2). Taken together, this revalidates the *frq*[luc] system (*30*) as a reliable reporter of the *Neurospora* circadian oscillator.

FRQ-LUC oscillations in strains lacking the COP9 signalosome

To confirm that these results were not restricted to only FWD-1 loss-of-function strains, we examined rhythms in strains bearing mutations in one of several components of the COP9 signalosome (CSN), which is required to deneddylate and thereby stabilize the class of SCF E3 ubiquitin ligases for which proteins like FWD-1 facilitate substrate recognition (*34*). For instance, loss of CSN-2 reduces CSN activity, causing a sharp decrease in amounts of FWD-1, and therefore stabilizing FRQ (*25*). This strain shows no rhythms in bulk FRQ amounts, and overt circadian rhythms

are replaced by unstable developmental rhythms having periods between 40 and 60 hours (*25*). In our hands, analysis of rhythmic spore production (race-tube assay) (Fig. 1) of the Δ*csn-2* strain confirmed the loss of overt circadian rhythms and the presence of unstable long-period cycles in conidiation, whereas real-time quantification of FRQ synthesis using the *frq*[luc] reporter confirmed the coexistence of both circadian and developmental rhythms of differing period lengths (fig. S3, and movie S2). Thus, in Δ*csn-2* cells, although stability of FRQ is increased (*25*), circadian rhythms in FRQ expression are still readily detectable; overt circadian developmental rhythms, however, are masked by long-period developmental cycles, a scenario similar to that in the *Neurospora chol-1* mutant (*29*). In light of recent reports that other CSN components influence FRQ stability and compromise both molecular and overt circadian rhythms (*26*, *27*), we also examined those strains for cryptic circadian rhythmicity with the *frq*[luc] reporter. In agreement with what we had observed for Δ*csn-2*, we confirmed circadian

rhythms in Δ*csn-1*, Δ*csn-4*, and Δ*csn-5* strains (fig. S4), providing additional evidence of circadian rhythms despite altered FRQ stability.

Synthesis of new FRQ in the presence of hyperphosphorylated FRQ

In general, *Neurospora* circadian protein expression analyses have used samples from liquid cultures (*35*). Because the luciferase assays reported herein were conducted on agar plates, we confirmed that media conditions (solid versus liquid) are not producing major differences in FRQ stability. Comparisons of FRQ abundance in wild-type (WT) and Δ*fwd-1* strains grown on solid media confirmed that, as observed for liquid cultures, degradation of FRQ was impaired in the absence of FWD-1 (fig. S5A). Time courses under these conditions showed clear oscillations of FRQ abundance in WT cells and revealed that although FRQ is more abundant and stable in Δ*fwd-1*, it is nonetheless possible to distinguish its turnover and new synthesis (fig. S5, B and C), something not easily observed in samples coming from liquid

Fig. 1. FRQ expression oscillates in the absence of FWD-1. (A) Strains were inoculated into 1-cm-diameter glass tubes partially filled with agar [race tubes, e.g., (*4*, *14*)], grown for 24 hours in constant light and then transferred to darkness to elicit circadian control of growth and conidial development ("banding"). Assessment of rhythmic conidiation (banding) through this race-tube assay confirms the absence of overt circadian rhythmicity in *ras-1*[bd], *frq*[luc], Δ*fwd-1* strains compared with a *ras-1*[bd], *frq*[luc], *fwd-1*[+] control. Nevertheless, quantification of FRQ-LUC bioluminescence throughout the entire race tube (**A**) or close to the beginning of the race tube (**B** to **D**) reveals the presence of oscillations in FRQ-LUC expression in the strains lacking FWD-1 as well as in FWD-1^{+}. In (**B**) and (**C**), each line corresponds to the average of three different quantifications (±SEM) of luminescence from within each demarked region across sequential time points.
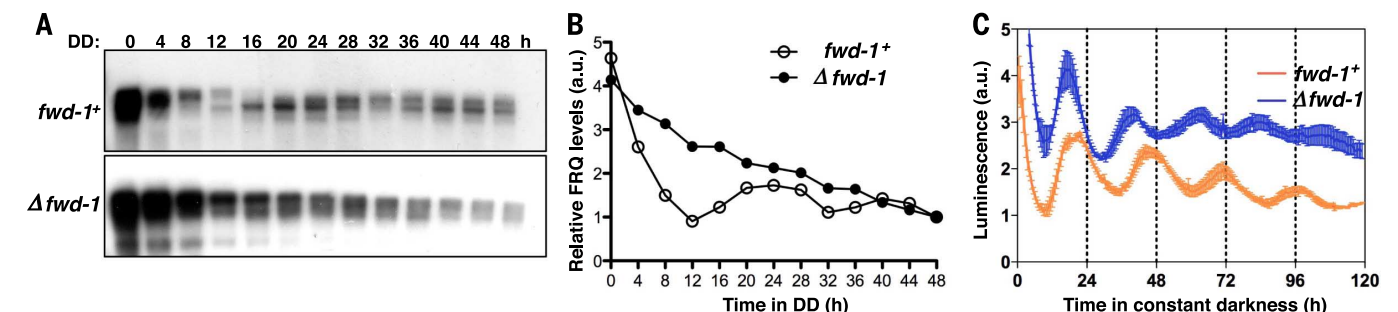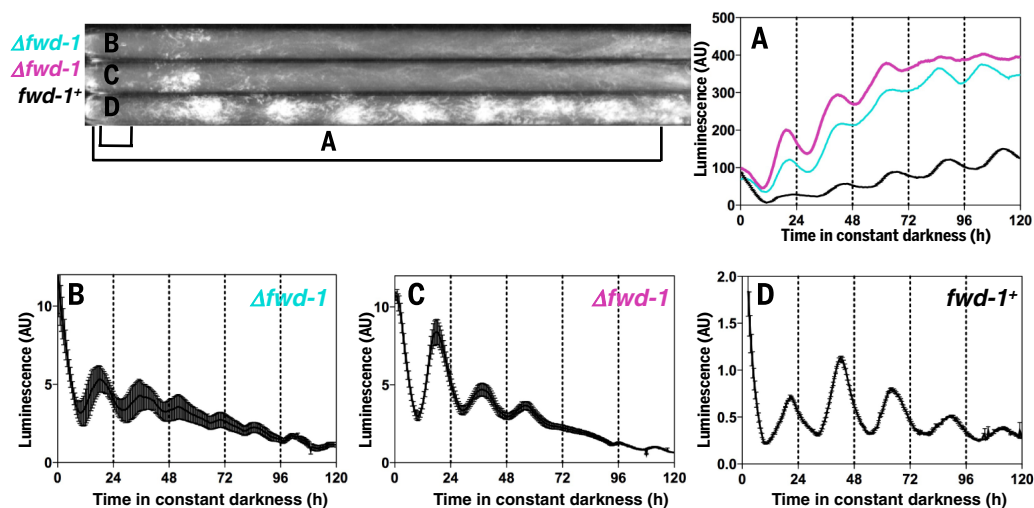
Fig. 2. Lack of clear oscillations in abundance of FRQ in the absence of FWD-1 under standard culture conditions. (A) *ras-1*[bd], *frq*[luc], *fwd-1*[+] (top) and *ras-1*[bd], *frq*[luc], Δ*fwd-1* (bottom) strains were grown in 2% LCM in darkness, and samples were harvested every 4 hours for 48 hours; proteins were extracted, and FRQ-LUC was detected with antibody to FRQ. (**B**) Densitometric analysis of the gels confirming elevated expression and loss of normal rhythmic FRQ expression in Δ*fwd-1*. (**C**) Quantification of bioluminescence of static cultures, in 96-well plates with solid race-tube media, reveals the presence of oscillations in FRQ-LUC levels in the Δ*fwd-1* strain. Each curve corresponds to the average of three independent wells.

cultures. In the aggregate, these results confirm that new FRQ can be produced in a timely manner even in the presence of hyperphosphorylated FRQ and that although FRQ degradation is impaired, molecular rhythms can still persist.

frq expression in Δfwd-1 reflects the allelic state of the oscillator

To further corroborate the existence of a functional circadian oscillator in strains devoid of fwd-1 (Δfwd-1), we employed a reporter in which only the frq CLOCK-Box of the frq promoter (36) drives luc expression (frq_{c-box}-luc) (Fig. 3). Rhythms were visualized in these strains, indicating that the WCC is active and therefore can still drive tran-

scription from circadian cis elements even in the presence of high amounts of FRQ.

That these rhythms depend on the circadian oscillator in the normal manner was evidenced by the characteristic systematic alteration of period length seen in strains bearing various frq alleles, whether or not they were devoid of FWD-1. Rhythmicity persisted in the absence of proper FRQ turnover in Δfwd-1, displayed a long period in the presence of long-period frq alleles such as frq^7 or frq^{S548A}, and was short in the presence of short-period alleles such as frq^1 or frq^{S900A} (Fig. 3 and table S2). However, periodicity was influenced by FWD-1, although the variation appeared to show no obvious pattern: Loss of FWD-1 altered the pe-

riod of strains with less stable FRQ—as frq^+ or frq^{S900A}—as well as of strains with more stable FRQ, as frq^7 or frq^{S548A} (Fig. 3, B and C). Loss of FWD-1 even made an arrhythmic strain rhythmic (frq^{5xS→D}), having clustered S to D mutations at phosphorylated residues S538, S540, S541, S545, and S548 within the PEST1 region (17) (Fig. 3C).

Half-life of FRQ is a correlative measurement, and not a determinant factor, of period length

The above-mentioned results emphasized the unforeseen nature of these circadian rhythms: The period alterations in strains such as frq^1, frq^7, or
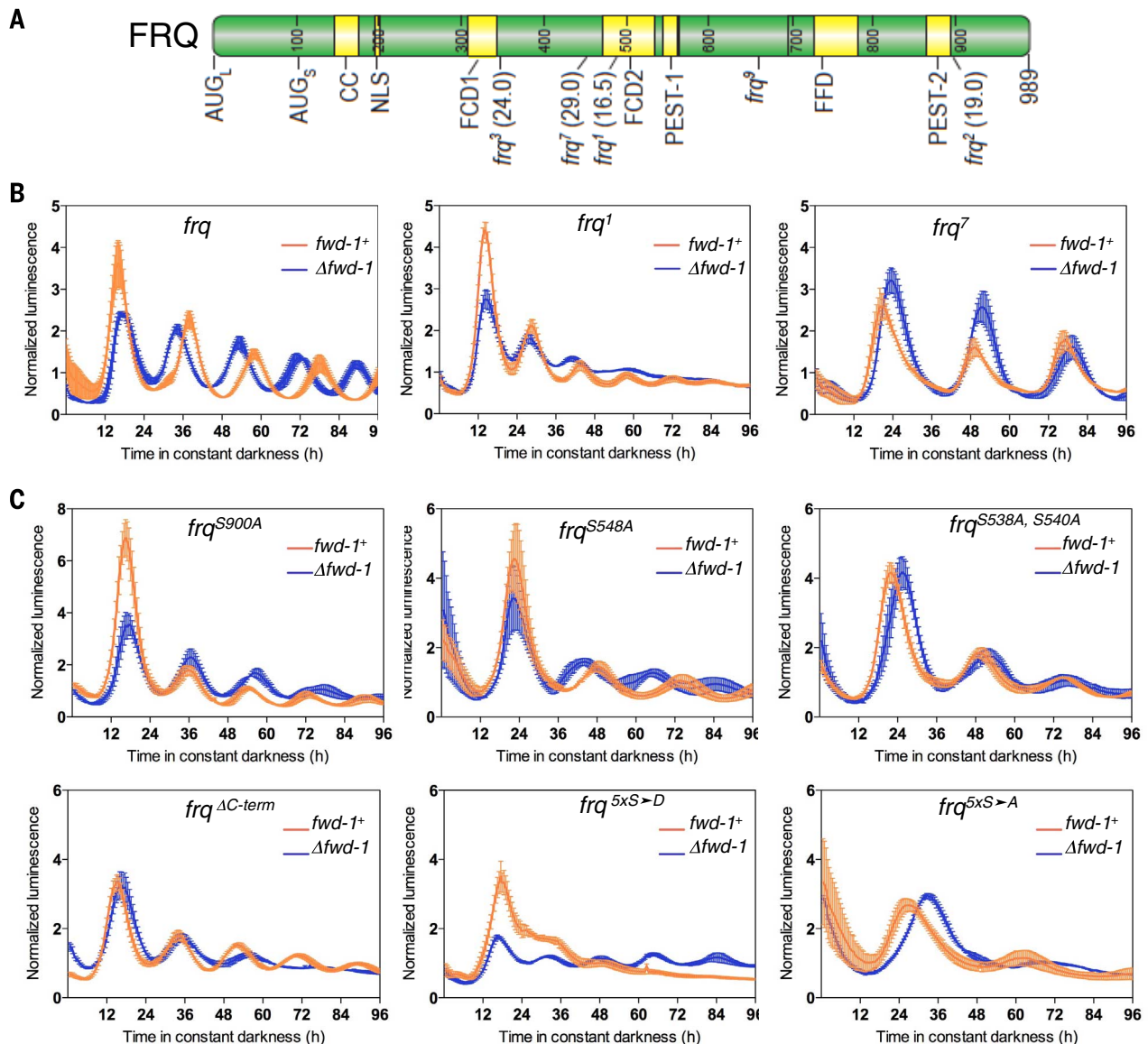
Fig. 3. Rhythmicity in the absence of FWD-1 depends on the FRQ-WCC oscillator. (A) Scheme depicting the main features of FRQ, including domains and the position of the mutations of the main frq alleles and their period alterations. AUG_L and AUG_S, starts of long and short FRQ proteins; CC, coiled coil region; NLS, nuclear localization; FCD, CK1 interaction domains; PEST, domains enriched in proline, aspartate, glutamate, serine, and threonine associated with turnover; FFD, FRQ-FRH interaction. **(B)** A frq_{c-box}-luc reporter was used to monitor the status of the oscillator by following frq expression in strain containing different isolated frq alleles or **(C)** V5-tagged frq mutants as indicated on top of each graph, in the strains with (fwd-1^+) or without (Δfwd-1) FWD-1. LUC activity was quantified for both WT and Δfwd-1 strains. Each line corresponds to the average of three different wells ±SEM. Periods for each strain can be found in table S2.

frq^{S900A} have been explained by changes in FRQ stability, and indeed FRQ half-life strongly correlates with period in these strains (*9*) (Fig. 4) in a manner similar to the correlation of locomotor rhythm period with PER half-life in *Drosophila* (*13*). That is, although in a WT *Neurospora* strain with a period of about 22 hours FRQ had a half-life of close to 2.8 hours, in *frq*^{7} cells (period ~29 hours), FRQ half-life was about 3.8 hours, whereas in *frq*^{1} cells (period ~16 hours) half-life was ~2 hours (*9*), yielding a strong correlation (Fig. 4D). However, examination of *Δfwd-1* strains confirmed that, in agreement with previous reports (*19*), FRQ half-life is increased (Fig. 4, A and B). Current models would predict that these increased half-lives would yield circadian periods of 39 hours or more (Fig. 4C). Instead, for all six *frq* alleles examined, we observed that period lengths in the absence of *fwd-1* remained close to those reported for turnover-proficient strains. Similar apparent inconsistencies between observed period length and stability can be found in the literature for other clustered FRQ phosphosite mutants that appear to cripple FRQ degradation without undue effects on clock-signaling phosphorylations (*18, 37, 38*), as well as the presence of altered FRQ profiles in overtly rhythmic strains (*18*). Although period was not unaffected

by loss of FWD-1, a finding consistent with possible side effects of its loss on other cellular proteins, the decisive finding is that period length is not correlated with FRQ half-life: Clock protein stability does not determine clock period length and, in this canonical TTFL, the circadian negative element does not have to be completely or even substantially removed to release repression by the negative arm of the circadian feedback loop.

Inhibition of kinase activity lengthens period independently of FRQ stability

We and others were initially led to hypotheses positing an essential role for protein turnover in the clock, both from the observed rhythms in negative element abundance—among the first and most solid generalizations to arise in the comparative molecular clocks literature (*1–3, 10, 11*)—and also from the clear cycles in phosphorylation of negative elements that precede turnover (*14*). Thus, given the inescapable conclusion from our data that total clearance of the negative element is not an essential step in the TTFL, we were led to reexamine phosphorylation. We used 6-dimethylaminopurine (6-DMAP), a broad-spectrum kinase inhibitor that blocks clock pro-

tein phosphorylation, and examined its effects in both WT (*fwd-1*$^+$) strains and in *Δfwd-1* strains deficient in clock protein turnover. Consistent with previous data (*14*), we observed that 6-DMAP lengthened period in a dose-dependent manner and did so independently of changing the inherent stability of FRQ as influenced by FWD-1 (fig. S6, A and B). Inhibition of kinase activity also had similar effects in the long-period *frq*^{7} mutant that has a more stable FRQ protein (fig. S6), but the pertinent question in light of the clock model is whether this period lengthening is accompanied by changes in FRQ stability. We examined FRQ stability in two concentrations of inhibitor that lengthen period (150 μM and 250 μM 6-DMAP) in three genetic backgrounds and found that the period lengthening was not accompanied by stabilization of FRQ, as previous models would predict (fig. S7, A to D). We reconfirmed published data (*14*) showing that higher doses (5 mM of 6-DMAP) can stabilize FRQ, but note that the stabilization effect was reduced in *Δfwd-1* strains in which FRQ has already been stabilized by loss of its primary connection to the proteasome (fig. S7, E and F). Overall, these data confirm the importance of daily phosphorylation to circadian cycling and period length but support a model in which the
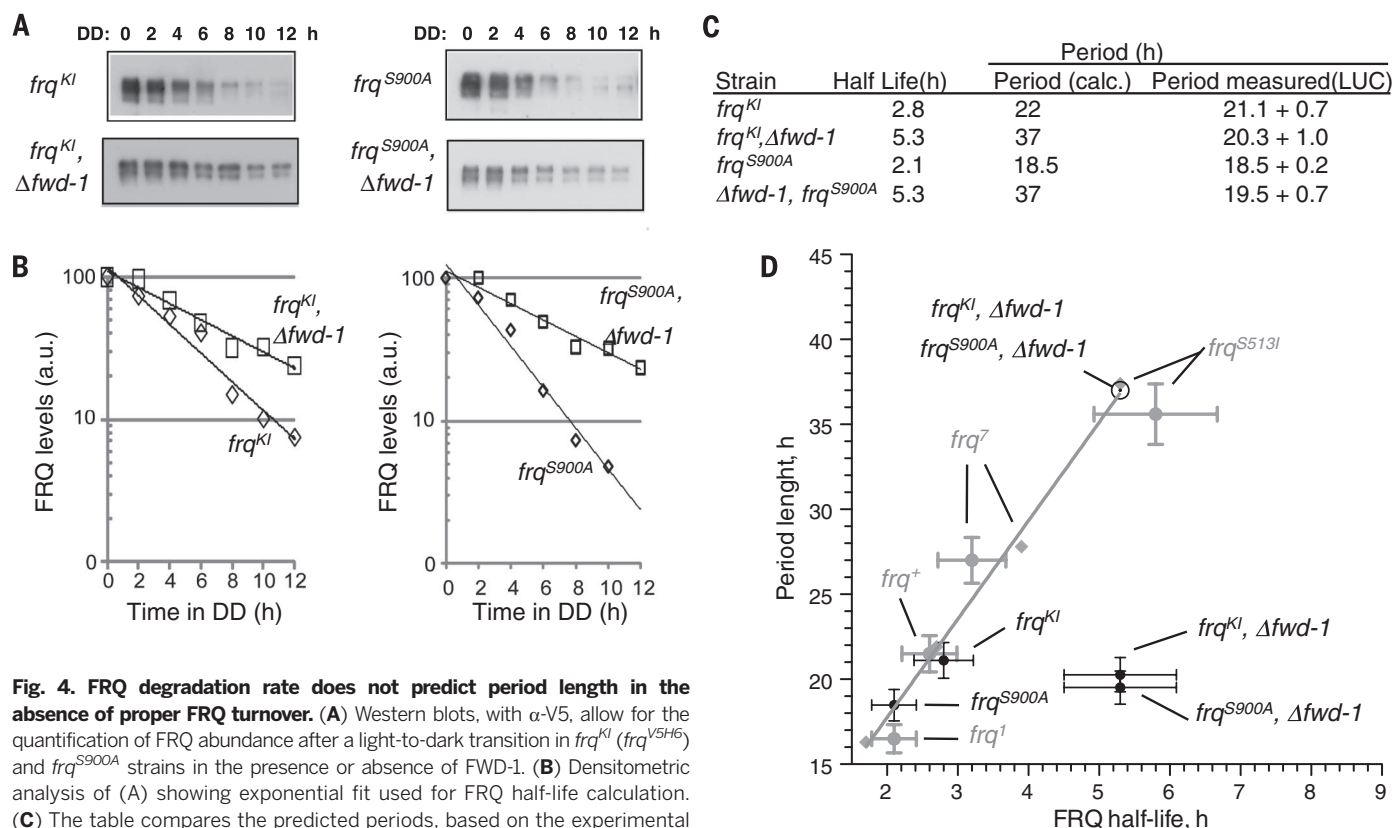
Fig. 4. FRQ degradation rate does not predict period length in the absence of proper FRQ turnover. (**A**) Western blots, with α-V5, allow for the quantification of FRQ abundance after a light-to-dark transition in *frq*^{KI} (*frq*^{V5H6}) and *frq*^{S900A} strains in the presence or absence of FWD-1. (**B**) Densitometric analysis of (A) showing exponential fit used for FRQ half-life calculation. (**C**) The table compares the predicted periods, based on the experimental half-lives (*9*), with the ones obtained with the *frq*$_{c-box}$-*luc* reporter for each strain. (**D**) These values were plotted along with the data from Ruoff *et al*. (*9*). Experimental data for period length (gray dots) correlates well with protein half-life, leading to a model (gray line) in which periods can be predicted for each strain (gray diamonds). Period lengths for *frq*^{S900A} and *frq*^{KI} (black dots) nicely fit the model. In the absence of FWD-1, the model predicts these two strains to have a period of 37 hours (open circle). Nevertheless, luciferase analysis reveals a period of about 20 hours (black dots), close to the original *frq* allele present in each strain. Uncertainties in period and half-life determinations were considered as an average of 5 or 15%, respectively (*9*).

half-life of a circadian negative element is a correlative measurement, and not a determinant factor, of period length.

Discussion

Revaluating the relation between FRQ half-life and period determination

Our data lead us to several seemingly inescapable conclusions. One is that the long-standing relation between clock protein phosphorylation, clock protein stability, and period determination ought to be revisited. The data indicate that it is the qualities of FRQ rather than its quantity that are crucial and that the strong correlations between clock protein phosphorylation and half-life and between half-life and period length are, in fact, just correlations that do not imply in all cases cause and effect. Equally important is the related conclusion that clock proteins such as FRQ acting as negative elements do not need to be mostly eliminated by turnover before the next cycle of their synthesis can start. Thus, although degradation is the final outcome of FRQ posttranslational modifications, phosphorylation may be the key mechanism determining clock speed and the point at which the next cycle of *frq* synthesis is initiated. Figure 5 presents a cartoon context summarizing both the obligate and the associated events in the circadian cycle as an aid in viewing these distinctions. Our data indicate two general classes of conceptual phosphorylation events on a clock protein, clock-signaling phosphorylations (CSP) and termination-signaling phosphorylations (TSP). In this model, clock speed is dictated by the rate at which a sequential series of CSP—and the associated secondary, tertiary, and quaternary structural as well as intracellular localization changes resulting from these CSP—take place in and among the clock protein complex of FRQ/FRH/CK1/WC-1/WC-2 (*17*). Under normal circumstances, these sequential CSP events will lead inexorably to TSP and to degradation of the negative element (e.g., FRQ) that may ordinarily be extremely rapid (unless strains have impaired protein turnover). However, once CSPs are completed, the rate of clock protein turnover per se is not a factor in determining circadian period length. This allows many predictions, among them that mutations causing a long period may delay CSP (pre-TSP) either directly by affecting phosphorylation sites or by eliciting structural changes that delay some key phosphorylation events. In this context, longer half-life of the clock protein does not cause a longer period by delaying the subsequent onset of new clock protein synthesis but rather is a consequence of a delayed cascade of phosphorylation events (including, necessarily, TSPs).

Predictions derived from the proposed model

This model provides novel perspectives and makes several predictions. For instance, clearance of the TTFL negative element (here FRQ) is not required before reinitiation of its synthesis (Fig. 2); changes in phosphorylation, turnover, and period length

do not need to be correlated (Fig. 4); and a broad-spectrum kinase inhibitor can lengthen period without changing negative element stability (figs. S7 and S8). We predicted that CSP and TSP would be distinct and identifiable; however, this was problematic. For instance, TSP (*sensu stricto*) were predicted to alter stability but not period and might include the "recreational phosphorylation" sites in FRQ (*17*), especially those residues phosphorylated late in the cycle whose mutation has no effect on period. However, these have not been seen, perhaps because phosphodegrons act as charged domains rather than as just one or two charged amino acids. The distinction between CSP and TSP may, however, explain the anomalous $frq^{5xS \rightarrow D}$ mutant (Fig. 3C) whose arrhythmicity is suppressed by

Δfwd-1. The revised TTFL model would view these mid- to late-cycle PEST1 region phosphorylations (*17*) primarily as CSP that lead to later separate events, including degradation. In Δfwd-1, mutation of these serines to phosphomimic aspartates propels a premature closing of the negative arm and a shorter than WT period length. CSPs would also include phosphorylations that regulate the ability of the negative element to act as a repressor. For instance, hyperphosphorylated FRQ interacts poorly, if at all, with the WCC (*17*) or with CK1a (*39*) and is impaired in repression of WCC activity (*40*), all consistent with a clock that has become blind to FRQ after all CSPs have been achieved. Premature phosphorylation can influence period by affecting CSP or stability, but once CSPs of the negative element deactivate its
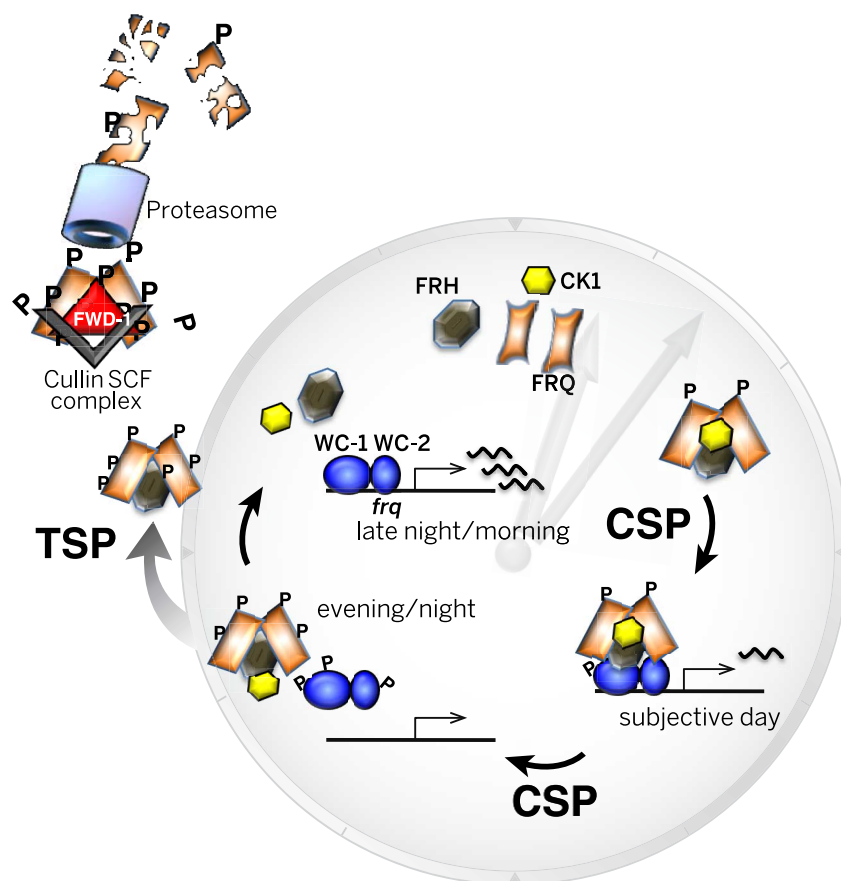
Fig. 5. A model describing distinct roles for clock protein phosphorylation and degradation through time. Essential events in the circadian cycle are shown within the shaded clock face. In the late night, WC-1 and WC-2 interact via PAS domains and assemble as the WCC at the Clock-box on the *frq* promoter to drive transcription, which leads to WC-1 destabilization. FRQ is expressed as a largely unstructured protein, adopting a defined and functional structure as it dimerizes and forms a complex with FRH (*6*). As part of this complex, CK1 is recruited (*17*). Hypophosphorylation of FRQ begins the CSP, whose kinetics determine the long time constant of the cycle, thereby setting circadian period length. FRQ promotes phosphorylation of WC-1 by CK1 and other kinases, eventually reducing *frq* expression to low levels and thereby stabilizing WC-1. Phosphorylated WCC leaves the *frq* promoter. As FRQ becomes hyperphosphorylated, it loses its ability to interact with CK1 (*39*) and WCC (*17*), becoming therefore a weak repressor of WCC (*40*). In addition, dephosphorylation of WCC, as well as new synthesis of these proteins, provide active WC-1 and WC-2 to reinitiate the cycle. Independently, and with kinetics that do not affect timekeeping, TSPs on FRQ lead to its recognition by FWD-1 and its associated cullin-SCF complex, leading to FRQ ubiquitylation and turnover in the proteasome.

ability to repress, later phosphorylations can no longer affect clock function.

It is premature to broadly generalize these findings to all TTFLs; however, data from animal clocks are not inconsistent with these ideas. For instance, phosphorylation of *Drosophila* PER (dPER) by Doubletime kinase (DBT) at Ser47 (S47), a key step in controlling the speed of that clock, elicits phosphorylation of nearby residues to generate a high-affinity atypical SLIMB-binding site that leads to PER turnover (*12*). Ablation of SLIMB is correlated with constitutively high amounts of negative elements and behavioral arrhythmicity (*23*); however, a dPER S47A mutant showing reduced affinity for SLIMB and a long period length displayed persistent multiply phosphorylated dPER at all times of day, including times coincident with cyclical synthesis of new PER; this result is most straightforwardly interpreted as reinitiation of new PER synthesis in the presence of inactive old PER (*12*). The existence of such a class of PER invisible to the feedback loop is a prediction from the revised model, and identification of DBT-driven phosphorylation of S47 as a period-determining step (CSP in our terminology) does not contradict the revised model presented here. Although in most cases in *Drosophila*, alterations in period have been attributed to changes in PER degradation rates, the effect of some mutants such as DBT^S cannot be simply explained by effects on PER stability (*13*). In mammals, epistasis among mutations that impact the stability of PER and CRY proteins is unexpectedly absent (*41*). Consistent with data from *Neurospora*, including those reported here, inhibition of kinases (casein kinase I, among others) in animals reliably lengthens circadian period in whole organisms or in cell lines by up to 6 hours (*10, 16–18, 22, 37, 42, 43*); although these data are usually interpreted in terms of phosphorylation promoting F-box protein substrate recognition leading to turnover, the effects of reduction of these F-box protein levels have been less consistent. Knockdown of β-TRCP1 lengthened rhythms in NIH3T3 cells by only ~1 hour (*42*), and the circadian period of β-TrCP1 homozygote knockout mice is identical to that of WT animals (*43*); in contrast, knockdown of β-TRCP2 in U2OS cells leads to more dramatic period lengthening that is further enhanced when RNA interference is directed to both β-TRCPs (*44*). Mutation or knockdown of FBXL3 leads to increased CRY1 amounts and marked period lengthening (*44–46*), an effect that can be minimized by suppressing FBXL21 expression (*47, 48*); both results suggest that CRY1 levels and stability mediate the period effect. However, changes in CRY1 stability observed by eliminating FBXL21 alone (an F-Box protein that stabilizes CRYs) or in combination with FBXL3 (*47*), or by mutating phosphosites within CRY1 (*49*), do not clearly correlate with the observed changes in period. Plausible explanations for some of these data may exist, among them possible paralog compensation, cellular compartment–specific effects, or effects of F-box protein ablation on

proteins other than PERs and CRYs; however, another possibility is that in these strains it is the phosphorylation status per se of the clock proteins that is crucial, rather than the derivative effects of phosphorylation on their stability or the timing of their ultimate turnover, each of which can be uncoupled from period determination. It may be that in these systems, the heretofore obligate coupling between clock protein stability and period determination, as well as the requirement of negative element turnover to reinitiate the circadian feedback loop, warrant a closer look.

Materials and methods

Strains

Strains used in this study are listed in table S1. Knockouts for *csn* components, *fwd-1* or *wc-1*, generated by the *Neurospora* functional genomics program (*50*) as well as *frq^7* and *frq^1* strains, were obtained from the Fungal Genetics Stock Center (Kansas City, Missouri, USA) (*51*). Strains containing the *frq^{V5H6}* (herein indistinctively mentioned as *frq^{V5}* or *frq^{KI}*) or other mutant *frq* alleles based on this knock-in construct have already been described (*17*), as well as the *frh^{R806H}* mutant (*32*).

Crosses between reporter strains and strains of interest were conducted as described in www.fgsc.net/Neurospora/NeurosporaProtocolGuide.htm and www.fgsc.net/methods/stanford.html. For race-tube analyses, progeny bearing the *ras-1^{bd}* allele [as determined by PCR (*52*)] were selected. Importantly, we did not observe differences between *ras-1^{wt}* or *ras-1^{bd}* in luciferase analyses. The reporter strains used in these studies correspond to (i) A *frq^{luc}* translational fusion in which the *luc* sequence has been fused in frame to the second-to-last codon of the *frq* gene, as already reported (*30*), and (ii) a reporter in which the Clock-box of the *frq* promoter (*53*) drives the expression of *luc* (*28*). Briefly, this construct, called *frq$_{c-box}$-luc*, contains a modified promoter region present in plasmid pAF 45 (*36*), where the pLRE (proximal light regulatory element) has been mutated, whereas the dLRE (Clock-box element) has been left intact (*36*). This reporter plasmid, which contains a resected *frq* promoter, was transformed into a *Neurospora* histidine auxotrophic strain (no. 87-74, *ras-1^{bd}* *his-3*), thereby targeting the transgene to *his-3*, and then backcrossed to strain 74A. Progeny from this cross were selected, genotyped, and used as a parental in the crosses described in this study. Genotypes of the different strains used herein were confirmed by PCR (see below).

Culture conditions

Race-tube studies were conducted as previously described (*14*). Liquid culture media (LCM 2%) consisted of 2% glucose, 0.5% arginine, 50 ng/ml biotin, and 1x Vogel's salts. Circadian cultures and FRQ degradation experiments were performed as already reported (*14, 54*). Race tubes that were examined for bioluminescence were supplemented with a sterile luciferin solution to a final concentration of 25 μM. Solid LCM 2% media refers to LCM 2% supplemented with 1.5% agar.

For in vivo monitoring of bioluminescence in multiple strains, 96-well plates were used. Liquid nitrogen–cooled charge-coupled device (LN-CCD) media (0.03% glucose, 0.05% arginine, 50 ng/ml biotin, 1.5% agar, and 25 uM luciferin) supplemented with quinic acid (QA) (to a final concentration of 0.01 M) were used as solid media for the 96-well plate assays throughout the studies. Although quinic acid does not affect the *Neurospora* circadian clock (*55*), we found it to dramatically increase the amplitude of the luciferase reporter signals when performing assays in 96-well plates, probably due to an increase of a metabolizable carbon source. Routinely, three wells were inoculated for each strain, using a freshly prepared spore suspension. Plates were covered with a sterile film permeable to O_2 and CO_2 (USA Scientific) and incubated at 25°C under constant light in a Percival incubator, before transferring to DD conditions to be examined for dynamic luciferase expression. 6-DMAP (Sigma) was added to liquid or solid media in the concentrations indicated.

Protein analyses from solid media cultures

Analyses were performed from samples grown on Petri plates containing agar media, as described above (LN-CCD + QA). These plates were overlaid with sterile wet cellophane, on top of which, at the center of the plate, 5 μl of a 10^5-spore suspension were inoculated. Plates were kept in an upside-up position at 25° C LL (constant light) for 4 hours, after which they were transferred to DD (constant darkness) conditions to then be harvested after a conventional staggered culture protocol schedule (*35*). For FRQ stability analyses, plates were grown for 36 hours in 25°C LL, previous to the transfers until completing 12 hours in DD. To harvest the biomass, a microscope slide was used to collect the fungal tissue growing on top of the cellophane and frozen immediately in an Eppendorf tube in liquid nitrogen. Samples were then processed for protein extraction.

Luciferase-based analyses

Bioluminescence analyses were conducted using either a VersArray 1300B or a 1024B PIXIS CCD system from Princeton Instruments. Both cameras were housed within Percival incubators, under constant dark conditions and constant temperature (25°C). The cameras are controlled with the WinView software (Princeton Instruments), and acquisition times were set to 10 min with a 20-min delay between images (two frames per hour). Data from the image series were extracted with a customized macro developed for ImageJ (http://rsbweb.nih.gov/ij) and customized with an Excel interface. Data were plotted as raw bioluminescence or normalized by dividing each frame of an individual region of interest (ROI) by the average luminescence registered in that particular ROI over time. Period determination was assessed with the BRASS software (Biological Rhythms Analysis Software System, P.E. Brown, Warwick University).

Protein preparation and Western blots

Protein extractions, analyses, and Western blots were conducted as previously described (*17*), using either FRQ antisera or α-V5 antibody (Invitrogen, Carlsbad, CA) at a 1:250 or 1:5000 dilution respectively.

DNA analyses

Neurospora genomic DNA was prepared from small liquid cultures using the Puregene DNA isolation kit (Gentra Systems). Genotyping was performed using sequence-specific primers for the amplification of *fwd-1* [Forward (Fwd), ATGGCC-GGCTTTCCTCCACGA; Reverse (Rev), ATCCTCAT-CAGCGGGCAACA; product size, 711 base pairs (bp)], *csn-2* (Fwd, ATGTCCGACGACGATTTCATG; Rev, GTAGTGTGAGGGAGTAGAAT; product size, 470 bp), *csn-1* (Fwd, ATGGACGACCGCAAATTAGC; Rev, CGCCGGAGCTGGCTTCGACA; product size, 980 bp), *csn-4* (fwd, ATGGTCTCCTCGGAAGTAAG; Rev, CATCTTCTCCAGGATGCCGA; product size, 858 bp), and *csn-5* (Fwd, GCTCGGCGAGAGCAA-CCGTT; Rev, GAGGGACGCTCTGTCCATCA; product size, 713 bp), and the amplification of the *mus-51* locus was used as amplification control in the multiplexing PCR reactions (Fwd, TGGAGGAA-GGATCAGGATGAG; Rev, CTGGTTGGCGCAGAA-GAGCA; product size, 522 bp). The presence of the *ras-1^bd* mutation was evaluated as previously reported (*52*).

REFERENCES AND NOTES

1. J. C. Dunlap, Molecular bases for circadian clocks. *Cell* **96**, 271–290 (1999). doi: 10.1016/S0092-8674(00)80566-8; pmid: 9988221

2. M. Rosbash, The implications of multiple circadian clock origins. *PLOS Biol.* **7**, e62 (2009). doi: 10.1371/journal.pbio.1000062; pmid: 19296723

3. D. Bell-Pedersen *et al.*, Circadian rhythms from multiple oscillators: Lessons from diverse organisms. *Nat. Rev. Genet.* **6**, 544–556 (2005). doi: 10.1038/nrg1633; pmid: 15951747

4. A. Montenegro-Montero, L. F. Larrondo, in *Neurospora: Genomics and Molecular Biology*, K. McCluskey, D. P. Kasbekar, Eds. (Caister Academic Press, Norfolk, 2013), pp. 243–271.

5. H. A. Duong, M. S. Robles, D. Knutti, C. J. Weitz, A molecular mechanism for circadian clock negative feedback. *Science* **332**, 1436–1439 (2011). doi: 10.1126/science.1196766; pmid: 21680841

6. J. M. Hurley, L. F. Larrondo, J. J. Loros, J. C. Dunlap, Conserved RNA helicase FRH acts nonenzymatically to support the intrinsically disordered *Neurospora* clock protein FRQ. *Mol. Cell* **52**, 832–843 (2013). doi: 10.1016/j.molcel.2013.11.005; pmid: 24316221

7. J. S. O'Neill, A. B. Reddy, Circadian clocks in human red blood cells. *Nature* **469**, 498–503 (2011). doi: 10.1038/nature09702; pmid: 21270888

8. J. S. O'Neill *et al.*, Circadian rhythms persist without transcription in a eukaryote. *Nature* **469**, 554–558 (2011). doi: 10.1038/nature09654; pmid: 21270895

9. P. Ruoff, J. J. Loros, J. C. Dunlap, The relationship between FRQ-protein stability and temperature compensation in the *Neurospora* circadian clock. *Proc. Natl. Acad. Sci. U.S.A.* **102**, 17681–17686 (2005). doi: 10.1073/pnas.0505137102; pmid: 16314576

10. S. A. Brown, E. Kowalska, R. Dallmann, (Re)inventing the circadian feedback loop. *Dev. Cell* **22**, 477–487 (2012). doi: 10.1016/j.devcel.2012.02.007; pmid: 22421040

11. J. Blau, PERspective on PER phosphorylation. *Genes Dev.* **22**, 1737–1740 (2008). doi: 10.1101/gad.1696408; pmid: 18593875

12. J. C. Chiu, J. T. Vanselow, A. Kramer, I. Edery, The phospho-occupancy of an atypical SLIMB-binding site on PERIOD that is phosphorylated by DOUBLETIME controls the pace

of the clock. *Genes Dev.* **22**, 1758–1772 (2008). doi: 10.1101/gad.1682708; pmid: 18593878

13. S. Syed, L. Saez, M. W. Young, Kinetics of doubletime kinase-dependent degradation of the *Drosophila* period protein. *J. Biol. Chem.* **286**, 27654–27662 (2011). doi: 10.1074/jbc.M111.243618; pmid: 21659538

14. Y. Liu, J. Loros, J. C. Dunlap, Phosphorylation of the *Neurospora* clock protein FREQUENCY determines its degradation rate and strongly influences the period length of the circadian clock. *Proc. Natl. Acad. Sci. U.S.A.* **97**, 234–239 (2000). doi: 10.1073/pnas.97.1.234; pmid: 10618401

15. Q. He, Y. Liu, Degradation of the *Neurospora* circadian clock protein FREQUENCY through the ubiquitin-proteasome pathway. *Biochem. Soc. Trans.* **33**, 953–956 (2005). doi: 10.1042/BST20050953; pmid: 16246019

16. S. Reischl, A. Kramer, Kinases and phosphatases in the mammalian circadian clock. *FEBS Lett.* **585**, 1393–1399 (2011). doi: 10.1016/j.febslet.2011.02.038; pmid: 21376720

17. C. L. Baker, A. N. Kettenbach, J. J. Loros, S. A. Gerber, J. C. Dunlap, Quantitative proteomics reveals a dynamic interactome and phase-specific phosphorylation in the *Neurospora* circadian clock. *Mol. Cell* **34**, 354–363 (2009). doi: 10.1016/j.molcel.2009.04.023; pmid: 19450533

18. C. T. Tang *et al.*, Setting the pace of the *Neurospora* circadian clock by multiple independent FRQ phosphorylation events. *Proc. Natl. Acad. Sci. U.S.A.* **106**, 10722–10727 (2009). doi: 10.1073/pnas.0904898106; pmid: 19506251

19. Q. He *et al.*, FWD1-mediated degradation of FREQUENCY in *Neurospora* establishes a conserved mechanism for circadian clock regulation. *EMBO J.* **22**, 4421–4430 (2003). doi: 10.1093/emboj/cdg425; pmid: 12941694

20. C. Heintzen, Y. Liu, The *Neurospora crassa* circadian clock. *Adv. Genet.* **58**, 25–66 (2007). doi: 10.1016/S0065-2660(06)58002-2; pmid: 17452245

21. C. Querfurth *et al.*, Circadian conformational change of the *Neurospora* clock protein FREQUENCY triggered by clustered hyperphosphorylation of a basic domain. *Mol. Cell* **43**, 713–722 (2011). doi: 10.1016/j.molcel.2011.06.033; pmid: 21884974

22. E. J. Eide *et al.*, Control of mammalian circadian rhythm by CKIepsilon-regulated proteasome-mediated PER2 degradation. *Mol. Cell. Biol.* **25**, 2795–2807 (2005). doi: 10.1128/MCB.25.7.2795-2807.2005; pmid: 15767683

23. B. Grima *et al.*, The F-box protein slimb controls the levels of clock proteins period and timeless. *Nature* **420**, 178–182 (2002). doi: 10.1038/nature01122; pmid: 12432393

24. H. W. Ko, J. Jiang, I. Edery, Role for Slimb in the degradation of *Drosophila* Period protein phosphorylated by Doubletime. *Nature* **420**, 673–678 (2002). doi: 10.1038/nature01272; pmid: 12442174

25. Q. He, P. Cheng, Q. He, Y. Liu, The COP9 signalosome regulates the *Neurospora* circadian clock by controlling the stability of the SCFFWD-1 complex. *Genes Dev.* **19**, 1518–1531 (2005). doi: 10.1101/gad.1322205; pmid: 15961524

26. J. Wang *et al.*, Role of individual subunits of the *Neurospora crassa* CSN complex in regulation of deneddylation and stability of cullin proteins. *PLOS Genet.* **6**, e1001232 (2010). doi: 10.1371/journal.pgen.1001232; pmid: 21151958

27. Z. Zhou, Y. Wang, G. Cai, Q. He, *Neurospora* COP9 signalosome integrity plays major roles for hyphal growth, conidial development, and circadian function. *PLOS Genet.* **8**, e1002712 (2012). doi: 10.1371/journal.pgen.1002712; pmid: 22589747

28. V. D. Gooch *et al.*, Fully codon-optimized luciferase uncovers novel temperature characteristics of the *Neurospora* clock. *Eukaryot. Cell* **7**, 28–37 (2008). doi: 10.1128/EC.00257-07; pmid: 17766461

29. M. Shi, L. F. Larrondo, J. J. Loros, J. C. Dunlap, A developmental cycle masks output from the circadian oscillator under conditions of choline deficiency in *Neurospora*. *Proc. Natl. Acad. Sci. U.S.A.* **104**, 20102–20107 (2007). doi: 10.1073/pnas.0706631104; pmid: 18056807

30. L. F. Larrondo, J. J. Loros, J. C. Dunlap, High-resolution spatiotemporal analysis of gene expression in real time: In vivo analysis of circadian rhythms in *Neurospora crassa* using a FREQUENCY-luciferase translational reporter. *Fungal Genet. Biol.* **49**, 681–683 (2012). doi: 10.1016/j.fgb.2012.06.001; pmid: 22695169

31. J. Guo, P. Cheng, Y. Liu, Functional significance of FRH in regulating the phosphorylation and stability of

Neurospora circadian clock protein FRQ. *J. Biol. Chem.* **285**, 11508–11515 (2010). doi: 10.1074/jbc.M109.071688; pmid: 20159972

32. M. Shi, M. Collett, J. J. Loros, J. C. Dunlap, FRQ-interacting RNA helicase mediates negative and positive feedback in the *Neurospora* circadian clock. *Genetics* **184**, 351–361 (2010). doi: 10.1534/genetics.109.111393; pmid: 19948888

33. P. Cheng, Q. He, Q. He, L. Wang, Y. Liu, Regulation of the *Neurospora* circadian clock by an RNA helicase. *Genes Dev.* **19**, 234–241 (2005). doi: 10.1101/gad.1266805; pmid: 15625191

34. N. Wei, G. Serino, X. W. Deng, The COP9 signalosome: More than a protease. *Trends Biochem. Sci.* **33**, 592–600 (2008). doi: 10.1016/j.tibs.2008.09.004; pmid: 18926707

35. G. Duffield, J. J. Loros, J. C. Dunlap, Analysis of circadian output rhythms of gene expression in *Neurospora* and mammalian cells in culture. *Methods Enzymol.* **393**, 315–341 (2005). doi: 10.1016/S0076-6879(05)93014-0; pmid: 15817297

36. A. C. Froehlich, Y. Liu, J. J. Loros, J. C. Dunlap, White Collar-1, a circadian blue light photoreceptor, binding to the *frequency* promoter. *Science* **297**, 815–819 (2002). doi: 10.1126/science.1073681; pmid: 12098706

37. A. Mehra *et al.*, A role for casein kinase 2 in the mechanism underlying circadian temperature compensation. *Cell* **137**, 749–760 (2009). doi: 10.1016/j.cell.2009.03.019; pmid: 19450520

38. M. Görl *et al.*, A PEST-like element in FREQUENCY determines the length of the circadian period in *Neurospora crassa*. *EMBO J.* **20**, 7074–7084 (2001). doi: 10.1093/emboj/20.24.7074; pmid: 11742984

39. L. Lauinger, A. Diernfellner, S. Falk, M. Brunner, The RNA helicase FRH is an ATP-dependent regulator of CK1a in the circadian clock of *Neurospora crassa*. *Nat. Commun.* **5**, 3598 (2014). doi: 10.1038/ncomms4598; pmid: 24710172

40. J. Cha, H. Yuan, Y. Liu, Regulation of the activity and cellular localization of the circadian clock protein FRQ. *J. Biol. Chem.* **286**, 11469–11478 (2011). doi: 10.1074/jbc.M111.219782; pmid: 21300798

41. E. S. Maywood *et al.*, Tuning the period of the mammalian circadian clock: Additive and independent effects of CK1εTau and Fbxl3Afh mutations on mouse circadian behavior and molecular pacemaking. *J. Neurosci.* **31**, 1539–1544 (2011). doi: 10.1523/JNEUROSCI.4107-10.2011; pmid: 21273438

42. S. Reischl *et al.*, Beta-TrCP1-mediated degradation of PERIOD2 is essential for circadian dynamics. *J. Biol. Rhythms* **22**, 375–386 (2007). doi: 10.1177/0748730407303926; pmid: 17876059

43. K. Ohsaki *et al.*, The role of beta-TrCP1 and beta-TrCP2 in circadian rhythm generation by mediating degradation of clock protein PER2. *J. Biochem.* **144**, 609–618 (2008). doi: 10.1093/jb/mvn112; pmid: 18782782

44. B. Maier *et al.*, A large-scale functional RNAi screen reveals a role for CK2 in the mammalian circadian clock. *Genes Dev.* **23**, 708–718 (2009). doi: 10.1101/gad.512209; pmid: 19299560

45. L. Busino *et al.*, SCFFbxl3 controls the oscillation of the circadian clock by directing the degradation of cryptochrome proteins. *Science* **316**, 900–904 (2007). doi: 10.1126/science.1141194; pmid: 17463251

46. G. Shi *et al.*, Dual roles of FBXL3 in the mammalian circadian feedback loops are important for period determination and robustness of the clock. *Proc. Natl. Acad. Sci. U.S.A.* **110**, 4750–4755 (2013). doi: 10.1073/pnas.1302560110; pmid: 23471982

47. A. Hirano *et al.*, FBXL21 regulates oscillation of the circadian clock through ubiquitination and stabilization of cryptochromes. *Cell* **152**, 1106–1118 (2013). doi: 10.1016/j.cell.2013.01.054; pmid: 23452856

48. S. H. Yoo *et al.*, Competing E3 ubiquitin ligases govern circadian periodicity by degradation of CRY in nucleus and cytoplasm. *Cell* **152**, 1091–1105 (2013). doi: 10.1016/j.cell.2013.01.055; pmid: 23452855

49. P. Gao *et al.*, Phosphorylation of the cryptochrome 1 C-terminal tail regulates circadian period length. *J. Biol. Chem.* **288**, 35277–35286 (2013). doi: 10.1074/jbc.M113.509604; pmid: 24158435

50. H. V. Colot *et al.*, A high-throughput gene knockout procedure for *Neurospora* reveals functions for multiple transcription factors. *Proc. Natl. Acad. Sci. U.S.A.* **103**, 10352–10357 (2006). doi: 10.1073/pnas.0601456103; pmid: 16801547

51. K. McCluskey, A. Wiest, M. Plamann, The Fungal Genetics Stock Center: A repository for 50 years of fungal genetics research. *J. Biosci.* **35**, 119–126 (2010). doi: 10.1007/s12038-010-0014-6; pmid: 20413916

52. W. J. Belden *et al.*, The band mutation in *Neurospora crassa* is a dominant allele of ras-1 implicating RAS signaling in circadian output. *Genes Dev.* **21**, 1494–1505 (2007). doi: 10.1101/gad.1551707; pmid: 17575051

53. A. C. Froehlich, J. J. Loros, J. C. Dunlap, Rhythmic binding of a WHITE COLLAR-containing complex to the *frequency* promoter is inhibited by FREQUENCY. *Proc. Natl. Acad. Sci. U.S.A.* **100**, 5914–5919 (2003). doi: 10.1073/pnas.1030057100; pmid: 12714686

54. P. Ruoff, M. K. Christensen, V. K. Sharma, PER/TIM-mediated amplification, gene dosage effects and temperature compensation in an interlocking-feedback loop model of the *Drosophila* circadian clock. *J. Theor. Biol.* **237**, 41–57 (2005). doi: 10.1016/j.jtbi.2005.03.030; pmid: 15935389

55. B. D. Aronson, K. A. Johnson, J. J. Loros, J. C. Dunlap, Negative feedback defining a circadian clock: Autoregulation of the clock gene *frequency*. *Science* **263**, 1578–1584 (1994). doi: 10.1126/science.8128244; pmid: 8128244

REPORTS

Low trap-state density and long carrier diffusion in organolead trihalide perovskite single crystals

Dong Shi,[1]* Valerio Adinolfi,[2]* Riccardo Comin,[2] Mingjian Yuan,[2] Erkki Alarousu,[1] Andrei Buin,[2] Yin Chen,[1] Sjoerd Hoogland,[2] Alexander Rothenberger,[1] Khabiboulakh Katsiev,[1] Yaroslav Losovyj,[3] Xin Zhang,[4] Peter A. Dowben,[4] Omar F. Mohammed,[1] Edward H. Sargent,[2] Osman M. Bakr[1]†

The fundamental properties and ultimate performance limits of organolead trihalide MAPbX$_3$ (MA = CH$_3$NH$_3^+$; X = Br$^-$ or I$^-$) perovskites remain obscured by extensive disorder in polycrystalline MAPbX$_3$ films. We report an antisolvent vapor-assisted crystallization approach that enables us to create sizable crack-free MAPbX$_3$ single crystals with volumes exceeding 100 cubic millimeters. These large single crystals enabled a detailed characterization of their optical and charge transport characteristics. We observed exceptionally low trap-state densities on the order of 10^9 to 10^{10} per cubic centimeter in MAPbX$_3$ single crystals (comparable to the best photovoltaic-quality silicon) and charge carrier diffusion lengths exceeding 10 micrometers. These results were validated with density functional theory calculations.

Solution-processed hybrid organolead trihalide (MAPbX$_3$) perovskite solar cells (PSCs) have now achieved 20.1% certified power conversion efficiencies (1), following a rapid surge of development since perovskite-based devices were first reported in 2009 (2). A key to the success of PSCs is the long diffusion length of charge carriers in the absorber perovskite layer (3). This parameter is expected to depend strongly on film crystallinity and morphology. Thermally evaporated MAPbI$_3$ films fabricated using a Cl$^-$-based metal salt precursor were reported to exhibit carrier diffusion lengths three times those of the best solution-processed materials, yet no measurable Cl$^-$ was incorporated in the final films, hinting at a major but unclear mechanism in the control of crystallinity and morphology (4, 5). These observations suggest that there may be room to improve upon already remarkable PSC efficiencies via the optimization of three key parameters: charge carrier lifetime, mobility, and diffusion length.

The quest for further improvements in these three figures of merit motivated our exploration of experimental strategies for the synthesis of large single-crystal MAPbX$_3$ perovskites that would exhibit phase purity and macroscopic (millimeter) dimensions. Unfortunately, previously published methods failed to produce single crystals with macroscopic dimensions large enough to enable electrode deposition and practical characterization of electrical properties (6). Past efforts based on cooling-induced crystallization were hindered by (i) the limited extent to which solubility could be influenced by controlling temperature, (ii) the complications arising from temperature-dependent phase transitions in MAPbX$_3$, and (iii) the impact of convective currents (arising from thermal gradients in the growth solution) that disturb the ordered growth of the crystals.

We hypothesized that a strategy using antisolvent vapor-assisted crystallization (AVC), in which an appropriate antisolvent is slowly diffused into a solution containing the crystal precursors, could lead to the growth of sizable MAPbX$_3$ crystals of high quality (with crack-free, smooth surfaces, well-shaped borders, and clear bulk transparency). Prior attempts to grow hybrid perovskite crystals with AVC have fallen short of these qualities—a fact we tentatively attributed to the use of alcohols as antisolvents (7). Alcohols act as good solvents for the organic salt MAX (8) due to solvent-solute hydrogen bond interactions; as a result, they can solvate MA$^+$ during the ionic assembly of the crystal, potentially disrupting long-range lattice order.

We instead implemented AVC (Fig. 1A) using a solvent with high solubility and moderate coordination for MAX and PbX$_2$ [N,N-dimethylformamide (DMF) or γ-butyrolactone (GBA)] and an antisolvent in which both perovskite precursors are completely insoluble [dichloromethane (DCM)]. We reasoned that DCM, unlike alcohols, is an extremely poor solvent for both

MAX and PbX$_2$ and lacks the ability to form hydrogen bonds, thus minimizing asymmetric interactions with the ions during their assembly into crystal form. When combined with a slow and controlled diffusion rate into DMF or GBA, our approach established the conditions for all the ionic building blocks of the perovskite to be coprecipitated from solution stoichiometrically.

Using this method, we grew high-quality, millimeter-sized MAPbBr$_3$ and MAPbI$_3$ single crystals (fig. S1) (9) whose shape conformed to the underlying symmetry of the crystal lattice. The phase purity of the as-grown crystals was confirmed by x-ray diffraction (XRD) performed on powder ground from a large batch of crystals (Fig. 1B).

The synthesized crystals were of sufficient quality and macroscopic dimensions to enable a detailed investigation of the optical and charge transport properties. The absorbance of MAPbX$_3$ (X = Br$^-$ or I$^-$) (Fig. 2) shows a clear band edge cutoff with no excitonic signature, which suggests a minimal number of in-gap defect states. For comparison, the absorption spectrum from the polycrystalline MAPbBr$_3$ (fig. S2) (9) and MAPbI$_3$ (5) thin films shows a peak near the band gap, which is often attributed to an excitonic transition. This observation is consistent with a substantial amount of disorder and lack of long-range structural coherence in nanostructured thin films (10). By extrapolating the linear region of the absorption edge to the energy-axis intercept (fig. S3) (9), we determined the optical band gaps of MAPbBr$_3$ and MAPbI$_3$ single
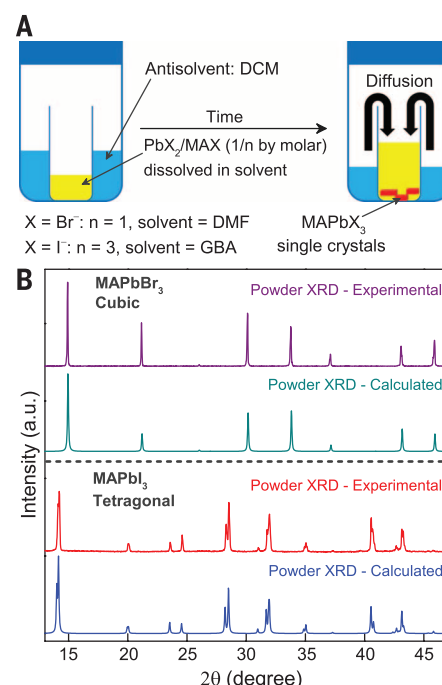
Fig. 1. Crystal growth and diffraction. (A) Schematic diagram of the crystallization process. **(B)** Experimental and calculated powder XRD profiles confirming the phase purity of MAPbX$_3$ crystals grown at room temperature (fig. S1). Single-crystal XRD data are given in (9).

[1]Solar and Photovoltaic Engineering Research Center (SPERC), King Abdullah University of Science and Technology (KAUST), 23955-6900 Thuwal, Saudi Arabia. [2]Department of Electrical and Computer Engineering, University of Toronto, Toronto, Ontario M5S 3G4, Canada. [3]Department of Chemistry, Indiana University, Bloomington, IN 47405, USA. [4]Department of Physics and Astronomy, University of Nebraska, Lincoln, NE 68588, USA.
*These authors contributed equally to this work. †Corresponding author. E-mail: osman.bakr@kaust.edu.sa

crystals to be 2.21 and 1.51 eV (Fig. 2), respectively. Both materials in their single-crystalline form exhibit a substantially narrower band gap than the corresponding films, which could enhance photon harvesting and hence improve photocurrent generation.

As also shown in Fig. 2, both MAPbBr$_3$ and MAPbI$_3$ exhibit a narrow photoluminescence (PL) that peaks near the band edge. A noticeable

Fig. 2. Steady-state absorbance and photoluminescence.
(**A**) MAPbBr$_3$ single crystal.
(**B**) MAPbI$_3$ single crystal. Insets: Absorbance versus photon energy and the determined band gap Eg. PL excitation wavelength was 480 nm.
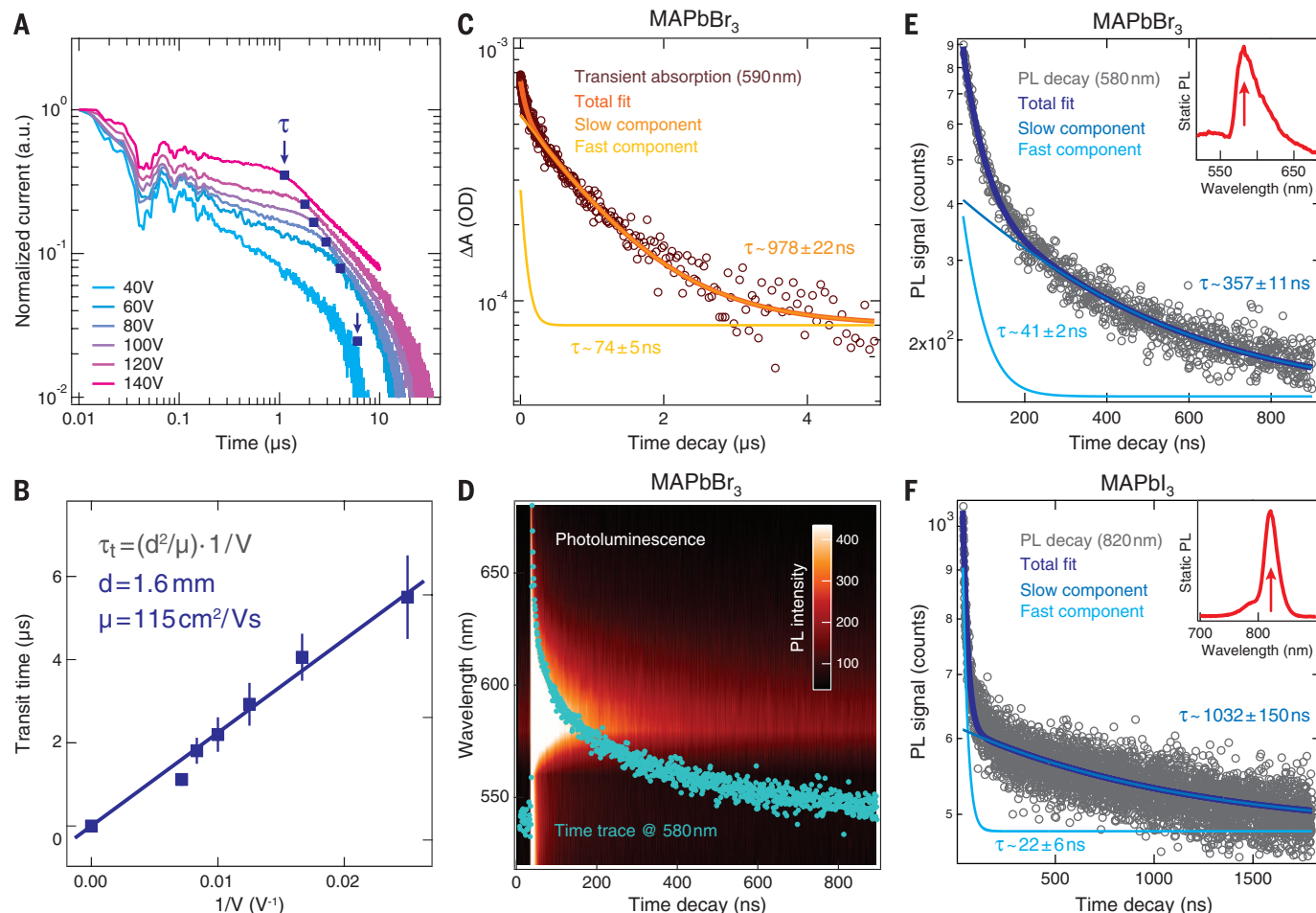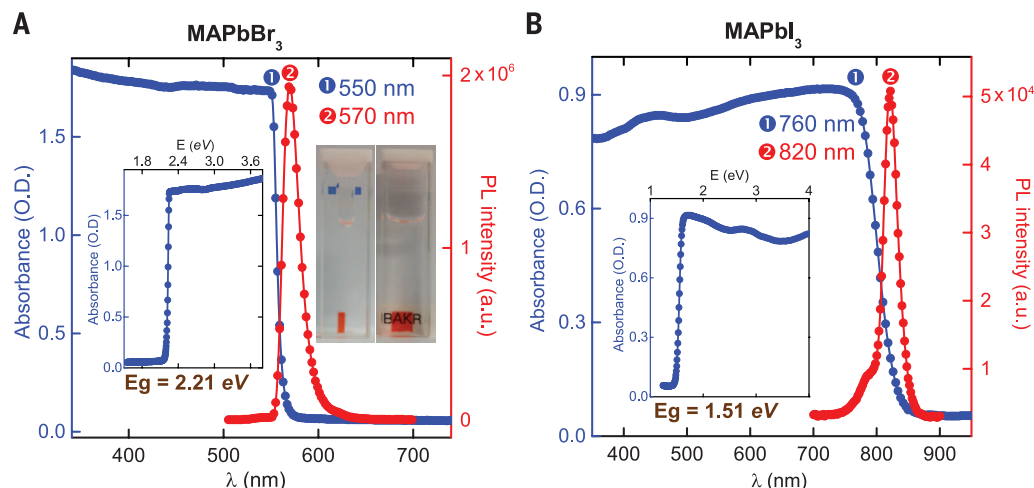
Fig. 3. Carrier mobility and lifetime measurements. (**A**) Time-of-flight traces showing the transient current after photoexcitation at time $t = 0$ in a bilogarithmic plot; the transit time τ_t is identified by the corner in each trace and marked by blue squares. (**B**) Linear fit of transit time versus inverse voltage V^{-1}. (**C**) Transient absorption in MAPbBr$_3$ crystals, evaluated at 590 nm, showing a fast component ($\tau \approx 74 \pm 5$ ns) together with a slower decay ($\tau \approx 978 \pm 22$ ns). (**D**) Time- and wavelength-dependent photoluminescence (PL) color map, with the time trace at $\lambda = 580$ nm superimposed (blue markers). (**E**) PL time decay trace on a MAPbBr$_3$ crystal at $\lambda = 580$ nm, with biexponential fits showing a fast ($\tau \approx 41 \pm 2$ ns) and a slow transient ($\tau \approx 357 \pm 11$ ns). (**F**) PL time decay trace on a MAPbI$_3$ crystal ($\lambda = 820$ nm, also showing a fast ($\tau \approx 22 \pm 6$ ns) and a slow ($\tau \approx 1032 \pm 150$ ns) component.

shoulder at ~790 nm in the PL of MAPbI$_3$ single crystals is in agreement with the PL from thin films [5], with the main PL peaking at 820 nm attributed to the intrinsic PL from the MAPbI$_3$ crystal lattice. A more structured PL spectrum was observed for polycrystalline MAPbBr$_3$ thin films (fig. S2) [9].

We investigated the key quantities that directly affect a material's potential for application in PSCs: carrier lifetime τ, carrier mobility μ, and carrier diffusion length L_D. In addition, we estimated the in-gap trap density n_{traps} in order to correlate the trap density with the observed diffusion length. For MAPbBr$_3$ single crystals, we first measured carrier mobility using the time-of-flight technique [11]. The transient current was measured for various driving voltages (V), and the corresponding traces are shown in Fig. 3A on a bilogarithmic scale. The transit time τ_t, defined as the position of the kink in the time traces, is marked by the blue squares, and the corresponding values are plotted in Fig. 3B as a function of V^{-1}. The mobility μ [$\mu = \mu_p \approx \mu_n$, where μ_p and μ_n are the hole and electron mobility, respectively [12, 13]] can be directly estimated from the transit time τ_t, sample thickness d, and applied voltage V as $\mu = d^2/V\tau_t$ (Fig. 3B) [9]. Estimating mobility via a linear fit of τ_t versus V^{-1} led to an estimate of 115 cm^2 V^{-1} s^{-1}. Complementary Hall effect measurements at room temperature confirmed a carrier (holes) concentration of between 5×10^9 and 5×10^{10} cm^{-3}, and provided a mobility estimate in the range from 20 to 60 cm^2 V^{-1} s^{-1}. Slightly lower mobilities obtained via the Hall effect may be ascribed to surface effects that are negligible for time-of-flight, which constitutes a bulk probe.

For MAPbI$_3$ single crystals, we estimated the carrier mobility using the space-charge-limited current (SCLC) technique. We measured the current-voltage (I-V) trace for the crystals and observed a region showing a clear quadratic dependency of the current on the applied voltage at 300 K (see fig. S8 for details). From this region, we could conservatively estimate the carrier mobility, obtaining the value μ = 2.5 cm^2 V^{-1} s^{-1}.

From the linear ohmic region, we also identified the conductivity of the crystal to be $\sigma = 1 \times 10^{-8}$ (ohm·cm)$^{-1}$. Combining the information on mobility and conductivity, we estimated a carrier concentration of $n_c = \sigma/e\mu \approx 2 \times 10^{10}$ cm^{-3} (where e is the electronic charge).

We estimated the carrier lifetime τ from transient absorption (TA) and PL spectra. Nanosecond pump-probe TA spectroscopy was carried out over a window covering the nanosecond-to-microsecond time scales in order to evaluate the fast ($\tau \approx 74$ ns) as well as the slow ($\tau \approx 978$ ns) carrier dynamics, as determined from biexponential fits. Time (t)– and wavelength (λ)–resolved PL maps $IPP(t, \lambda)$ (Fig. 3D) of single-crystalline MAPbBr$_3$ were acquired in the wavelength region around the main band-to-band recombination peak at 580 nm (λ = 500 to 680 nm). The time-dependent PL signals in single-crystalline samples of MAPbBr$_3$ and MAPbI$_3$ are shown in Fig. 3, E and F, respectively; the data were measured at the wavelength of the main PL peak—i.e., λ = 580 nm and λ = 820 nm for MAPbBr$_3$ and MAPbI$_3$, respectively (see insets).

The time-resolved traces are representative of the transient evolution of the electron-hole population after impulsive ($\Delta t \approx 0.7$ ns) photo-excitation. Biexponential fits were performed to quantify the carrier dynamics (fig. S4, blue traces) [9]. Both the bromide- and iodide-based perovskite crystals exhibited a superposition of fast and slow dynamics: $\tau \approx 41$ and 357 ns for MAPbBr$_3$, and $\tau \approx 22$ and 1032 ns for MAPbI$_3$. We assign these two very different time scales to the presence of a surface component (fast) together with a bulk component (slow), which reveals the lifetime of carriers propagating deeper in the material. The relative contribution of these two terms to the static PL can be readily evaluated by integrating the respective exponential traces (the integral is equal to the product of the amplitude A and the decay time τ), which shows that the fast (tentatively surface) component amounts to only 3.6% of the total TA signal in MAPbBr$_3$, and to 12% and 7% of the total PL signal in MAPbBr$_3$ and MAPbI$_3$, respectively.

Ultimately, by combining the longer (bulk) carrier lifetimes with the higher measured bulk mobility, we obtained a best-case carrier diffusion length $L_D = (k_B T/e \cdot \mu \cdot \tau)^{1/2}$ (where k_B is Boltzmann's constant and T is the sample temperature) of ~17 μm in MAPbBr$_3$; use of the shorter lifetime and lower mobility led to an estimate of ~3 μm. The same considerations were applied for the MAPbI$_3$ crystals to obtain a best-case diffusion length of ~8 μm and a worst-case length of ~2 μm.

For comparison, we also investigated the PL decay of solution-processed thin films of MAPbBr$_3$ (fig. S5). We again found two dynamics: a fast decay ($\tau \approx 13$ ns) and a longer-lived component ($\tau \approx 168$ ns), in both cases faster than the single crystals. This result suggests a larger trap-induced recombination rate in the thin films, which are expected to possess a much higher trap density than the single crystals. Previous studies on non–Cl-doped MAPbI$_3$ nanostructured thin films also corroborate this trend, revealing a PL lifetime of ~10 ns and a carrier diffusion length of ~100 nm [3, 5].

Crystalline MAPbX$_3$ is characterized by a charge transport efficiency that outperforms thin film–based materials in mobility, lifetime, and diffusion length. To unveil the physical origins of this difference, we investigated the concentration of in-gap deep electronic trap states. We measured the I-V response of the crystals in the SCLC regime (Fig. 4). Three regions were evident in the experimental data. At low voltages, the I-V response was ohmic (i.e., linear), as confirmed by the fit to an $I \approx V$ functional dependence (blue line). At intermediate voltages, the current exhibited a rapid nonlinear rise (set in at V_{TFL} = 4.6 V for MAPbBr$_3$ and 24.2 V for MAPbI$_3$) and signaled the transition onto the trap-filled limit (TFL)—a regime in which all the available trap states were filled by the injected carriers [14]. The onset voltage V_{TFL} is linearly proportional to the density of trap states n_{traps} (Fig. 4A). Correspondingly, we found for MAPbBr$_3$ single crystals a remarkably low trap density n_{traps} = 5.8×10^9 cm^{-3}, which, together with the extremely clean absorption and PL profiles (see again Fig. 2A), points to a nearly defect-free electronic structure. At high fields, the current showed a quadratic voltage dependence in the Child's regime. In this region, we extracted the value for the trap-free mobility μ. We found μ = 38 cm^2 V^{-1} s^{-1} (Fig. 4A), a value in good agreement with the mobility extracted using time-of-flight and Hall effect measurements (fig. S7) [9]. We determined a comparable low trap density n_{traps} = 3.3×10^{10} cm^{-3} for MAPbI$_3$ single crystals using the same method (Fig. 4B).

The defect density measured for the room temperature–grown MAPbX$_3$ crystals was superior to a wide array of established and emerging optoelectronic inorganic semiconductors including polycrystalline Si ($n_{traps} \approx 10^{13}$ to 10^{14} cm^{-3}) [15, 16], CdTe/CdS ($n_{traps} \approx 10^{11}$ to 10^{13} cm^{-3}) [17], and copper indium gallium selenide (CIGS) ($n_{traps} \approx 10^{13}$ cm^{-3}) thin films [18], as well as organic materials such as single-crystal rubrene ($n_{traps} \approx 10^{16}$ cm^{-3}) [19] and pentacene ($n_{traps} \approx 10^{14}$ to 10^{15} cm^{-3}) [20]. Only
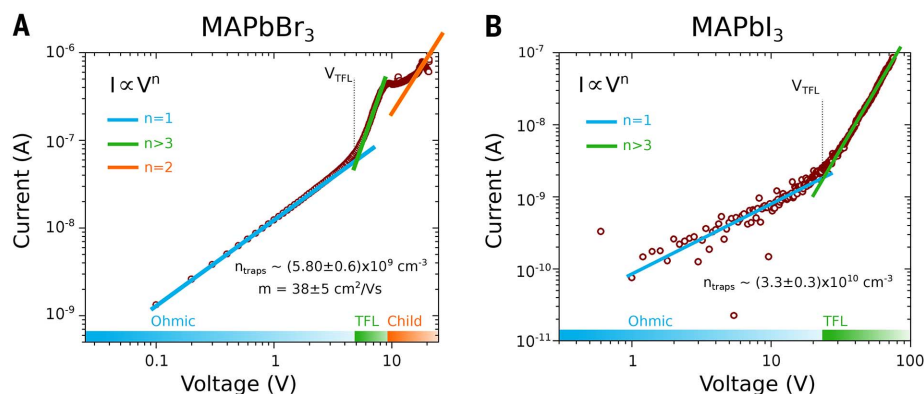
Fig. 4. Current-voltage traces and trap density. Characteristic I-V trace (purple markers) showing three different regimes for (**A**) MAPbBr$_3$ (at 300 K) and (**B**) MAPbI$_3$ (at 225 K). A linear ohmic regime ($I \propto V$, blue line) is followed by the trap-filled regime, marked by a steep increase in current ($I \propto V^{n>3}$, green line). The MAPbBr$_3$ trace shows a trap-free Child's regime ($I \propto V^2$, green line) at high voltages.

ultrahigh-quality crystalline silicon, grown at high temperatures, offers comparable or better deep trap densities ($10^8 < n_{traps} < 10^{15}$ cm^{-3}) (21, 22). The exceptionally low trap density found experimentally can be explained with the aid of density functional theory (DFT) calculations performed on MAPbBr$_3$, which predict a high formation energy for deep trap defects when MAPbBr$_3$ is synthesized under Br-rich conditions (e.g., from PbBr$_2$ and MABr), such as is the case in this study (9).

REFERENCES AND NOTES

1. National Renewable Energy Laboratory, Best Research-Cell Efficiencies; www.nrel.gov/ncpv/images/efficiency_chart.jpg.
2. A. Kojima, K. Teshima, Y. Shirai, T. Miyasaka, *J. Am. Chem. Soc.* **131**, 6050–6051 (2009).
3. T. C. Sum, N. Mathews, *Energy Environ. Sci.* **7**, 2518–2534 (2014).
4. C. Wehrenfennig, M. Liu, H. J. Snaith, M. B. Johnston, L. M. Herz, *Energy Environ. Sci.* **7**, 2269–2275 (2014).
5. S. D. Stranks et al., *Science* **342**, 341–344 (2013).
6. D. B. Mitzi, *Prog. Inorg. Chem.* **48**, 1–121 (1999).
7. Y. Tidhar et al., *J. Am. Chem. Soc.* **136**, 13249–13256 (2014).
8. M. Xiao et al., *Angew. Chem. Int. Ed.* **53**, 9898–9903 (2014).
9. See supplementary materials on *Science* Online.
10. J. J. Choi, X. Yang, Z. M. Norman, S. J. L. Billinge, J. S. Owen, *Nano Lett.* **14**, 127–133 (2014).
11. J. R. Haynes, W. Shockley, *Phys. Rev.* **81**, 835–843 (1951).
12. G. Giorgi, K. Yamashita, *J. Mater. Chem. A* 10.1039/C4TA05046K (2015).
13. E. Edri, S. Kirmayer, D. Cahen, G. Hodes, *J. Phys. Chem. Lett.* **4**, 897–902 (2013).
14. M. A. Lampert, P. Mark, *Current Injection in Solids* (Academic Press, New York, 1970).
15. J. R. Ayres, *J. Appl. Phys.* **74**, 1787–1792 (1993).
16. I. Capan, V. Borjanović, B. Pivac, *Sol. Energy Mater. Sol. Cells* **91**, 931–937 (2007).
17. A. Balcioglu, R. K. Ahrenkiel, F. Hasoon, *J. Appl. Phys.* **88**, 7175–7178 (2000).
18. L. L. Kerr et al., *Solid-State Electron.* **48**, 1579–1586 (2004).
19. C. Goldmann et al., *J. Appl. Phys.* **99**, 034507 (2006).
20. Y. S. Yang et al., *Appl. Phys. Lett.* **80**, 1595–1597 (2002).
21. J. R. Haynes, J. A. Hornbeck, *Phys. Rev.* **100**, 606–615 (1955).
22. J. A. Hornbeck, J. R. Haynes, *Phys. Rev.* **97**, 311–321 (1955).

High-efficiency solution-processed perovskite solar cells with millimeter-scale grains

Wanyi Nie,[1]* Hsinhan Tsai,[2]* Reza Asadpour,[3]† Jean-Christophe Blancon,[2]† Amanda J. Neukirch,[4,5] Gautam Gupta,[1] Jared J. Crochet,[2] Manish Chhowalla,[6] Sergei Tretiak,[4] Muhammad A. Alam,[3] Hsing-Lin Wang,[2]‡ Aditya D. Mohite[1]‡

State-of-the-art photovoltaics use high-purity, large-area, wafer-scale single-crystalline semiconductors grown by sophisticated, high-temperature crystal growth processes. We demonstrate a solution-based hot-casting technique to grow continuous, pinhole-free thin films of organometallic perovskites with millimeter-scale crystalline grains. We fabricated planar solar cells with efficiencies approaching 18%, with little cell-to-cell variability. The devices show hysteresis-free photovoltaic response, which had been a fundamental bottleneck for the stable operation of perovskite devices. Characterization and modeling attribute the improved performance to reduced bulk defects and improved charge carrier mobility in large-grain devices. We anticipate that this technique will lead the field toward synthesis of wafer-scale crystalline perovskites, necessary for the fabrication of high-efficiency solar cells, and will be applicable to several other material systems plagued by polydispersity, defects, and grain boundary recombination in solution-processed thin films.

T he recent discovery of organic-inorganic perovskites offers promising routes for the development of low-cost, solar-based clean global energy solutions for the future (1–4). Solution-processed organic-inorganic hybrid perovskite planar solar cells, such as CH$_3$NH$_3$PbX$_3$ (X = Cl, Br, I), have achieved high average power conversion efficiency (PCE) values of ~16% using a titania-based planar structure (1–7) or ~10 to 13% in the phenyl-C$_{61}$-butyric acid methyl ester (PCBM)–based architecture (8–10). Such high PCE values have been attributed to strong light absorption and weakly bound excitons that easily dissociate into free carriers with large diffusion length (11–13). The average efficiency is typically lower by 4 to 10% relative to the reported most efficient device, indicating persistent challenges of stability and reproducibility. Moreover, hysteresis during device operation, possibly due to defect-assisted trapping, has been identified as a critical roadblock to the commercial viability of perovskite photovoltaic technology (14–17). Therefore, recent efforts in the field have focused on improving film surface coverage (18) by increasing the crystal size and improving the crystalline quality of the grains (19), which is expected to reduce the overall bulk defect density and mitigate hysteresis by suppressing charge trapping during solar cell operation. Although approaches such as thermal annealing (20, 21), varying of precursor concentrations and carrier solvents (22), and using mixed solvents (23) have been investigated, control over structure, grain size, and degree of crystallinity remain key scientific challenges for the realization of high-performance devices.

Here, we report a solution-based hot-casting technique to achieve ~18% solar cell efficiency based on millimeter-scale crystalline grains, with relatively small variability (~2%) in the overall PCE from one solar cell to another. Figure 1A schematically describes our hot-casting process for deposition of organometallic perovskite thin films. Our approach involves casting a hot (~70°C) mixture of lead iodide (PbI$_2$) and methylamine hydrochloride (MACl) solution onto a substrate maintained at a temperature of up to 180°C and subsequently spin-coated (15 s) to obtain a uniform film (Fig. 1A). In the conventional scheme, the mixture of PbI$_2$ and MACl is spin-coated at room temperature and then post-annealed for 20 min on a hot plate maintained at 100°C. Figure 1, B to D, illustrates the obtained crystal grain structures using this hot-casting technique for various substrate temperatures and processing solvents. We chose a PbI$_2$/MACl molar ratio of 1:1 in all experiments described in this Report to achieve the basic perovskite composition and the best morphology (see fig. S1 for images). We observed large, millimeter-scale crystalline grains with a unique leaf-like pattern radiating from the center of the grain [see scanning electron microscopy (SEM) image of microstructure in fig. S2]. The x-ray diffraction (XRD) pattern shows sharp and strong perovskite (110) and (220) peaks for the hot-casted film, indicating a highly oriented crystal structure (fig. S3). The grain size increases markedly (Fig. 1, B and D) as the substrate temperature increases from room temperature up to 190°C or when using solvents with a higher boiling point, such

[1]Materials Physics and Application Division, Los Alamos National Laboratory, Los Alamos, NM 87545, USA. [2]Physical Chemistry and Applied Spectroscopy Division, Los Alamos National Laboratory, Los Alamos, NM 87545, USA. [3]School of Electrical and Computer Engineering, Purdue University, West Lafayette, IN 47907, USA. [4]Theoretical Chemistry and Molecular Physics Division, Los Alamos National Laboratory, Los Alamos, NM 87545, USA. [5]Center for Nonlinear Studies, Los Alamos National Laboratory, Los Alamos, NM 87545, USA. [6]Materials Science and Engineering, Rutgers University, Piscataway, NJ 08854, USA. *These authors contributed equally to this work. †These authors contributed equally to this work. ‡Corresponding author. E-mail: amohite@lanl.gov (A.D.M.); hwang@lanl.gov (H.-L.W.)
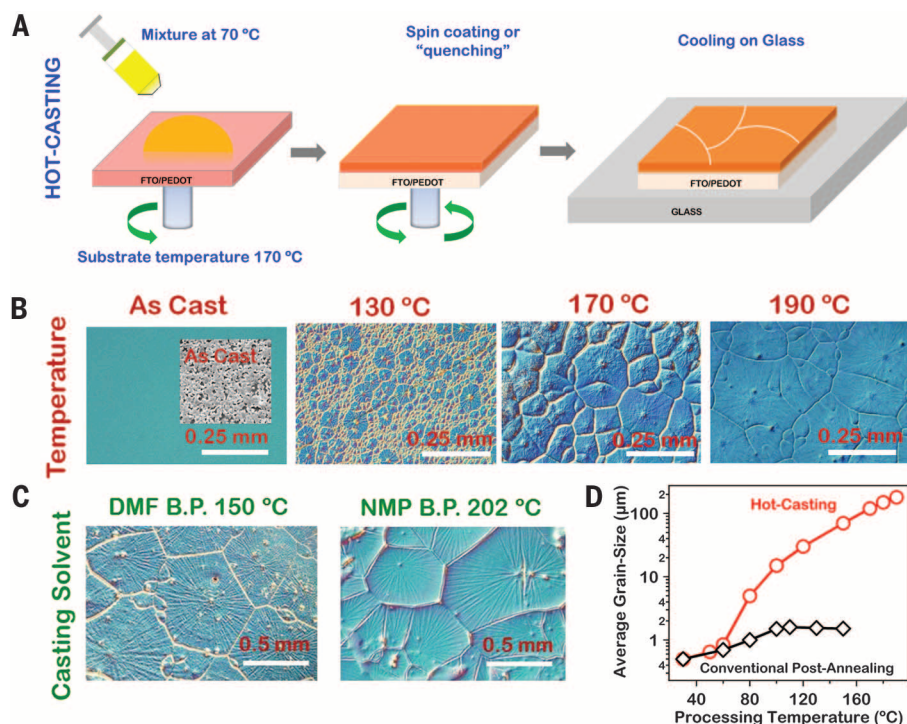
Fig. 1. Processing scheme for perovskite thin-film using hot-casting methods and observations for large-area millimeter-scale crystal grain formation for a perovskite (PbCH$_3$NH$_3$I$_{3-x}$Cl$_x$)–based thin film. (**A**) Hot-casting scheme for large-area crystal growth [ITO, indium tin oxide; FTO, fluorine-doped tin oxide; PEDOT, poly(3,4-ethylenedioxythiophene) polystyrene sulfonate]. (**B**) Optical micrographs illustrating grain formation as a function of substrate temperature with the casting solution maintained at 70°C. (**C**) Large-area grain formation using casting solvents with high boiling points. (**D**) Comparison of grain size as a function of processing temperature obtained for the hot-casting and conventional post-annealing methods.
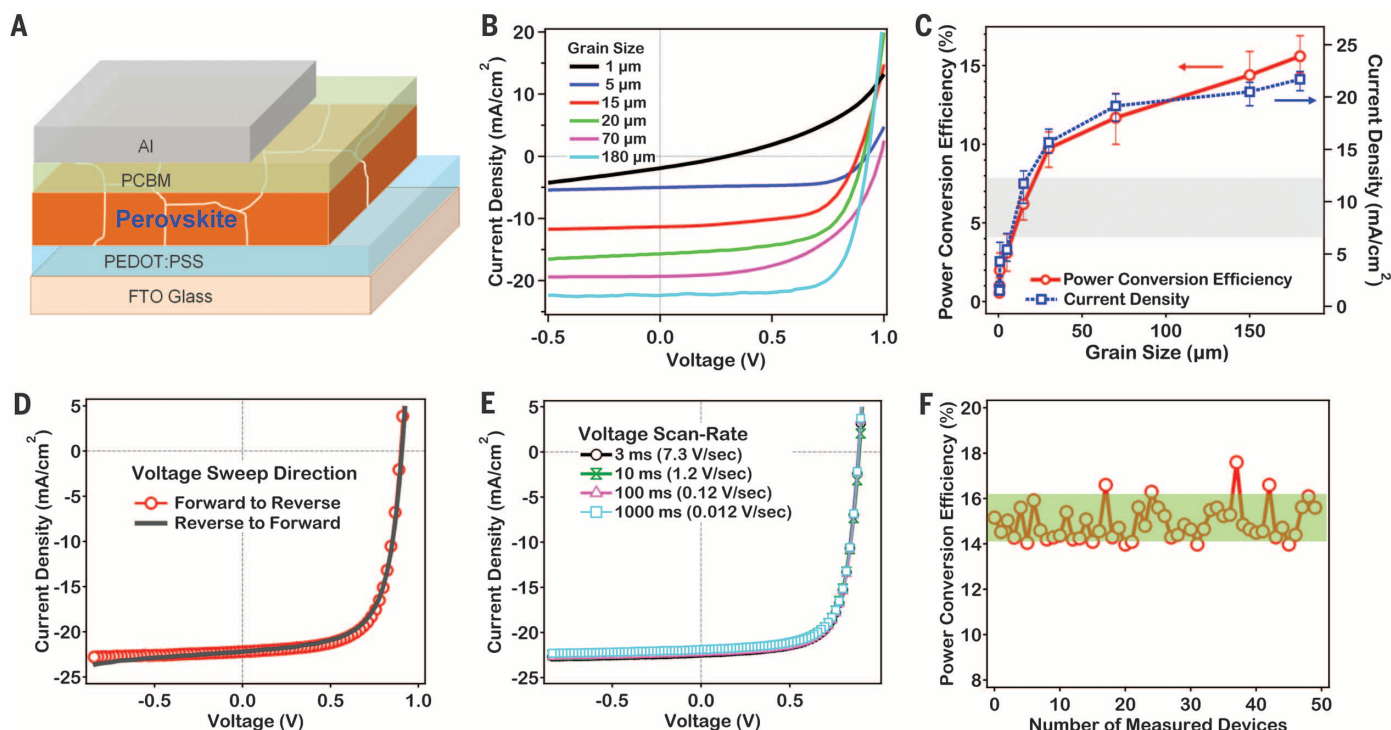
Fig. 2. Solar cell device architecture and performance. (**A**) Planar device configuration used for this study. (**B**) J-V curves obtained under AM 1.5 illumination. (**C**) Average overall PCE (left) and J_{SC} (right) as a function of crystalline grain size. The average values were obtained by averaging the PCE and J_{SC} for 25 devices; error bars were calculated by subtracting the average value from max or min values. Gray box represents the range of PCE values obtained using the conventional post-annealing process. (**D**) Average J-V characteristics resulted by sweeping the voltage from forward to reverse and from reverse to forward bias demonstrates the absence of hysteresis. These curves were obtained by averaging 15 sweeps in each direction. (**E**) J-V curves at different voltage scan rates in voltage delay time (ms) or V/s again demonstrate negligible hysteresis. (**F**) Variation in PCE for 50 measured devices.

as N,N-dimethylformamide (DMF) or N-methyl-2-pyrrolidone (NMP) (Fig. 1C).

Our method leads to grain sizes as large as 1 to 2 mm, in comparison with the grain sizes of ~1 to 2 μm typically obtained using the conventional post-annealing process. (See fig. S4 for details of the average grain size calculation procedure.) The major difference between hot-casting and conventional post-annealing is the presence of solvent when heating the substrate. For hot-casting, there is excess solvent present when the substrate is maintained above the crystallization temperature for the formation of the perovskite phase. This allows for the prolonged growth of the perovskite crystals, yielding large crystalline grains. Thus, the use of high–boiling point solvents (see Fig. 1C) provides the ideal conditions for the growth of large crystalline grains, as the excess solvent allows more time for their growth (24) (fig. S5).

Optical images (Fig. 1, B and C) and SEM images (fig. S2) illustrate that the perovskite thin films produced with the hot-casting method (from 100°C up to 180°C) are uniform, pinhole-free, and cover the entire substrate. We also used high-resolution SEM imaging to evaluate the morphology of the large- and small-area grains and found that except for the size of the grain, there was no observable difference in micromorphology (fig. S2). Preliminary analysis using high-resolution cross-sectional SEM imaging coupled with optical polarization microscopy and photoluminescence spectral imaging (figs. S18 to S20) shows consistency of the bulk single-crystalline nature over a large area of the perovskite film. The hot-casting method is applicable for both pure and mixed-halide perovskite combinations (fig. S6) and may lead to the realization of industrially scalable large-area crystalline thin films made from other materials [such as copper zinc tin sulfide (CZTS), copper indium gallium selenide (CIGS), and cadmium telluride (CdTe)] by means of low-temperature, solution-processed, large-area crystal growth.

We fabricated the mixed-halide organometallic perovskite photovoltaic devices using the hot-casting technique in a planar device architecture (Fig. 2A). The current density–voltage (J-V) curves

for devices fabricated at various temperatures measured under simulated air mass (AM) 1.5 irradiance of 100 mW/cm^2, calibrated using a NIST-certified monocrystalline Si solar cell (Newport 532 ISO1599), are shown in Fig. 2B. During measurements, a mask was used to confine the illuminated active area to avoid edge effects (25). PCE and short-circuit current density (J_{SC}) are plotted as a function of perovskite grain size in Fig. 2C. An optimal perovskite film thickness of ~450 nm was fixed for all devices to exclude variations in optical absorption or interference effects due to changes in film thickness. (See fig. S7 and table S1 for details of film thickness optimization and calibration.) We observed a marked increase in J_{SC} (3.5 mA/cm^2 to 22.4 mA/cm^2), open-circuit voltage (V_{OC}) (0.4 V to 0.92 V; fig. S8A), and fill factor (FF) (0.45 to 0.82; fig. S8B) when the grain size increased from ~1 μm up to ~180 μm, which translated into an increase in the overall PCE from 1% to ~18%. The J_{SC} of the devices is in good agreement with the calculated J_{SC} obtained by integrating the external quantum efficiency (fig. S9). In addition to the high PCE, we found that the solar cell device performance was hysteresis-free, with negligible change in the photocurrent density with either the direction of voltage sweep or the scan rate (or voltage delay time) (Fig. 2, D and E, and fig. S10). The devices exhibited a high degree of reproducibility in the overall PCE (Fig. 2F). We also applied the hot-casting technique with the conventional mixed-halide precursor (PbCl$_2$ and MAI, 1:3 molar ratio) but were not able to obtain high-performing devices, most likely because of differences in film morphology and uniformity (fig. S21).

High-performance cells have previously been reported with micrometer-sized grains (1, 26–28). We believe that there are two primary benefits of growing crystals with large grain size: (i) The reduced interfacial area associated with large grains suppresses charge trapping and eliminates hysteresis (irrespective of the direction of voltage sweep or the scan rate), and (ii) larger grains have lower bulk defects and higher mobility, allowing for the photogenerated carriers to propagate through the

device without frequent encounters with defects and impurities.

The J-V curves in Fig. 2B support the hypothesis. For example, the reduction in defect-assisted recombination in larger grains is reflected in the observed increase in V_{OC} from 0.4 V to 0.94 V and in FF from 0.4 to 0.83 with increased grain size. The J_{SC} value, 22.4 mA/cm^2, is on par with the highest values reported in literature. Indeed, the measured J_{SC}, V_{OC}, and FF values for the large-grain device compare favorably with the Shockley-Queisser theoretical limit ($J_{SC} \approx 26.23$ mA/cm^2, $V_{OC} \approx 1.02$ V, and FF ≈ 0.90) for the given device architecture and band alignment (24).

We performed a self-consistent optoelectronic simulation (involving solution of the Maxwell, Poisson, and drift-diffusion equations), which also supports the hypothesis of improved material quality for larger grains (Fig. 3, A to C). On the basis of material parameters from the literature (tables S2 to S5) and bulk defect density and mobility as fitting parameters, the model quantitatively reproduces all the salient features of the J-V characteristic (Fig. 3A) of both 17.7% (large grain) and 9.1% (small grain) cells. The key to the efficiency gain is the suppression of defect-assisted recombination in the bulk region: According to the normalized recombination distribution profile across the film thickness (fig. S11B), the majority of recombination for the small-grain device comes from the bulk defect (40% of the loss distributed in the bulk), which suggests that most of the loss comes from defect-assisted recombination. By contrast, for the large-grain device, recombination in the bulk is reduced to 5% of the overall recombination profile. Moreover, the energy band diagram of the large-grain 17.7% cell (Fig. 3B) shows that the absorber region is fully depleted, and the built-in electrical field and high mobility allow efficient charge collection. Consistent with the hypothesis, we find that the experimental results can be interpreted only if one assumes that mobility is correlated to grain size (Fig. 3C).

To understand recombination of photogenerated carriers during device operation, we measured
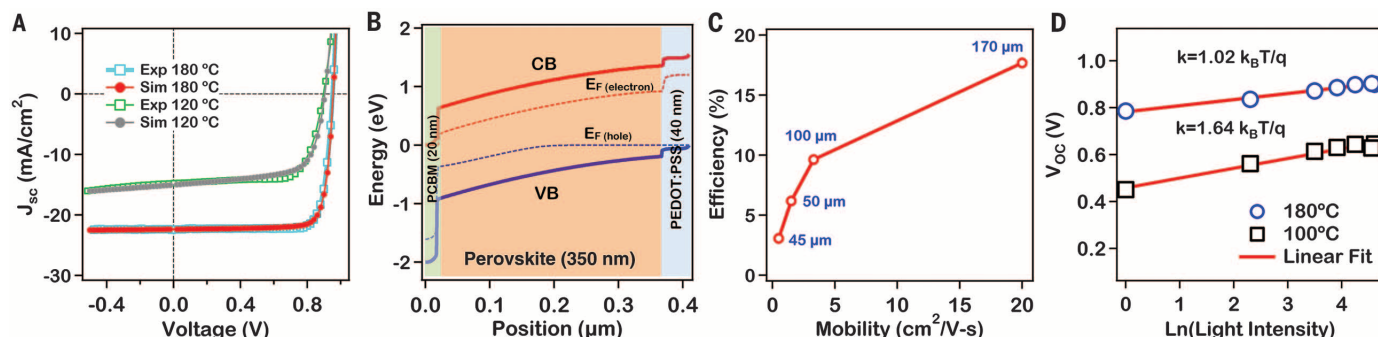
Fig. 3. Self-consistent device simulation attributes the process-dependent PCE gain to the improved mobility of films with larger grains. (**A**) The simulated J-V characteristics for large- and small-grain devices reproduce the salient features of the corresponding experimental data. (**B**) Typical energy band diagram at short circuit (SC) indicates the importance of a semi-intrinsic (reduced self-doping) fully depleted absorber in directing the charge carriers to their respective contacts; otherwise, the charge carrier would be lost to recombination in the field-free regions. (**C**) With all other parameters characterized and/or obtained from the literature, the PCE values appear to be correlated to the bulk mobility of the absorber (labels correspond to the average grain size). (**D**) Experimental data for V_{OC} as a function of illumination light intensity for a large-grain device (180°C) and a small-grain device (100°C) along with the linear fit (red line).

V_{OC} as a function of light intensity for large- and small-grain devices (Fig. 3D). By linearly fitting V_{OC} versus log-scaled light intensity [ln(I)], we obtained a slope of ~1.0 $k_B T/q$ (where k_B is the Boltzmann constant, T is absolute temperature, and q is elementary charge) for a large-grain device (hot-cast at 180°C), which suggests that a bimolecular recombination process dominates during device operation (29–31), similar to that observed in high-quality semiconductors such as silicon and GaAs. In contrast, for the small-grain device (hot-cast at 100°C), a slope of 1.64 $k_B T/q$ is measured, that is an indicator of trap-assisted recombination (Fitting details can be found in (24)).

Finally, direct optical characterization of the material characteristics also supports the hypothesis that material crystalline quality is correlated to grain size. Specifically, we evaluated the overall crystalline quality of large-area grains (24) by performing microphotoluminescence, absorption spectroscopy, and time-resolved photoluminescence measurements on large and small grains. The band-edge emission and absorption for large grains (>10^3 μm^2) were observed at 1.627 eV and 1.653 eV, respectively (Fig. 4A). As the grain size decreased, two concomitant effects were observed: (i) a blue shift of the band-edge photoluminescence by ~25 meV (Fig. 4B), and (ii) linewidth broadening of ~20 meV (Fig. 4C). Such blue shifts were predicted by our density functional theory (DFT) simula-tions (24) (fig. S12) and are possibly attributed to the composition change at the grain boundaries. The increase of emission line width at grain boundaries can be attributed to disorder and defects. We observed a bimolecular recombination process of free electrons and holes for the large-grain crystals by means of time-resolved photoluminescence spectroscopy (Fig. 4D), which is a strong indicator of good crystalline quality (24) (fig. S13). This is in contrast to a mono-exponential decay observed in previous reports for small grain size or mesoporous structures (11, 12, 32) and with our measurements on small grains, and is representative of nonradiative decay due to trap states. These results are also consistent with our earlier measurements of V_{OC} as a function of light intensity, which suggest reduced trap-assisted recombination in large-area grains.

Beyond our results described above, further enhancements in efficiency can be expected by improving the interface between perovskite and PCBM, obtaining better band alignment, and using an inverted structure. From the perspective of the global photovoltaics community, these results are expected to lead the field toward the reproducible synthesis of wafer-scale crystalline perovskites, which are necessary for the fabrication of high-efficiency single-junction and hybrid (semiconductor and perovskite) planar cells.

REFERENCES AND NOTES

1. J. Burschka et al., Nature 499, 316–319 (2013).
2. M. M. Lee, J. Teuscher, T. Miyasaka, T. N. Murakami, H. J. Snaith, Science 338, 643–647 (2012).
3. A. Mei et al., Science 345, 295–298 (2014).
4. H. Zhou et al., Science 345, 542–546 (2014).
5. H.-S. Kim et al., Sci. Rep. 2, 591 (2012).
6. M. Liu, M. B. Johnston, H. J. Snaith, Nature 501, 395–398 (2013).
7. N. J. Jeon et al., Nat. Mater. 13, 897–903 (2014).
8. P. Docampo, J. M. Ball, M. Darwich, G. E. Eperon, H. J. Snaith, Nat. Commun. 4, 2761 (2013).
9. O. Malinkiewicz et al., Nat. Photonics 8, 128–132 (2014).
10. J. Seo et al., Energy Environ. Sci. 7, 2642–2646 (2014).
11. S. D. Stranks et al., Science 342, 341–344 (2013).
12. G. Xing et al., Science 342, 344–347 (2013).
13. J. S. Manser, P. V. Kamat, Nat. Photonics 8, 737–743 (2014).
14. M. Grätzel, Nat. Mater. 13, 838–842 (2014).
15. M. D. McGehee, Nat. Mater. 13, 845–846 (2014).
16. R. S. Sanchez et al., J. Phys. Chem. Lett. 5, 2357–2363 (2014).
17. H. J. Snaith et al., J. Phys. Chem. Lett. 5, 1511–1515 (2014).
18. G. E. Eperon, V. M. Burlakov, P. Docampo, A. Goriely, H. J. Snaith, Adv. Funct. Mater. 24, 151–157 (2014).
19. M. Xiao et al., Angew. Chem. Int. Ed. 53, 9898–9903 (2014).
20. B. Conings et al., Adv. Mater. 26, 2041–2046 (2014).
21. A. Dualeh et al., Adv. Funct. Mater. 24, 3250–3258 (2014).
22. Q. Wang et al., Energy Environ. Sci. 7, 2359–2365 (2014).
23. H.-B. Kim et al., Nanoscale 6, 6679–6683 (2014).
24. See supplementary materials on Science Online.
25. [Editorial] Nat. Photonics 8, 665 (2014).
26. Q. Chen et al., J. Am. Chem. Soc. 136, 622–625 (2014).
27. G. Grancini et al., J. Phys. Chem. Lett. 5, 3836–3842 (2014).
28. Z. Xiao et al., Adv. Mater. 26, 6503–6509 (2014).
29. S. R. Cowan, A. Roy, A. J. Heeger, Phys. Rev. B 82, 245207 (2010).
30. C. M. Proctor, C. Kim, D. Neher, T.-Q. Nguyen, Adv. Funct. Mater. 23, 3584–3594 (2013).
31. C. M. Proctor, M. Kuik, T.-Q. Nguyen, Prog. Polym. Sci. 38, 1941–1960 (2013).
32. C. Wehrenfennig et al., Adv. Mater. 26, 1584–1589 (2014).

Fig. 4. Spectrally, spatially, and temporally resolved microphotoluminescence spectroscopy. (**A**) Normalized absorbance (black) and microscopically resolved PL emission spectra (red) obtained for a large-grain sample. (**B**) Normalized, microscopically resolved emission spectra for different grain sizes. (**C**) Relative shift and linewidth broadening of the band-edge emission as a function of grain area (with respect to the largest grain). (**D**) Normalized, microscopically resolved time-correlated single-photon histograms of both a large and a small grain (black). The red and blue lines are fits to the intensity decay considering interband relaxation, radiative bimolecular recombination, and nonradiative decay into states below the gap (see figs. S13 and S14).

SUPERNOVAE

The bubble-like interior of the core-collapse supernova remnant Cassiopeia A

Dan Milisavljevic[1]* and Robert A. Fesen[2]

The death of massive stars is believed to involve aspheric explosions initiated by the collapse of an iron core. The specifics of these catastrophic explosions remain uncertain, due partly to limited observational constraints on asymmetries deep inside the star. Here we present near-infrared observations of the young supernova remnant Cassiopeia A, descendant of a type IIb core-collapse explosion, and a three-dimensional map of its interior unshocked ejecta. The remnant's interior has a bubble-like morphology that smoothly connects to and helps explain the multiringed structures seen in the remnant's bright reverse-shocked main shell of expanding debris. This internal structure may originate from turbulent mixing processes that encouraged outwardly expanding plumes of radioactive ^{56}Ni-rich ejecta. If this is true, substantial amounts of its decay product, ^{56}Fe, may still reside in these interior cavities.

Computer simulations have long shown that the collapse of a high-mass star's dense iron-rich core into a neutron star generates an outward-moving shock wave that is unable to disrupt the star into a supernova (SN) under spherical conditions (1). This is because the outgoing shock wave is too weak to overcome the infalling outer layers of the star and stalls, thus requiring some postbounce revival (2, 3). It is now believed that explosion

[1]Harvard-Smithsonian Center for Astrophysics, 60 Garden Street, Cambridge, MA 02138, USA. [2]Department of Physics and Astronomy, Dartmouth College, Hanover, NH 03755, USA.
*Corresponding author. E-mail: dmilisav@cfa.harvard.edu

asymmetries introduced by dynamical instabilities and the influences of rotation and magnetic fields must contribute to the core-collapse process (4, 5), but their relative contributions are uncertain. Some aspects of these explosion processes have been successfully probed by observations of extragalactic supernovae (SNe) (6, 7). However, even with the Hubble Space Telescope (HST), distant SNe appear as unresolved point sources, which limits our ability to unravel the three-dimensional (3D) structure of the expanding ejecta that can reveal key properties of the explosion mechanism.

An alternative approach to understanding core-collapse SN explosions is through studies

of their remnants in our own Milky Way galaxy that are still young enough to be in free expansion and near enough to permit detailed studies of the expanding debris field. Such investigations can provide information on the explosion-driven mixing of the progenitor star's chemically distinct layers, the star's mass loss history before explosion, and the fate of its remnant core. With an age of around 340 years (8), a distance of only 11,000 light years (9), and its status as a known descendant of a type IIb explosion (10), Cassiopeia A (Cas A) is one of the best specimens for postmortem examination. Cas A is visible today through the heating effects of a reflected or "reverse" shock generated when the original SN's high-velocity blast wave ran into the surrounding interstellar medium. Cas A's metal-rich debris is arranged in large ringlike structures that together form a roughly spherical shell (commonly referred to as the main shell) approximately 6 light years in radius, with an overall velocity range of −4000 to +6000 km s^{-1} (11, 12). These and many other properties of Cas A, such as its wide-angle (≈40°) opposing streams of Si- and S-rich ejecta seen in the northeast and southwest regions traveling at unusually high velocities of up to 15,000 km s^{-1} (13, 14), an uneven expansion of the photosphere at the time of outburst (15), and an overall high chemical abundance ratio of ^{44}Ti/^{56}Ni with a nonuniform distribution (16, 17), all point to an asymmetric explosion.

In order to investigate possible asymmetries in Cas A's interior debris, we obtained near-infrared spectra of the remnant in 2011 and 2013 using the Mayall 4-m telescope at Kitt Peak National Observatory, in combination with instrumental setups particularly sensitive to the wavelength region from 900 to 1000 nm covering the [S III] 906.9- and 953.1-nm line emissions from Cas A's
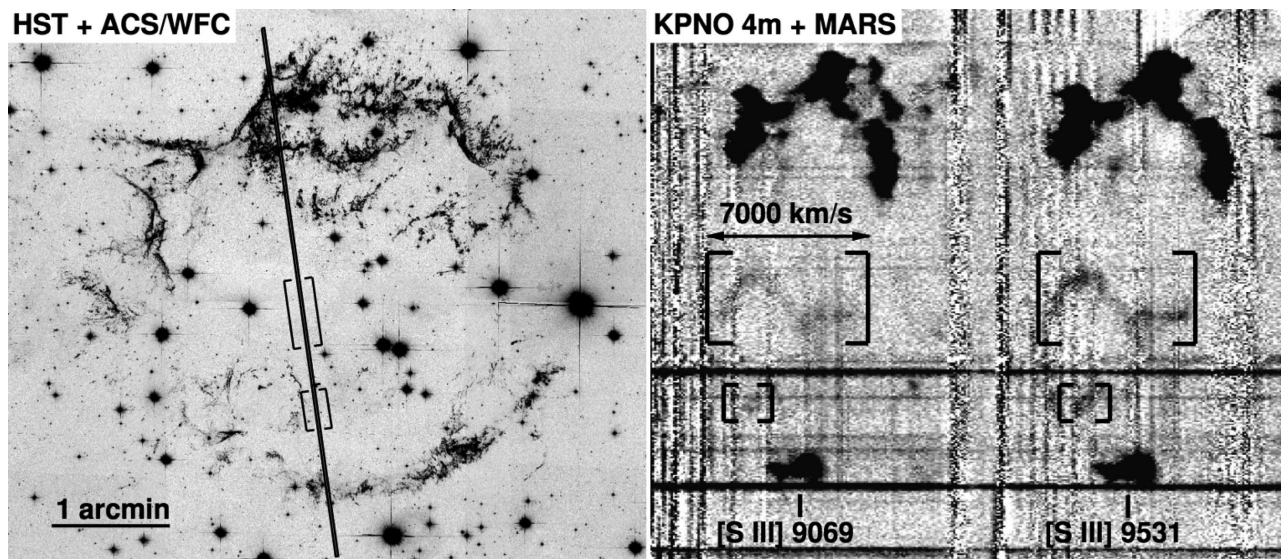
Fig. 1. Representative near-infrared observation of the [S III] 906.9- and 953.1-nm line emission from Cas A. (Left) A finding chart of a single long-slit position, which was rotated to optimize coverage of particular interior emission regions. The background image is a mosaic created from 2004 HST observations sensitive to O and S emissions (31). ACS/WFC, Advanced Camera for Surveys/Wide Field Channel. (**Right**) The corresponding 2D spectrum. Square brackets highlight regions where interior unshocked ejecta have been detected. See fig. S1 for a map of all slit positions used in the survey. KPNO, Kitt Peak National Observatory; MARS, Multi-Aperture Red Spectrograph.

sulfur-rich ejecta. Closely spaced long-slit spectra were taken across the remnant's central regions (*18*). The resulting data were transformed into three-dimensional coordinates and incorporated into our existing reconstruction of the optical main shell and high-velocity outer knots (*12*).

Faint and patchy [S III] emission can be seen interior to Cas A's bright main shell, with radial velocities spanning –3000 to +4000 km s^{-1} in a continuous manner (Fig. 1). The emission is diffuse, in sharp contrast with the bright main-shell ejecta that are compressed into small knots and filaments by the reverse shock. Most of our detections are located in the southern half of the remnant, but some are found in the northern half as well (Fig. 2). Presumably, the [S III] emission arises from unshocked interior material being photoionized by ultraviolet and x-ray flux from the main-shell ejecta that has been heated to temperatures up to several million degrees kelvin by the reverse shock.

The majority of the unshocked ejecta exhibit coherent structure (Fig. 3) in the form of large cavities or "bubbles" that appear to be physically connected to the main-shell rings. At least two cavities are well defined. A cavity seen in the southeast with the largest range of blue-shifted velocities extends outward from just below the remnant's approximate center and smoothly connects with a pair of optically bright curved filaments sometimes referred to as the "Parentheses." Opposite this, in the northwest and immediately below the remnant's largest main-shell ring of redshifted material, is the largest internal cavity. These two cavities intersect along a concentration of central emission that runs from the front to the back of the remnant.

The larger northern cavity dominates the remnant's interior volume and has a radius of approximately 3 light years, whereas the southeast cavity is approximately half as large. Both cavities exhibit a few S-rich clumps or filaments, indicating that neither cavity is completely empty of ejecta. Although it is difficult to accurately assess the total number of cavities, the diameters
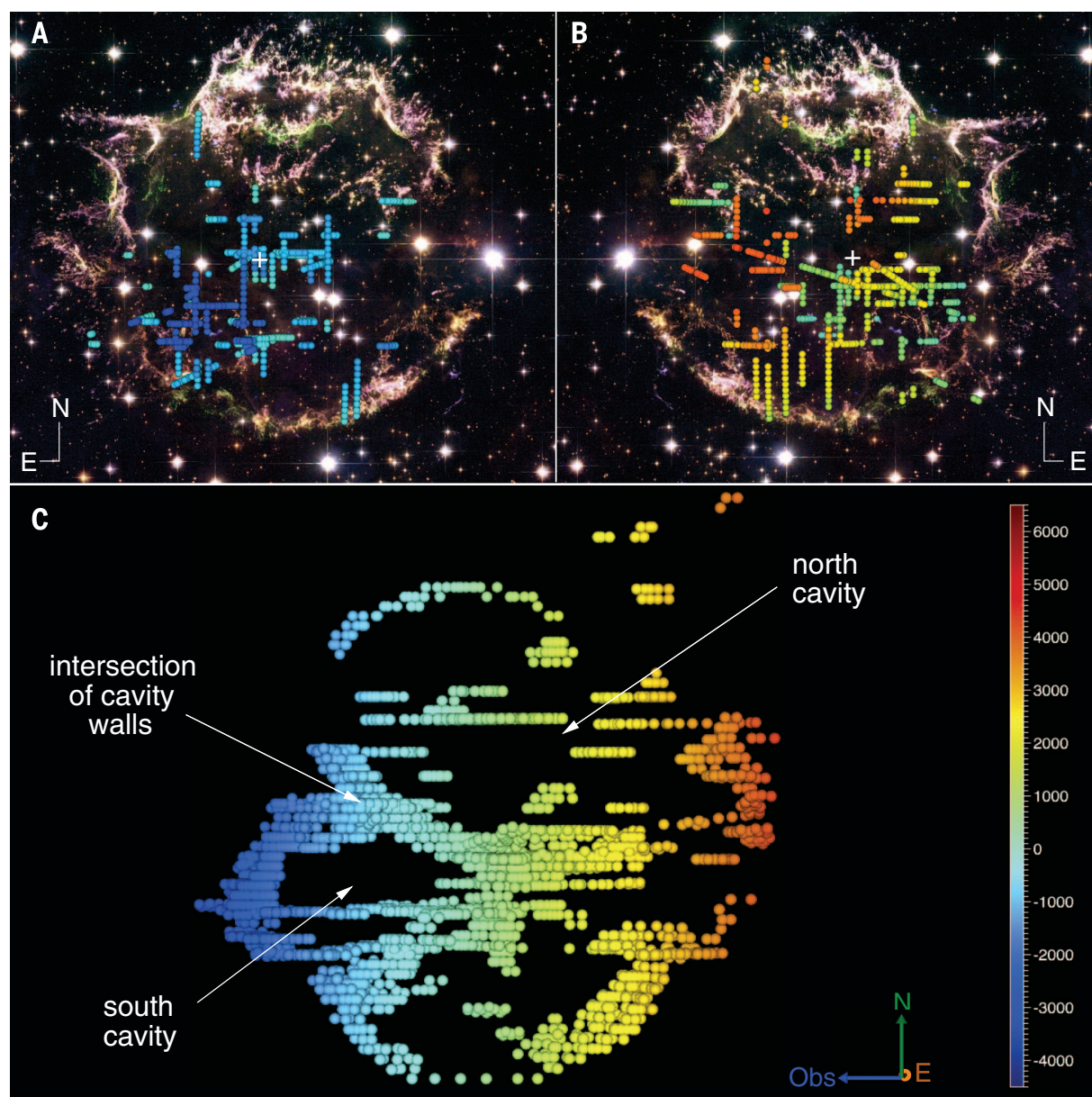
Fig. 2. Map of [S III] 906.9- and 953.1-nm line emission detected by our survey. The blue-to-red color gradient represents the range of measured Doppler velocities. Spheres mark individual measurements. (**A**) All blueshifted emission (<0 km s^{-1}) and (**B**) all redshifted emission (>0 km s^{-1}). The background is a composite HST image sensitive to the remnant's O and S emissions retrieved from www.spacetelescope.org. The center of expansion is shown as a white cross. (**C**) A perspective rotated 90° toward the west along the north-south axis. The north and south interior cavities are highlighted, as well as the wall of ejecta where the two cavities intersect.

of the main-shell rings are comparable to the diameters of the cavities, which suggests that they are approximately equal in number (about six). These properties, along with the fact that the main-shell rings extend radially outward along gently sloped paths that follow the circumference of the cavities, support the notion that the reverse-shocked rings and unshocked cavities of ejecta share a common formation origin.
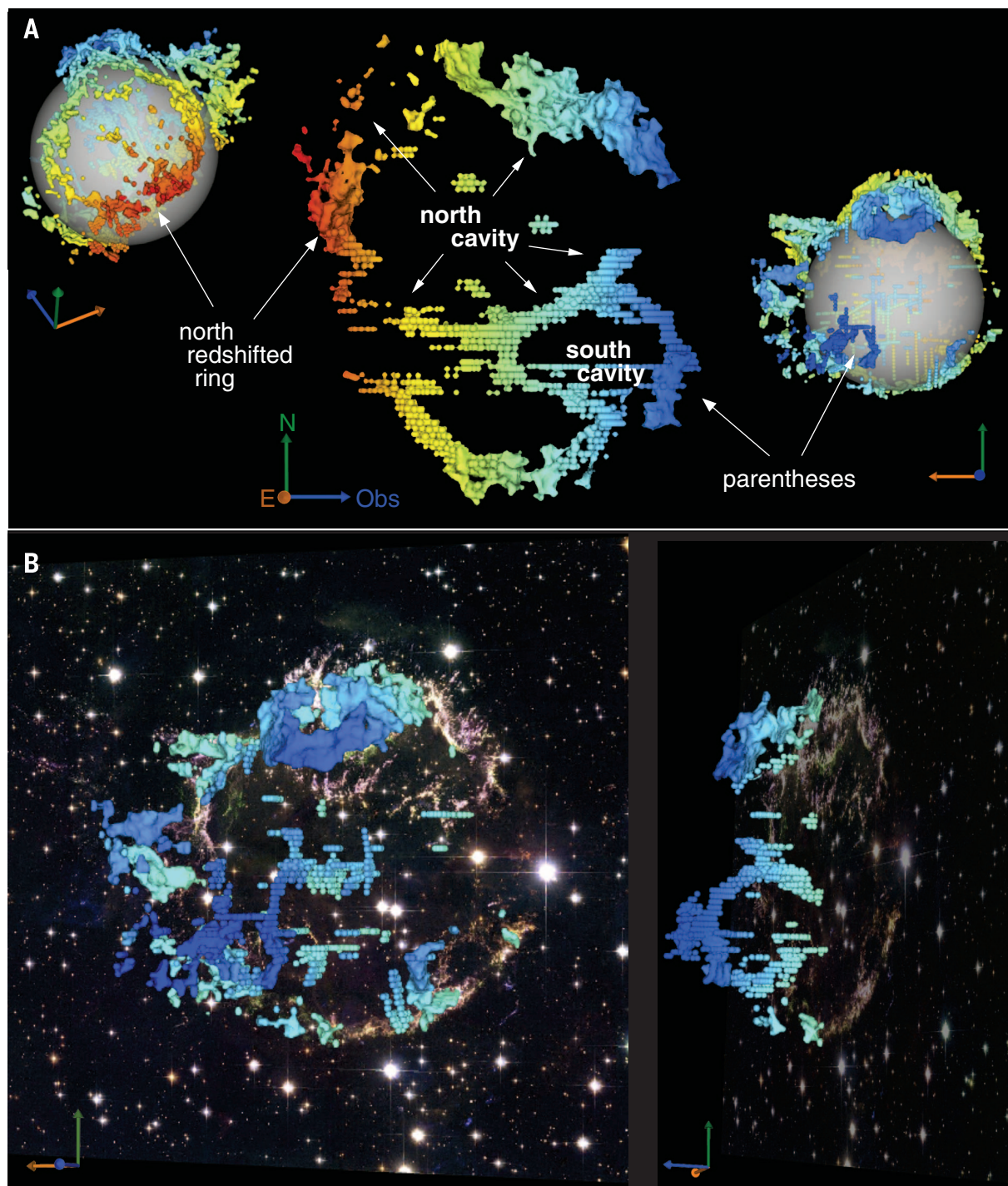
Fig. 3. Doppler reconstruction of Cas A made from the [S III] 906.9- and 953.1-nm emission map presented here and previous optical observations of main-shell ejecta (*12*). The blue-to-red color gradient corresponds to Doppler velocities that range from −4000 to 6000 km s^{-1}. [S III] measurements are individual spheres, and previous optical data are smoothed with a surface reconstruction. (**A**) A side perspective of a portion of the remnant spanning all material located between 15″ east of the center of expansion to 50″ west of the center of expansion to emphasize the two conspicuous interior cavities and their connections to main-shell ejecta. The translucent sphere centered on the center of expansion is a visual aid to differentiate between front and back material. (**B**) Two angled perspectives highlighting the south cavity. The first perspective angled 20° away from the observer's line of sight shows all data, and the second perspective angled 70° away from the observer's line of sight shows the same portion of the remnant as displayed in (A). The background image representing the plane of the sky as seen from Earth is the same shown in Fig. 2. An animation of the entire reconstruction is provided in movie S1.

Portions of Cas A's interior unshocked ejecta that were surveyed by our near-infrared observations are also visible in previous observations taken at longer wavelengths. Infrared images of Cas A taken with the Spitzer spacecraft show [S III] 33.48-μm and [S IV] 10.51-μm emission inside the boundary of the main shell at locations coincident with regions where we detect the strongest [S III] 906.9- and 953.1-nm emissions (19). Follow-up Spitzer infrared spectra in the central region showed line emission from interior O, Si, and S ejecta in sheetlike structures and filaments with inferred radial velocities approaching ±5000 km s^{-1} (20). Those spectroscopic Spitzer observations covered a smaller 50″ × 40″ area of Cas A, whereas our survey encompasses the entire remnant and reveals a far larger extent of the remnant's internal debris.

We interpret Cas A's main-shell rings of ejecta to be the cross sections of reverse-shock–heated cavities in the remnant's internal ejecta now made visible by our survey. A cavity-filled interior is in line with prior predictions for the arrangement of expanding debris created by a postexplosion input of energy from plumes of radioactive ^{56}Ni-rich ejecta (21, 22). Such plumes can push the nuclear burning zones located around the Fe core outward, creating dense shells separating zones rich in O, S, and Si from the Ni-rich material. Compression of surrounding nonradioactive material by hot expanding plumes of radioactive ^{56}Ni-rich ejecta generates a "Swiss cheese"–like structure that is frozen into the homologous expansion during the first few weeks after the SN explosion, when the radioactive power of ^{56}Ni is strongest.

In this scenario, the decay chain of ^{56}Ni → ^{56}Co → ^{56}Fe should eventually make these bubble-like structures enriched in Fe. Doppler reconstruction of Chandra x-ray observations sensitive to Fe K emissions shows that the three most significant regions of Fe-rich ejecta are located within three of Cas A's main-shell rings (11, 12). Thus, the coincidence of Fe-rich material with rings of O- and S-rich debris is consistent with the notion of ^{56}Ni bubbles.

However, Fe-rich ejecta associated with the Ni bubble effect should be characterized by diffuse morphologies and low ionization ages, and yet the x-ray bright Fe emissions we currently see are at an advanced ionization age relative to the other elements (23, 24). Furthermore, not all main-shell rings have associated x-ray–emitting Fe-rich ejecta, and there is no clear relationship between the locations of the internal bubbles we have detected and the spatial distribution of ^{44}Ti recently mapped by NASA's NuSTAR (Nuclear Spectroscopic Telescope Array) (17).

One solution is that Fe-rich ejecta associated with some of the remnant's internal cavities remain undetected. Low-density Fe could be present in ionization states between those detectable by optical or infrared line emission and those in x-rays. The total mass of unshocked Fe that is potentially contained in the bubbles is constrained by the total nucleosynthetic yield of Fe in the original SN explosion, which

is estimated to be less than ~0.2 solar mass ($M_\odot$) (25), and the amount of shocked Fe that is observed today, which is estimated to be 0.09 to 0.13 $M_\odot$ (24). Together these estimates imply that no more than an additional ~0.1 $M_\odot$ of Fe could potentially be located within Cas A's reverse shock.

Whatever their true cause, Cas A's bubble-like interior and outer ringlike structures observed in the main shell suggest that large-scale mixing greatly influences the overall arrangement of ejecta in core-collapse SNe. Presently, the extent of such mixing and how it takes place are not well known. A variety of potential dynamical processes may contribute to the redistribution of chemical layers, including uneven neutrino heating, axisymmetric magnetorotational effects, and Rayleigh-Taylor and Kelvin-Helmholtz instabilities [e.g. (26, 27)].

Compelling evidence for large-scale mixing involving considerable nonradial flow was first observed in the nearest and brightest SN seen in modern times, SN 1987A. In that case, high-energy gamma rays and x-rays with broad emission line widths from the decay of ^{56}Ni were detected only months after the explosion, implying that Ni-rich material was near the star's surface well before 1D progenitor models had predicted, assuming spherical symmetry (28).

Since SN 1987A, state-of-the-art 3D computer simulations of core-collapse explosions have confirmed that large-scale mixing can lead to Ni-dominated plumes overtaking the star's outer oxygen- and carbon-rich layers with velocities up to 4000 km s^{-1} (29). However, the majority of these simulations show that the mass density should essentially be unaffected. Although mixing can affect the species distribution, the bulk of the Ni mass should remain inside the remnant with velocities below 2000 km s^{-1}. This is, in fact, opposite to what we currently see in Cas A, where the x-ray bright Fe has velocities around the 4000 km s^{-1} limit (11). Thus, either the simulations are not adequately following the dynamics of mixing or, as we suspect, more Fe remains to be detected in Cas A's interior.

An additional consideration in interpreting a SN debris field is the chemical makeup of the star at the time of outburst. The evolution of massive stars toward the ends of their life cycles is likely to be nonspherical and may produce extensive intershell mixing. If strong enough, these dynamical interactions lead to Rayleigh-Taylor instabilities in the progenitor structure that can contribute to the formation of Ni-rich bubbles and influence the overall progression of the explosion (30). Thus, asymmetries introduced by a turbulent progenitor star interior, in addition to those initiated by the explosion mechanism, could contribute to the bubble-like morphology observed in Cas A.

Because Cas A's opposing streams of Si- and S-rich debris have kinematic and chemical properties indicative of an origin deep within the progenitor star (12), we searched for evidence of any structure joining the high-velocity material with the interior ejecta mapped in our survey.

However, we were not able to find any clear relationship between them. An indirect association is hinted at by the inferred projected motion of Cas A's central x-ray point source (XPS) that is thought to be the remnant neutron star. Its motion toward the southwest of the center of expansion is (i) roughly opposite to and moving away from the direction of the largest internal cavity in our reconstruction that is coincident with a sizable concentration of reverse-shocked Fe and (ii) nearly perpendicular to the axis of the high-velocity jets (31). The XPS, conserving momentum, could have been kicked in a direction opposite the largest plume of Fe-rich material (15) and released an energetic proto–neutron star wind that shaped the jets shortly after the core-collapse explosion (32).

The apparent mismatch of Ti-rich and Fe-rich ejecta regions uncovered by NuSTAR is a reminder that unresolved key issues surrounding Cas A still linger despite decades of scrutiny. Our 3D map of its interior is an important step forward, as it represents a rare look at the geometry of a SN remnant's inner volume of debris unmodified by reverse-shock instabilities. Because Cas A shows many striking similarities with SNe young and old (33, 34), its dynamical properties described in this work are probably not unique and can be used to help interpret other SN explosions and remnants that cannot be resolved.

Our data make it clear that Cas A's dominant ejecta structure is in the form of large internal cavities whose cross sections are the prominent rings of the reverse-shock–heated main shell. What is not clear, however, is why only half a dozen bubbles—not dozens—are present. SN explosion models can explore this issue, as well as better understand how the remnant's interior bubbles fit into a single coherent picture with its opposing high-velocity jets. A crucial test of the origin of these cavities would be a confirmation of the "missing" internal Fe we predict to be located in the remnant's interior, but conclusive observations may not be possible until the next generation of infrared and x-ray space telescopes comes online.

REFERENCES AND NOTES

1. S. Colgate, R. H. White, *Astrophys. J.* **143**, 626 (1966).
2. J. R. Wilson, in *Numerical Astrophysics: Proceedings of a Symposium in Honor of J. R. Wilson Held at the University of Illinois*, J. M. Centrella, J. M. LeBlanc, R. L. Bowers, Eds. (Jones and Bartlett Publishers, Boston, MA, 1982), pp. 422–434.
3. H. A. Bethe, J. R. Wilson, *Astrophys. J.* **295**, 14 (1985).
4. H. Th. Janka, *Annu. Rev. Nucl. Part. Sci.* **62**, 407–451 (2012).
5. A. Burrows, *Rev. Mod. Phys.* **85**, 245–261 (2013).
6. K. Maeda et al., *Science* **319**, 1220–1223 (2008).
7. L. Wang, J. C. Wheeler, *Annu. Rev. Astron. Astrophys.* **46**, 433–474 (2008).
8. J. R. Thorstensen, R. A. Fesen, S. van den Bergh, *Astron. J.* **122**, 297–307 (2001).
9. J. E. Reed, J. J. Hester, A. C. Fabian, P. F. Winkler, *Astrophys. J.* **440**, 706 (1995).
10. O. Krause et al., *Science* **320**, 1195–1197 (2008).
11. T. DeLaney et al., *Astrophys. J.* **725**, 2038–2058 (2010).
12. D. Milisavljevic, R. A. Fesen, *Astrophys. J.* **772**, 134 (2013).
13. R. A. Fesen, *Astrophys. J. Suppl. Ser.* **133**, 161–186 (2001).
14. U. Hwang et al., *Astrophys. J.* **615**, L117 (2004).
15. A. Rest et al., *Astrophys. J.* **732**, 3 (2011).
16. S. Nagataki, M. Hashimoto, K. Sato, S. Yamada, Y. S. Mochizuki, *Astrophys. J.* **492**, L45–L48 (1998).
17. B. W. Grefenstette et al., *Nature* **506**, 339–342 (2014).

18. See the supplementary materials for details of the observations obtained and data reduction.
19. J. D. T. Smith *et al.*, *Astrophys. J.* **693**, 713–721 (2009).
20. K. Isensee *et al.*, *Astrophys. J.* **725**, 2059–2070 (2010).
21. H. Li, R. McCray, R. A. Sunyaev, *Astrophys. J.* **419**, 824 (1993).
22. J. M. Blondin, K. J. Borkowski, S. P. Reynolds, *Astrophys. J.* **557**, 782–791 (2001).
23. U. Hwang, M. J. Laming, *Astrophys. J.* **597**, 362–373 (2003).
24. U. Hwang, M. J. Laming, *Astrophys. J.* **746**, 130 (2012).
25. K. Eriksen, D. Arnett, D. W. McCarthy, P. Young, *Astrophys. J.* **697**, 29–36 (2009).
26. J. C. Wheeler, D. L. Meier, J. R. Wilson, *Astrophys. J.* **568**, 807–819 (2002).
27. K. Kifonidis, T. Plewa, H.-Th. Janka, E. Müller, *Astron. Astrophys.* **408**, 621–649 (2003).
28. M. Itoh, S. Kumagai, T. Shigeyama, K. Nomoto, J. Nishimura, *Nature* **330**, 233–235 (1987).
29. N. J. Hammer, H.-Th. Janka, E. Müller, *Astrophys. J.* **714**, 1371–1385 (2010).
30. W. Arnett, C. Meakin, *Astrophys. J.* **741**, 33 (2011).
31. R. A. Fesen *et al.*, *Astrophys. J.* **645**, 283–292 (2006).
32. A. Burrows, in *1604–2004: Supernovae as Cosmological Lighthouses, ASP Conference Series*, vol. 342, M. Turatto, S. Benetti, L. Zampieri, W. Shea, Eds. (Astronomical Society of the Pacific, San Francisco, CA, 2005).
33. D. Milisavljevic *et al.*, *Astrophys. J.* **751**, 25 (2012).
34. K. A. Eriksen, J. A. Morse, R. P. Kirshner, P. R. Winkler, *AIP Conf. Proc.* **565**, 193–196 (2001).

REACTION DYNAMICS

Vibrational relaxation and microsolvation of DF after F-atom reactions in polar solvents

G. T. Dunning,[1] D. R. Glowacki,[1,2,3,4]* T. J. Preston,[1] S. J. Greaves,[5] G. M. Greetham,[6] I. P. Clark,[6] M. Towrie,[6] J. N. Harvey,[1] A. J. Orr-Ewing[1]*

Solvent-solute interactions influence the mechanisms of chemical reactions in solution, but the response of the solvent is often slower than the reactive event. Here, we report that exothermic reactions of fluorine (F) atoms in d_3-acetonitrile and d_2-dichloromethane involve efficient energy flow to vibrational motion of the deuterium fluoride (DF) product that competes with dissipation of the energy to the solvent bath, despite strong solvent coupling. Transient infrared absorption spectroscopy and molecular dynamics simulations show that after DF forms its first hydrogen bond on a subpicosecond time scale, DF vibrational relaxation and further solvent restructuring occur over more than 10 picoseconds. Characteristic dynamics of gas-phase F-atom reactions with hydrogen-containing molecules persist in polar organic solvents, and the spectral evolution of the DF products serves as a probe of solvent reorganization induced by a chemical reaction.

Elementary reactions of fluorine atoms are central to the development of our understanding of rates, dynamics, and mechanisms of chemical reactions (*1, 2*). Evidence for rich and subtle dynamical behavior has come from studying hydrogen atom abstractions by F atoms from molecules such as H_2, H_2O, and CH_4 (or deuterium abstraction from their isotopologs) under isolated-collision conditions in the gas phase. In partnership with quantum-mechanical scattering calculations, sophisticated experiments have probed the transition state (TS) region directly (*3, 4*), identified nonclassical processes that contribute to reaction (*5–8*), and observed breakdown of the Born-Oppenheimer approximation (*9*). Early TSs for these exothermic F-atom reactions favor highly vibrationally excited HF or DF molecules (*10, 11*), consistent with expectations from the Polanyi rules (*12*). For reactions of F atoms with hydrocarbons, similar dynamics persist at the gas-liquid interface (*13*). Here, we extend mechanistic studies of F-atom reactions to the bulk liquid phase and report coupled DF-product and solvent dynamics on the picosecond time scale.

Bimolecular chemical reactions in solution are of considerable importance in both chemical synthesis and the biochemistry of living organisms. Under thermal conditions, these reactions typically occur on the ground-state potential energy surface (PES). The mechanisms of the reactions and the influence of the solvent can be explored using time-resolved spectroscopy and nonequilibrium molecular dynamics (MD) simulations (*14–18*), but examples of ultrafast studies of the dynamics of bimolecular reactions of ther-

malized reagents in liquids remain rare. The current study shows that exothermic F-atom reactions in CD_3CN or CD_2Cl_2 solutions, to produce DF and an organic radical [$\Delta_r H_0 \approx -150$ kJ mol^{-1} (*11*)], exhibit comparably rich dynamics to their gas-phase counterparts and examines the evolving postreaction microsolvation environment. The propensity of nascent DF to hydrogen bond promotes strong solute-solvent coupling, which might be expected to quench the state-specific dynamics. Nevertheless, we observe the formation of highly vibrationally excited DF, with subsequent rapid relaxation by energy transfer to the solvent bath. Evidence for a solvent response to the chemical reaction also emerges.

Figure 1 presents frames from an MD simulation that illustrate the early-time dynamics of reaction in d_3-acetonitrile. Despite reagents that are thermalized, the reaction results in strikingly nonthermal microscopic dynamics in the wake of transition-state passage. At the instant of reactive formation, DF molecules have multiple quanta of vibrational excitation, and the surrounding solvent molecules are not oriented to solvate the DF optimally. The solvent environment is thus intermediate between the noninteracting gas-phase limit and the strongly interacting equilibrium limit. Initial hydrogen-bond formation is the first step toward equilibrium solvation of the nascent DF and occurs within a few hundred femtoseconds. Subsequent time-dependent shifts in the DF vibrational frequency over several picoseconds signify both vibrational relaxation and restructuring of the microsolvation environment to accommodate this reaction product.

Figure 2 shows time-resolved infrared (TRIR) absorption spectra of DF after F-atom reactions in CD_3CN and CD_2Cl_2. One-photon photolysis of XeF_2 with 50-fs laser pulses centered at 267 nm promptly generated F atoms in solution (*19*), and DF products were probed using 50-fs IR laser pulses with >500 cm^{-1} bandwidth (*20*). The broad, unstructured IR bands are characteristic of DF solutes in organic solvents (*21*). However, the spectral features evolve in time, with a component that moves from lower to higher wave number within ~5 ps and a further shift of ~90 cm^{-1} from higher to lower wave number over the first 30 ps.

[1]School of Chemistry, University of Bristol, Cantock's Close, Bristol BS8 1TS, UK. [2]Department of Computer Science, Merchant Venturers Building, Woodland Road, Bristol BS8 1UB, UK. [3]Photon Ultrafast Laser Science and Engineering (PULSE) Institute and Department of Chemistry, Stanford University, Stanford, CA 94305, USA. [4]SLAC National Accelerator Laboratory, Menlo Park, CA 94025, USA. [5]School of Engineering and Physical Sciences, Heriot-Watt University, Edinburgh EH14 4AS, UK. [6]Central Laser Facility, Research Complex at Harwell, Science and Technology Facilities Council, Rutherford Appleton Laboratory, Harwell Oxford, Didcot, Oxfordshire OX11 0QX, UK.
*Corresponding author. E-mail: a.orr-ewing@bristol.ac.uk (A.J.O.-E.);

Figure 2 also displays the time-dependent band intensities of the DF (v = 1 and 0) component absorptions obtained by decomposition of the time-dependent spectra (20). (Here, v denotes the vibrational quantum number of the DF.) This decomposition makes use of the displacement of the DF ($v = 2 \leftarrow v = 1$) absorption band by more than 100 cm^{-1} to the low wave-number side of the ($v = 1 \leftarrow v = 0$) fundamental band because of the large anharmonicity of the DF vibrational levels. The solid lines are the outcomes of fits to a kinetic model in which the F + CD$_3$CN or CD$_2$Cl$_2$ reaction produces DF in vibrational levels v = 2, 1, and 0, and vibrational relaxation occurs in single-quantum steps from $v = 2 \rightarrow 1$ and $v = 1 \rightarrow 0$. The kinetic fits are constrained by data derived from further experiments using ultraviolet/visible spectroscopy to monitor the reactive loss of the F atoms (19) (with time-constant τ_F = 4.0 ± 0.2 ps in CD$_3$CN and 4.5 ± 0.8 ps in CD$_2$Cl$_2$) and by IR-pump and IR-probe experiments that determined the DF(v = $1 \rightarrow 0$) vibrational relaxation time constant in solution ($\tau_{1\rightarrow0}$ = 3.1 ± 0.6 ps in CD$_3$CN, compared with 2.8 ± 0.3 ps from our MD simulation) (20). All quoted uncertainties herein correspond to 2 SDs.

We concentrate mostly on the outcomes of the F + CD$_3$CN reaction, for which both experimental studies and MD simulations were performed. From the fitted rate coefficients obtained from analysis of five independent data sets, we deduce a branching of 55% to DF(v = 2) and 44% to DF(v = 1) products with ±15% uncertainty and negligible direct production of DF(v = 0) molecules. Multistate reactive nonequilibrium atomistic MD simulations of the F + CD$_3$CN reaction in a periodic box of 62 fully flexible solvent molecules (20) predict very similar vibrational excitation of DF. Figure 3 illustrates the outcomes of the MD simulations for DF production and relaxation in

the immediate wake of the reaction. The computed average energy in vibrational motion of the newly formed DF is almost 100 kJ mol^{-1} and mostly corresponds to DF(v = 2 and 3). Subpicosecond relaxation of the DF(v = 3) population is too fast to be resolved experimentally. The vibrational excitation decays through coupling to the solvent bath with two time constants that have a weighted average of 3.9 ± 0.18 ps, in good agreement with the experimentally determined rise of DF(v = 0) absorption.

The negative intensities assigned to DF(v = 1) in Fig. 2C indicate stimulated emission because of an initially greater population of DF(v = 2). This population inversion is sustained by faster $v = 1 \rightarrow v = 0$ than $v = 2 \rightarrow v = 1$ relaxation. Strong coupling of the DF vibrational motion to solvent modes facilitates rapid transfer of excess energy to the bath, and the solvent Fourier transform infrared (FTIR) spectrum (Fig. 2) can help identify candidate modes but cannot predict their quenching ability. The $v = 1 \leftarrow 0$ transition of incompletely solvated DF temporarily overlaps the CD$_3$CN vibrational mode at 2600 cm^{-1}, enabling efficient energy redistribution. In contrast, the solvent bands below 2330 cm^{-1} lie more than 100 cm^{-1} lower than the DF($v = 2 \leftarrow 1$) band center in the early time spectra. The dynamics of F-atom reactions in CD$_2$Cl$_2$ (Fig. 2D) are similar to those observed in CD$_3$CN, although $v = 2 \rightarrow 1$ relaxation is now found to be faster than $v = 1 \rightarrow 0$, as expected without resonant coupling to solvent modes. Initial relative populations of DF(v) levels are 77% in v = 2 and 22% in v = 1 (±11%).

We were unable to find a gas-phase study of the F + CD$_3$CN reaction with which to compare the liquid-phase DF(v) branching. The outcomes of measurements of HF from the F + CH$_3$CN reaction in the gas phase instead serve as a

benchmark (22), and we deduce lower, but still substantial, vibration of the emergent products of reaction in solution despite the strongly interacting solvent. For the F + CD$_2$Cl$_2$ reaction, direct comparison with gas-phase data also indicates partial solvent quenching of the nascent DF vibrational excitation (11).

Vibrational frequencies are sensitive reporters of the local, dynamic environment of the molecule and provide information on vibrational cooling and solvent restructuring as the system approaches postreaction equilibrium. Immediately upon formation, DF is vibrationally excited and in an orientation that cannot participate in hydrogen bonding to the solvent (Fig. 1). Different types of nonequilibrium MD simulations help to reveal the microscopic mechanisms at play for short-time relaxation of the nascent DF to equilibrium. The full simulations mimicked the experiments, treating the abstraction and relaxation dynamics, and generated the transient DF spectra shown in Fig. 4. Subsequent simulations indicated two different contributions to DF relaxation in the immediate wake of the abstraction event, as a result of (i) energy flow from vibrationally excited DF to the solvent and (ii) changes in the DF microsolvation environment leading to hydrogen bonds. As shown in Fig. 4, these two dynamical relaxation processes have opposite effects on the transient DF spectra (20). Relaxation from more energetic vibrational quantum states drives a shift of the DF band to a higher wave number, as observed experimentally, because of the anharmonicity of the mode. Conversely, reorientation of the DF within its microsolvation environment to form hydrogen-bonded complexes shifts the DF band to lower wave number. The MD simulations predict that the latter effect causes a 220 cm^{-1} shift of the vibrational band center to lower wave number, with a time constant <1 ps that accords with previous studies of fast-solvation dynamics in acetonitrile (23). This process cannot be followed experimentally because of insufficient build-up of reaction products on this short time scale. However, the computational prediction is consistent with experimental observations of absorption bands below 2600 cm^{-1} at every time delay, shifted from the 2907 cm^{-1} fundamental band origin of isolated DF, and also with spectra of CD$_3$CN–DF complexes (24). The DF subsequently exchanges hydrogen-bonded solvent partners at intervals on the order of 10 ps.

The time-resolved IR spectra (Fig. 2) indicate that a second mechanism further contributes to the reduction in DF vibrational wave number on a ≤30-ps time scale. Fits to the experimental spectra incorporate a red shift of the DF($v = 0 \rightarrow 1$ and $1 \rightarrow 2$) absorption bands of 90 cm^{-1}, with a time constant of 9 to 11 ps (20). MD spectral analysis (e.g., Fig. 4, A1 to A3) reveals a spectral feature to the high wave-number side of the primary DF band center. This feature arises from DF molecules with a distribution of solvation environments that are not completely relaxed; solute-solvent hydrogen bonding is not fully established, even at longer times. In qualitative agreement with experimental observations, this peak eventually shifts to
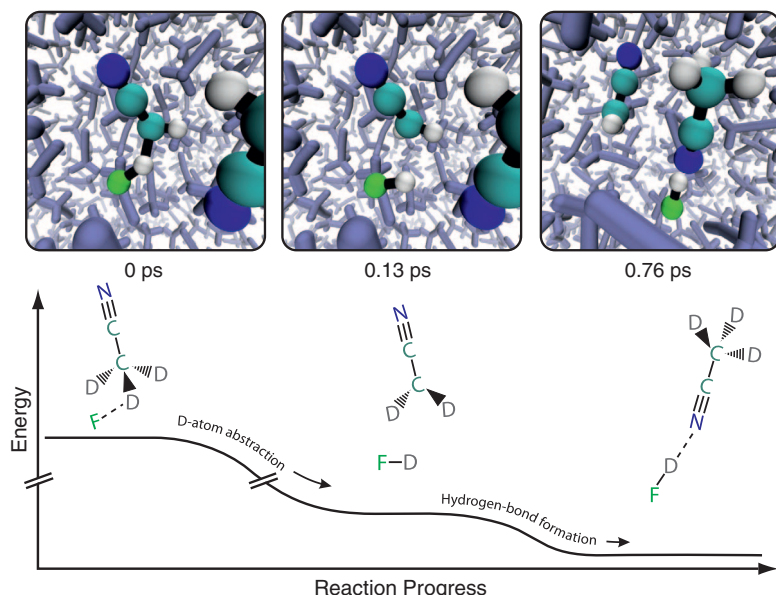
Fig. 1. Snapshots from an MD simulation of an F atom reaction in d_3-acetonitrile, superimposed on a schematic energy profile. The snapshots show the instant of transition state passage (t = 0 ps), initial separation of CD$_2$CN and vibrationally excited DF (t = 0.13 ps), and reorientation of the DF and a solvent molecule to establish a hydrogen bond (t = 0.76 ps). Other solvent molecules are shown in gray.

lower wave number as the DF microsolvation environment approaches equilibrium. We therefore attribute the experimentally observed spectral change to additional restructuring of the solvent around the reaction products, facilitated by hydrogen-bond dynamics (25). The combined experimental and computational outcomes provide the following picture for shifts in the DF fundamental frequency: The initial DF vibrational wave number approaches that of an isolated molecule [2907 cm^{-1} for DF($v = 0$)], but incipient H bonding to a CD$_3$CN molecule with time constant <1 ps reduces it by ≥200 cm^{-1}. Further relaxation to the equilibrated 2480 cm^{-1} band center results from solvent restructuring with time constant ~10 ps. These spectral shifts oppose those associated with vibrational cooling of nascent DF($v > 0$).

Multiple relaxation time scales have been observed in many solvents (23), and acetonitrile's extensive first- and second-solvent shell structure is consistent with their occurrence here (26). A similar time constant is observed for recovery of the equilibrated DF absorption spectrum when we excite a subset of the DF molecules with an IR laser tuned to be resonant only with the high wave-number wing of the fundamental band (20). In these latter experiments, the time constant derives solely from changes in the DF solvation environment, but for the reactive results, we cannot rule out solvent restructuring associated with replacement of XeF by one or more CD$_3$CN molecules after XeF$_2$ photolysis (19).

The minimum energy pathway for the reaction of an F atom with a solvent molecule in liquid CD$_3$CN is dominated by electronic configurations corresponding to neutral species, with negligible contributions from states deriving from D$^+$ transfer to the solvent [the pK_a (where K_a is the acid dissociation constant) of HF in acetonitrile is estimated to be >20 (27)]. However, at the energies of vibrationally excited DF, our MD simulations demonstrate the transient influence of diabatic states with deuteron-transfer character on the products' side of the TS. These states are required for an accurate description of the anharmonicity in the solute-solvent coupling and must be included in our treatment of the reaction PES to give the reported agreement between the MD simulations and experimental measurements of energy disposal to the DF and its subsequent relaxation to the solvent bath.

The current work extends to the liquid-phase prior dynamical studies of benchmark fluorine-atom reactions with organic molecules. As we have found in other bimolecular reactions (14, 16), we can apply, with certain caveats, intuition derived from the gas-phase reaction dynamics to the complicated realm of liquids. Despite strong solute-solvent coupling, highly vibrationally excited DF products form after reaction in liquid CD$_3$CN and CD$_2$Cl$_2$, but this excitation is lower than for reactions in the gas phase. Solvent damping of the nascent DF vibration may derive from coupling
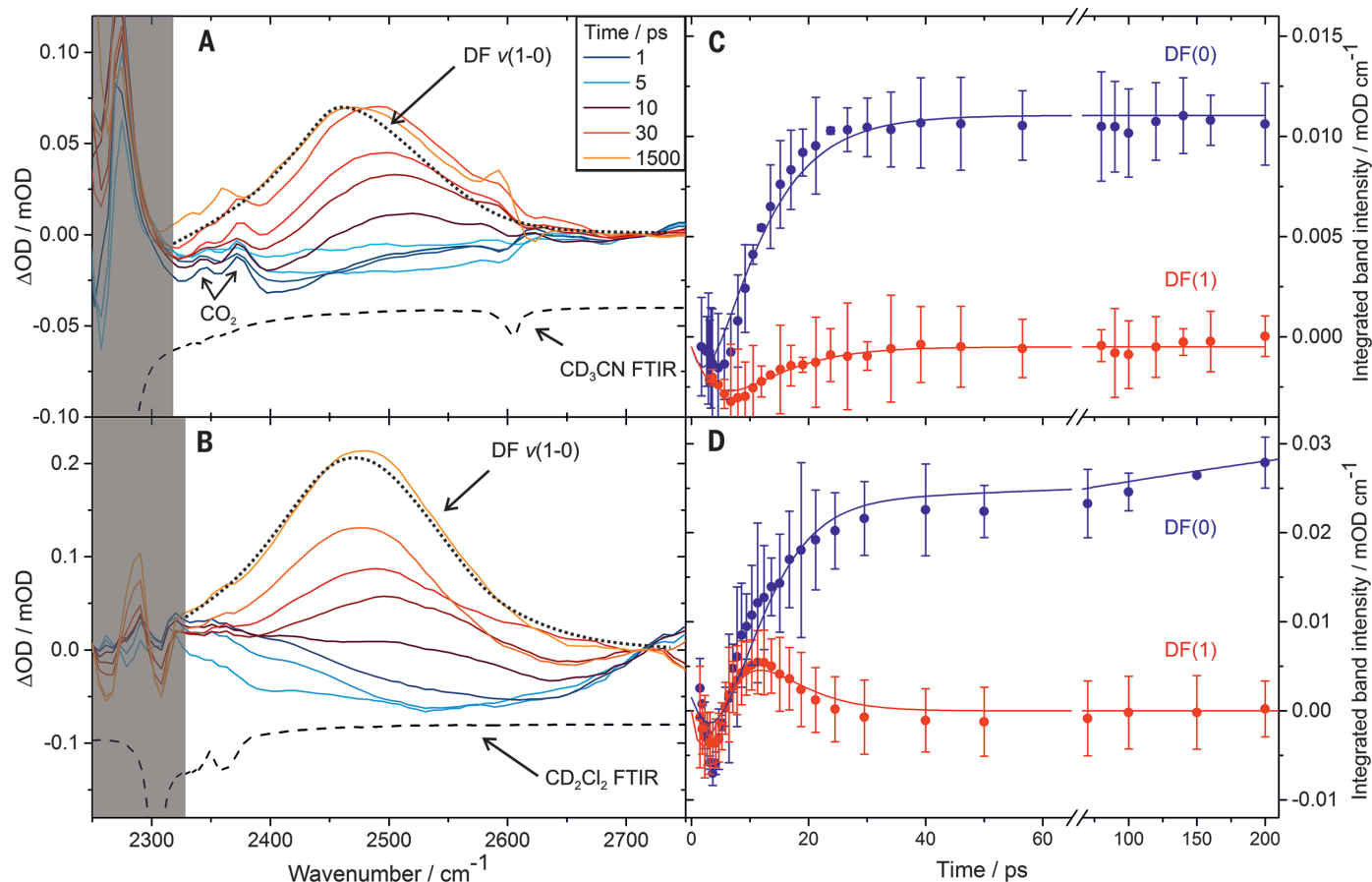
Fig. 2. TRIR absorption spectra and DF band intensities for reactions of F atoms in polar solvents. (**A** and **C**) Results in CD$_3$CN. (**B** and **D**) Results in CD$_2$Cl$_2$. The inset key shows selected time delays at which the transient spectra were obtained. Negative intensities indicate stimulated emission because of vibrational population inversions. The black dotted lines are steady-state FTIR spectra of DF in each solvent, and inverted solvent spectra are shown as dashed lines. Gray shading masks regions of strong solvent absorption. Decomposition of the spectra into $v = 1 \leftarrow v = 0$ and $v = 2 \leftarrow v = 1$ bands uses the anharmonicity of the DF vibrational levels, which shifts the ($2 \leftarrow 1$) band more than 100 cm^{-1} lower than the ($1 \leftarrow 0$) band. Fitting of time-resolved spectra for complete sets of time delays, subsets of which are shown in (A) and (B), gives the integrated DF($v = 0$) (blue circles) and DF($v = 1$) (red circles) absorption band intensities in (C) and (D), respectively. Uncertainties (2-SD error bars) are obtained from comparison of the fitted band intensities for separately acquired sets of time-resolved spectra and illustrate the reproducibility of the results. Kinetic fits (solid lines) use a model described in the supplementary materials (20): Independent fits to separately acquired sets of pairs of time-dependent ($2 \leftarrow 1$) and ($1 \leftarrow 0$) band intensities give the rate coefficients, mean values, and 2-SD uncertainties (from five data sets for F + CD$_3$CN and three for F + CD$_2$Cl$_2$) presented in tables S1 and S2.

to the energized products as they emerge from the TS and displacement of the TS later along the reaction coordinate. Equilibration of the excess DF vibrational energy takes 3 to 4 ps in both solvents. Further solvent restructuring to accommodate reaction products continues over the ensuing 10 ps. This depth of understanding of a condensed-phase reaction mechanism requires

knowledge not only of the PES but also of the dynamical interplay between solute and solvent. Vibrational probes of reactions in solution and nonequilibrium MD simulations provide penetrating insights into the dynamics of bond-making and subsequent dissipation of excess chemical energy to the solvent. Further exploration using this combined methodology will pro-

vide increasingly detailed descriptions of the effect of emergent product vibrational excitation on reaction outcomes in complex systems.

REFERENCES AND NOTES

1. R. D. Levine, *Molecular Reaction Dynamics* (Cambridge Univ. Press, Cambridge, 2005).
2. D. M. Neumark, A. M. Wodtke, G. N. Robinson, C. C. Hayden, Y. T. Lee, *J. Chem. Phys.* **82**, 3045–3066 (1985).
3. W. Dong *et al.*, *Science* **327**, 1501–1502 (2010).
4. D. E. Manolopoulos *et al.*, *Science* **262**, 1852–1855 (1993).
5. M. Tizniti *et al.*, *Nat. Chem.* **6**, 141–145 (2014).
6. M. Qiu *et al.*, *Science* **311**, 1440–1443 (2006).
7. T. Wang *et al.*, *Science* **342**, 1499–1502 (2013).
8. R. Otto *et al.*, *Science* **343**, 396–399 (2014).
9. L. Che *et al.*, *Science* **317**, 1061–1064 (2007).
10. J. J. Lin, J. Zhou, W. Shiu, K. Liu, *Science* **300**, 966–969 (2003).
11. M. A. Wickramaaratchi, D. W. Setser, H. Hildebrandt, B. Körbitzer, H. Heydtmann, *Chem. Phys.* **94**, 109–129 (1985).
12. J. C. Polanyi, *Acc. Chem. Res.* **5**, 161–168 (1972).
13. A. M. Zolot, P. J. Dagdigian, D. J. Nesbitt, *J. Chem. Phys.* **129**, 194705 (2008).
14. S. J. Greaves *et al.*, *Science* **331**, 1423–1426 (2011).
15. R. A. Rose *et al.*, *J. Chem. Phys.* **134**, 244503 (2011).
16. A. J. Orr-Ewing, *J. Chem. Phys.* **140**, 090901 (2014).
17. D. R. Glowacki, A. J. Orr-Ewing, J. N. Harvey, *J. Chem. Phys.* **134**, 214508–214511 (2011).
18. D. R. Glowacki, R. A. Rose, S. J. Greaves, A. J. Orr-Ewing, J. N. Harvey, *Nat. Chem.* **3**, 850–855 (2011).
19. G. T. Dunning *et al.*, *Phys. Chem. Chem. Phys.* **16**, 16095–16102 (2014).
20. Materials and methods are available as supporting material on *Science* Online.
21. R. M. Adams, J. J. Katz, *J. Mol. Spectrosc.* **1**, 306–332 (1957).
22. K. Dehe, H. Heydtmann, *Chem. Phys. Lett.* **262**, 683–688 (1996).
23. B. Bagchi, B. Jana, *Chem. Soc. Rev.* **39**, 1936–1954 (2010).
24. G. L. Johnson, L. Andrews, *J. Phys. Chem.* **87**, 1852–1859 (1983).
25. R. Rey, K. B. Møller, J. T. Hynes, *J. Phys. Chem. A* **106**, 11993–11996 (2002).
26. W. L. Jorgensen, J. M. Briggs, *Mol. Phys.* **63**, 547–558 (1988).
27. C. R. Nicoleti, V. G. Marini, L. M. Zimmermann, V. G. Machado, *J. Braz. Chem. Soc.* **23**, 1488–1500 (2012).

Fig. 3. Transient DF vibrational energy content following D-atom abstractions in d_3-acetonitrile, obtained from the MD simulations. (**A**) DF vibrational energy averaged over 200 trajectories, with time constants obtained from a biexponential fit. (**B1** to **B4**) Normalized transient vibrational energy content in the $v = 0$ to 3 vibrational levels. Exponential fits to the decaying populations of $v = 3$, 2, and 1 and the rise in $v = 0$ give time constants of $\tau_{3\to2} = 0.37 \pm 0.20$ ps, $\tau_{2\to1} = 3.6 \pm 1.8$ ps, and $\tau_{1\to0} = 6.9 \pm 1.4$ ps.
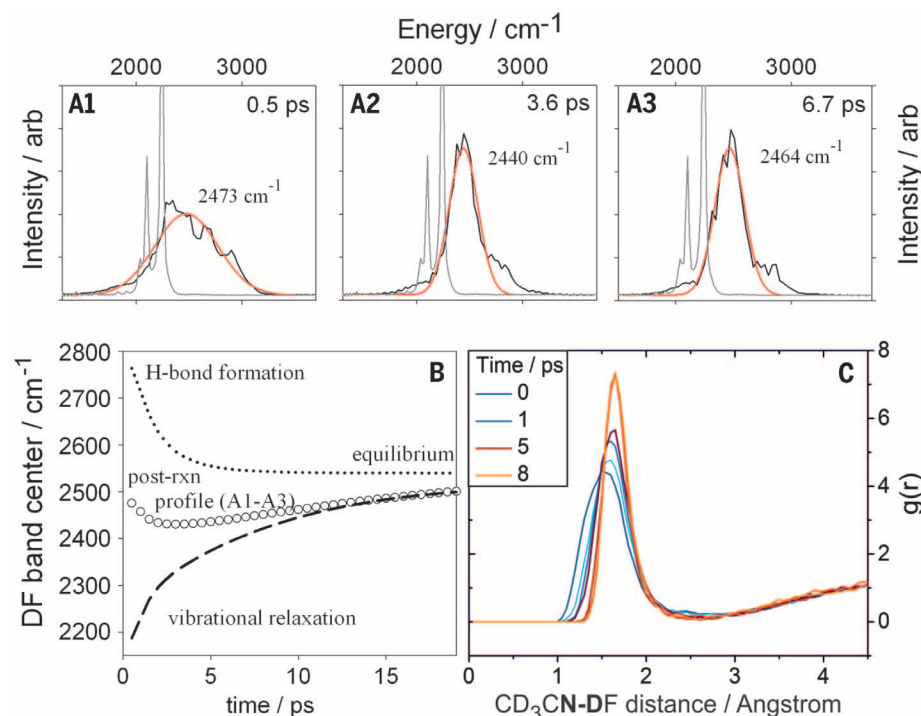
Fig. 4. MD simulations of transient power spectra and radial distribution functions. (**A**) Transient DF spectral bands (black lines), Gaussian fits to the simulated DF spectra (red lines), and the simulated solvent spectrum (gray lines). (**B**) Time-dependent postreaction profile of the DF band center (circles), together with results from separate simulations that identify spectral effects of hydrogen-bond formation with CD_3CN (dotted line) and relaxation of vibrationally excited DF (dashed line). (**C**) Time evolution of the radial distribution function, $g(r)$, which describes the changing distribution of distances of the D atom (in DF) to the N atoms of the CD_3CN solvent molecules.

ANIMAL COGNITION

Number-space mapping in the newborn chick resembles humans' mental number line

Rosa Rugani,[1,2]* Giorgio Vallortigara,[2] Konstantinos Priftis,[1] Lucia Regolin[1]

Humans represent numbers along a mental number line (MNL), where smaller values are located on the left and larger on the right. The origin of the MNL and its connections with cultural experience are unclear: Pre-verbal infants and nonhuman species master a variety of numerical abilities, supporting the existence of evolutionary ancient precursor systems. In our experiments, 3-day-old domestic chicks, once familiarized with a target number (5), spontaneously associated a smaller number (2) with the left space and a larger number (8) with the right space. The same number (8), though, was associated with the left space when the target number was 20. Similarly to humans, chicks associate smaller numbers with the left space and larger numbers with the right space.

Number knowledge and processing are fundamental to everyday life. There is now considerable empirical evidence that numbers may be represented along a continuous, left-to-right–oriented, mental number line (MNL) (1); however, the origin of this orientation is debated. In humans (2) and nonhuman animals (3, 4), numerical judgments become easier as the difference between the numbers increases (the distance effect) and harder as the magnitude of numbers increases (the size effect). Interspecific similarities suggest a continuous

and analogical nonverbal representation of numerical magnitude (3). This indicates that numerical competence did not emerge de novo in linguistic humans but was probably built on a precursor nonverbal number system (1, 5).

The size and distance effects, though, are not informative about the origin of the orientation of the MNL. Indeed, the MNL has been, up to now, demonstrated solely among humans (6–8), where its orientation may be influenced by cultural factors, such as reading direction. People primarily educated in Arabic show an inverted spatial-numerical association of response codes (SNARC) (9) effect (10), whereas people with mixed reading habits (such as Israelis) show no SNARC at all (11).

It remains unclear whether the MNL orientation is simply modulated or entirely produced by educational factors. Seven-month-old infants prefer increasing (e.g., 1-2-3) to decreasing (e.g., 3-2-1) magnitudes displayed from left to right, (12), showing that spatial-numerical association does exist before mathematics and linguistic education. A tendency to count from left to right has also been found in domestic chicks (13), adult Clark's nutcrackers (14), and adult Rhesus macaques (15). In these studies, animals were trained to identify a target element in a sagitally oriented series of identical elements. When required to repeat the task with an identical series of elements rotated by 90°, animals identified as correct the target positioned from the left end (14). However, this left-sided preference could depend on a general bias in the allocation of spatial attention (16). Both humans (17) and birds (18, 19) primarily attend to objects in the left side of space, a phenomenon termed "pseudo-neglect." When a different paradigm was used, adult chimpanzees were trained to touch in ascendant order Arabic numerals (1 to 9) randomly displayed on a computer screen. At testing, they were presented with only two numerals (1 and 9) displayed horizontally, one on the left and the other on the right; chimpanzees responded faster to the left-right (1-9) than to the right-left condition (9-1) (20). However, these results are not conclusive concerning the spontaneous mapping of magnitudes onto space, because apes required intensive sequential learning during training.

The spatial arrangement of numbers is highly flexible in humans: A fundamental characteristic of the human MNL is its relativity. In the 1-9 range, for instance, responding to 9 is faster when responses are executed on the right; but in

[1]Department of General Psychology, University of Padova, Padova, Italy. [2]Center for Mind/Brain Sciences, University of Trento, Rovereto (Trento), Italy.
*Corresponding author. E-mail: rosa.rugani@unipd.it
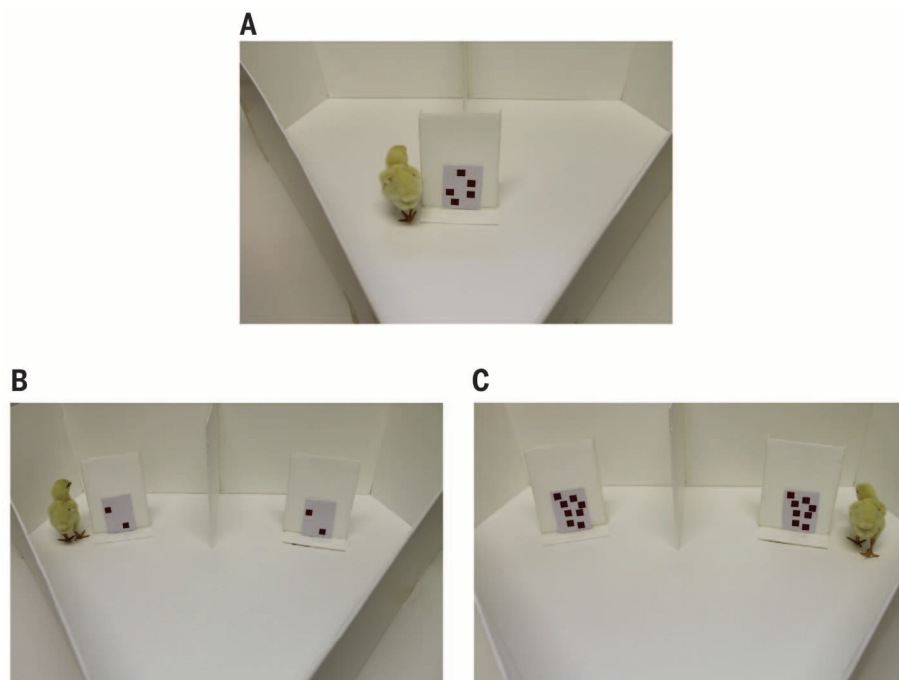
Fig. 1. Experimental settings of experiment 1. Chicks were trained to circumnavigate a panel, located in the center of the apparatus, depicting 5 identical elements (i.e., the target number). (**A**) In all experiments, we used 20 different training stimuli, differing in the spatial disposition of the elements. The training finished whenever the chick circumnavigated the screen and reached the food reward 20 consecutive times. After training, each chick underwent two tests in random order: a small number test (2 versus 2) (**B**) and a large number test (8 versus 8) (**C**). In all experiments, each test consisted of five nonreinforced trials (a novel pair of stimuli was employed on each trial). On each test trial, we scored the panel first inspected by the chick and computed the mean percentage of choices for the left panel.

the 9-18 range, responding to 9 is faster when responses are executed on the left (1). No evidence of this has been reported in nonhuman species.

To avoid the influence of pseudoneglect and to ascertain the relativity of the MNL and its dependence on the number magnitude, we devised a new experimental paradigm (21). Three-day-old domestic chicks (*Gallus gallus*) learned to circumnavigate a panel to reach a food reward (fig. S1). At training, the panel depicted a target number of elements (5 in experiment 1; Fig. 1A). At testing, we presented each chick with two panels, one on its left side and one on its right side, both depicting the same number of elements, which was, however, a different number from the target. Each chick underwent two tests: a small number test in which the panels depicted a number of elements smaller than the target (2 in experiment 1; Fig. 1B), and a large number test in which the number of elements was larger than the target (8 in experiment 1; Fig. 1C). The test stimuli looked identical. Moreover, birds could not rely on familiar information concerning their spatial position or appearance to choose which panel to approach first when looking for food. Any facilitation in processing a number smaller than the target to the left (or larger to the right), resulting in a coherent preferential choice for one side, would support the hypothesis of a left-to-right–oriented spatial numerical association. On each of five testing trials, for each test, we scored the first panel (left or right) inspected by the chick (fig. S2). In the small number test (2 versus 2), chicks chose the left panel 70.67% and the right panel 29.33% of the times. In the large number test (8 versus 8), the chicks chose the left panel 29% and the right panel 71% of the times (Fig. 3). In experiment 2, a new group of chicks was presented with the target number "20" (Fig. 2A). Now 8 versus 8 constituted the small number test (Fig. 2B), and chicks chose the left panel 70% and the right panel 30% of the time. In the large number test, 32 versus 32 (Fig. 2C), chicks chose the left panel 22.5% and the right panel 77.5% of the times (Fig. 3). The association of a certain number on the left or on the right was not absolute but depended on the relative magnitude of the number with respect to the target. Chicks that had experienced the number "5" as the target, associated the number "8" with the right side of space. On the contrary, chicks that had experienced the number "20" as the target, associated the number "8" with the left side of the space. These results were confirmed in experiment 3, in which we controlled for the effect of the following non-numerical cues on number-space
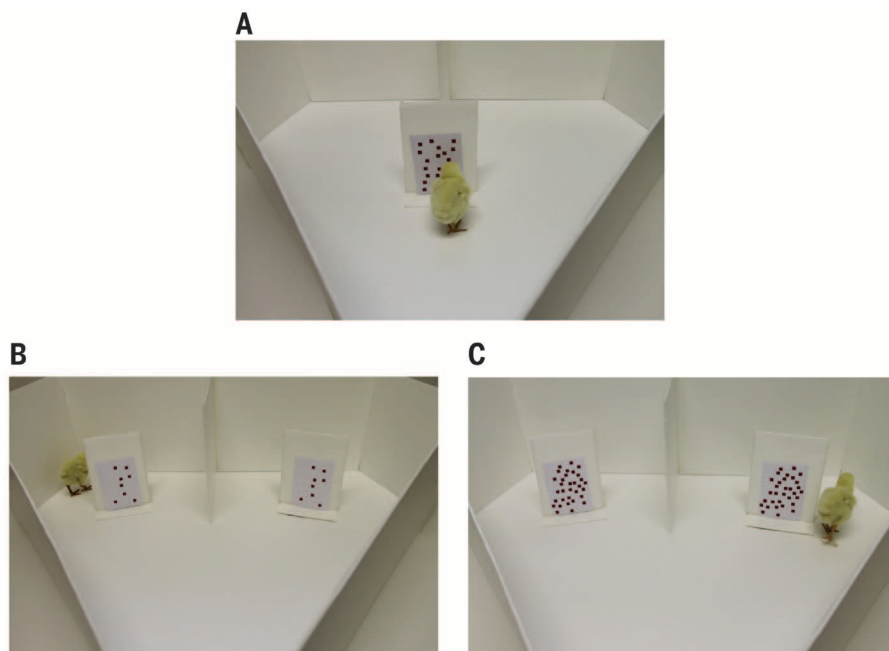
Fig. 2. Experimental settings of experiment 2. We trained a new group of chicks on the target number 20 (**A**). Birds then underwent both a small number test (8 versus 8) (**B**) and a large number test (32 versus 32) (**C**).

Fig. 3. Results of all the experiments. For each experiment, we calculated the percentage of the times each chick chose the left panel [range: 0 (left panel never chosen) – 100 (left panel always chosen)]. Experiment 1: A Mann-Whitney U test on the percentage of choices for the left panel did not reveal any difference between chicks that underwent the small number test first (*n* = 8) or second (*n* = 7) (*U* = 24.50, *P* = 0.66), nor between chicks that underwent the large number test first (*n* = 7) or second (*n* = 8) (*U* = 24.50, *P* = 0.68). Data were merged and compared with chance level (50%) with a *t* test. In the small number test, chicks preferred the left panel (*n* = 15 chicks, mean = 70.67%, SE = 5.81, *t*(14) = 3.56, *P* < 0.01). In the large number test, chicks preferred the right panel (*n* = 15, mean = 29%, SE = 7.37, *t*(14) = −2.85, *P* = 0.01). Experiment 2: A Mann-Whitney U test did not reveal any difference between chicks that underwent the small number test first (*n* = 6) or second (*n* = 6) (*U* = 18, *P* = 1), nor between chicks that underwent the large number test first (*n* = 6) or second (*n* = 6) (*U* = 16, *P* = 0.72).

In the small number test, chicks preferred the left panel (*n* = 12, mean = 70%, SE = 5.77, *t*(11) = 3.46, *P* < 0.01). In the large number test, chicks preferred the right panel (*n* = 12, mean = 22.5%, SE = 6.53, *t*(11) = −4.21, *P* < 0.01). In experiment 3, we ran a two-way mixed analysis of variance [between-subjects factor: condition (1, 2, 3); within-subjects factor: number (8 versus 8, 32 versus 32)] to control for the effect of non-numerical cues. Only the main effect of number was significant [*F*(1, 34) = 98.71, *P* < 0.01, partial eta squared = 0.74]. In the small number test, chicks preferred the left panel (*n* = 37, mean = 69.46%, SE = 2.94, *t*(36) = 6.61, *P* < 0.01). In the large number test, chicks preferred the right panel (*n* = 37, mean = 25.27%, SE = 3.36, *t*(36) = −7.35, *P* < 0.01).
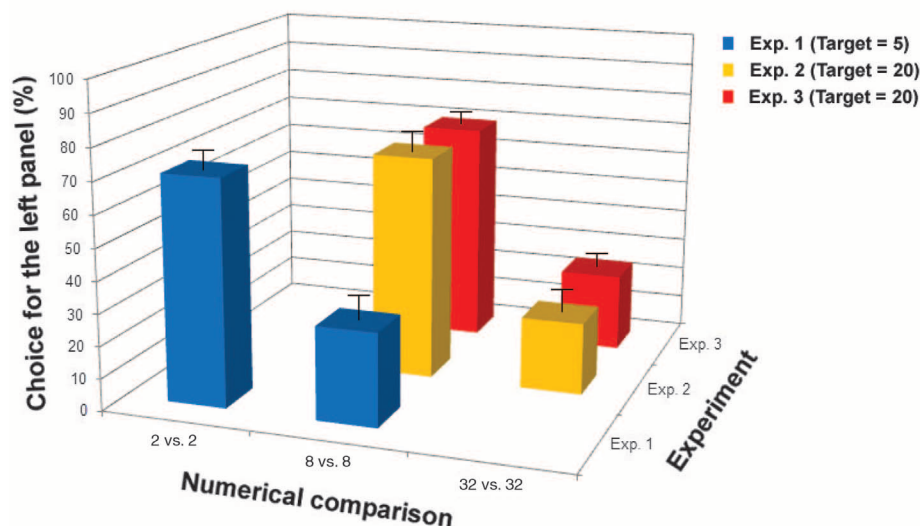
mapping: condition 1: shape, color, and size of each element; condition 2: overall area (summation of the areas of all elements depicted in each stimulus); condition 3: overall perimeter (summation of the perimeters of all elements depicted in each stimulus) and density (the mean distance among the elements). Moreover, in condition 3, there was a negative correlation between overall area and number: The overall area of the 8 elements was larger than that of the 32 elements. Furthermore, the elements of each stimulus occupied the same overall spatial frame in conditions 2 and 3. If the overall area, in the presence of the same perimeter, was the crucial factor underlying number-space mapping, chicks would have chosen the right panel in the small number test and the left panel in the large number test. The results showed that in the small number test (8 versus 8), chicks chose the left panel 69.46% and the right panel 30.54% of the times. In the large number test (32 versus 32), chicks chose the left panel 25.27% and the right panel 74.73% of the times (Fig. 3). Therefore, the results of experiment 3 demonstrate that spatial mapping relates to the abstract numerical magnitude, independently of non-numerical cues.

Our results indicate that a disposition to map numerical magnitudes onto a left-to-right–oriented MNL exists independently of cultural factors and can be observed in animals with very little nonsymbolic numerical experience, supporting a nativistic foundation of such orientation. Spatial mapping of numbers from left to right may be a universal cognitive strategy available soon after birth. Experience and, in humans, culture and education (e.g., reading habits and formal mathematics education) may modulate or even be modulated by this innate number sense.

During evolution, the direction of mapping from left to right rather than vice versa, although in principle arbitrary, may have been imposed by brain asymmetry, a common and ancient trait in vertebrates (22), prompted by a right hemisphere dominance in attending visuospatial and/or numerical information. Recent studies have suggested that numerical knowledge constitutes a domain-specific cognitive ability, with a dedicated neural substrate located in the inferior parietal cortices (1, 23). Moreover, number-space mapping is implemented in humans through a topographical representation in the right posterior parietal cortex (24). Such topography has not yet been found in neurons responding to number in animals (25, 26).

Because nonverbal numerical cognition is shared by many animal classes (1, 27, 28), we suggest that a similar predisposition to map numbers onto space is embodied in the architecture of the animal neural systems.

REFERENCES AND NOTES

1. S. Dehaene, *The Number Sense* (Oxford Univ. Press, New York, 2011).
2. R. S. Moyer, T. K. Landauer, *Nature* **215**, 1519–1520 (1967).
3. J. F. Cantlon, E. M. Brannon, *PLOS Biol.* **5**, e328 (2007).
4. D. Scarf, H. Hayne, M. Colombo, *Science* **334**, 1664 (2011).
5. E. S. Spelke, K. D. Kinzler, *Dev. Sci.* **10**, 89–96 (2007).
6. S. Dehaene, S. Bossini, P. Giraux, *J. Exp. Psychol. Gen.* **122**, 371–396 (1993).
7. M. Zorzi, K. Priftis, C. Umiltà, *Nature* **417**, 138–139 (2002).
8. C. Umiltà, K. Priftis, M. Zorzi, *Exp. Brain Res.* **192**, 561–569 (2009).
9. The SNARC effect refers to the fact that humans respond faster to small numbers when responses are executed on the left side rather than on the right, but they respond faster to large numbers when responses are executed on the right side rather than on the left.
10. S. Zebian, *J. Cogn. Cult.* **5**, 165–190 (2005).
11. S. Shaki, M. H. Fischer, W. M. Petrusic, *Psychon. Bull. Rev.* **16**, 328–331 (2009).
12. M. D. de Hevia, L. Girelli, M. Addabbo, V. Macchi Cassia, *PLOS ONE* **9**, e96412 (2014).
13. R. Rugani, L. Regolin, G. Vallortigara, *J. Exp. Psychol. Anim. Behav. Process.* **33**, 21–31 (2007).
14. R. Rugani, D. M. Kelly, I. Szelest, L. Regolin, G. Vallortigara, *Biol. Lett.* **6**, 290–292 (2010).
15. C. B. Drucker, E. M. Brannon, *Cognition* **132**, 57–67 (2014).
16. R. Rugani, G. Vallortigara, B. Vallini, L. Regolin, *Neurobiol. Learn. Mem.* **95**, 231–238 (2011).
17. G. Jewell, M. E. McCourt, *Neuropsychologia* **38**, 93–110 (2000).
18. B. Diekamp, L. Regolin, O. Güntürkün, G. Vallortigara, *Curr. Biol.* **15**, R372–R373 (2005).
19. L. Regolin, *Cortex* **42**, 101–103 (2006).
20. I. Adachi, *PLOS ONE* **9**, e90373 (2014).
21. Materials and methods are available as supplementary materials on *Science* Online.
22. L. J. Rogers, G. Vallortigara, R. J. Andrew, *Divided Brains* (Cambridge Univ. Press, New York, 2013).
23. A. Nieder, D. J. Freedman, E. K. Miller, *Science* **297**, 1708–1711 (2002).
24. B. M. Harvey, B. P. Klein, N. Petridou, S. O. Dumoulin, *Science* **341**, 1123–1126 (2013).
25. J. D. Roitman, E. M. Brannon, M. L. Platt, *Front. Integr. Neurosci.* **6**, 25 (2012).
26. A. Nieder, *J. Comp. Physiol. A Neuroethol. Sens. Neural Behav. Physiol.* **199**, 1–16 (2013).
27. E. M. Brannon, H. S. Terrace, *Science* **282**, 746–749 (1998).
28. R. Rugani, L. Fontanari, E. Simoni, L. Regolin, G. Vallortigara, *Proc. Biol. Sci.* **276**, 2451–2460 (2009).

IDENTITY AND PRIVACY

Unique in the shopping mall: On the reidentifiability of credit card metadata

Yves-Alexandre de Montjoye,[1]* Laura Radaelli,[2] Vivek Kumar Singh,[1,3] Alex "Sandy" Pentland[1]

Large-scale data sets of human behavior have the potential to fundamentally transform the way we fight diseases, design cities, or perform research. Metadata, however, contain sensitive information. Understanding the privacy of these data sets is key to their broad use and, ultimately, their impact. We study 3 months of credit card records for 1.1 million people and show that four spatiotemporal points are enough to uniquely reidentify 90% of individuals. We show that knowing the price of a transaction increases the risk of reidentification by 22%, on average. Finally, we show that even data sets that provide coarse information at any or all of the dimensions provide little anonymity and that women are more reidentifiable than men in credit card metadata.

Large-scale data sets of human behavior have the potential to fundamentally transform the way we fight diseases, design cities, or perform research. Ubiquitous technologies create personal metadata on a very large scale. Our smartphones, browsers, cars, or credit cards generate information about where we are, whom we call, or how much we spend. Scientists have compared this recent availability of large-scale behavioral data sets to the invention of the microscope (1). New fields such as computational social science (2–4) rely on metadata to address crucial questions such as fighting malaria, studying the spread of information, or monitoring poverty (5–7). The same metadata data sets are also used by organizations and governments. For example, Netflix uses viewing patterns to recommend movies, whereas Google uses location data to provide real-time traffic information, allowing drivers to reduce fuel consumption and time spent traveling (8).

The transformational potential of metadata data sets is, however, conditional on their wide availability. In science, it is essential for the data to be available and shareable. Sharing data allows

[1]Media Lab, Massachusetts Institute of Technology (MIT), 20 Amherst Street, Cambridge, MA 02139, USA. [2]Department of Computer Science, Aarhus University, Aabogade 34, Aarhus, 8200, Denmark. [3]School of Communication and Information, Rutgers University, 4 Huntington Street, New Brunswick, NJ 08901, USA.
*Corresponding author. E-mail: yvesalexandre@demontjoye.com
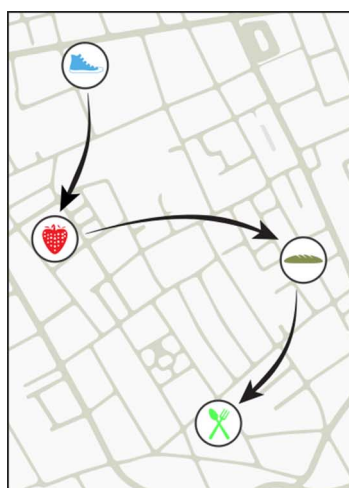
Fig. 1. Financial traces in a simply anonymized data set such as the one we use for this work. Arrows represent the temporal sequence of transactions for user 7abc1a23 and the prices are grouped in bins of increasing size (29).

scientists to build on previous work, replicate results, or propose alternative hypotheses and models. Several publishers and funding agencies now require experimental data to be publicly available (9–11). Governments and businesses are similarly realizing the benefits of open data (12). For example, Boston's transportation authority makes the real-time position of all public rail vehicles available through a public interface (13), whereas Orange Group and its subsidiaries make large samples of mobile phone data from Côte d'Ivoire and Senegal available to selected researchers through their Data for Development challenges (14, 15).

These metadata are generated by our use of technology and, hence, may reveal a lot about an individual (16, 17). Making these data sets broadly available, therefore, requires solid quantitative guarantees on the risk of reidentification. A data set's lack of names, home addresses, phone numbers, or other obvious identifiers [such as required, for instance, under the U.S. personally identifiable information (PII) "specific-types" approach (18)], does not make it anonymous nor safe to release to the public and to third parties. The privacy of such simply anonymized data sets has been compromised before (19–22).

Unicity quantifies the intrinsic reidentification risk of a data set (19). It was recently used to show that individuals in a simply anonymized mobile phone data set are reidentifiable from only four pieces of outside information. Outside information could be a tweet that positions a user at an approximate time for a mobility data set or a publicly available movie review for the Netflix data set (20). Unicity quantifies how much outside information one would need, on average, to reidentify a specific and known user in a simply anonymized data set. The higher a data set's unicity is, the more reidentifiable it is. It consequently also quantifies the ease with which a simply anonymized data set could be merged with another.

Financial data that include noncash and digital payments contain rich metadata on individuals' behavior. About 60% of payments in the United States are made using credit cards (23),

Fig. 2. The unicity ε of the credit card data set given p points. The green bars represent unicity when spatiotemporal tuples are known. This shows that four spatiotemporal points taken at random (p = 4) are enough to uniquely characterize 90% of individuals. The blue bars represent unicity when using spatial-temporal-price triples (a = 0.50) and show that adding the approximate price of a transaction significantly increases the likelihood of reidentification. Error bars denote the 95% confidence interval on the mean.
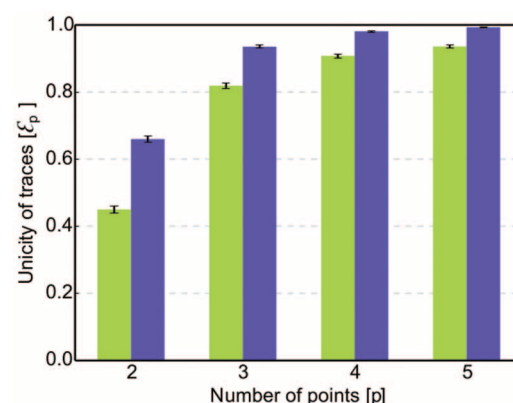
and mobile payments are estimated to soon top $1 billion in the United States (24). A recent survey shows that financial and credit card data sets are considered the most sensitive personal data worldwide (25). Among Americans, 87% consider credit card data as moderately or extremely private, whereas only 68% consider health and genetic information private, and 62% consider location data private. At the same time, financial data sets have been used extensively for credit scoring (26), fraud detection (27), and understanding the predictability of shopping patterns (28). Financial metadata have great potential, but they are also personal and highly sensitive. There are obvious benefits to having metadata data sets broadly available, but this first requires a solid understanding of their privacy.

To provide a quantitative assessment of the likelihood of identification from financial data, we used a data set D of 3 months of credit card transactions for 1.1 million users in 10,000 shops in an Organisation for Economic Co-operation and Development country (Fig. 1). The data set was simply anonymized, which means that it did not contain any names, account numbers, or obvious identifiers. Each transaction was time-stamped with a resolution of 1 day and associated with one shop. Shops are distributed throughout the country, and the number of shops in a district scales with population density (r^2 = 0.51, P < 0.001) (fig. S1).

We quantified the risk of reidentification of D by means of unicity ε (19). Unicity is the risk of reidentification knowing p pieces of outside information about a user (29). We evaluate ε_p of D as the percentage of its users who are reidentified with p randomly selected points from their financial trace. For each user, we extracted the subset $S(I_p)$ of traces that match the p known points (I_p). A user was considered reidentified in this correlation attack if $|S(I_p)| = 1$.

For example, let's say that we are searching for Scott in a simply anonymized credit card data set (Fig. 1). We know two points about Scott: he went to the bakery on 23 September and to the restaurant on 24 September. Searching through the data set reveals that there is one and only one person in the entire data set who went to these two places on these two days. $|S(I_p)|$ is thus equal to 1, Scott is reidentified, and we now know all of his other transactions, such as the fact that he went shopping for shoes and groceries on 23 September, and how much he spent.

Figure 2 shows that the unicity of financial traces is high (ε_4 > 0.9, green bars). This means that knowing four random spatiotemporal points or tuples is enough to uniquely reidentify 90% of the individuals and to uncover all of their records. Simply anonymized large-scale financial metadata can be easily reidentified via spatiotemporal information.
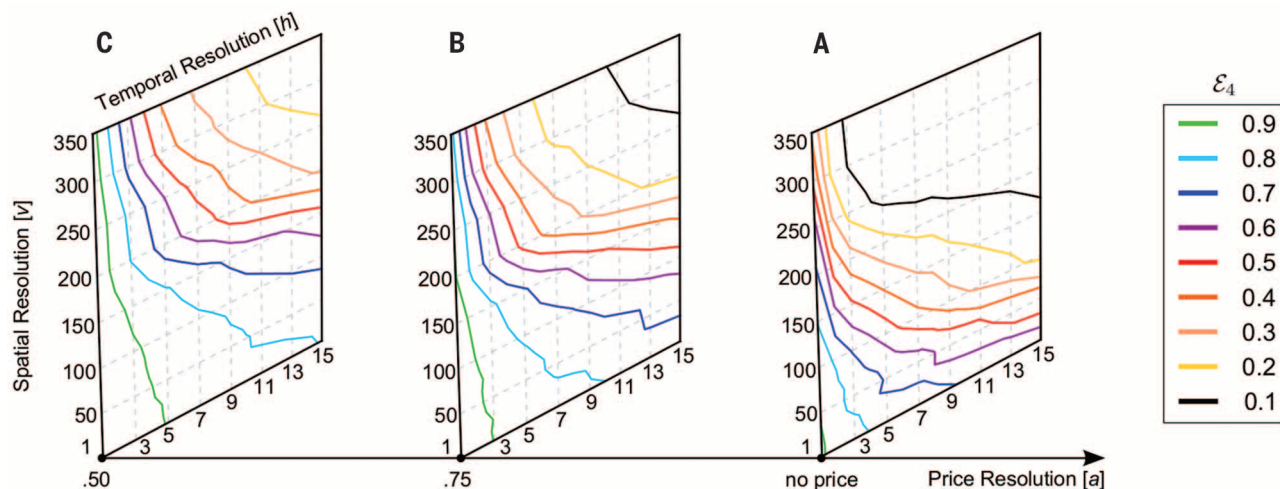
Fig. 3. Unicity (ε_4) when we lower the resolution of the data set on any or all of the three dimensions; with four spatiotemporal tuples [(A), no price] and with four spatiotemporal-price triples [(B), a = 0.75; (C), a = 0.50]. Although unicity decreases with the resolution of the data, the decrease is easily overcome by collecting a few more points. Even at very low resolution (h = 15 days, v = 350 shops, price a = 0.50), we have more than an 80% chance of reidentifying an individual with 10 points ($\varepsilon_{10} > 0.8$) (table S1).

Fig. 4. Unicity for different categories of users ($v = 1$, $h = 1$). (**A**) It is significantly easier to reidentify women ($\varepsilon_4 = 0.93$) than men ($\varepsilon_4 = 0.89$). (**B**) The higher a person's income is, the easier he or she is to reidentify. High-income people ($\varepsilon_4 = 0.93$) are significantly easier to reidentify than medium-income people ($\varepsilon_4 = 0.91$), and medium-income people are themselves significantly easier to reidentify than low-income people ($\varepsilon_4 = 0.88$). Significance levels were tested with a one-tailed t test ($P < 0.05$). Error bars denote the 95% confidence interval on the mean.
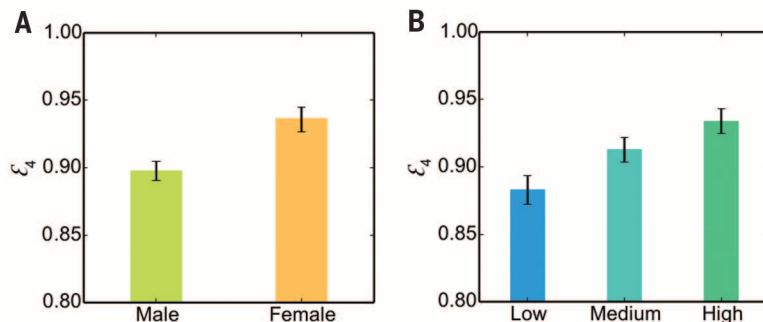
Furthermore, financial traces contain one additional column that can be used to reidentify an individual: the price of a transaction. A piece of outside information, a spatiotemporal tuple can become a triple: space, time, and the approximate price of the transaction. The data set contains the exact price of each transaction, but we assume that we only observe an approximation of this price with a precision a we call price resolution. Prices are approximated by bins whose size is increasing; that is, the size of a bin containing low prices is smaller than the size of a bin containing high prices. The size of a bin is a function of the price resolution a and of the median price m of the bin (29). Although knowing the location of my local coffee shop and the approximate time I was there this morning helps to reidentify me, Fig. 2 (blue bars) shows that also knowing the approximate price of my coffee significantly increases the chances of reidentifying me. In fact, adding the approximate price of the transaction increases, on average, the unicity of the data set by 22% (fig. S2, when a =0.50, $\langle \Delta\varepsilon \rangle$ = 0.22).

The unicity ε of the data set naturally decreases with its resolution. Coarsening the data along any or all of the three dimensions makes reidentification harder. We artificially lower the spatial resolution of our data by aggregating shops in clusters of increasing size v based on their spatial prox-

imity (29). This means that we do not know the exact shop in which the transaction happened, but only that it happened in this geographical area. We also artificially lower the temporal resolution of the data by increasing the time window h of a transaction from 1 day to up to 15 days. Finally, we increase the size of the bins for price a from 50 to 75%. In practice, this means that the bin in which a $15.13 transaction falls into will go from $5 to $16 ($a$ = 0.50) to $5 to $34 ($a$ = 0.75) (table S2).

Figure 3 shows that coarsening the data is not enough to protect the privacy of individuals in financial metadata data sets. Although unicity decreases with the resolution of the data, it only decreases slowly along the spatial (v), temporal (h), and price (a) axes. Furthermore, this decrease is easily overcome by collecting a few more points (table S1). For instance, at a very low resolution of h = 15 days, v = 350 shops, and an approximate price a = 0.50, we have less than a 15% chance of reidentifying an individual knowing four points ($\varepsilon_4 < 0.15$). However, if we know 10 points, we now have more than an 80% chance of reidentifying this person ($\varepsilon_{10} > 0.8$). This means that even noisy and/or coarse financial data sets along all of the dimensions provide little anonymity.

We also studied the effects of gender and income on the likelihood of reidentification. Figure 4A shows that women are easier to reiden-

tify than men, whereas Fig. 4B shows that the higher somebody's income is, the easier it is to reidentify him or her. In fact, in a generalized linear model (GLM), the odds of women being reidentified are 1.214 times greater than for men. Similarly, the odds of high-income people (and, respectively, medium-income people) to be reidentified are 1.746 times (and 1.172 times) greater than for low-income people (29). Although a full causal analysis or investigation of the determinants of reidentification of individuals is beyond the scope of this paper, we investigate a couple of variables through which gender or income could influence unicity. A linear discriminant analysis shows that the entropy of shops, how one shares his or her time between the shops he or she visits, is the most discriminative factor for both gender and income (29).

Our estimation of unicity picks the points at random from an individual's financial trace. These points thus follow the financial trace's non-uniform distributions (Fig. 5A and fig. S3A). We are thus more likely to pick a point where most of the points are concentrated, which makes them less useful on average. However, even in this case, seven points were enough to reidentify all of the traces considered (fig. S4). More sophisticated reidentification strategies could collect points that would maximize the decrease in unicity.
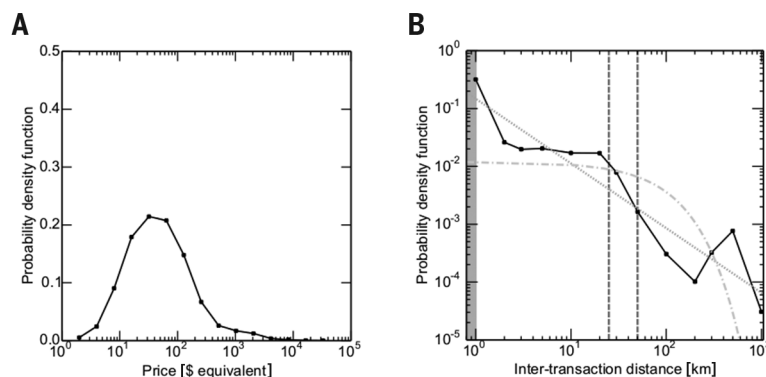
Fig. 5. Distributions of the financial records. (**A**) Probability density function of the price of a transaction in dollars equivalent. (**B**) Probability density function of spatial distance between two consecutive transactions of the same user. The best fit of a power law (dotted line) and an exponential distribution (dot-dashed line) are given as a reference. The dashed lines are the diameter of the first and second largest cities in the country. Thirty percent of the successive transactions of a user are less than 1 km apart (the shaded area), followed by, an order of magnitude lower, a plateau between 2 and 20 km, roughly the radius of the two largest cities in the country. This shows that financial metadata are different from mobility data: The likelihood of short travel distance is very high and then plateaus, and the overall distribution does not follow a power-law or exponential distribution.

Although future work is needed, it seems likely that most large-scale metadata data sets—for example, browsing history, financial records, and transportation and mobility data—will have a high unicity. Despite technological and behavioral differences (Fig. 5B and fig. S3), we showed credit card records to be as reidentifiable as mobile phone data and their unicity to be robust to coarsening or noise. Like credit card and mobile phone metadata, Web browsing or transportation data sets are generated as side effects of human interaction with technology, are subjected to the same idiosyncrasies of human behavior, and are also sparse and high-dimensional (for example, in the number of Web sites one can visit or the number of possible entry-exit combinations of metro stations). This means that these data can probably be relatively easily reidentified if released in a simply anonymized form and that they can probably not be anonymized by simply coarsening of the data.

Our results render the concept of PII, on which the applicability of U.S. and European Union (EU) privacy laws depend, inadequate for metadata data sets (18). On the one hand, the U.S. specific-types approach—for which the lack of names, home addresses, phone numbers, or other listed PII is enough to not be subject to privacy laws—is obviously not sufficient to protect the privacy of individuals in high-unicity metadata data sets. On the other hand, open-ended definitions expanding privacy laws to "any information concerning an identified or identifiable person" (30) in the EU proposed data regulation or "[when the] re-identification to a particular person is not possible" (31) for Deutsche Telekom are probably impossible to prove and could very strongly limit any sharing of the data (32).

From a technical perspective, our results emphasize the need to move, when possible, to more advanced and probably interactive individual (33) or group (34) privacy-conscientious technologies, as well as the need for more research in computational privacy. From a policy perspective, our findings highlight the need to reform our data protection mechanisms beyond PII and anonymity and toward a more quantitative assessment of the likelihood of reidentification. Finding the right balance between privacy and utility is absolutely crucial to realizing the great potential of metadata.

REFERENCES AND NOTES

1. S. Higginbotham, "For science, big data is the microscope of the 21st century" (2011); http://gigaom.com/2011/11/08/for-science-big-data-is-the-microscope-of-the-21st-century/.
2. D. Lazer et al., Science 323, 721–723 (2009).
3. J. Giles, Nature 488, 448–450 (2012).
4. D. J. Watts, Winter Issue of The Bridge on Frontiers of Engineering 43, 5–10 (2013).
5. A. Wesolowski et al., Science 338, 267–270 (2012).
6. S. Charaudeau, K. Pakdaman, P.-Y. Boëlle, PLOS ONE 9, e83002 (2014).
7. N. Eagle, M. Macy, R. Claxton, Science 328, 1029–1031 (2010).
8. V. Padmanabhan, R. Ramjee, P. Mohan, U.S. Patent 8,423,255 (2013).
9. G. Boulton, Nature 486, 441 (2012).
10. M. McNutt, Science 346, 679 (2014).
11. T. Bloom, "Data access for the open access literature: PLOS's data policy" (2013); www.plos.org/data-access-for-the-open-access-literature-ploss-data-policy.
12. K. Burns, "In US cities, open data is not just nice to have; it's the norm" The Guardian, 21 October 2013; www.theguardian.com/local-government-network/2013/oct/21/open-data-us-san-francisco.
13. Massachusetts Bay Transportation Authority, "Real-time commuter rail data" (2010); www.mbta.com/rider_tools/developers/default.asp?id=21899.
14. Y.-A. de Montjoye, Z. Smoreda, R. Trinquart, C. Ziemlicki, V. D. Blondel, D4D-Senegal: The second mobile phone data for development challenge. (2014); http://arxiv.org/abs/1407.4885.
15. V. D. Blondel et al., Data for Development: The D4D challenge on mobile phone data. (2012); http://arxiv.org/abs/1210.0137.
16. P. Mutchler, "MetaPhone: The sensitivity of telephone metadata" (2014); http://webpolicy.org/2014/03/12/metaphone-the-sensitivity-of-telephone-metadata/.
17. Y.-A. de Montjoye, J. Quoidbach, F. Robic, A. Pentland, Predicting personality using novel mobile phone-based metrics. in Proc. SBP (Springer, Berlin, Heidelberg, 2013), pp. 48–55.
18. P. M. Schwartz, D. J. Solove, Calif. Law Rev. 102, 877–916 (2014).
19. Y.-A. de Montjoye, C. A. Hidalgo, M. Verleysen, V. D. Blondel, Sci. Rep. 3, 1376 (2013).
20. A. Narayanan, V. Shmatikov, Robust de-anonymization of large sparse datasets. in IEEE Symposium on Security and Privacy, Oakland, CA, 18 to 22 May 2008 (IEEE, New York, 2008), pp. 111–125.
21. A. C. Solomon, R. Hill, E. Janssen, S. A. Sanders, J. R. Heiman, Uniqueness and how it impacts privacy in health-related social science datasets. in Proc. IHI (Association for Computing Machinery, New York, 2012), pp. 523–532.
22. L. Sweeney, Int. J. Unc. Fuzz. Knowl. Based Syst. 10, 557–570 (2002).
23. 2013 Federal Reserve payments study (2013); www.frbservices.org/files/communications/pdf/research/2013_payments_summary.pdf.
24. eMarketer, "US mobile payments to top $ 1 billion in 2013" (2013); www.emarketer.com/Article/US-Mobile-Payments-Top-1-Billion-2013/1010035.
25. "The trust advantage: How to win with big data" (2013); www.bcgperspectives.com/content/articles/information_technology_strategy_consumer_products_trust_advantage_win_big_data/.
26. C.-L. Huang, M.-C. Chen, C.-J. Wang, Expert Syst. Appl. 33, 847–856 (2007).
27. S. Bhattacharyya, S. Jha, K. Tharakunnel, J. C. Westland, Decis. Support Syst. 50, 602–613 (2011).
28. C. Krumme, A. Llorente, M. Cebrian, A. S. Pentland, E. Moro, Sci. Rep. 3, 1645 (2013).
29. Materials and methods are available as supplementary materials on Science Online.
30. European Commission, "General data protection regulation" (2012); http://ec.europa.eu/justice/data-protection/document/review2012/com_2012_11_en.pdf.
31. Deutsche Telekom, "Guiding principle big data" (2014); www.telekom.com/static/-/205808/1/guiding-principles-big-data-si.
32. Y.-A. de Montjoye, J. Kendall, C. Kerry, Enabling Humanitarian Use of Mobile Phone Data. Brookings Issues in Technology Innovation Series (Brookings Institution, Washington, DC, 2014), vol. 26.
33. Y.-A. de Montjoye, S.S. Wang, A.S. Pentland, IEEE Data Eng. Bull. 35, 5–8 (2012).
34. C. Dwork, in Automata, Languages and Programming (Lecture Notes in Computer Science Series, Springer, Berlin, Heidelberg, 2006), vol. 4052, pp. 1–12.

ATMOSPHERIC DYNAMICS

Constrained work output of the moist atmospheric heat engine in a warming climate

F. Laliberté,[1]* J. Zika,[2] L. Mudryk,[3] P. J. Kushner,[1] J. Kjellsson,[3] K. Döös[4]

Incoming and outgoing solar radiation couple with heat exchange at Earth's surface to drive weather patterns that redistribute heat and moisture around the globe, creating an atmospheric heat engine. Here, we investigate the engine's work output using thermodynamic diagrams computed from reanalyzed observations and from a climate model simulation with anthropogenic forcing. We show that the work output is always less than that of an equivalent Carnot cycle and that it is constrained by the power necessary to maintain the hydrological cycle. In the climate simulation, the hydrological cycle increases more rapidly than the equivalent Carnot cycle. We conclude that the intensification of the hydrological cycle in warmer climates might limit the heat engine's ability to generate work.

As a reflection of the seminal work of Carnot, atmospheric motions have been described as an important component of the planetary heat engine (1). The concept of a heat engine is closely associated with the idea of work: For two cycles that transport the same amount of heat between the same two reservoirs, the one that generates the least irreversible entropy will produce the most work (2). We quantify the atmosphere's work output through a budget of its entropy production. Previous attempts at obtaining such a budget either resulted in gross estimates (3, 4) or required highly specific data from climate models for a precise analysis (5–8). Some of these studies showed that the hydrological cycle was an important contributor to the generation of irreversible entropy (6, 9, 10), suggesting that moist processes, including the frictional dissipation associated with falling hydrometeors (11, 12), tend to limit the work output of the atmospheric heat engine. On a warming Earth, the increase in precipitable water (13) has been identified as a reason for the tropical overturning to slow down (14), and studies over a wide range of climates suggest that global atmospheric motions are reduced in extremely warm climates (15–17). Models forced according to a climate change scenario also exhibit this behavior in their tropical circulation (18). Here, we employ a method that uses high-frequency and high-resolution data to obtain an atmospheric entropy budget from climate models and reanalyses. This method does not depend on specialized model output, making the diagnostic applicable to the suite of models produced for the Climate Model Intercomparison Project phase 5 (CMIP5) and paving the way to

a systematic analysis of the entropy budget in climate models, as proposed by some authors (8).

We base our analysis on the first law of thermodynamics describing moist air (19, 20).

$$Tds/dt = dh/dt - \alpha dp/dt + \mu dq_T/dt.$$

The material derivatives of moist enthalpy h and moist entropy s (19–21) are given by dh/dt and ds/dt, respectively.

The equation of state used here provides a comprehensive treatment of moist thermodynamics, including the effect of the latent heat of fusion on h and s (19, 20). The specific ratio q_T represents the total mass of water divided by the total mass of wet air (humid air plus water condensate). The work output $-\alpha dp/dt$ is given by the product of the specific volume α with the vertical velocity in pressure coordinates $-dp/dt$. The chemical potential μ quantifies the effect of adding or removing moisture; it is equal to the sum of two terms with different physical meanings (see the supplementary text). The first of these terms accounts for the moistening inefficiencies that accompany the irreversible entropy production associated with the addition of water vapor to unsaturated air (9, 10). The second term accounts for the enthalpy changes associated with the drying and moistening of air. For the atmospheric thermodynamic cycle, we will show that when μ is positive, $\mu dq_T/dt$ primarily quantifies the moistening inefficiencies accounted for by the first term, and when μ is negative $\mu dq_T/dt$ primarily quantifies how much power is associated with combined moisture and dry air fluxes between the surface and the precipitation level accounted for by the second term.

Averaging the first law using a mass-weighted annual and global spatial mean [denoted as $\{\cdot\}$] results in simplification. First, $\{dh/dt\}$ equals the difference between interior moist enthalpy sinks and the moist enthalpy sources at Earth's surface stemming from diffusive fluxes. If we assume that the atmospheric system is in steady state

(and therefore approximately yearly periodic), the sinks cancel the sources and $\{dh/dt\}$ vanishes. Moreover, under this averaging, $\dot{Q}_{moist} = \{\mu dq_T/dt\}$ is positive because it quantifies the power necessary to maintain the hydrological cycle and accounts for the moistening inefficiencies (10), and $W = \{-\alpha dp/dt\}$ is also positive because it is associated with the dissipation of kinetic energy at the viscous scale (22). Writing $\dot{Q}_{total} = \{Tds/dt\}$, then, the first law reads [equation 4 in (10)]

$$W = \dot{Q}_{total} - \dot{Q}_{moist}$$

W is thus reduced by the moistening inefficiencies accounted for by $\dot{Q}_{moist}$. In the following sections, we obtain a diagnostic for $\dot{Q}_{total}$ and $\dot{Q}_{moist}$ based on the area occupied by the atmospheric thermodynamic cycle in a temperature-entropy diagram (hereafter $T-s$ diagram) and in a specific humidity-chemical potential diagram (hereafter $q_T-\mu$ diagram), respectively.

We analyze two different data sources. The first source is a coupled climate model simulation using the Community Earth System Model (CESM) version 1.0.2 (23). The time period 1981 to 2098 is simulated using a combination of historical radiative forcing estimates and the Representative Concentration Pathway 4.5 (24) future scenario (hereafter historical RCP45). The second source is the period 1981 to 2012 of the Modern-Era Retrospective Analysis for Research and Applications (MERRA) reanalysis (25). For these two data sets, we use a recently developed method (20) to project the material derivative ds/dt from eulerian space to $\dot{s}(s,T)$, its representation in the $T-s$ diagram. We use the same method to project dq_T/dt to $\dot{q}_T(\mu,q_T)$, its representation in the $q_T-\mu$ diagram. Each of these quantities is associated with a closed, uniquely defined mass flux stream function in its respective coordinate system.

$$\Psi^{total}(s,T) = \int_T^\infty \dot{s}(s,T')dT',$$
$$(\dot{s},\dot{T}) = (-\partial_T\Psi^{total}, \partial_s\Psi^{total}),$$
$$\Psi^{moist}(\mu,q_T) = \int_\mu^\infty \dot{q}_T(\mu',q_T)d\mu',$$
$$(\dot{\mu},\dot{q}_T) = (-\partial_{q_T}\Psi^{moist}, \partial_\mu\Psi^{moist})$$

Each stream function describes a separate aspect of the large-scale atmospheric thermodynamic cycle. This approach is similar to a method that has been previously used to study the atmospheric and oceanic circulations in thermodynamic coordinates (26–29).

In a $T-s$ diagram, the quantity Ψ^{total} describes a clockwise cycle (Fig. 1, A and B) with three main branches. In the lower branch, a large fraction of air is transported along the surface saturation curve (1000 hPa, 100% relative humidity) and, as it moves toward warmer temperatures, picks up heat through exchanges at Earth's surface. In the tropical branch, air is transported from warm temperatures to colder temperatures at almost constant moist entropy along the zonal-mean tropical (15°S to 15°N) profile. The zonal-mean tropical profile thus represents the transformations that tropical air masses undergo

[1]Department of Physics, University of Toronto, Ontario, Canada. [2]University of Southampton, National Oceanography Centre, Southampton, UK. [3]British Antarctic Survey, Cambridge, UK. [4]Department of Meteorology, Stockholm University, Stockholm, Sweden.
*Corresponding author. E-mail: frederic.laliberte@utoronto.ca

when they convect, detrain, and mix with environmental midtropospheric air masses (30). In the third branch, radiative cooling acts to reduce entropy as air is transported from high moist entropy and cold temperatures to low moist entropy and warmer temperatures. The thermodynamic cycles in CESM and MERRA have a similar shape, but MERRA's is stronger (larger maximum stream

function value). In the region of the $T - s$ diagram rightward of the zonal-mean subtropical profile (25°N to 35°N) and at temperatures lower than 280 K, the saturation specific humidity is small, so that pressure is approximately a function of temperature and moist entropy. In this region, thermodynamic transformations that occur along discrete pressure levels [diagnosed by $\dot{s}(p,q_T,s,t)$, $\dot{q}_T(p,q_T,s,t)$, and $\omega(p,q_T,s,t)$ (20) but not explicitly demonstrated here] yield the prominent sawtooth patterns seen in the CESM cycle. Although the same patterns appear in the MERRA cycle, they are not as prominent because the vertical resolution is finer by a factor of three, so that a smaller portion of the thermodynamic cycle is sampled along a given pressure level.

Another difference between the CESM and MERRA thermodynamic cycles is found along the zonal-mean tropical profile. At low temperatures, MERRA's Ψ^{total} is weaker than that of CESM, which suggests that MERRA's thermodynamic cycle represents a tropical heat engine more confined to the lower half of the troposphere.

The power associated with the motions described in the $T - s$ diagram can be computed as the area occupied by the stream function Ψ^{total} in a similar way that one would quantify the work output of an equivalent Carnot cycle.

$$\dot{Q}_{total} = \left\{ T \frac{ds}{dt} \right\} = -\int_{-\infty}^{\infty} \int_{0}^{\infty} \Psi^{total}(s,T)dTds$$

The averages of $\bar{\dot{Q}}_{total}$ over the 1981 to 2012 period for MERRA (6.34 Wm^{-2}) and for CESM (6.36 Wm^{-2}) have a similar magnitude (Fig. 2, A and C).

In a $q_T - \mu$ diagram, the quantity Ψ^{moist} describes a clockwise cycle (Fig. 1, C and D) restricted to $q_T \geq 0$ comprising three main branches. In the dry branch, air is transported from $\mu = 0$ to low relative humidity (high μ) near the $q_T = 0$ line. In the moistening branch, air is transported from low q_T and low relative humidity to high q_T at saturation. The cycle to the right of the $\mu = 0$ line, formed by the dry and moistening branches, primarily quantifies the moistening inefficiencies (as can be seen by comparing Fig. 1, C and D, with fig. S1). At high q_T the moistening branch follows the zonal-mean tropical (15°S to 15°N) profile from 600 hPa down in the CESM but only from 800 hPa down in MERRA. Because of this important difference, moistening air masses between 800 hPa and 600 hPa are drier than the tropical environment in MERRA but not in CESM, leading to fewer moistening inefficiencies in CESM. This difference in how air masses are moistened could arise if, for example, the data assimilation in MERRA corrected the tendency of parameterized convection to detrain and mix with its environment. In both cases, the tropical environment nevertheless determines the highest q_T values that can be produced by the atmospheric circulation.

In the dehumidification branch, air is kept close to $\mu \approx 0$ and transported from high q_T to low q_T. We note that in MERRA, the dehumidification branch reaches into negative μ values between

Fig. 1. Thermodynamic diagrams for years 1981–2012. (**A** and **C**) CESM. (**B** and **D**) MERRA. [(A) and (B)] $T - s$ diagram. Ψ^{total} in color shading and gray contours (−75, −225, −375, and −525 Sv). Thick dashed lines represents the zonal-mean vertical profile in different latitude bands. Dotted lines give the 100% relative humidity curves at 1000 hPa, 500 hPa, and 200 hPa. Axes are oriented so that the lower left corner is closest to typical tropical surface $T - s$ values, the upper left corner is closest to typical tropical upper tropospheric $T - s$ values, and the right side of the graph is closest to typical polar $T - s$ values. The correspondence between the equivalent potential temperature θ_e and s (21) is indicated on the top abscissa. [(C) and (D)] $q_T - \mu$ diagram. Ψ^{moist} in color shading and gray contours (−333, −667, −1000, and −1333 Sv). The thick dashed line represents the zonal-mean vertical profile in the tropics. Pressure levels are indicated along this profile. Axes are oriented so that the lower left corner is closest to typical tropical surface $q_T - \mu$ values. [(A) to (D)] Thin black curves indicate where $\Psi^{total} = -1$ Sv or $\Psi^{moist} = -1$ Sv. They indicate the small-magnitude cutoff over which $\dot{Q}_{total}$ or $\dot{Q}_{moist}$ were computed to avoid floating-point errors.

Fig. 2. Time series of 1-year running mean. (**A**) $\dot{Q}_{total}$ CESM. (**B**) $\dot{Q}_{moist}$ CESM. (**C**) $\dot{Q}_{total}$ MERRA. (**D**) $\dot{Q}_{moist}$ MERRA. Gray shadings quantify W.

$q_T = 5$ g kg^{-1} and $q_T = 10$ g kg^{-1}, whereas the dehumidification branch in CESM follows the $\mu = 0$ line (thin dashed line) more closely in this region of the $q_T - \mu$ diagram.

The power necessary to maintain the global moistening and remoistening motions described in this diagram can also be written as the area occupied by the stream function Ψ^{moist}.

$$\dot{Q}_{moist} = \left\{\mu \frac{dq_T}{dt}\right\} = -\int_{-\infty}^{\infty}\int_{0}^{\infty} \Psi^{moist}(\mu, q_T) d\mu dq_T$$

The average $\overline{\dot{Q}_{moist}}$ over the 1981 to 2012 period for MERRA (2.68 Wm^{-2}) (Fig. 2D) is 18% larger than for CESM (2.27 Wm^{-2}) (Fig. 2B). The difference in $\overline{\dot{Q}_{moist}}$ is mostly explained by a reduced amplitude of moistening inefficiencies in CESM (1.97 Wm^{-2}) (fig. S2B) as compared to MERRA (2.40 Wm^{-2}) (fig. S2D). Because the values of $\overline{\dot{Q}_{total}}$ are similar for the MERRA and the CESM data, but those for $\overline{\dot{Q}_{moist}}$ differ, values for W (Fig. 2, A and C) differ when averaged over the period (3.66 Wm^{-2} for MERRA, 4.09 Wm^{-2} for CESM). Computing W from an $\alpha-p$ diagram gives the same results and shows that the CESM has a larger work output between 500 hPa and 200 hPa (fig. S3). This suggests that the smaller amplitude of moistening inefficiencies in CESM might allow more deep convection than in MERRA.

The climate change response of Ψ^{total} (Fig. 3A) to an anthropogenic forcing scenario takes the shape of a dipole centered along the zonal-mean tropical profile. The mass flux stream function strengthens at higher moist entropy values and weakens at lower moist entropy values, indicative of a translation to higher moist entropy values. The same response is observed for the zonal-mean profiles.

The response of Ψ^{moist} (Fig. 3B) does not exhibit a dipole as in the $T - s$ diagram. Instead, it is strengthened almost everywhere in the $q_T - \mu$ diagram by a mostly uniform value. Accordingly, the zonal-mean tropical profile does not move appreciably. The strengthening is particularly concentrated along the outermost streamline, suggesting a slight dilatation of the cycle that results in more moistening happening at higher q_T toward the end of the 21st century.

By changing the footprint and magnitude of Ψ^{total} and Ψ^{moist}, the effect of anthropogenic forcing will also influence W. Both $\delta\dot{Q}_{total}$ and $\delta\dot{Q}_{moist}$ (Fig. 4A) exhibit large interannual variability of comparable magnitude but substantially smaller interdecadal variability. Both sets of time series demonstrate that, while both $\delta\dot{Q}_{total}$ and $\delta\dot{Q}_{moist}$ increase in response to projected climate change, $\delta\dot{Q}_{moist}$ increases more rapidly.

The evolution of W in response to anthropogenic forcing indicates a trend of -0.038 ± 0.08 Wm^{-2} [one-sided t test, 95% confidence interval (CI)] per 100 years for the 10-year running mean (Fig. 4B). Over the 21st century, this amounts to a small reduction in W ($\approx$–1%). In an $\alpha-p$ diagram, the W response at the end of the 21st century exhibits a reduction of -0.102 Wm^{-2} per 100 years below 300 hPa and an increase of 0.073 Wm^{-2} per 100 years above 300 hPa (fig.

S4); at 500 hPa, it is reduced by more than 5% per 100 years. This response is compatible with a general weakening of tropospheric motions accompanied with a strengthening of deep convective motions that have enough energy to reach the upper troposphere.

Because $\dot{Q}_{moist}$ is proportional to the material derivative dq_T/dt, we might expect its response to scale like the near-surface specific humidity and therefore be directly related to changes in global surface temperature through a surface Clausius-Clapeyron scaling. Indeed, the specific humidity on the model level nearest to the surface explains 94% of the variance of $\delta\dot{Q}_{moist}$ over

the entire 1981 to 2099 period (Fig. 4A). Both the near-surface specific humidity and $\delta\dot{Q}_{moist}$ increase by 5.4% per K global surface warming, which is slightly less than the 7% per K surface warming increase associated with a tropical Clausius-Clapeyron scaling (14). In fact, most of the increase in $\delta\dot{Q}_{moist}$ can be attributed to an increase in the moistening inefficiencies (fig. S5A). Moreover, this increase alone compensates for the increase in $\delta\dot{Q}_{total}$ (fig. S5B) and is therefore sufficient to constrain the atmospheric heat engine's work output.

Previous theoretical analyses of the entropy cycle (6, 31) suggest that $\dot{Q}_{total}$ should scale like
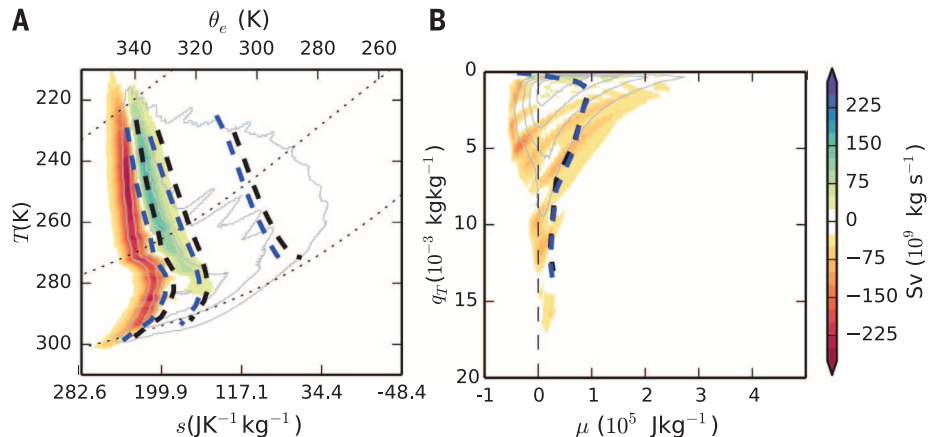
Fig. 3. Response of CESM thermodynamic diagrams between years 1981 to 2012 and years 2067 to 2098. (**A**) Response of Ψ^{total} (color shading). Gray contours indicate the 1981 to 2012 streamlines (Fig. 1A). Thick dashed lines show the change in zonal-mean vertical profiles for different latitude bands between the 1981 to 2012 (black) and the 2067 to 2098 (blue) periods. Dotted lines illustrate the 100% relative humidity curves at 1000 hPa, 500 hPa, and 200 hPa. (**B**) Response of Ψ^{moist} (color shading). Thick dashed lines (black and blue overlapping) as in (A) but only for the tropical (15°S to 15°N) profile. Gray contours indicate the 1981 to 2012 streamlines (Fig. 1C).

Fig. 4. Evolution of the different components of the first law over the 21st century. (**A**) Difference of $\dot{Q}_{total}$ (red, 1-year running mean in pale, 10-year running mean in solid) and $\dot{Q}_{moist}$ (blue, 1-year running mean in pale, 10-year running mean in solid) from the 1981 to 2012 control period. Theoretical scaling of $\dot{Q}_{moist}$ according to the increase in global specific humidity on the model level nearest to the surface in green (1-year running mean in pale, 10-year running mean in solid). (**B**) W (1-year running mean in gray, 10-year running mean in black), its trend (black line), and the 95% one-sided t test CI for the trend (gray shading).

$\dot{R}_{out}\, T_d(T_{out}^{-1} - T_{in}^{-1})$, where $\dot{R}_{out}$ is the outgoing long-wave radiation and T_{in}, T_{out}, and T_d are the mean temperature of atmospheric heat input, output, and dissipation, respectively. Observations of recent tropospheric warming [figures 2.26 and 2.27 in (32)] show that temperature trends are somewhat uniform in the vertical, which suggests that the difference $T_{out}^{-1} - T_{in}^{-1}$ might increase more slowly than either T_{in} or T_{out}. This slower increase may explain why $\delta\dot{Q}_{total}$ does not follow a surface Clausius-Clapeyron scaling and why one would expect moist processes to limit the work output in simulations with anthropogenic forcing. Simulations over a wider range of climates would help verify this hypothesis.

Our comparison of thermodynamic cycles in CESM and MERRA show many similarities; however, we find that CESM requires less power to maintain its hydrological cycle than the reanalysis, due to the smaller amplitude of its moistening inefficiencies. We suggest that this difference might be a consequence of the idealized nature of parameterized convection schemes, and it is likely that it might also influence the response of CESM to anthropogenic forcing. Typically, convection schemes artificially transport moisture along a moist adiabat without accounting for the work needed to lift this moisture, but in the real world, this work is necessary to sustain precipitation. Any increase in global precipitation therefore requires an increase in work output; otherwise, precipitation would have to become more efficient, for example, by reducing the frictional dissipation of falling hydrometeors (11, 12). This is one reason we should interpret the constraint in work output in CESM as a constraint on the large-scale motions and not on the unresolved subgrid-scale convective events.

Our work illustrates a major constraint on the large-scale global atmospheric engine: As the climate warms, the system may be unable to increase its total entropy production enough to offset the moistening inefficiencies associated with phase transitions. This suggests that in a future climate, the global atmospheric circulation might comprise highly energetic storms due to explosive latent heat release, but in such a case, the constraint on work output identified here will result in fewer numbers of such events. Earth's atmospheric circulation thus suffers from the "water in gas problem" observed in simulations of tropical convection (6), where its ability to produce work is constrained by the need to convert liquid water into water vapor and back again to tap its fuel.

REFERENCES AND NOTES

1. L. Barry, G. C. Craig, J. Thuburn, *Nature* **415**, 774–777 (2002).
2. M. H. P. Ambaum, *Thermal Physics of the Atmosphere* (Wiley, Hoboken, 2010), pp. 203–220.
3. O. R. Wulf, L. Davis Jr., *J. Meteorol.* **9**, 80–82 (1952).
4. J. P. Peixoto, A. H. Oort, M. De Almeida, A. Tomé, *J. Geophys. Res.* **96** (D6), 10981 (1991).
5. R. Goody, *Q. J. R. Meteorol. Soc.* **126**, 1953–1970 (2000).
6. O. Pauluis, I. M. Held, *J. Atmos. Sci.* **59**, 125–139 (2002).
7. D. M. Romps, *J. Atmos. Sci.* **65**, 3779–3799 (2008).
8. S. Pascale, J. Gregory, M. Ambaum, R. Tailleux, *Clim. Dyn.* **36**, 1189–1206 (2011).
9. O. Pauluis, I. M. Held, *J. Atmos. Sci.* **59**, 140–149 (2002).
10. O. Pauluis, *J. Atmos. Sci.* **68**, 91–102 (2011).
11. O. Pauluis, V. Balaji, I. M. Held, *J. Atmos. Sci.* **57**, 989–994 (2000).
12. O. Pauluis, J. Dias, *Science* **335**, 953–956 (2012).
13. S. Sherwood, R. Roca, T. Weckwerth, N. Andronova, *Rev. Geophys.* **48**, RG2001 (2010).
14. I. Held, B. Soden, *J. Clim.* **19**, 5686–5699 (2006).
15. R. Caballero, P. L. Langen, *Geophys. Res. Lett.* **32**, L02705 (2005).
16. P. O'Gorman, T. Schneider, *J. Clim.* **21**, 5797–5806 (2008).
17. T. Schneider, P. A. O'Gorman, X. Levine, *Rev. Geophys.* **48**, RG3001 (2010).
18. G. Vecchi, B. Soden, *J. Clim.* **20**, 4316–4340 (2007).
19. R. Feistel *et al.*, *Ocean Science* **6**, 91–141 (2010).
20. Materials and methods are available as supplementary material on *Science* Online.
21. K. Emanuel, *Atmospheric Convection* (Oxford Univ. Press, MIT, Oxford, 1994).
22. D. R. Johnson, *International Geophysics*, D. A. Randall, Ed. (Academic Press, Waltham, 2001), pp. 659–720.
23. P. R. Gent *et al.*, *J. Clim.* **24**, 4973–4991 (2011).
24. R. H. Moss *et al.*, *Nature* **463**, 747–756 (2010).
25. M. M. Rienecker *et al.*, *J. Clim.* **24**, 3624–3648 (2011).
26. J. D. Zika, M. H. England, W. P. Sijp, *J. Phys. Oceanogr.* **42**, 708–724 (2012).
27. K. Döös, J. Nilsson, J. Nycander, L. Brodeau, M. Ballarotta, *J. Phys. Oceanogr.* **42**, 1445–1460 (2012).
28. J. Kjellsson, K. Döös, F. B. Laliberté, J. D. Zika, *J. Atmos. Sci.* **71**, 916–928 (2014).
29. S. Groeskamp, J. D. Zika, T. J. McDougall, B. M. Sloyan, F. Laliberté, *J. Phys. Oceanogr.* **44**, 1735–1750 (2014).
30. O. M. Pauluis, A. A. Mrowiec, *J. Atmos. Sci.* **70**, 3673–3688 (2013).
31. V. Lucarini, K. Fraedrich, F. Ragone, *J. Atmos. Sci.* **68**, 2438–2458 (2011).
32. D. L. Hartmann *et al.*, Climate Change 2013: The Physical Science Basis. Contribution of Working Group I to the Fifth Assessment Report of the Intergovernmental Panel on Climate Change, T. F. Stocker *et al.*, Eds. (Cambridge Univ. Press, Cambridge and New York, NY, USA, 2013).

OPTICAL IMAGING

Expansion microscopy

Fei Chen,[1]* **Paul W. Tillberg,**[2]* **Edward S. Boyden**[1,3,4,5,6]†

In optical microscopy, fine structural details are resolved by using refraction to magnify images of a specimen. We discovered that by synthesizing a swellable polymer network within a specimen, it can be physically expanded, resulting in physical magnification. By covalently anchoring specific labels located within the specimen directly to the polymer network, labels spaced closer than the optical diffraction limit can be isotropically separated and optically resolved, a process we call expansion microscopy (ExM). Thus, this process can be used to perform scalable superresolution microscopy with diffraction-limited microscopes. We demonstrate ExM with apparent ~70-nanometer lateral resolution in both cultured cells and brain tissue, performing three-color superresolution imaging of ~10^7 cubic micrometers of the mouse hippocampus with a conventional confocal microscope.

Microscopy has facilitated the discovery of many biological insights by optically magnifying images of structures in fixed cells and tissues. We here report that physical magnification of the specimen itself is also possible.

We first set out to see whether a well-known property of polyelectrolyte gels—namely, that dialyzing them in water causes expansion of the polymer network into extended conformations (Fig. 1A) (1)—could be performed in a biological sample. We infused into chemically

fixed and permeabilized brain tissue (Fig. 1B) sodium acrylate, a monomer used to produce superabsorbent materials (2, 3), along with the comonomer acrylamide and the cross-linker N-N′-methylenebisacrylamide. After triggering free radical polymerization with ammonium persulfate (APS) initiator and tetramethylethylenediamine (TEMED) accelerator, we treated the tissue-polymer composite with protease to homogenize its mechanical characteristics. After proteolysis, dialysis in water resulted in a 4.5-fold linear expansion, without distortion at the level of gross anatomy (Fig. 1C). Digestion was uniform throughout the slice (fig. S1). Expanded specimens were transparent (fig. S2) because they consist largely of water. Thus, polyelectrolyte gel expansion is possible when the polymer is embedded throughout a biological sample.

We developed a fluorescent labeling strategy compatible with the proteolytic treatment and subsequent tissue expansion described above,

[1]Department of Biological Engineering, Massachussetts Institute of Technology (MIT), Cambridge, MA, USA. [2]Department of Electrical Engineering and Computer Science, MIT, Cambridge, MA, USA. [3]Media Lab, MIT, Cambridge, MA, USA. [4]McGovern Institute, MIT, Cambridge, MA, USA. [5]Department of Brain and Cognitive Sciences, MIT, Cambridge, MA, USA. [6]Center for Neurobiological Engineering, MIT, Cambridge, MA, USA.
*These authors contributed equally to this work. †Corresponding author. E-mail: esb@media.mit.edu

$\dot{R}_{out}\, T_d(T_{out}^{-1} - T_{in}^{-1})$, where $\dot{R}_{out}$ is the outgoing long-wave radiation and T_{in}, T_{out}, and T_d are the mean temperature of atmospheric heat input, output, and dissipation, respectively. Observations of recent tropospheric warming [figures 2.26 and 2.27 in (32)] show that temperature trends are somewhat uniform in the vertical, which suggests that the difference $T_{out}^{-1} - T_{in}^{-1}$ might increase more slowly than either T_{in} or T_{out}. This slower increase may explain why $\delta \dot{Q}_{total}$ does not follow a surface Clausius-Clapeyron scaling and why one would expect moist processes to limit the work output in simulations with anthropogenic forcing. Simulations over a wider range of climates would help verify this hypothesis.

Our comparison of thermodynamic cycles in CESM and MERRA show many similarities; however, we find that CESM requires less power to maintain its hydrological cycle than the reanalysis, due to the smaller amplitude of its moistening inefficiencies. We suggest that this difference might be a consequence of the idealized nature of parameterized convection schemes, and it is likely that it might also influence the response of CESM to anthropogenic forcing. Typically, convection schemes artificially transport moisture along a moist adiabat without accounting for the work needed to lift this moisture, but in the real world, this work is necessary to sustain precipitation. Any increase in global precipitation therefore requires an increase in work output; otherwise, precipitation would have to become more efficient, for example, by reducing the frictional dissipation of falling hydrometeors (11, 12). This is one reason we should interpret the constraint in work output in CESM as a constraint on the large-scale motions and not on the unresolved subgrid-scale convective events.

Our work illustrates a major constraint on the large-scale global atmospheric engine: As the climate warms, the system may be unable to increase its total entropy production enough to offset the moistening inefficiencies associated with phase transitions. This suggests that in a future climate, the global atmospheric circulation might comprise highly energetic storms due to explosive latent heat release, but in such a case, the constraint on work output identified here will result in fewer numbers of such events. Earth's atmospheric circulation thus suffers from the "water in gas problem" observed in simulations of tropical convection (6), where its ability to produce work is constrained by the need to convert liquid water into water vapor and back again to tap its fuel.

REFERENCES AND NOTES

1. L. Barry, G. C. Craig, J. Thuburn, *Nature* **415**, 774–777 (2002).
2. M. H. P. Ambaum, *Thermal Physics of the Atmosphere* (Wiley, Hoboken, 2010), pp. 203–220.
3. O. R. Wulf, L. Davis Jr., *J. Meteorol.* **9**, 80–82 (1952).
4. J. P. Peixoto, A. H. Oort, M. De Almeida, A. Tomé, *J. Geophys. Res.* **96** (D6), 10981 (1991).
5. R. Goody, *Q. J. R. Meteorol. Soc.* **126**, 1953–1970 (2000).
6. O. Pauluis, I. M. Held, *J. Atmos. Sci.* **59**, 125–139 (2002).
7. D. M. Romps, *J. Atmos. Sci.* **65**, 3779–3799 (2008).
8. S. Pascale, J. Gregory, M. Ambaum, R. Tailleux, *Clim. Dyn.* **36**, 1189–1206 (2011).
9. O. Pauluis, I. M. Held, *J. Atmos. Sci.* **59**, 140–149 (2002).
10. O. Pauluis, *J. Atmos. Sci.* **68**, 91–102 (2011).
11. O. Pauluis, V. Balaji, I. M. Held, *J. Atmos. Sci.* **57**, 989–994 (2000).
12. O. Pauluis, J. Dias, *Science* **335**, 953–956 (2012).
13. S. Sherwood, R. Roca, T. Weckwerth, N. Andronova, *Rev. Geophys.* **48**, RG2001 (2010).
14. I. Held, B. Soden, *J. Clim.* **19**, 5686–5699 (2006).
15. R. Caballero, P. L. Langen, *Geophys. Res. Lett.* **32**, L02705 (2005).
16. P. O'Gorman, T. Schneider, *J. Clim.* **21**, 5797–5806 (2008).
17. T. Schneider, P. A. O'Gorman, X. Levine, *Rev. Geophys.* **48**, RG3001 (2010).
18. G. Vecchi, B. Soden, *J. Clim.* **20**, 4316–4340 (2007).
19. R. Feistel *et al.*, *Ocean Science* **6**, 91–141 (2010).
20. Materials and methods are available as supplementary material on Science Online.
21. K. Emanuel, *Atmospheric Convection* (Oxford Univ. Press, MIT, Oxford, 1994).
22. D. R. Johnson, *International Geophysics*, D. A. Randall, Ed. (Academic Press, Waltham, 2001), pp. 659–720.
23. P. R. Gent *et al.*, *J. Clim.* **24**, 4973–4991 (2011).
24. R. H. Moss *et al.*, *Nature* **463**, 747–756 (2010).
25. M. M. Rienecker *et al.*, *J. Clim.* **24**, 3624–3648 (2011).
26. J. D. Zika, M. H. England, W. P. Sijp, *J. Phys. Oceanogr.* **42**, 708–724 (2012).
27. K. Döös, J. Nilsson, J. Nycander, L. Brodeau, M. Ballarotta, *J. Phys. Oceanogr.* **42**, 1445–1460 (2012).
28. J. Kjellsson, K. Döös, F. B. Laliberté, J. D. Zika, *J. Atmos. Sci.* **71**, 916–928 (2014).
29. S. Groeskamp, J. D. Zika, T. J. McDougall, B. M. Sloyan, F. Laliberté, *J. Phys. Oceanogr.* **44**, 1735–1750 (2014).
30. O. M. Pauluis, A. A. Mrowiec, *J. Atmos. Sci.* **70**, 3673–3688 (2013).
31. V. Lucarini, K. Fraedrich, F. Ragone, *J. Atmos. Sci.* **68**, 2438–2458 (2011).
32. D. L. Hartmann *et al.*, Climate Change 2013: The Physical Science Basis. Contribution of Working Group I to the Fifth Assessment Report of the Intergovernmental Panel on Climate Change, T. F. Stocker *et al.*, Eds. (Cambridge Univ. Press, Cambridge and New York, NY, USA, 2013).

OPTICAL IMAGING

Expansion microscopy

Fei Chen,[1]* Paul W. Tillberg,[2]* Edward S. Boyden[1,3,4,5,6]†

In optical microscopy, fine structural details are resolved by using refraction to magnify images of a specimen. We discovered that by synthesizing a swellable polymer network within a specimen, it can be physically expanded, resulting in physical magnification. By covalently anchoring specific labels located within the specimen directly to the polymer network, labels spaced closer than the optical diffraction limit can be isotropically separated and optically resolved, a process we call expansion microscopy (ExM). Thus, this process can be used to perform scalable superresolution microscopy with diffraction-limited microscopes. We demonstrate ExM with apparent ~70-nanometer lateral resolution in both cultured cells and brain tissue, performing three-color superresolution imaging of ~10^7 cubic micrometers of the mouse hippocampus with a conventional confocal microscope.

Microscopy has facilitated the discovery of many biological insights by optically magnifying images of structures in fixed cells and tissues. We here report that physical magnification of the specimen itself is also possible.

We first set out to see whether a well-known property of polyelectrolyte gels—namely, that dialyzing them in water causes expansion of the polymer network into extended conformations (Fig. 1A) (1)—could be performed in a biological sample. We infused into chemically

[1]Department of Biological Engineering, Massachussetts Institute of Technology (MIT), Cambridge, MA, USA. [2]Department of Electrical Engineering and Computer Science, MIT, Cambridge, MA, USA. [3]Media Lab, MIT, Cambridge, MA, USA. [4]McGovern Institute, MIT, Cambridge, MA, USA. [5]Department of Brain and Cognitive Sciences, MIT, Cambridge, MA, USA. [6]Center for Neurobiological Engineering, MIT, Cambridge, MA, USA.
*These authors contributed equally to this work. †Corresponding author. E-mail: esb@media.mit.edu

fixed and permeabilized brain tissue (Fig. 1B) sodium acrylate, a monomer used to produce superabsorbent materials (2, 3), along with the comonomer acrylamide and the cross-linker N-N′-methylenebisacrylamide. After triggering free radical polymerization with ammonium persulfate (APS) initiator and tetramethylethylenediamine (TEMED) accelerator, we treated the tissue-polymer composite with protease to homogenize its mechanical characteristics. After proteolysis, dialysis in water resulted in a 4.5-fold linear expansion, without distortion at the level of gross anatomy (Fig. 1C). Digestion was uniform throughout the slice (fig. S1). Expanded specimens were transparent (fig. S2) because they consist largely of water. Thus, polyelectrolyte gel expansion is possible when the polymer is embedded throughout a biological sample.

We developed a fluorescent labeling strategy compatible with the proteolytic treatment and subsequent tissue expansion described above,

to see whether fluorescence nanoscopy would be possible. We designed a custom fluorescent label (Fig. 1D) that can be incorporated directly into the polymer network and thus survives the proteolytic digestion of endogenous biomolecules. This label is trifunctional, comprising a methacryloyl group capable of participating in free radical polymerization, a chemical fluorophore for visualization, and an oligonucleotide that can hybridize to a complementary sequence attached to an affinity tag (such as a secondary antibody) (Fig. 1, E and F). Thus, the fluorescent tag is targeted to a biomolecule of interest yet remains anchored covalently with high yield (table S1) to the polymer network. The entire process of labeling, gelation, digestion, expansion, and imaging we call expansion microscopy (ExM).

We performed fluorescence imaging using ExM, examining microtubules in fixed human embryonic kidney (HEK) 293 cells labeled with the trifunctional label and imaged with confocal laser scanning microscopy pre- versus post-ExM processing. The post-ExM image (Fig. 2B) was registered to the pre-ExM image (Fig. 2A) via a similarity transformation, resulting in visually indistinguishable images. To quantify the isotropy of ExM, we calculated the deformation vector field between the images via a nonrigid registration process (fig. S3). From this vector field, we quantified the root-mean-square (RMS) error of feature measurements post-ExM. The

errors in length were small (<1% of distance, for errors larger than the imaging system point spread function size; $n = 4$ samples) (Fig. 2C). Throughout the paper, all distances measured in the post-expansion specimen are reported divided by the expansion factor (supplementary materials, materials and methods).

We next compared pre-ExM conventional superresolution images to post-ExM confocal images. We labeled features traditionally used to characterize the performance of superresolution microscopes, including microtubules (4, 5) and clathrin coated pits (6), and imaged them with a superresolution structured illumination microscope (SR-SIM) pre-ExM, and a spinning disk confocal post-ExM. Qualitatively (Fig. 2, D and E), the images were similar, and quantitatively (Fig. 2I), measurement errors were again on the order of 1% and well within the point spread function size of the SR-SIM microscope ($n = 4$ samples). Microtubule networks were more sharply resolved in ExM (Fig. 2G) than with SR-SIM (Fig. 2F). ExM resolved individual microtubules that could not be distinguished with SR-SIM (Fig. 2H). Microtubules imaged with ExM presented a full-width at half-maximum (FWHM) (Fig. 2J) of 83.8 ± 5.68 nm (mean ± SD, $n = 24$ microtubules from 3 samples). This FWHM reflects the effective resolution of ExM convolved by the width of the labeled microtubule. To estimate the effective resolution of ExM, we deconvolved [as in (7)] our observed microtubule

FWHM by the known immunostained microtubule width [55 nm (6)], conservatively ignoring the width of the trifunctional label, and obtained an effective resolution for ExM of ~60 nm. This conservative estimate is comparable with the diffraction-limited confocal resolution [~250-nm lateral resolution (8)] divided by the expansion factor (~4.5).

Clathrin-coated pits were also well resolved (Fig. 2, K and L). ExM resolved the central nulls of the pits better than SR-SIM (Fig. 2, M and N). Clathrin-coated pit radii measured via ExM and SR-SIM were highly correlated, with a slope of 1.001 (total least squares regression, confidence interval 0.013 with $P < 0.05$, $n = 50$ pits from three samples) (Fig. 2O). Forty-nine of the 50 points lay within a half-pixel distance of the unity slope line, suggesting that variation in the ExM versus SR-SIM comparison was within the digitization error of the measurement.

We next applied ExM to fixed brain tissue. Slices of brain from Thy1-YFP-H mice expressing cytosolic yellow fluorescent protein (YFP) under the Thy1 promoter in a subset of neurons (9) were stained with a trifunctional label bearing Alexa 488, using primary antibodies to green fluorescent protein (GFP) (which also bind YFP). Slices expanded fourfold, similar to the expansion factor in cultured cells. We compared pre- versus post-ExM images taken on an epifluorescence microscope. As with cultured cells, the post-ExM image (Fig. 3B) was registered to the pre-ExM

Fig. 1. Expansion microscopy (ExM) concept. (**A**) Schematic of (i) collapsed polyelectrolyte network, showing crosslinker (dot) and polymer chain (line), and (ii) expanded network after H_2O dialysis. (**B**) Photograph of fixed mouse brain slice. (**C**) Photograph, post-ExM, of the sample (B) under side illumination. (**D**) Schematic of label that can be anchored to the gel at site of a biomolecule. (**E**) Schematic of microtubules (green) and polymer network (orange). (**F**) The label of (D), hybridized to the oligo-bearing secondary antibody top (top gray shape) bound via the primary (bottom gray shape) to microtubules (purple), is incorporated into the gel (orange lines) via the methacryloyl group (orange dot) and remains after proteolysis (dotted lines). Scale bars, (B) and (C) 5 mm. Schematics are not to scale.
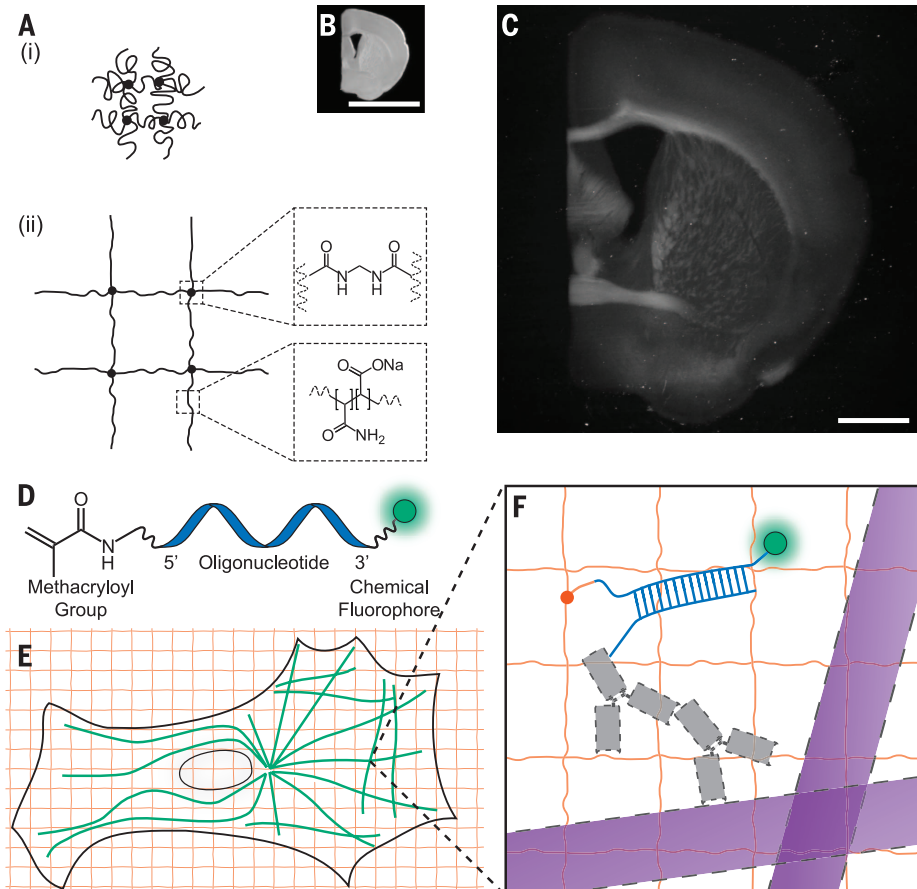
image (Fig. 3A) via a similarity transformation. The registered images closely matched, although some features moved in or out of the depth of field because of the axial expansion post-ExM. Quantitatively, post-ExM measurement errors (Fig. 3C, n = 4 cortical slices) were 2 to 4%.

We synthesized trifunctional labels with different colors and oligonucleotides (supplementary materials, materials and methods) to enable multicolor ExM. We obtained pre- (Fig. 3D) ver-

sus post-ExM (Fig. 3E) images of Thy1-YFP-H mouse cortex with ExM labels directed against YFP (Fig. 3E, green) and the pre- and postsynaptic scaffolding proteins Bassoon (Fig. 3E, blue) and Homer1 (Fig. 3E, red). In the pre-ExM image, Bassoon and Homer1 staining form overlapping spots at each synapse (Fig. 3F), whereas the post-ExM image (Fig. 3G) shows clearly distinguishable pre- and postsynaptic labeling. We quantified the distance between the Bassoon and

Homer1 scaffolds, as measured with ExM. We fit the distributions of Bassoon and Homer1 staining intensity, taken along the line perpendicular to the synaptic cleft (Fig. 3H, boxed region), to Gaussians (Fig. 3I). The Bassoon-Homer1 separation was 169 ± 32.6 nm (Fig. 3J, n = 277 synapses from four cortical slices), similar to a previous study using stochastic optical reconstruction microscopy (STORM) in the ventral cortex and olfactory bulb, which obtained ~150 nm
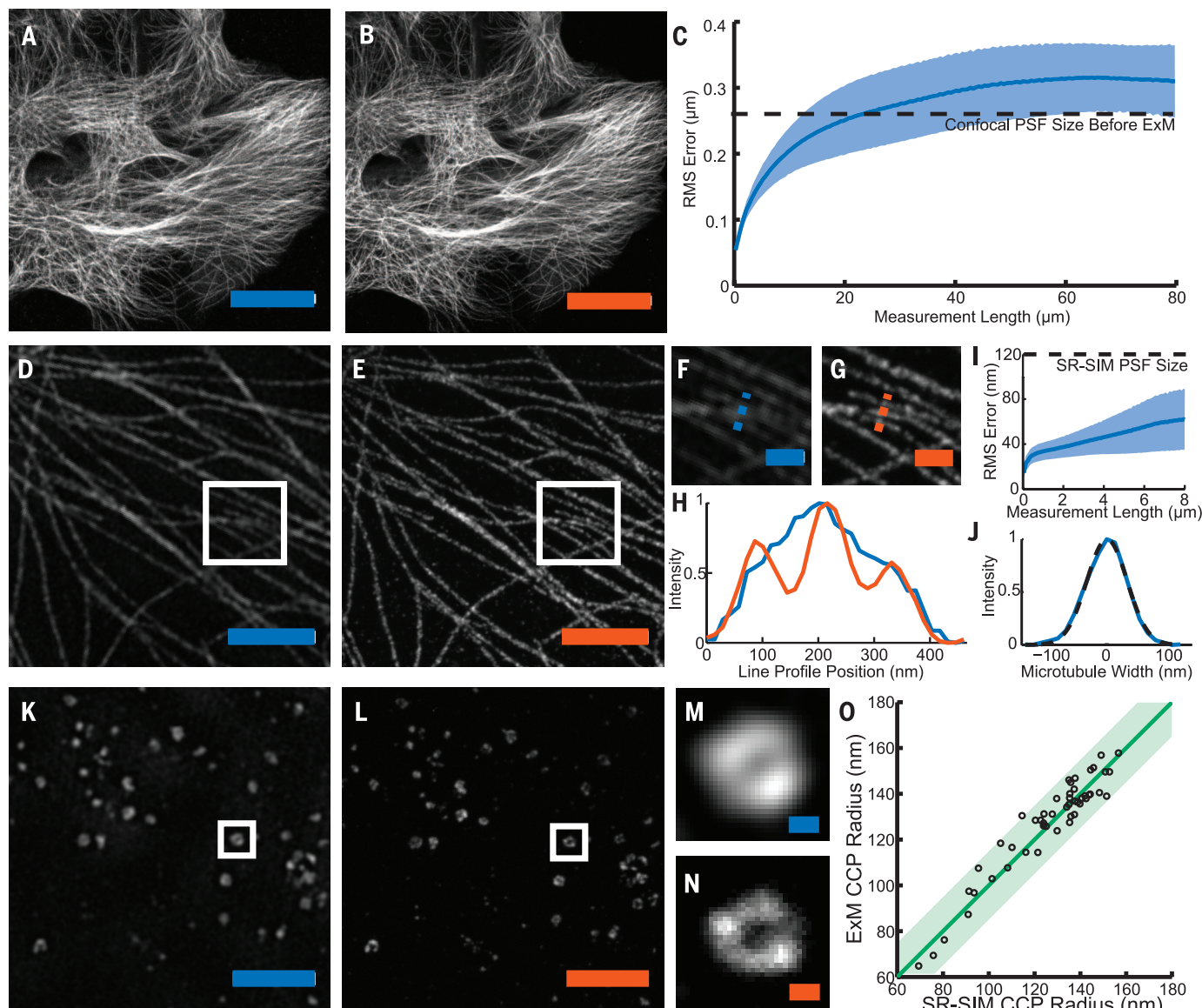
Fig. 2. Expansion microscopy physically magnifies, with nanoscale isotropy. We compared images acquired via conventional microscopy (blue scale bars) versus images acquired post-expansion (orange scale bars). (**A**) Confocal image of microtubules in HEK293 cells. (**B**) Post-expansion confocal image of sample (A). (**C**) RMS length measurement error of pre- versus post-ExM confocal images of cultured cells (blue line, mean; shaded area, standard deviation; n = 4 samples). (**D**) SR-SIM image of microtubules. (**E**) Post-expansion confocal image of the sample of (D). (**F** and **G**) Magnified views of boxed regions of (D) and (E), respectively. (**H**) Profiles of microtubule intensity taken along the blue and orange dotted lines in (F) and (G). (**I**) RMS length measurement error of ExM versus SR-SIM images (blue line,

mean; shaded area, standard deviation; n = 4 samples). (**J**) Transverse profile of a representative microtubule (blue line), with Gaussian fit (black dotted line). (**K**) SR-SIM image of clathrin-coated pits (CCPs) in HEK293 cells. (**L**) Post-expansion confocal image of the sample of (K). (**M** and **N**) Magnified views of a single CCP in the boxed regions of (K) and (L), respectively. (**O**) Scatterplot of radii of CCPs measured via ExM versus SR-SIM (n = 50 CCPs from 3 samples). Green line, $y = x$ line; shaded green region, half-pixel width of digitization error about the $y = x$ line. Scale bars for pre- versus post-ExM images, (A) 20 μm; (B) 20 μm (physical size post-expansion, 81.6 μm); (D) 2 μm; (E) 2 μm (9.1 μm); (F) 500 nm; (G) 500 nm (2.27 μm); (K) 2 μm; (L) 2 μm (8.82 μm); (M) 100 nm; (N) 100 nm (441 nm).

separation (*10*). We also imaged other antibody targets of interest in biology (fig. S4).

To explore whether expanded samples, scanned on fast diffraction-limited microscopes, could support scalable superresolution imaging, we imaged a volume of the adult Thy1-YFP-H mouse brain spanning 500 by 180 by 100 μm (tissue slice thickness), with three labels (antibody to

GFP, green; antibody to Homer1, red; antibody to Bassoon, blue) (Fig. 4A). The diffraction limit of our confocal spinning disk microscope (with 40×, 1.15 NA, water immersion objective), divided by the expansion factor, yields an estimated effective resolution of ~70 nm laterally and ~200 nm axially. Shown in Fig. 4A is a three-dimensional (3D) rendered image of the data set (an ani-

mated rendering is provided in movie S1). Zooming into the raw data set, nanoscale features emerge (Fig. 4, B to D). We performed a volume rendering of the YFP-expressing neurons in a subset of CA1 stratum lacunosum moleculare (slm), revealing spine morphology (Fig. 4B and movie S2). Focusing on a dendrite in CA1 slm, we observed the postsynaptic protein Homer1
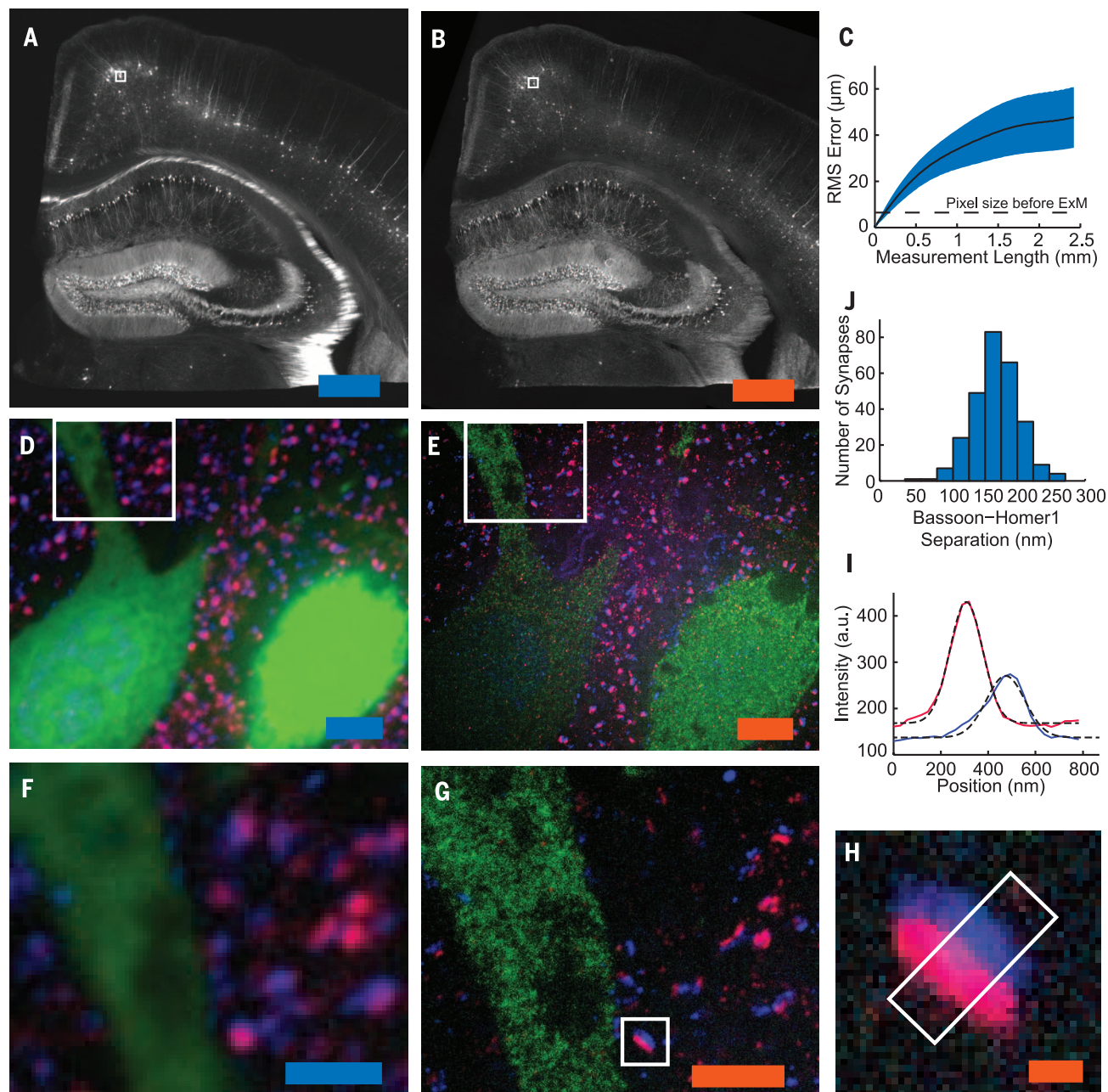
Fig. 3. ExM imaging of mammalian brain tissue. (**A**) Widefield fluorescence (white) image of Thy1-YFP mouse brain slice. (**B**) Post-expansion widefield image of sample (A). (**C**) RMS length measurement error for pre- versus post-ExM images of brain slices (blue line, mean; shaded area, SD; *n* = 4 samples). (**D** and **E**) Confocal fluorescence images of boxed regions in (A) and (B), respectively, stained with presynaptic (anti-Bassoon, blue) and postsynaptic (anti-Homer1, red) markers, in addition to antibody to GFP (green), pre- (D) versus post- (E) expansion. (**F** and **G**) Details of boxed regions in (D) and (E), respectively. (**H**) Single representative synapse highlighted in (G). (**I**) Staining intensity for Bassoon (blue) and Homer1 (red) of the sample of (H) along white box long axis. Dotted black lines, Gaussian fits. a.u., arbitrary units. (**J**) Bassoon-Homer1 separation (*n* = 277 synapses from four cortical slices). Scale bars for pre- versus post-ExM images, (A) 500 μm; (B) 500 μm (physical size post-expansion 2.01 mm); (D) 5 μm; (E) 5 μm (20.1 μm); (F) 2.5 μm; (G) 2.5 μm (10.0 μm); and (H) 250 nm (1.00 μm).

to be well localized to dendritic spine heads, with the presynaptic molecule Bassoon in apposition (Fig. 4C and movie S3). Examination of a mossy fiber bouton in the hilus of the dentate gyrus reveals invaginations into the bouton by spiny excrescences of the opposing dendrite, as observed previously via electron microscopy (Fig. 4D) (11). Thus, ExM enables multiscale imaging and visualization of nanoscale features, across length scales relevant to understanding neural circuits.

We report the discovery of a new modality of magnification, namely that fixed cells and tissues, appropriately labeled and processed, can be physically magnified, with isotropic nanoscale resolution (effective ~60-nm lateral resolution). Although acrylate esters have been used for

antigen-preserving embedding for electron microscopy (12, 13), ExM represents the first use of an embedded polyelectrolyte gel, used here to expand the specimen. Superresolution imaging methods are slower than their diffraction-limited counterparts because they must resolve more voxels per unit volume. ExM achieves this by expanding the voxels physically. ExM achieves the same voxel throughputs as a diffraction-limited microscope, but at the voxel sizes of a superresolution microscope. Ongoing technology trends for faster diffraction-limited microscopy (14) will continue to boost ExM speed.

The physical magnification of ExM enables superresolution imaging with several fundamental new properties. The axial effective resolution is improved by the same factor as the

lateral effective resolution. ExM can achieve superresolution with standard fluorophores, and on a diffraction-limited microscope. Superresolution imaging is often performed within ~10 μm of the sample surface because of low signal-to-noise, scattering, and refractive index mismatch. We were able to perform three-color superresolution imaging of a large volume of brain tissue over an axial extent of 100 μm with a spinning disk confocal microscope. Because the ExM-processed sample is almost entirely water, eliminating scattering, ExM may empower fast methods such as light-sheet microscopy (15) to become superresolution methods. ExM potentially enables labels to be situated within a well-defined, in vitro–like environment, facilitating in situ analysis (16). Because the
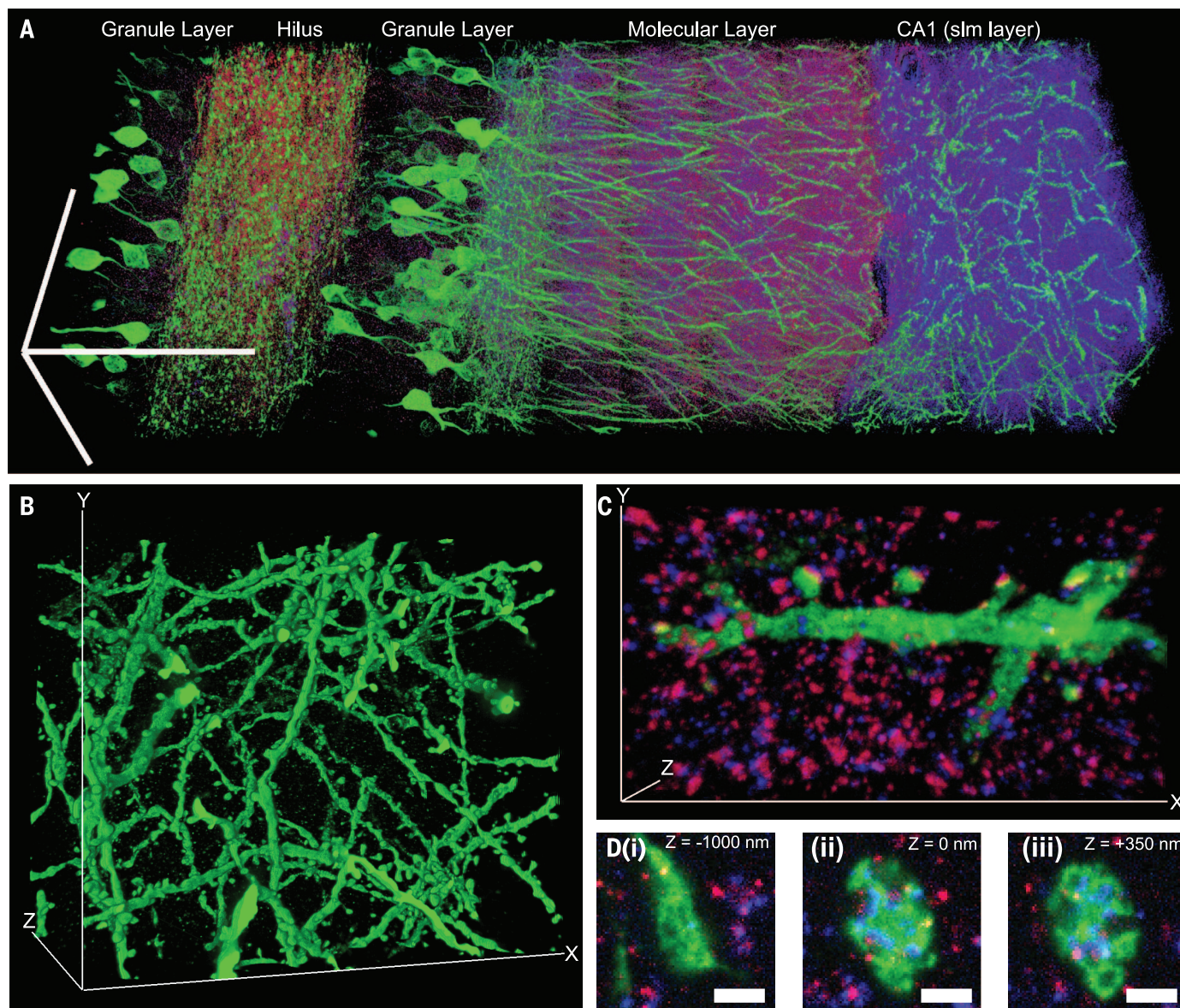
Fig. 4. Scalable 3D superresolution microscopy of mouse brain tissue. (**A**) Volume rendering of a portion of hippocampus showing neurons (expressing YFP, shown in green) and synapses [marked with anti-Bassoon (blue) and antibody to Homer1 (red)]. (**B**) Volume rendering of dendrites in CA1 slm. (**C**) Volume rendering of dendritic branch in CA1 slm. (**D**) Mossy fiber bouton in hilus of the dentate gyrus. (i) to (iii), selected z-slices. Scale bars, (A) 100 μm in each dimension; (B) 52.7 μm (x); 42.5 μm (y); and 35.2 μm (z); (C) 13.5 μm (x); 7.3 μm (y); and 2.8 μm (z); (D), (i) to (iii) 1 μm.

sample is physically larger, any mechanical errors in post-expansion sectioning, or stage drift, are divided by the expansion factor.

The performance of ExM suggests that despite statistical fluctuations in polymer chain length at the molecular scale, at the nanoscale distances here examined these fluctuations average out, yielding isotropy. Estimates of mesh size for comparable gels suggest that the distance between nearest-neighbor polymer chains are in the ~1 to 2 nm range (*17*, *18*). By tuning the material properties of the ExM polymer, such as the density of cross-links, yet higher effective resolutions may be possible.

REFERENCES AND NOTES

1. T. Tanaka et al., *Phys. Rev. Lett.* **45**, 1636–1639 (1980).
2. I. Ohmine, *J. Chem. Phys.* **77**, 5725 (1982).
3. F. L. Buchholz, *Superabsorbent Polymers* **573**, 27–38 (1994).
4. B. Huang, S. A. Jones, B. Brandenburg, X. Zhuang, *Nat. Methods* **5**, 1047–1052 (2008).
5. E. H. Rego et al., *Proc. Natl. Acad. Sci. U.S.A.* **109**, E135–E143 (2012).
6. M. Bates, B. Huang, G. T. Dempsey, X. Zhuang, *Science* **317**, 1749–1753 (2007).
7. N. Olivier, D. Keller, P. Gönczy, S. Manley, *PLOS One* **8**, (2013).
8. R. W. Cole, T. Jinadasa, C. M. Brown, *Nat. Protoc.* **6**, 1929–1941 (2011).
9. G. Feng et al., *Neuron* **28**, 41–51 (2000).
10. A. Dani, B. Huang, J. Bergan, C. Dulac, X. Zhuang, *Neuron* **68**, 843–856 (2010).
11. A. Rollenhagen, J. H. R. Lübke, *Front. Synaptic Neurosci.* **2**, 2 (2010).
12. G. R. Newman, B. Jasani, E. D. Williams, *Histochem. J.* **15**, 543–555 (1983).
13. K. D. Micheva, S. J. Smith, *Neuron* **55**, 25–36 (2007).
14. B.-C. Chen et al., *Science* **346**, 1257998 (2014).
15. J. Huisken, J. Swoger, F. Del Bene, J. Wittbrodt, E. H. K. Stelzer, *Science* **305**, 1007–1009 (2004).
16. J. H. Lee et al., *Science* **343**, 1360–1363 (2014).
17. A. M. Hecht, R. Duplessix, E. Geissler, *Macromolecules* **18**, 2167–2173 (1985).
18. D. Calvet, J. Y. Wong, S. Giasson, *Macromolecules* **37**, 7762–7771 (2004).

MITOCHONDRIAL BIOLOGY

Replication-transcription switch in human mitochondria

Karen Agaronyan, Yaroslav I. Morozov, Michael Anikin, Dmitry Temiakov*

Coordinated replication and expression of the mitochondrial genome is critical for metabolically active cells during various stages of development. However, it is not known whether replication and transcription can occur simultaneously without interfering with each other and whether mitochondrial DNA copy number can be regulated by the transcription machinery. We found that interaction of human transcription elongation factor TEFM with mitochondrial RNA polymerase and nascent transcript prevents the generation of replication primers and increases transcription processivity and thereby serves as a molecular switch between replication and transcription, which appear to be mutually exclusive processes in mitochondria. TEFM may allow mitochondria to increase transcription rates and, as a consequence, respiration and adenosine triphosphate production without the need to replicate mitochondrial DNA, as has been observed during spermatogenesis and the early stages of embryogenesis.

The maternally inherited circular mitochondrial DNA (mtDNA) encodes subunits of complexes of the oxidative phosphorylation chain, as well as transfer RNAs (tRNAs) and ribosomal RNAs (*1*, *2*). Transcription of human mtDNA is directed by two promoters, the LSP (light-strand promoter) and the HSP (heavy-strand promoter) located in opposing mtDNA strands, which results in two almost-genome-sized polycistronic transcripts that undergo extensive processing before polyadenylation and translation (*3*, *4*). Note that transcription terminates prematurely about 120 base pairs (bp) downstream of LSP at a vertebrate-conserved G-rich region, called conserved sequence block II (CSBII), as a result of formation of a hybrid G-quadruplex between nascent RNA and the nontemplate strand of DNA (*5*–*7*). This termination event occurs near the origin of replication of the heavy strand (oriH) (*8*) and generates a replication primer. According to the asymmetric model (*9*), replication then proceeds through about two-thirds of the mtDNA, until the oriL sequence in the opposing strand becomes single stranded and forms a hairpin structure. The oriL hairpin is then recognized by mitochondrial RNA polymerase (mtRNAP), which primes replication of the light strand (*10*). Because replication of mtDNA coincides with transcription in time and space, collisions between transcription and replication machineries are inevitable and, similarly to bacterial and eukaryotic systems, likely have detrimental effects on mtDNA gene expression (*11*).

We analyzed the effects of a mitochondrial transcription elongation factor, TEFM, recently described by Minczuk and colleagues (*12*), on transcription of mtDNA. This protein was pulled down from mitochondrial lysates via mtRNAP and was found to stimulate nonspecific transcription on promoterless DNA; however, its effect on promoter-driven transcription had not been

Department of Cell Biology, School of Osteopathic Medicine, Rowan University, 2 Medical Center Drive, Stratford, NJ 08084, USA.
*Corresponding author. E-mail:temiakdm@rowan.edu

determined (*12*). We found that in the presence of TEFM, mtRNAP efficiently transcribes through CSBII (Fig. 1, A and B). Thus, TEFM acts as a factor that prevents termination at CSBII and synthesis of a primer for mtDNA polymerase. We identified the exact location of the termination point in CSBII (fig. S1). MtRNAP terminates at the end of a U6 sequence (positions 287 to 283 in mtDNA), 16 to 18 nucleotides (nt) downstream of the G-quadruplex (Fig. 1A). At this point, the 9-bp RNA-DNA hybrid in the elongation complex (EC) is extremely weak, as it is composed of only A-U and T-A pairs. This is reminiscent of intrinsic termination signals in prokaryotes—where the formation of an RNA hairpin is thought to disrupt the upstream region of the RNA-DNA hybrid—and is followed by the run of six to eight uridine 5′-monophosphate residues that further destabilizes the complex (*5*, *13*).

Human mtDNA is highly polymorphic in the CSBII region; coincidently, the reference mitochondrial genome (Cambridge) contains a rare polymorphism in the G-quadruplex—namely, G5AG7—whereas the majority of mtDNAs from various haplogroups have two additional G residues (G6AG8) (*14*). We found that the termination efficiency of mtRNAP was substantially lower at G5AG7-CSBII (Fig. 1C), which suggested an effect of G run length on quadruplex formation and underscored the importance of further studies of various polymorphisms in this region.

In considering a putative mechanism of TEFM antitermination activity, we investigated whether it can interact with the nascent transcript and, thus, interfere with the formation of the quadruplex structure. We assembled ECs on a nucleic acid scaffold containing a photoreactive analog of uridine, 4-thio-uridine, 13 nt downstream from the 3′ end of RNA, and walked mtRNAP along the template by incorporation of appropriate substrate nucleoside triphosphates (NTPs) (Fig. 2A). We observed efficient cross-linking between TEFM and RNA when the photoreactive base was 15 to 16 bp away from the 3′ end of RNA. Additionally, using a template DNA containing the LSP promoter and

sample is physically larger, any mechanical errors in post-expansion sectioning, or stage drift, are divided by the expansion factor.

The performance of ExM suggests that despite statistical fluctuations in polymer chain length at the molecular scale, at the nanoscale distances here examined these fluctuations average out, yielding isotropy. Estimates of mesh size for comparable gels suggest that the distance between nearest-neighbor polymer chains are in the ~1 to 2 nm range (17, 18). By tuning the material properties of the ExM polymer, such as the density of cross-links, yet higher effective resolutions may be possible.

REFERENCES AND NOTES

1. T. Tanaka et al., Phys. Rev. Lett. 45, 1636–1639 (1980).
2. I. Ohmine, J. Chem. Phys. 77, 5725 (1982).
3. F. L. Buchholz, Superabsorbent Polymers 573, 27–38 (1994).
4. B. Huang, S. A. Jones, B. Brandenburg, X. Zhuang, Nat. Methods 5, 1047–1052 (2008).
5. E. H. Rego et al., Proc. Natl. Acad. Sci. U.S.A. 109, E135–E143 (2012).
6. M. Bates, B. Huang, G. T. Dempsey, X. Zhuang, Science 317, 1749–1753 (2007).
7. N. Olivier, D. Keller, P. Gönczy, S. Manley, PLOS One 8, (2013).
8. R. W. Cole, T. Jinadasa, C. M. Brown, Nat. Protoc. 6, 1929–1941 (2011).
9. G. Feng et al., Neuron 28, 41–51 (2000).
10. A. Dani, B. Huang, J. Bergan, C. Dulac, X. Zhuang, Neuron 68, 843–856 (2010).
11. A. Rollenhagen, J. H. R. Lübke, Front. Synaptic Neurosci. 2, 2 (2010).
12. G. R. Newman, B. Jasani, E. D. Williams, Histochem. J. 15, 543–555 (1983).
13. K. D. Micheva, S. J. Smith, Neuron 55, 25–36 (2007).
14. B.-C. Chen et al., Science 346, 1257998 (2014).
15. J. Huisken, J. Swoger, F. Del Bene, J. Wittbrodt, E. H. K. Stelzer, Science 305, 1007–1009 (2004).
16. J. H. Lee et al., Science 343, 1360–1363 (2014).
17. A. M. Hecht, R. Duplessix, E. Geissler, Macromolecules 18, 2167–2173 (1985).
18. D. Calvet, J. Y. Wong, S. Giasson, Macromolecules 37, 7762–7771 (2004).

Replication-transcription switch in human mitochondria

Karen Agaronyan, Yaroslav I. Morozov, Michael Anikin, Dmitry Temiakov*

Coordinated replication and expression of the mitochondrial genome is critical for metabolically active cells during various stages of development. However, it is not known whether replication and transcription can occur simultaneously without interfering with each other and whether mitochondrial DNA copy number can be regulated by the transcription machinery. We found that interaction of human transcription elongation factor TEFM with mitochondrial RNA polymerase and nascent transcript prevents the generation of replication primers and increases transcription processivity and thereby serves as a molecular switch between replication and transcription, which appear to be mutually exclusive processes in mitochondria. TEFM may allow mitochondria to increase transcription rates and, as a consequence, respiration and adenosine triphosphate production without the need to replicate mitochondrial DNA, as has been observed during spermatogenesis and the early stages of embryogenesis.

The maternally inherited circular mitochondrial DNA (mtDNA) encodes subunits of complexes of the oxidative phosphorylation chain, as well as transfer RNAs (tRNAs) and ribosomal RNAs (1, 2). Transcription of human mtDNA is directed by two promoters, the LSP (light-strand promoter) and the HSP (heavy-strand promoter) located in opposing mtDNA strands, which results in two almost-genome-sized polycistronic transcripts that undergo extensive processing before polyadenylation and translation (3, 4). Note that transcription terminates prematurely about 120 base pairs (bp) downstream of LSP at a vertebrate-conserved G-rich region, called conserved sequence block II (CSBII), as a result of formation of a hybrid G-quadruplex between nascent RNA and the nontemplate strand of DNA (5–7). This termination event occurs near the origin of replication of the heavy strand (oriH) (8) and generates a replication primer. According to the asymmetric model (9), replication then proceeds through about two-thirds of the mtDNA, until the oriL sequence in the opposing strand becomes single stranded and forms a hairpin structure. The oriL hairpin is then recognized by mitochondrial RNA polymerase (mtRNAP), which primes replication of the light strand (10). Because replication of mtDNA coincides with transcription in time and space, collisions between transcription and replication machineries are inevitable and, similarly to bacterial and eukaryotic systems, likely have detrimental effects on mtDNA gene expression (11).

We analyzed the effects of a mitochondrial transcription elongation factor, TEFM, recently described by Minczuk and colleagues (12), on transcription of mtDNA. This protein was pulled down from mitochondrial lysates via mtRNAP and was found to stimulate nonspecific transcription on promoterless DNA; however, its effect on promoter-driven transcription had not been

Department of Cell Biology, School of Osteopathic Medicine, Rowan University, 2 Medical Center Drive, Stratford, NJ 08084, USA.
*Corresponding author. E-mail:temiakdm@rowan.edu

determined (12). We found that in the presence of TEFM, mtRNAP efficiently transcribes through CSBII (Fig. 1, A and B). Thus, TEFM acts as a factor that prevents termination at CSBII and synthesis of a primer for mtDNA polymerase. We identified the exact location of the termination point in CSBII (fig. S1). MtRNAP terminates at the end of a U6 sequence (positions 287 to 283 in mtDNA), 16 to 18 nucleotides (nt) downstream of the G-quadruplex (Fig. 1A). At this point, the 9-bp RNA-DNA hybrid in the elongation complex (EC) is extremely weak, as it is composed of only A-U and T-A pairs. This is reminiscent of intrinsic termination signals in prokaryotes—where the formation of an RNA hairpin is thought to disrupt the upstream region of the RNA-DNA hybrid—and is followed by the run of six to eight uridine 5′-monophosphate residues that further destabilizes the complex (5, 13).

Human mtDNA is highly polymorphic in the CSBII region; coincidently, the reference mitochondrial genome (Cambridge) contains a rare polymorphism in the G-quadruplex—namely, G5AG7—whereas the majority of mtDNAs from various haplogroups have two additional G residues (G6AG8) (14). We found that the termination efficiency of mtRNAP was substantially lower at G5AG7-CSBII (Fig. 1C), which suggested an effect of G run length on quadruplex formation and underscored the importance of further studies of various polymorphisms in this region.

In considering a putative mechanism of TEFM antitermination activity, we investigated whether it can interact with the nascent transcript and, thus, interfere with the formation of the quadruplex structure. We assembled ECs on a nucleic acid scaffold containing a photoreactive analog of uridine, 4-thio-uridine, 13 nt downstream from the 3′ end of RNA, and walked mtRNAP along the template by incorporation of appropriate substrate nucleoside triphosphates (NTPs) (Fig. 2A). We observed efficient cross-linking between TEFM and RNA when the photoreactive base was 15 to 16 bp away from the 3′ end of RNA. Additionally, using a template DNA containing the LSP promoter and

CSBII, we probed interactions of TEFM with RNA having a photoreactive probe 6-thio guanosine-5′-monophosphate (6-thio GMP) 9 to 16 or 18 to 25 nt away from the 3′ end of RNA (fig. S2). We found that TEFM efficiently cross-linked to the G-quadruplex region of RNA, which further confirmed its interactions with the nascent transcript (fig. S2).

The catalytic domains of mtRNAP and the single-subunit RNAP from bacteriophage T7 share high sequence and structural homology (15). When we compared the structural organization of human mtRNAP EC (15) and T7 RNAP EC (16), one striking difference became apparent—the former polymerase makes very few contacts with the downstream DNA duplex (fig. S3). In contrast,

in T7 RNAP EC, the N terminus of the polymerase makes extensive interactions with the entire downstream duplex. These extensive interactions with the downstream DNA may explain the high processivity of T7 RNAP (16). Because TEFM binds the C terminus of mtRNAP (12), we hypothesized that it may also bind the downstream DNA to compensate for the lack of mtRNAP-DNA interactions. To evaluate this, we incorporated 4-thio-2′-deoxythymidine-5′-monophosphate (4-thio dTMP) into the DNA template in the downstream region and assembled the EC using RNA-DNA scaffolds. We found that TEFM efficiently cross-linked to the +7 and +8 bases in the DNA template strand (Fig. 2B and fig. S4A). The DNA-TEFM cross-linking was species-specific, as no efficient cross-

linking was detected when yeast mtRNAP was used (fig. S4B).

The binding site of TEFM on mtRNAP has been previously identified in the C-terminal region, between residues 768 and 1230 (12). These data, taken together with the RNA and DNA cross-linking data, suggest that TEFM likely binds to the palm subdomain of mtRNAP in proximity to the PPR domain and interacts with the emerging RNA transcript (Fig. 2C). It is therefore likely that TEFM antitermination activity is due to direct interference with the formation of the bulky G-quadruplex structure between the palm subdomain and the PPR domain of mtRNAP or due to the allosteric effect of quadruplex formation on complex stability. Similar mechanisms of
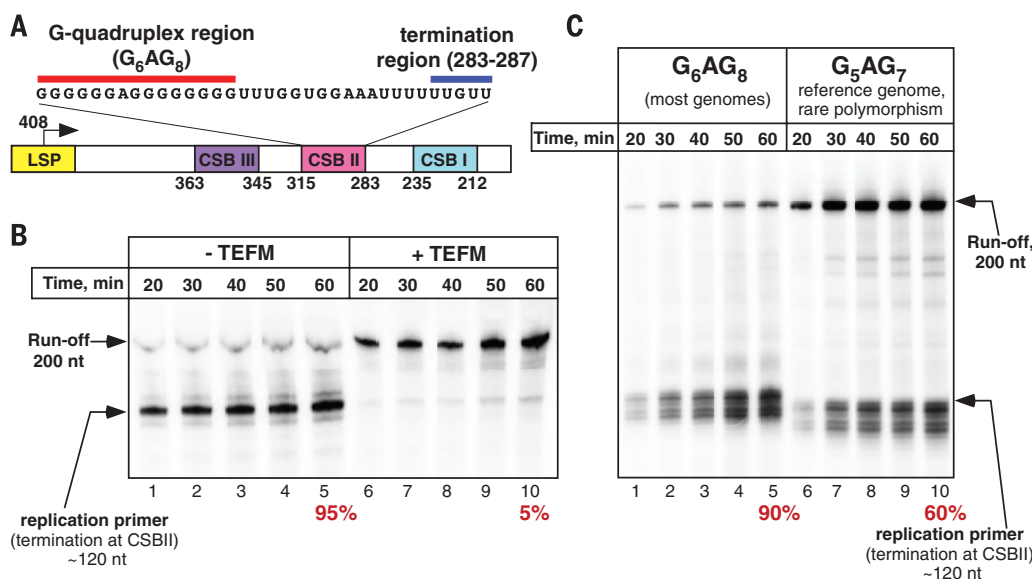
Fig. 1. TEFM prevents termination at CSBII. (A) Schematic illustration of the human mtDNA region downstream of the LSP promoter. The numbers below the scheme correspond to the reference human mtDNA; the transcribed sequence of CSBII is shown at the top. (B) MtRNAP does not terminate at CSBII in the presence of TEFM. Termination efficiency (%) is indicated below the panel. (C) A rare polymorphism in a reference mtDNA results in a decreased efficiency of transcription termination at CSBII.
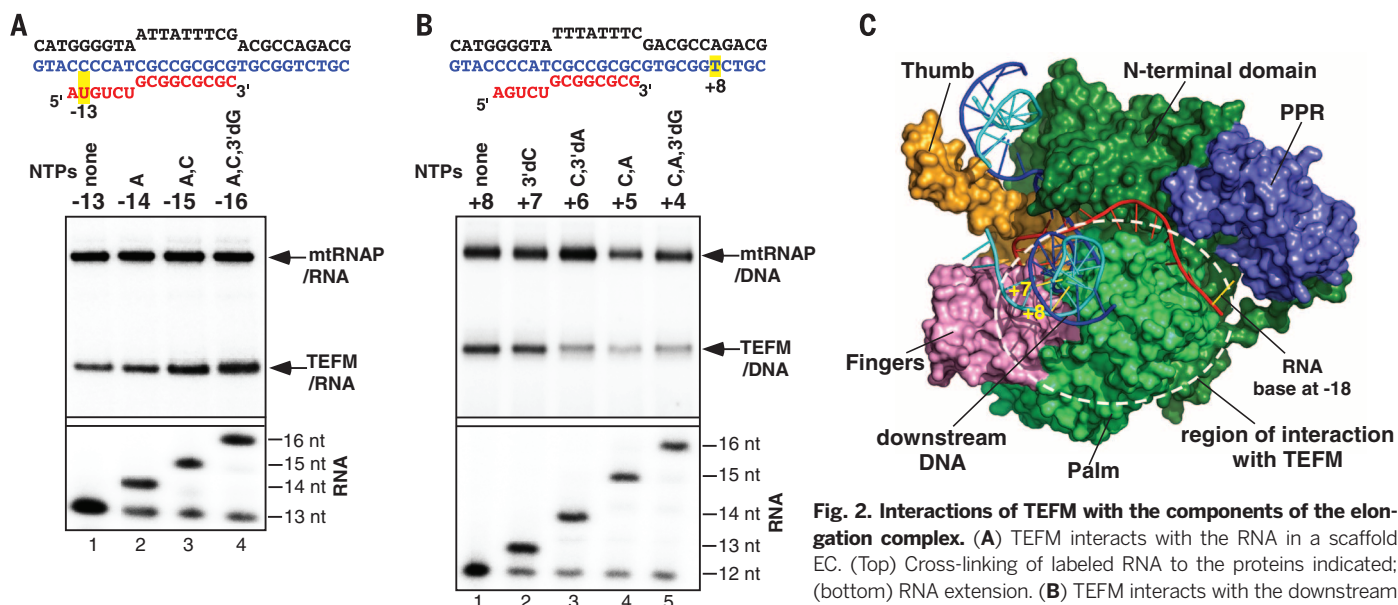
Fig. 2. Interactions of TEFM with the components of the elongation complex. (A) TEFM interacts with the RNA in a scaffold EC. (Top) Cross-linking of labeled RNA to the proteins indicated; (bottom) RNA extension. (B) TEFM interacts with the downstream DNA. (C) Putative region of interaction with TEFM. Structure of human mtRNAP EC (surface representation, PDB ID 4BOC) is shown with the major domains indicated (fingers, pink; palm, light green; N-terminal domain, dark green; thumb, orange; DNA template strand, blue; nontemplate strand, cyan; and RNA, red). The 9-nt-long RNA in the EC is extended by 9 nt to model the trajectory of the nascent RNA.

antitermination have been suggested for lambda phage antiterminators Q and N and a number of bacterial antiterminators that were shown to interact with both RNAP and its nascent transcript that would otherwise form a hairpin structure (17, 18).

Because TEFM interacts with the downstream DNA (which may stabilize the EC), we decided to investigate its effect on mtRNAP processivity. We found that the efficiency of runoff synthesis by mtRNAP was low if the size of the product exceeded 500 nt (Fig. 3, A and B). Indeed, the processivity of mtRNAP was substantially lower than that of a related T7 RNAP (which is known to transcribe large fragments of DNA) and was apparently not sufficient to transcribe a 16,000-bp-long mtDNA. In the presence of TEFM, the efficiency of synthesis of long RNA was significantly increased (Fig. 3, A and B), which suggested that TEFM indeed acts as a processivity factor, as was originally proposed (12).

We next probed if TEFM contributes to the stability of the elongating mtRNAP and, as a consequence, to its antitermination activity. To demonstrate this, we halted the EC 35 bp downstream of the promoter start site by omitting one of the substrate NTPs [cytidine 5′-triphosphate (CTP)] (Fig. 3C and fig. S5), in the presence or absence of TEFM. After 10 to 40 min, the complexes were chased to allow synthesis of a runoff product. In the absence of TEFM, accumulation of a 35-oligomer RNA product predominated, with little production of runoff, which indicates that the halted EC is unstable, rapidly dissociates and reinitiates, but is inefficiently chased (Fig. 3C and fig. S5). In contrast, in the presence of TEFM, little, if any, of 35-oligomer RNA product accumulates, but more efficient synthesis of full-length products is observed, which indicates that, under these conditions, the EC is stable and may subsequently be extended.

Our in vitro data demonstrate that TEFM increases the overall processivity of ECs. In the absence of TEFM, mtRNAP is unable to efficiently produce long transcripts and, instead, terminates at CSBII, which primes replication of the heavy strand of mtDNA (Fig. 4). Consistent with this, a knockdown of TEFM in human cells results in a decrease of promoter-distal RNA transcripts (12). We therefore propose that replication and transcription are mutually exclusive processes in human mitochondria that allow the corresponding machineries to avoid the detrimental consequences of head-on collisions (Fig. 4). As such, TEFM serves as a molecular switch that would allow the organelles to either replicate the mtDNA and regulate its copy number or to elevate its transcription rates. This switch can be important for a number of developmental processes, such as embryogenesis and spermatogenesis, during which an active transcription of mtDNA is observed without replication (19–25). Although TEFM may not be the only factor affecting mtDNA copy number (26), the proposed mechanism provides a solution to these important biological processes. Further in vivo analysis will be required to address the question as to how this switch is regulated in mitochondria of actively metabolizing cells.
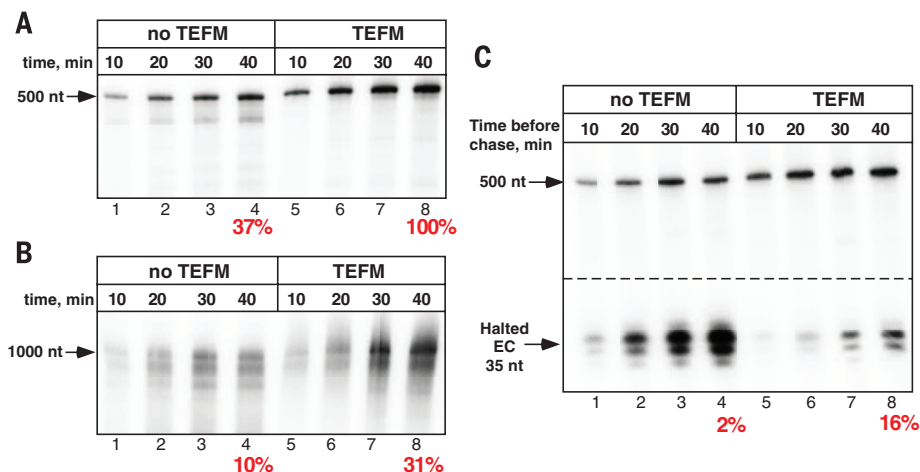
Fig. 3. TEFM increases processivity and stability of mtRNAP EC. (**A** and **B**) TEFM increases the EC processivity. Transcription was performed using LSP templates lacking CSBII sequence to generate 500-nt (A) or 1000-nt (B) runoff products. Efficiency of synthesis of 500 nt of RNA in the presence of TEFM is taken as 100%. (**C**) TEFM increases the EC stability. Complexes halted at +35 in the presence or absence of TEFM were incubated for the times indicated and chased with CTP. Numbers below indicate efficiency of a halted EC extension (%).
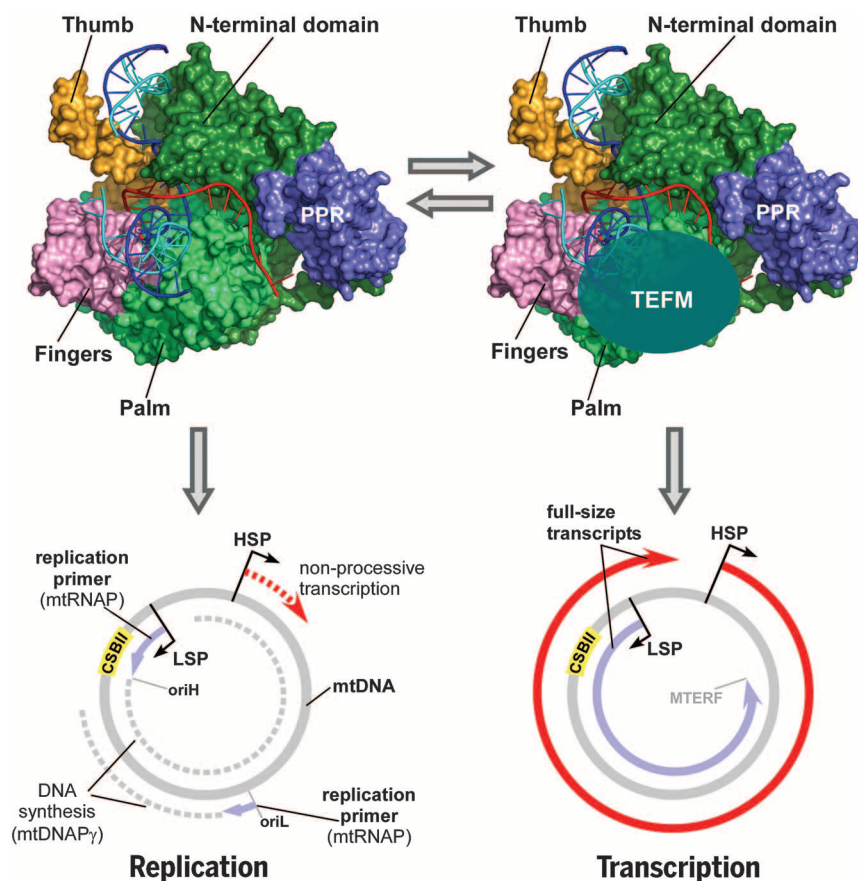
Fig. 4. Model for a replication-transcription switch in mitochondria. In the absence of TEFM, mtRNAP initiates transcription at the LSP promoter but terminates at CSBII and produces a 120-nt replication primer at the replication origin oriH. The primer is used by replisome for replication of the heavy strand of mtDNA, during which a separate initiation event involving mtRNAP generates a replication primer at oriL. Because of low processivity, transcription from the HSP does not produce a full-size transcript (bottom left). When TEFM is bound (bottom right), transcription from HSP produces genome-length transcripts. At the same time, LSP-driven transcription is not terminated at CSBII and proceeds to the site of factor-dependent termination (MTERF).

REFERENCES AND NOTES

1. M. Falkenberg, N. G. Larsson, C. M. Gustafsson, *Annu. Rev. Biochem.* **76**, 679–699 (2007).
2. N. D. Bonawitz, D. A. Clayton, G. S. Shadel, *Mol. Cell* **24**, 813–825 (2006).
3. B. M. Hällberg, N. G. Larsson, *Cell Metab.* **20**, 226–240 (2014).
4. Y. I. Morozov *et al.*, *Nucleic Acids Res.* **42**, 3884–3893 (2014).
5. P. H. Wanrooij *et al.*, *Nucleic Acids Res.* **40**, 10334–10344 (2012).
6. P. H. Wanrooij, J. P. Uhler, T. Simonsson, M. Falkenberg, C. M. Gustafsson, *Proc. Natl. Acad. Sci. U.S.A.* **107**, 16072–16077 (2010).
7. D. D. Chang, D. A. Clayton, *Proc. Natl. Acad. Sci. U.S.A.* **82**, 351–355 (1985).
8. D. Kang, K. Miyako, Y. Kai, T. Irie, K. Takeshige, *J. Biol. Chem.* **272**, 15275–15279 (1997).
9. D. A. Clayton, *Cell* **28**, 693–705 (1982).
10. J. M. Fusté *et al.*, *Mol. Cell* **37**, 67–78 (2010).
11. R. T. Pomerantz, M. O'Donnell, *Cell Cycle* **9**, 2537–2543 (2010).
12. M. Minczuk *et al.*, *Nucleic Acids Res.* **39**, 4284–4299 (2011).
13. V. Epshtein, C. J. Cardinale, A. E. Ruckenstein, S. Borukhov, E. Nudler, *Mol. Cell* **28**, 991–1001 (2007).
14. R. M. Andrews *et al.*, *Nat. Genet.* **23**, 147 (1999).
15. K. Schwinghammer *et al.*, *Nat. Struct. Mol. Biol.* **20**, 1298–1303 (2013).
16. T. H. Tahirov *et al.*, *Nature* **420**, 43–50 (2002).
17. I. Gusarov, E. Nudler, *Cell* **107**, 437–449 (2001).
18. S. Shankar, A. Hatoum, J. W. Roberts, *Mol. Cell* **27**, 914–927 (2007).
19. A. Rantanen, N. G. Larsson, *Hum. Reprod.* **15** (suppl. 2), 86–91 (2000).
20. J. St John, *Biochim. Biophys. Acta* **1840**, 1345–1354 (2014).
21. T. Wai *et al.*, *Biol. Reprod.* **83**, 52–62 (2010).
22. P. J. Carling, L. M. Cree, P. F. Chinnery, *Mitochondrion* **11**, 686–692 (2011).
23. J. Van Blerkom, *Mitochondrion* **11**, 797–813 (2011).
24. S. Monnot *et al.*, *Hum. Mol. Genet.* **22**, 1867–1872 (2013).
25. D. C. Wallace, *Annu. Rev. Genet.* **39**, 359–407 (2005).
26. M. I. Ekstrand *et al.*, *Hum. Mol. Genet.* **13**, 935–944 (2004).

PROTEIN STRUCTURE

Structure and activity of tryptophan-rich TSPO proteins

Youzhong Guo,[1] Ravi C. Kalathur,[2] Qun Liu,[2,3] Brian Kloss,[2] Renato Bruni,[2] Christopher Ginter,[2] Edda Kloppmann,[2,4] Burkhard Rost,[2,4] Wayne A. Hendrickson[1,2,3,5]*

Translocator proteins (TSPOs) bind steroids and porphyrins, and they are implicated in many human diseases, for which they serve as biomarkers and therapeutic targets. TSPOs have tryptophan-rich sequences that are highly conserved from bacteria to mammals. Here we report crystal structures for *Bacillus cereus* TSPO (*Bc*TSPO) down to 1.7 Å resolution, including a complex with the benzodiazepine-like inhibitor PK11195. We also describe *Bc*TSPO-mediated protoporphyrin IX (PpIX) reactions, including catalytic degradation to a previously undescribed heme derivative. We used structure-inspired mutations to investigate reaction mechanisms, and we showed that TSPOs from *Xenopus* and man have similar PpIX-directed activities. Although TSPOs have been regarded as transporters, the catalytic activity in PpIX degradation suggests physiological importance for TSPOs in protection against oxidative stress.

The translocator protein (TSPO) is named for its putative roles in the transport of cholesterol, proteins, and porphyrins into mitochondria and elsewhere (*1*). TSPO was first identified as a peripheral-type benzodiazepine receptor in mammals (*2*)—attracting attention because of popular anxiolytic benzodiazepines such as diazepam (Valium)—and the tryptophan-rich sensory protein TspO of photosynthetic bacteria proved to be homologous (*3*). The sequences of TSPO proteins from diverse organisms are highly conserved in sequence (fig. S1) and also in function; notably, rat TSPO can substitute for the bacterial protein as a negative regulator of photosynthesis gene expression in *Rhodobacter sphaeroides* (*4*).

Benzodiazepine-like chemicals, such as PK11195, were found to bind to TSPO and regulate steroid biosynthesis (*5*), and porphyrins were identified as endogenous ligands of rat TSPO, with highest affinity for protoporphyrin IX (PpIX) (*6*). Many following studies have pursued TSPO interactions with cholesterol and PpIX (*7*, *8*). Most recently, the seeming essentiality of TSPO for steroidogenesis (*9*) has been challenged by the finding that TSPO1$^{-/-}$ mice are viable and without defects in steroid hormone biosynthesis (*10*), and the presumed role in PpIX transport (*11*) has been amended by the discovery that bacterial TSPOs catalyze a photooxidative degradation of PpIX (*12*).

Although the underlying biochemical mechanisms for its activities are not fully understood, TSPO has elicited considerable interest for medicine. Roles for TSPO have been imputed in apoptosis (*13*), inflammation (*14*), HIV biosynthesis (*15*), cancer (*16*), Alzheimer's disease (*17*), and cardiovascular diseases (*18*). TSPO is a therapeutic target (*13*, *18*–*20*) and has proven useful as a positron emission tomography–imaging biomarker (*14*, *17*, *21*, *22*).

The translocator protein has been characterized in monomer, dimer, and higher oligomeric states (*20*). An electron microscopy structure for TSPO from *R. sphaeroides* (*Rs*TSPO) revealed a dimer (*23*), and a nuclear magnetic resonance structure for a mouse TSPO showed a monomer comprising five transmembrane helices (*24*).

We produced recombinant TSPO proteins from several bacterial and vertebrate organisms and found *Bacillus cereus* TSPO (*Bc*TSPO) suitable for biochemical and structural characterization (see supplementary materials and methods). By size-exclusion chromatography, detergent-extracted *Bc*TSPO exists in at least three different oligomeric states (fig. S2A). Apo *Bc*TSPO crystallized from the monomer-dimer fraction (fig. S2, C and D) in two different lipidic cubic phase (LCP) conditions and also from the high-oligomer fraction as a detergent micelle; the *Bc*TSPO-PK11195 complex crystallized as a dimer in LCP. A structure obtained by single-wavelength anomalous diffraction analysis from iodinated *Bc*TSPO (fig. S2E) was the starting point for native structures that followed (tables S1 and S2). Refinements yielded structures at 1.7 Å (Fig. 1, A to E, and fig. S3) and 2.0 Å resolution for apo monomers in LCP, at 4.1 Å resolution for the apo dimer in detergent (Fig. 1F), and at 3.5 Å resolution for the dimeric ligand complex in LCP (Fig. 1G).

Each *Bc*TSPO protomer has five transmembrane (TM) α helices organized in clockwise order (TM1-TM2-TM5-TM4-TM3), as viewed from the C-terminal end (Fig. 1, A and B, and fig. S1) where a short extra-membranous helix ($\alpha_{1,2}$) between TM1 and TM2 caps a C-terminal pocket (Fig. 1C). The electrostatic potential surface defines a transmembrane orientation (Fig. 1C) having its N-terminal end heavily positive, likely cytoplasmic in *B. cereus*, and its C-terminal end largely negative (Fig. 1D and fig. S4, A to D). A mapping of sequence conservation onto the molecular surface shows a conservative band between TM2 and TM5, a highly conserved pocket opening between TM1 and TM2, and features more conserved at the C-terminal end than on most of the exterior (Fig. 1E and fig. S4, E to H).

[1]Department of Biochemistry and Molecular Biophysics, Columbia University, New York, NY 10032, USA. [2]The New York Consortium on Membrane Protein Structure (NYCOMPS), New York Structural Biology Center, 89 Convent Avenue, New York, NY 10027, USA. [3]New York Structural Biology Center, Synchrotron Beamlines, Brookhaven National Laboratory, Upton, NY 11973, USA. [4]Department of Informatics, Bioinformatics and Computational Biology, Technische Universität München, Garching 85748, Germany. [5]Department of Physiology and Cellular Biophysics, Columbia University, New York, NY 10032, USA.
*Corresponding author. E-mail: wayne@xtl.cumc.columbia.edu

REFERENCES AND NOTES

1. M. Falkenberg, N. G. Larsson, C. M. Gustafsson, *Annu. Rev. Biochem.* **76**, 679–699 (2007).
2. N. D. Bonawitz, D. A. Clayton, G. S. Shadel, *Mol. Cell* **24**, 813–825 (2006).
3. B. M. Hällberg, N. G. Larsson, *Cell Metab.* **20**, 226–240 (2014).
4. Y. I. Morozov *et al.*, *Nucleic Acids Res.* **42**, 3884–3893 (2014).
5. P. H. Wanrooij *et al.*, *Nucleic Acids Res.* **40**, 10334–10344 (2012).
6. P. H. Wanrooij, J. P. Uhler, T. Simonsson, M. Falkenberg, C. M. Gustafsson, *Proc. Natl. Acad. Sci. U.S.A.* **107**, 16072–16077 (2010).
7. D. D. Chang, D. A. Clayton, *Proc. Natl. Acad. Sci. U.S.A.* **82**, 351–355 (1985).
8. D. Kang, K. Miyako, Y. Kai, T. Irie, K. Takeshige, *J. Biol. Chem.* **272**, 15275–15279 (1997).
9. D. A. Clayton, *Cell* **28**, 693–705 (1982).
10. J. M. Fusté *et al.*, *Mol. Cell* **37**, 67–78 (2010).
11. R. T. Pomerantz, M. O'Donnell, *Cell Cycle* **9**, 2537–2543 (2010).
12. M. Minczuk *et al.*, *Nucleic Acids Res.* **39**, 4284–4299 (2011).
13. V. Epshtein, C. J. Cardinale, A. E. Ruckenstein, S. Borukhov, E. Nudler, *Mol. Cell* **28**, 991–1001 (2007).
14. R. M. Andrews *et al.*, *Nat. Genet.* **23**, 147 (1999).
15. K. Schwinghammer *et al.*, *Nat. Struct. Mol. Biol.* **20**, 1298–1303 (2013).
16. T. H. Tahirov *et al.*, *Nature* **420**, 43–50 (2002).
17. I. Gusarov, E. Nudler, *Cell* **107**, 437–449 (2001).
18. S. Shankar, A. Hatoum, J. W. Roberts, *Mol. Cell* **27**, 914–927 (2007).
19. A. Rantanen, N. G. Larsson, *Hum. Reprod.* **15** (suppl. 2), 86–91 (2000).
20. J. St John, *Biochim. Biophys. Acta* **1840**, 1345–1354 (2014).
21. T. Wai *et al.*, *Biol. Reprod.* **83**, 52–62 (2010).
22. P. J. Carling, L. M. Cree, P. F. Chinnery, *Mitochondrion* **11**, 686–692 (2011).
23. J. Van Blerkom, *Mitochondrion* **11**, 797–813 (2011).
24. S. Monnot *et al.*, *Hum. Mol. Genet.* **22**, 1867–1872 (2013).
25. D. C. Wallace, *Annu. Rev. Genet.* **39**, 359–407 (2005).
26. M. I. Ekstrand *et al.*, *Hum. Mol. Genet.* **13**, 935–944 (2004).

PROTEIN STRUCTURE

Structure and activity of tryptophan-rich TSPO proteins

Youzhong Guo,[1] Ravi C. Kalathur,[2] Qun Liu,[2,3] Brian Kloss,[2] Renato Bruni,[2] Christopher Ginter,[2] Edda Kloppmann,[2,4] Burkhard Rost,[2,4] Wayne A. Hendrickson[1,2,3,5]*

Translocator proteins (TSPOs) bind steroids and porphyrins, and they are implicated in many human diseases, for which they serve as biomarkers and therapeutic targets. TSPOs have tryptophan-rich sequences that are highly conserved from bacteria to mammals. Here we report crystal structures for *Bacillus cereus* TSPO (*Bc*TSPO) down to 1.7 Å resolution, including a complex with the benzodiazepine-like inhibitor PK11195. We also describe *Bc*TSPO-mediated protoporphyrin IX (PpIX) reactions, including catalytic degradation to a previously undescribed heme derivative. We used structure-inspired mutations to investigate reaction mechanisms, and we showed that TSPOs from *Xenopus* and man have similar PpIX-directed activities. Although TSPOs have been regarded as transporters, the catalytic activity in PpIX degradation suggests physiological importance for TSPOs in protection against oxidative stress.

The translocator protein (TSPO) is named for its putative roles in the transport of cholesterol, proteins, and porphyrins into mitochondria and elsewhere (*1*). TSPO was first identified as a peripheral-type benzodiazepine receptor in mammals (*2*)—attracting attention because of popular anxiolytic benzodiazepines such as diazepam (Valium)—and the tryptophan-rich sensory protein TspO of photosynthetic bacteria proved to be homologous (*3*). The sequences of TSPO proteins from diverse organisms are highly conserved in sequence (fig. S1) and also in function; notably, rat TSPO can sub-stitute for the bacterial protein as a negative regulator of photosynthesis gene expression in *Rhodobacter sphaeroides* (*4*).

Benzodiazepine-like chemicals, such as PK11195, were found to bind to TSPO and regulate steroid biosynthesis (*5*), and porphyrins were identified as endogenous ligands of rat TSPO, with highest affinity for protoporphyrin IX (PpIX) (*6*). Many following studies have pursued TSPO interactions with cholesterol and PpIX (*7*, *8*). Most recently, the seeming essentiality of TSPO for steroidogenesis (*9*) has been challenged by the finding that TSPO1$^{-/-}$ mice are viable and without defects in steroid hormone biosynthesis (*10*), and the presumed role in PpIX transport (*11*) has been amended by the discovery that bacterial TSPOs catalyze a photooxidative degradation of PpIX (*12*).

Although the underlying biochemical mechanisms for its activities are not fully understood, TSPO has elicited considerable interest for medicine. Roles for TSPO have been imputed in apoptosis (*13*), inflammation (*14*), HIV biosynthesis (*15*), cancer (*16*), Alzheimer's disease (*17*), and cardiovascular diseases (*18*). TSPO is a therapeutic target (*13*, *18–20*) and has proven useful as a pos-itron emission tomography–imaging biomarker (*14*, *17*, *21*, *22*).

The translocator protein has been characterized in monomer, dimer, and higher oligomeric states (*20*). An electron microscopy structure for TSPO from *R. sphaeroides* (*Rs*TSPO) revealed a dimer (*23*), and a nuclear magnetic resonance structure for a mouse TSPO showed a monomer comprising five transmembrane helices (*24*).

We produced recombinant TSPO proteins from several bacterial and vertebrate organisms and found *Bacillus cereus* TSPO (*Bc*TSPO) suitable for biochemical and structural characterization (see supplementary materials and methods). By size-exclusion chromatography, detergent-extracted *Bc*TSPO exists in at least three different oligomeric states (fig. S2A). Apo *Bc*TSPO crystallized from the monomer-dimer fraction (fig. S2, C and D) in two different lipidic cubic phase (LCP) conditions and also from the high-oligomer fraction as a detergent micelle; the *Bc*TSPO-PK11195 complex crystallized as a dimer in LCP. A structure obtained by single-wavelength anomalous diffraction analysis from iodinated *Bc*TSPO (fig. S2E) was the starting point for native structures that followed (tables S1 and S2). Refinements yielded structures at 1.7 Å (Fig. 1, A to E, and fig. S3) and 2.0 Å resolution for apo monomers in LCP, at 4.1 Å resolution for the apo dimer in detergent (Fig. 1F), and at 3.5 Å resolution for the dimeric ligand complex in LCP (Fig. 1G).

Each *Bc*TSPO protomer has five transmembrane (TM) α helices organized in clockwise order (TM1-TM2-TM5-TM4-TM3), as viewed from the C-terminal end (Fig. 1, A and B, and fig. S1) where a short extra-membranous helix ($\alpha_{1,2}$) between TM1 and TM2 caps a C-terminal pocket (Fig. 1C). The electrostatic potential surface defines a transmembrane orientation (Fig. 1C) having its N-terminal end heavily positive, likely cytoplasmic in *B. cereus*, and its C-terminal end largely negative (Fig. 1D and fig. S4, A to D). A mapping of sequence conservation onto the molecular surface shows a conservative band between TM2 and TM5, a highly conserved pocket opening between TM1 and TM2, and features more conserved at the C-terminal end than on most of the exterior (Fig. 1E and fig. S4, E to H).

[1]Department of Biochemistry and Molecular Biophysics, Columbia University, New York, NY 10032, USA. [2]The New York Consortium on Membrane Protein Structure (NYCOMPS), New York Structural Biology Center, 89 Convent Avenue, New York, NY 10027, USA. [3]New York Structural Biology Center, Synchrotron Beamlines, Brookhaven National Laboratory, Upton, NY 11973, USA. [4]Department of Informatics, Bioinformatics and Computational Biology, Technische Universität München, Garching 85748, Germany. [5]Department of Physiology and Cellular Biophysics, Columbia University, New York, NY 10032, USA.
*Corresponding author. E-mail: wayne@xtl.cumc.columbia.edu

All four crystallized copies of *Bc*TSPO are very similar: The two apo monomers have a root-mean-squared deviation (RMSD) of 0.64 Å for Cα positions, differing most in the TM1-TM2 loop, and protein conformations are essentially identical whether with or without the PK11195 ligand (Cα RMSDs between the 1.7 Å resolution apo monomer and subunits A and B of the PK11195 dimer are 0.51 and 0.59 Å, respectively). Dimeric associations in the detergent micelle and in LCP

are also nearly the same (Fig. 1, F and G), although the apo micelle may be a swapped dimer. The associated chains are cleanly resolved in the liganded complex.

In comparing our structures of *Bc*TSPO to that published for the mouse protein *Mus musculus* TSPO1 (*Mm*TSPO1) (*24*), we found limited similarity apart from the topological order of helices. Comparing all 148 residues in common between the two models (fig. S1; 26.6% identity), the Cα

RMSD equals 4.90 Å (PDB IDs 4RYQ versus 2MGY); when the comparison is restricted to the 54 positions that match within 3 Å, the RMSD value is still exceptionally high at 1.71 Å. TM2 and TM5 can be superimposed relatively well, but the other helices are rotated such that conserved residues that are inside in *Bc*TSPO move outside in *Mm*TSPO1 (fig. S5A). Having the sequence redisposed to the *Mm*TSPO1 model also removes pocket-lining conservation from interior surfaces

Fig. 1. Structures of *Bc*TSPO.
(**A** and **B**) Ribbon drawing of TSPO from the type 1 apo structure, as viewed from within the membrane plane (A) and from the periplasm above (B). Coloring progresses spectrally from the N terminus (blue) to the C terminus (red). Side chains are shown for conserved tryptophan residues Trp[31], Trp[40], Trp[51], and Trp[138]. (**C** and **D**) Electrostatic potential at the molecular surface of the apo monomer, as oriented in (A) and (B), respectively. Positive potentials are in degrees of blue; negatives are in red. Dotted planes show membrane boundaries computed by the Positioning of Proteins in Membranes (PPM) server. (**E**) Molecular surface as in (D) but colored by Consurf sequence conservation. Variable positions are in degrees of turquoise; conserved positions are in degrees of maroon. (**F**) Ribbon drawing of the apo dimer in detergent. Tryptophan residues and coloring are as in (A). (**G**) Ribbon drawing of the PK11195 dimer in LCP. The PK11195 moieties are drawn as pink sticks.
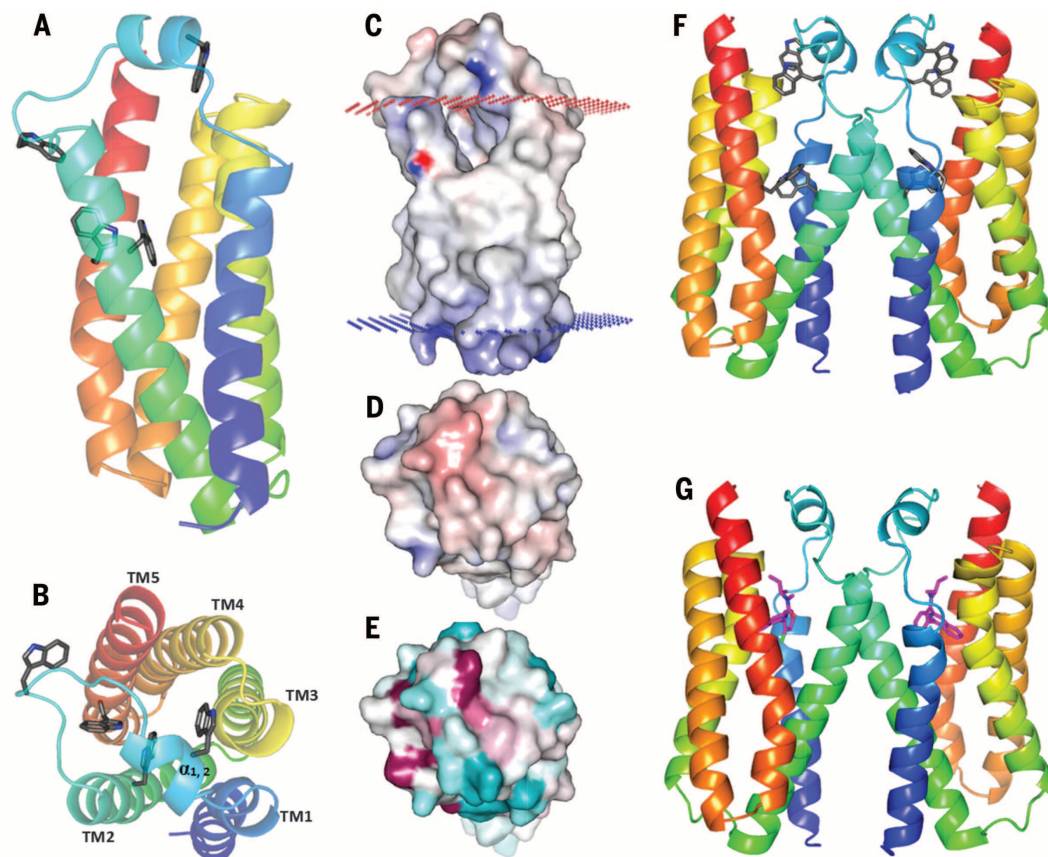
Fig. 2. Features of the ligand binding site in *Bc*TSPO. (**A**) PK11195 in the binding pocket. The ligand is drawn as a stick figure with atom coloring of carbon (light gray), nitrogen (blue), and oxygen (red). Portions of a ribbon drawing of the TSPO protein structure are displayed faintly with coloring as in Fig. 1A. Side chains that contact PK11195 are drawn in stick representation and have carbon atoms colored as for the backbone. (**B**) Cross-sectioned views of the ligand binding pocket. The surface of an apo monomer, oriented as in Fig. 1A and sliced by a vertical

plane perpendicular to the page, was opened as a book to show both sides of the invaginated pocket. The planar cut surfaces are gray, and exposed molecular surfaces and visible atomic structures are in ConSurf coloring as in Fig. 1E.
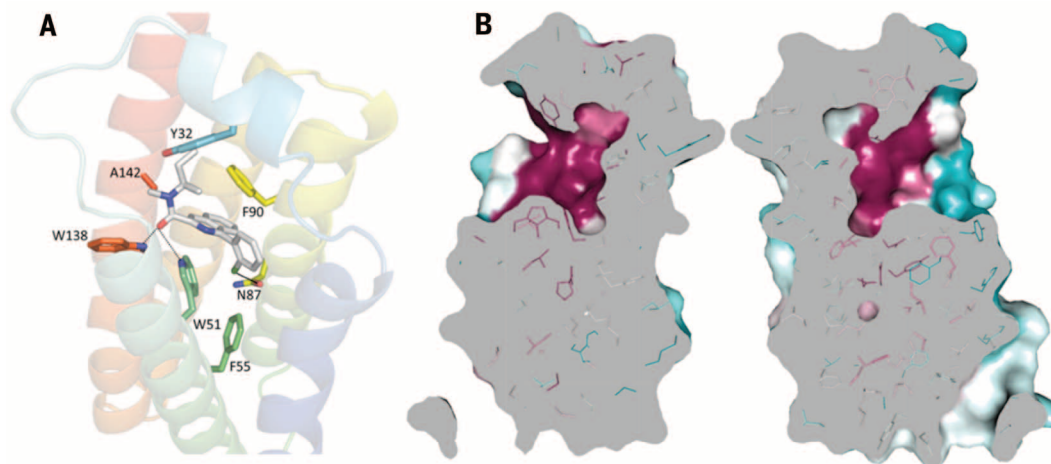
(fig. S5C). We also compared *Bc*TSPO to recent structures of *R. sphaeroides* TSPO (*Rs*TSPO) (*25*) and here found substantial similarity. On superimposition of those 126 of 148 Cα atoms within 3 Å of one another for *Bc*TSPO versus *Rs*TSPO Ala[139]→Thr[139] (A139T) (*26*) (PDB IDs 4RYQ versus 4UC1), the RMSD value was 1.17 Å, with TM1 helices most disparate (fig. S5B). TM1 is the least conserved helix (fig. S1), and it is at the dimer interface of *Rs*TSPO but not at that of *Bc*TSPO (fig. S5D).

Both protomers of the *Bc*TSPO-PK11195 dimer showed omit-map density in the pocket opening between TM1 and TM2 (fig. S2F). When fitted by the ligand structure, the resulting model has the carbonyl-oxygen atom of PK11195 hydrogen bonded to indole-NH groups of both Trp[51] and Trp[138], and the Cl atom of the ligand is in van der Waals contact with Asn[87] (Fig. 2A). PK11195 in *Bc*TSPO also makes van der Waals contacts with residues Ser[22], Tyr[32], Pro[42], Ile[47], Phe[55], Phe[90], Ser[91], Gln[94], Cys[107], Ala[142], and Leu[145]. These contacts emanate from each of the transmembrane helices plus

the TM1-TM2 loop. All among them except Ser[22] are widely conserved residues. Because the apo and ligated *Bc*TSPO proteins are essentially isostructural, the ligand-binding site is a highly conserved cavity in apo *Bc*TSPO (Fig. 2B). This cavity is water-filled in our high-resolution apo structures (fig. S6A), and PpIX can be satisfactorily docked into the cavity in a particular orientation (fig. S6, B and C). The PK11195 conformation, ligand binding pose, and protein contacts are very different in the model for *Mm*TSPO1 (fig. S5A).

The side chain of Ala[142] protrudes into the binding pocket such that its mutation would be expected to interfere with ligand binding. In accord, recent reports show that TSPO radioligands PBR28 (*21*) and [^{18}F]-FEPPA (*22*) have different binding affinities for the predominant Ala[147] and the minor Thr[147] polymorphic variants of human TSPO1 (position 142 in *Bc*TSPO).

In attempting to bind PpIX to *Bc*TSPO, we noticed that initially red mixtures turned blue on standing out in the light for a few minutes, but not when dark. Thus, considering the reported pho-

tooxidative degradation of PpIX by *Chlorobium tepidum* TSPO (*Ct*TSPO) (*12*), we characterized this activity of *Bc*TSPO toward PpIX. As for *Ct*TSPO, we observed a rapid decrease of the Soret absorbance at 405 nm when in the light (Fig. 3A) and a concomitant loss of the characteristic PpIX fluorescence at 629 and 697 nm (632 and 700 nm for *Bc*TSPO-PpIX) when illuminated by ultraviolet (UV) light (*27*, *28*). These changes were irreversible, and saturated PK11195 substantially inhibited the PpIX decay but did not entirely block it.

The post-illumination absorbance spectrum of *Bc*TSPO-PpIX is like that reported from *Ct*TSPO-PpIX (*12*), and the spectrum that we extracted for the photo-degradation product shows features like those of spectra from biliverdin and phycocyanobilin, but with absorption peaks further blue-shifted in series (Fig. 3B). By analogy with biliverdin and for its indigo color, we call this product bilindigin. Because the photooxidation of PpIX yields oxidized vinyl groups, predominantly generating formyl groups when in aqueous micelles
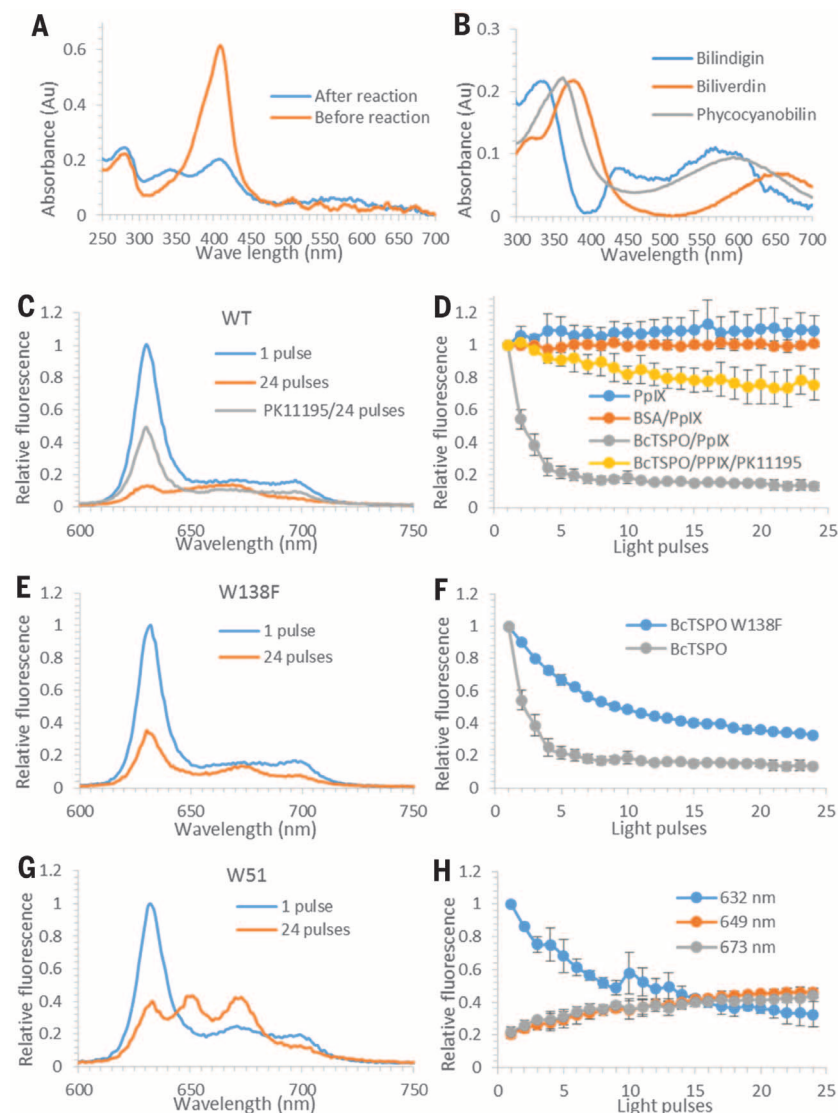
Fig. 3. Spectral analysis of bacterial TSPO-mediated activity in PpIX degradation and modulation. (**A**) UV-visible spectra of WT *Bc*TSPO with PpIX before and after reaction. AU, absorbance units. (**B**) Comparison of the spectrum for the bilindigin degradation product as extracted from the postreaction spectrum in (A), with spectra from biliverdin and phycocyanobilin. (**C** and **D**) Fluorescence analysis of WT *Bc*TSPO activity toward PpIX. Specta after indicated light exposures are shown in (C), and time courses of fluorescence at the 632-nm ground-state peak are tracked in (D). Exposure time is measured in light pulses, where each pulse comprised 50 s light plus 10 s read-out in the dark. Time courses are compared for PpIX in the indicated associations. (**E** and **F**) Fluorescence analysis of *Bc*TSPO W138F activity toward PpIX. Spectra and time courses are as described for (C) and (D). (**G** and **H**) Fluorescence analysis of *Bc*TSPO W51F activity toward PpIX. Spectra and time courses are as described for (C) and (D). Error bars in (D), (F), and (H) indicate SD.

Table 1. Reactions of PpIX with TSPO proteins. Down arrows denote the decrease with time in intensity of photostimulated fluorescence from the first excited state. Up arrows denote the increase with time of fluorescence from secondary excited states, presumably reached by oxidative photochemistry processes.

TSPO protein	Porphyrin cleavage	Fluorescence excitations		
		632 nm	649 nm	673 nm
*Bc*TSPO wild type	Fast	↓	No	No
*Bc*TSPO wild type	No	↓	↑	↑
*Bc*TSPO wild type	Slow	↓	No	No
*Bc*TSPO W51F/W138F	No	↓	No	↑
*Bc*TSPO A142T	No	↓	No	↑
*Xt*TSPO	Yes	↓	No	No
*Hs*TSPO1 T147	No	↓	No	↑
*Hs*TSPO2 T145	No	↓	No	↑

(29), and the modifications that distinguish phycocyanobilin from biliverdin are also at vinyl positions, we contemplate a formyl analog of biliverdin as a plausible product candidate (fig. S7). Thus, TSPO might catalyze both the vinyl-to-formyl oxidation and also the oxidative cleavage of PpIX at the methene bridge between vinyl-bearing pyrrole rings.

A mechanistic clue for TSPO-mediated degradation of PpIX comes from the observation that the W→F mutation of a conserved tryptophan was said to abrogate PpIX degradation by *Cf*TSPO without affecting PpIX binding (12). In our *Bc*TSPO-PpIX model (fig. S6C), both the corresponding residue, Trp[138], and another conserved tryptophan, Trp[51], are poised for potential interactions with the scissile methene bridge and with the vinyl groups. To examine the possible roles of these residues in PpIX degradation, we compared the reaction for the wild type with reactions for the W138F, W51F, W51F/W138F variants, and we also tested A142T because of its relation to the polymorphic variation at the analogous position (A/T147) in *Homo sapiens* TSPO1 (*Hs*TSPO1). We used the sensitive PpIX fluorescence spectrum (27, 28) to monitor the changes.

The prominent fluorescence features of free PpIX were shifted slightly and quenched appreciably (~30%) upon interaction with wild-type (WT) *Bc*TSPO, and these features disappeared within minutes during light exposure (Fig. 3, C and D). Preincubation with saturated PK11195 slowed the decay of PpIX greatly (Fig. 3D) but did not block it entirely. As for *Cf*TSPO, the W138F mutant of *Bc*TSPO greatly reduced the catalytic degradation of PpIX compared with the WT protein (Fig. 3, E and F); however, in this case, the degradation was not abolished altogether. For the W51F mutant, we saw no evidence of the product formed by WT and W138F *Bc*TSPO. Instead, we observed a rich fluorescence spectrum (Fig. 3, G and H) with new peaks growing at 649 and 673 nm as the primary peak at 632 nm decreased. We attribute the new peaks to secondary excited states, probably due to incipient photooxidation (29). These states are intrinsic to PpIX (fig. S8, A and B) but stabilized by TSPO (Fig. 3G and fig. S8C) and reversed on PpIX dis-

sociation (fig. S8, D and E). We conclude that Trp[51] is essential for PpIX cleavage and that Trp[138] participates in the reaction.

Neither the W51F/W138F double mutant nor the A142T showed any PpIX cleavage, but each generated reversible excitation at 673 nm as the primary 632-nm fluorescence decreased (Table 1 and fig. S9, A to D). To test for the greater generality of TSPO-mediated PpIX reactions, we produced various eukaryotic TSPO homologs. Among these we have been able to extract and purify three vertebrate proteins: *Xenopus tropicalis* TSPO (*Xt*TSPO), *Hs*TSPO1 A147T, and *Hs*TSPO2. From the sequences (fig. S1) considered in light of our analysis of *Bc*TSPO properties, we expected that *Xt*TSPO should degrade PpIX similarly to WT *Bc*TSPO but that the other two would show aberrant behavior. Indeed, *Xt*TSPO degraded PpIX, as monitored by our fluorescence assay, whereas both *Hs*TSPO1 (Thr[147]) and *Hs*TSPO2 (Thr[145]) showed growth of 673-nm fluorescence at the expense of 632-nm decay but no irreversible degradation (Table 1 and fig. S9, E to J). Because the latter behavior is as for *Bc*TSPO A142T, we infer that having threonine at position 142 precludes cleavage-appropriate binding of PpIX in each of them. Protein instability complicated our analysis of reaction rates for the vertebrate TSPOs.

What is the chemical basis for TSPO-mediated PpIX degradation? The intrinsic photochemistry of PpIX involves the generation of singlet oxygen $^1O_2$ and other reactive oxygen species (ROS) upon photostimulation (27–30), and it is evident from our observations that excited states of PpIX are stabilized when bound to TSPOs. Additionally, ROS interactions with tryptophan residues can generate tryptophan radicals, which are essential for the oxidation of aromatic substrates by lignin peroxidases (31). We suggest that such tryptophan radicals at Trp[51] and Trp[138] (*Bc*TSPO numbering) may be responsible for TSPO-mediated oxidation of PpIX. Radical interactions may work at a distance, and conserved Trp[31] and Trp[40] may also play a role (fig. S10). Although ROS come from light in our in vitro experiments, ROS-generating cellular processes may be responsible in vivo.

What physiological role might PpIX degradation serve? Porphyrins such as PpIX are tightly

controlled because they can generate toxic ROS, especially when excited by light. An incisive analysis of the role of TSPO in such control came in studies of oxidative stress in the moss *Physcomitrella patens* (32). Mitochondrial *Pp*TSPO1, which has catalytic residues the same as in *Bc*TSPO (fig. S1), was shown to be induced by oxidative stress from the inhibition of mitochondrial respiration, and knockout lines showed an accumulation of PpIX and ROS. In other studies, porphyrins exerted toxic effects on liver in the dark, generating hydroxyl radicals (33). Biliverdin is an oxyradical scavenger and is cytoprotective (34). We suggest that TSPO-mediated degradation of PpIX to bilindigin both reduces ROS generation and also promotes ROS neutralization.

REFERENCES AND NOTES

1. V. Papadopoulos et al., Trends Pharmacol. Sci. 27, 402–409 (2006).
2. C. Braestrup, R. F. Squires, Proc. Natl. Acad. Sci. U.S.A. 74, 3805–3809 (1977).
3. A. A. Yeliseev, S. Kaplan, J. Biol. Chem. 270, 21167–21175 (1995).
4. A. A. Yeliseev, K. E. Krueger, S. Kaplan, Proc. Natl. Acad. Sci. U.S.A. 94, 5101–5106 (1997).
5. A. G. Mukhin, V. Papadopoulos, E. Costa, K. E. Krueger, Proc. Natl. Acad. Sci. U.S.A. 86, 9813–9816 (1989).
6. A. Verma, J. S. Nye, S. H. Snyder, Proc. Natl. Acad. Sci. U.S.A. 84, 2256–2260 (1987).
7. V. Papadopoulos, W. L. Miller, Best Pract. Res. Clin. Endocrinol. Metab. 26, 771–790 (2012).
8. N. Rosenberg, O. Rosenberg, A. Weizman, L. Veenman, M. Gavish, J. Bioenerg. Biomembr. 45, 333–341 (2013).
9. V. Papadopoulos et al., Steroids 62, 21–28 (1997).
10. L. N. Tu et al., J. Biol. Chem. 289, 27444–27454 (2014).
11. G. Wendler, P. Lindemann, J. J. Lacapère, V. Papadopoulos, Biochem. Biophys. Res. Commun. 311, 847–852 (2003).
12. C. Ginter, I. Kiburu, O. Boudker, Biochemistry 52, 3609–3611 (2013).
13. L. Veenman, M. Gavish, W. Kugler, Anticancer. Agents Med. Chem. 14, 559–577 (2014).
14. F. M. Lartey et al., Mol. Imaging Biol. 16, 109–117 (2014).
15. T. Zhou, Y. Dang, Y.-H. Zheng, J. Virol. 88, 3474–3484 (2014).
16. T. Ruksha, M. Aksenenko, V. Papadopoulos, Arch. Dermatol. Res. 304, 839–845 (2012).
17. W. C. Kreisl et al., Brain 136, 2228–2238 (2013).
18. X. Qi, J. Xu, F. Wang, J. Xiao, Oxid. Med. Cell. Longev. 2012, 162934 (2012).
19. R. Rupprecht et al., Nat. Rev. Drug Discov. 9, 971–988 (2010).
20. F. Delavoie et al., Biochemistry 42, 4506–4519 (2003).
21. D. R. Owen et al., J. Cereb. Blood Flow Metab. 32, 1–5 (2012).
22. R. Mizrahi et al., J. Cereb. Blood Flow Metab. 32, 968–972 (2012).
23. V. M. Korkhov, C. Sachse, J. M. Short, C. G. Tate, Structure 18, 677–687 (2010).
24. Ł. Jaremko, M. Jaremko, K. Giller, S. Becker, M. Zweckstetter, Science 343, 1363–1366 (2014).
25. F. Li, J. Liu, Y. Zheng, R. M. Garavito, S. Ferguson-Miller, Science 347, 555–558 (2015).
26. Single-letter abbreviations for the amino acid residues are as follows: A, Ala; C, Cys; D, Asp; E, Glu; F, Phe; G, Gly; H, His; I, Ile; K, Lys; L, Leu; M, Met; N, Asn; P, Pro; Q, Gln; R, Arg; S, Ser; T, Thr; V, Val; W, Trp; and Y, Tyr.
27. A. Marcelli, I. Jelovica Badovinac, N. Orlic, P. R. Salvi, C. Gellini, Photochem. Photobiol. Sci. 12, 348–355 (2013).
28. S. Jockusch, C. Bonda, S. Hu, Photochem. Photobiol. Sci. 13, 1180–1184 (2014).
29. G. S. Cox, D. G. Whitten, J. Am. Chem. Soc. 104, 516–521 (1982).
30. J. Dalton, C. A. McAuliffe, D. H. Slater, Nature 235, 388 (1972).
31. R. Pogni et al., J. Biol. Chem. 281, 9517–9526 (2006).
32. W. Frank et al., Plant J. 51, 1004–1018 (2007).

33. J. C. Koningsberger et al., Eur. J. Clin. Invest. **23**, 716–723 (1993).
34. J.-A. Farrera et al., Bioorg. Med. Chem. **2**, 181–185 (1994).

PROTEIN STRUCTURE

Crystal structures of translocator protein (TSPO) and mutant mimic of a human polymorphism

Fei Li, Jian Liu, Yi Zheng,* R. Michael Garavito, Shelagh Ferguson-Miller†

The 18-kilodalton translocator protein (TSPO), proposed to be a key player in cholesterol transport into mitochondria, is highly expressed in steroidogenic tissues, metastatic cancer, and inflammatory and neurological diseases such as Alzheimer's and Parkinson's. TSPO ligands, including benzodiazepine drugs, are implicated in regulating apoptosis and are extensively used in diagnostic imaging. We report crystal structures (at 1.8, 2.4, and 2.5 angstrom resolution) of TSPO from Rhodobacter sphaeroides and a mutant that mimics the human Ala[147]→Thr[147] polymorphism associated with psychiatric disorders and reduced pregnenolone production. Crystals obtained in the lipidic cubic phase reveal the binding site of an endogenous porphyrin ligand and conformational effects of the mutation. The three crystal structures show the same tightly interacting dimer and provide insights into the controversial physiological role of TSPO and how the mutation affects cholesterol binding.

The 18-kD translocator protein (TSPO) was first discovered as a receptor for benzodiazepine drugs in peripheral tissues and is implicated in transport of cholesterol into mitochondria, the first and rate-limiting step of steroid hormone synthesis (1, 2). TSPO is also a major research focus due to its apparent involvement in a variety of human diseases (3–5). Of particular interest is a human single-nucleotide polymorphism [rs6971 = Ala[147]→Thr[147] (A147T) (6)] in a region of TSPO that is highly conserved between mammals and bacteria. The mutation is associated with diminished cholesterol metabolism (7), altered ligand binding to TSPO (8), and increased incidence of anxiety-related disorders in humans (9–11). Some understanding of how this mutation affects TSPO function has come from studies involving positron emission tomography (PET), which uses ligands of TSPO as sensitive imaging agents for detecting areas of inflammation in the brain (12). A lower binding affinity toward TSPO-specific PET ligands

and an increased incidence of several neurological diseases correlate directly with the presence and dosage of the allele harboring the A147T mutation (9–11). This indicates that the TSPO mutation is responsible for the observed phenotypes, but it remains unclear how this mutation in TSPO alters cholesterol metabolism or how it is related to multiple neurological diseases.

Translocator protein from Rhodobacter sphaeroides (RsTSPO) has a 34% sequence identity with the human protein (fig. S1) and is the best-characterized bacterial homolog in the extensive TSPO family (13–15). Functional and mutational studies in R. sphaeroides show that RsTSPO is involved in porphyrin transport, as also reported in human (16), and in regulating the switch from photosynthesis to respiration in response to increased oxygen (13, 17, 18). The knock-out phenotype in R. sphaeroides can be rescued by the rat homolog (17), indicating conserved functional properties between bacterial and mammalian organisms and establishing the value of R. sphaeroides, a close living relative of the mitochondrion (19), as a model system to investigate structure-function relationships in TSPO.

The human mutation, A147T, is one helical turn preceding the cholesterol recognition consensus sequence (CRAC) identified as a cholesterol bind-

ing site in TSPO (20), suggesting that altered cholesterol binding could be involved. To test this hypothesis, the corresponding mutation, A139T, was created in RsTSPO, and the binding properties of the purified protein were compared with those of the wild type. The observed lower binding affinity (four- to fivefold) for cholesterol and PK11195, as well as protoporphyrin IX (PpIX) (Fig. 1A), is consistent with the phenotypic behavior of the human A147T polymorphism (7, 8), further confirming RsTSPO as a valuable model system and providing strong evidence of a functional defect caused by the mutation.

In line with these observations, crystal structures of the wild type (at 2.5 Å resolution) and the A139T mutant (at 1.8 and 2.4 Å resolution) show substantial differences within the CRAC site and conformational changes that alter the structural environment within a potential ligand binding region. Although crystallized in three different space groups (fig. S2), all RsTSPO structures show an identical "parallel" dimer formed from compact monomers composed of five transmembrane helices (Fig. 1, B and C). The residues within the CRAC site and surrounding the mutation are clearly resolved in all structures, including the wild-type (WT) protein and the A139T mutant (fig. S3 and table S1), providing the molecular basis for understanding the effect of this mutation.

The dimer interface (Fig. 2) is primarily composed of 37 residues, contributed by transmembrane helices TM-III (16 residues), TM-I (12 residues), and TM-IV (3 residues) and covers ~1250 Å² (~15% of a monomer's surface area). The tight interface, unaltered by the mutation, is quite flat but displays two notable features. First, TM-III forms the central core of the hydrophobic interface, which is dominated by alanines and leucines, and reveals a G/A-xxx-G/A motif, which favors helical dimerization (21). Second, the central core of the interface is devoid of hydrogen interactions; the five observed hydrogen bonds are at the periphery between TM-I and TM-III. The tight fit suggests that the dimer interface is not likely to be a transport pathway (14). The biological relevance of a TSPO dimer is not well understood, but previous studies show that RsTSPO forms a stable dimer in detergent solution (14), and a similar dimeric structure is observed in the low-resolution cryo–electron microscopy (EM) structure (15) (fig. S4). Taken together, the dimer observed in these crystals is likely to be the primary structural and functional

Department of Biochemistry and Molecular Biology, Michigan State University, East Lansing, MI 48824, USA.
*Present address: Skaggs School of Pharmacy and Pharmaceutical Sciences, University of California, San Diego, La Jolla, CA 92093, USA. †Corresponding author. E-mail: fergus20@msu.edu
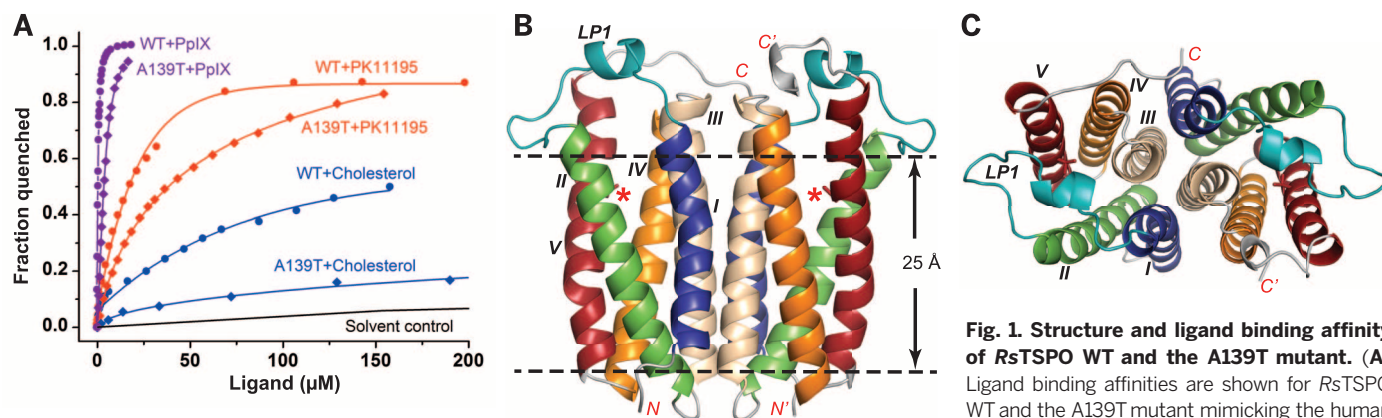
Fig. 1. Structure and ligand binding affinity of *Rs*TSPO WT and the A139T mutant. (**A**) Ligand binding affinities are shown for *Rs*TSPO WT and the A139T mutant mimicking the human A147T mutation. Dissociation constant (K_d) values are obtained as described in (*24*): 10 ± 1 μM for PK11195 with WT, 42 ± 4 μM with A139T; 0.3 ± 0.01 μM for PpIX with WT, 1.9 ± 0.3 with A139T; and ~80 μM for cholesterol with WT, >300 μM with A139T. WT data are from (*14*), reproduced for comparison. (**B**) Overall structure of the A139T dimer. The position of the A139T mutation is labeled with a red asterisk and shown in sticks; the five transmembrane helices (TM-I to TM-V) are colored blue, green, wheat, orange, and red, respectively; and loop 1 (LP1) is colored teal. (**C**) Top view of (B). *Rs*TSPO A139T crystallized in two different space groups (C2 and P2₁2₁2₁) that have identical overall structures except for the flexible C terminus, whereas WT crystallized in a P2₁ space group. In all three crystal forms, the identical parallel dimer of *Rs*TSPO was observed (Fig. 2). The A139T mutant in the C2 space group is shown here and used to discuss the major structural features of *Rs*TSPO, as it has the highest resolution and most complete structure of *Rs*TSPO. The N and C termini are labeled N/N′ and C/C′, respectively; the dashed lines highlight the approximate membrane region.
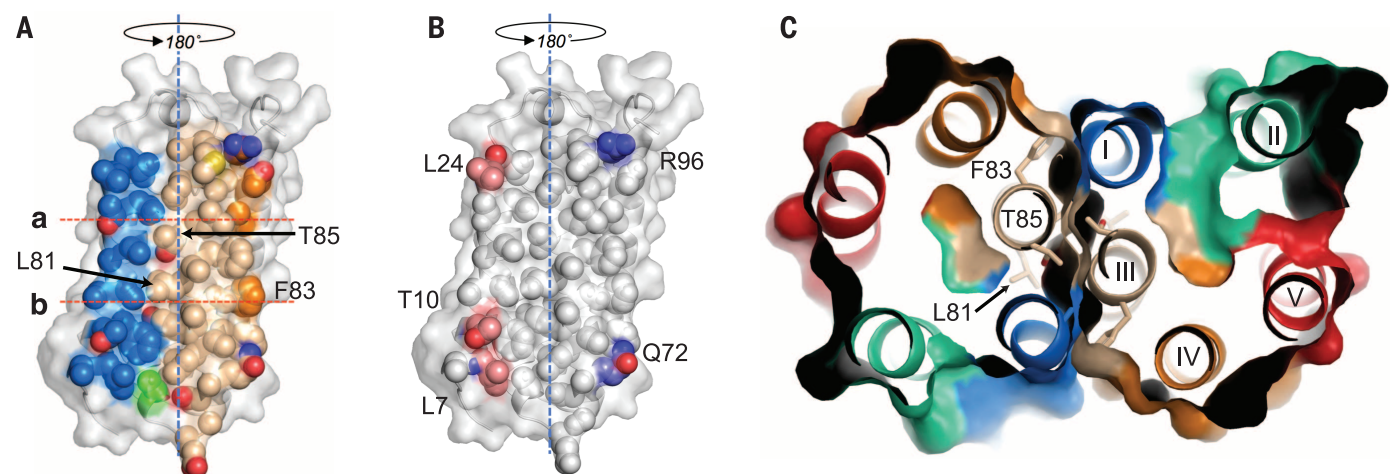
Fig. 2. Analysis of the dimer interface. (**A**) The dimer interface is primarily made up of TM-I and TM-III. Helices are colored the same as in Fig. 1 (blue, TM-I; gold, TM-III; orange, TM-IV) but are shown as space-filling models. TM-II and TM-IV make only minor contributions to the interface. Rotating the monomer by 180° about the dyad axis (blue dashed line) and overlaying it on top of itself creates the dimer. (**B**) Hydrophobic (white) and hydrogen bonding residues (blue, hydrogen bond donor atoms; red, hydrogen bond acceptor atoms) within the dimer interface. (**C**) Top view of a slab [between lines a and b in (A)]; residues forming strong interactions in the core of the dimer interface are labeled. The interface is essentially identical in all WT and A139T structures.

unit of *Rs*TSPO. How the *Rs*TSPO dimer is oriented in the *Rhodobacter* outer membrane is not well established and awaits further study.

Recently, a nuclear magnetic resonance (NMR) structure of the mouse TSPO (mTSPO) was determined in the presence of dodecylphoscholine (*22*). A monomeric species is observed with the same topology as the monomers in the crystal structures. However, the helices display substantial shifts in position and orientation relative to each other such that the overall tertiary structure is quite different (fig. S5). The major shifts in helix alignment in the NMR structure, particularly regarding TM-III, would markedly affect the dimer interface. Unlike the crystal structures, a stable tertiary structure for mTSPO is only achieved in

the presence of PK11195 at a roughly fivefold molar excess, which may account for the distinctively different conformation observed.

The structural differences between the WT and A139T proteins (Fig. 3 and fig. S6) are consistent with their differing ligand binding affinities (Fig. 1A). Superposition of the Cα atoms in the N-terminal side of each helix yields root mean square deviations of less than 0.3 Å. All of the major structural differences occur in the C-terminal side of the monomer, with helices TM-II and TM-V and loop 1 (LP-1) showing the most dramatic changes. TM-II tilts by 7.7° toward TM-V in the mutant structure, whereas TM-V becomes less kinked as the C-terminal portion of the helix straightens by 6.3°. This results in a closer asso-

ciation of TM-II and TM-V (Fig. 3A). TM-IV also shifts in concert with TM-V. In addition, the A139T mutation results in the movement and side-chain repositioning of F46 on TM-II, and L142 and F144 on TM-V, two of the critical residues of the CRAC (*20*) motif. The highly conserved W135 on TM-V is also flipped, resulting in a closer proximity to W50 on TM-II (Fig. 3B). These changes result in a substantially narrower gap between TM-II and TM-V in the A139T structure (fig. S7) and an altered surface in the CRAC region that may account for altered cholesterol and ligand binding.

The relatively long linker LP1, which connects TM-I and TM-II (Fig. 1, B and C), is the only long loop in the entire structure and is proposed to play a role in ligand binding based on mutagenesis
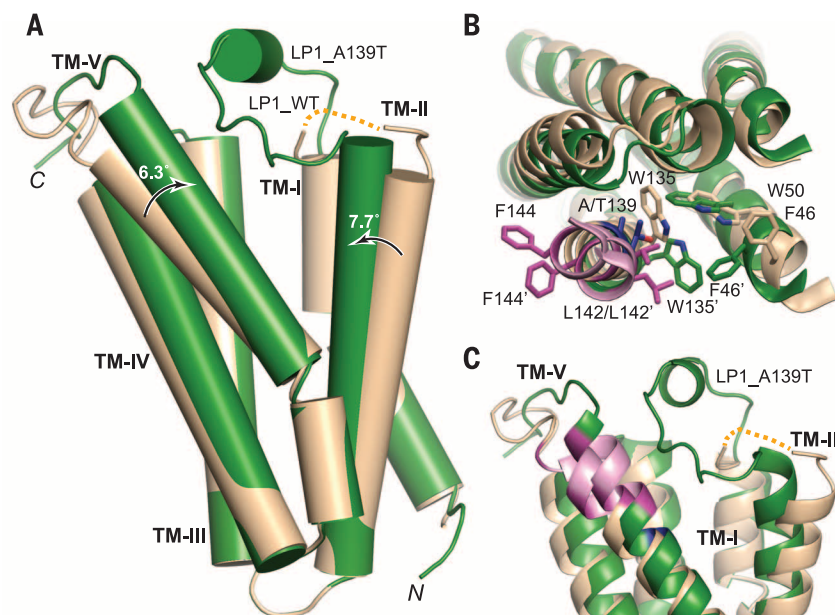
Fig. 3. Structural comparison of WT and A139T RsTSPO. Monomers of the WT (wheat) and A139T (green) are overlaid. (**A**) Overall structural alignment that highlights the degree and direction (arrows) of conformation change from WT to A139T for TM-II and TM-V. (**B**) Top view of the monomer, highlighting the side-chain rearrangements in sticks. Residue 139 is colored in blue; the CRAC site is colored in pink with two of three proposed critical residues (L142 and F144) highlighted in magenta. The prime symbol designates the mutant position. (**C**) Close-up side view of the potential ligand binding cavity, which reveals major differences in the conformations of LP1, TM-II, and TM-V between the WT and mutant proteins (fig. S7). The dotted yellow line denotes the location of unresolved LP1 in the WT structure (residues 29 to 40).

studies (2, 13). Within the loop is a short helical segment (residues 29 to 33) in monomers A and B of A139T in both C2 and P2₁2₁2₁ crystal forms; in monomer C of the C2 form, the helical segment is unwound and results in a more extended LP1 (fig. S6). Although the LP1 is not completely resolved in the WT structure, its configuration is quite distinct from that of the mutant (Fig. 3C). As the RsTSPO structures determined here display three different well-resolved conformations of LP1 (fig. S6), this loop may exist in several defined states, consistent with the hypothesis that structural changes in LP1 play an important role in regulation of ligand binding and the functions of TSPO (2). Similarly, the 10 residues at the C terminus of TM-V take on several different conformations (fig. S6) that may also relate to different ligand binding states (23).

Ligands bind to RsTSPO less strongly than to the human protein (14), but RsTSPO still displays affinities for PpIX, PK11195, and cholesterol in the high nanomolar to micromolar range (14). Cholesterol was added to the crystallization medium, along with PK11195, but neither ligand was resolved, even though their addition did improve the quality of RsTSPO crystals (24). In monomer A of the A139T structure, a cavity between TM-I and TM-II and underneath LP1 contained electron density that did not fit any of the known components in the crystallization medium. However, it did correspond to the size and shape of a porphyrin ring (Fig. 4A). As porphyrins are proposed natural ligands for RsTSPO (13), and purified RsTSPO binds porphyrins tightly in vitro (14, 15), we identify the ligand in the A139T mutant as a porphyrin compound that copurifies with the protein (fig. S8, A and B).

Lipids and considerable amounts of monoolein are observed in all three structures. The monooleins, which are primary components of the cubic-phase crystallization medium, most likely displace native lipids that would occupy the grooves
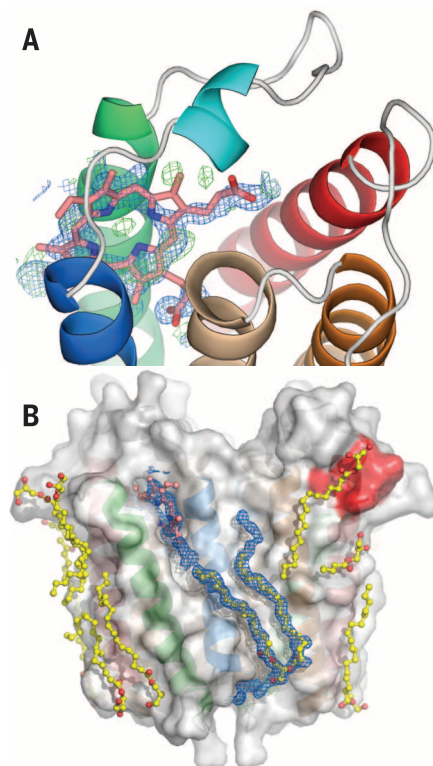
Fig. 4. Ligand binding and evidence for a transport pathway. Close-up view of the porphyrin binding site (**A**) with a porphyrin (pink) overlaid with feature enhanced map (FEM) omit map electron density (blue) and $F_o - F_c$ difference electron density (green), contoured at 1σ and ±3σ, respectively. A partially oxidized porphyrin is suggested by the spectrum (fig. S8A) that shows absence of a Soret band. (**B**) Surface groves on TSPO are occupied by monooleins and phospholipid (yellow). The CRAC site (red) is also interacting with lipids. Unusually long FEM omit map electron density (in blue and contoured at 1.0σ) extends from the porphyrin binding site to the bottom surface of the protein, beyond the bound phospholipid, suggesting an external transport pathway that involves both monomers of the dimer (see also fig. S9).

on the protein's surface (25), but the locations also provide insights into possible lipid and ligand binding sites. The polar head groups of the monooleins are observed in the porphyrin binding site in several monomers, whereas their lipidic tails lie along the surface grooves (fig. S8, C and D). The length of the electron density observed along several surface grooves in A139T is substantially longer than any known components of the crystallization conditions or *Escherichia coli* lipids (Fig. 4B and fig. S9), implying a continuous path occupied by several ligands or lipids bound

in different positions. These observations suggest a possible sliding mechanism of transport (Fig. 4B and fig. S9E), similar to maltoporin (26) but on the external protein surface. Such a transport pathway would require the association of TSPO with itself or other protein partners. In fact, StAR and VDAC have been reported to associate with TSPO in a cholesterol transport complex (1), whereas oligomerization of mouse TSPO has been observed (27). The EM structure and the crystal-packing arrangements (fig. S4) also suggest possibilities for homo-oligomerization of the TSPO

dimer. Models for TSPO-mediated ligand transport are somewhat constrained by the dimeric structure seen in *Rs*TSPO crystals, making unlikely an internal pore-like transport mechanism (*28*) through the monomer or transport via the tight dimer interface (*14*). Thus, an external surface-transport mechanism appears worthy of further investigation.

Based on the structures of *Rs*TSPO, WT, and A139T determined in this study and current understanding of TSPO function, we propose that the phenotype of the A147T mutation in humans arises from altered cholesterol binding and transport caused by the perturbed environment around the CRAC site, which modifies the binding surface for cholesterol. Concurrently, the changes in the tilt of the helices give rise to reduced binding of other ligands, suggesting that the A147T mutation overall favors a lower-affinity conformation. A proposed external surface-transport mechanism that probably requires protein partners is consistent with the complex functional and regulatory properties of this ancient multifaceted protein (*29–32*).

REFERENCES AND NOTES

1. J. Fan, V. Papadopoulos, *PLOS ONE* **8**, e76701 (2013).
2. J. Fan, P. Lindemann, M. G. Feuilloley, V. Papadopoulos, *Curr. Mol. Med.* **12**, 369–386 (2012).
3. J. L. Bird *et al.*, *Atherosclerosis* **210**, 388–391 (2010).
4. M. Hardwick *et al.*, *Cancer Res.* **59**, 831–842 (1999).
5. B. Ji *et al.*, *J. Neurosci.* **28**, 12255–12267 (2008).
6. Single-letter abbreviations for the amino acid residues are as follows: A, Ala; C, Cys; D, Asp; E, Glu; F, Phe; G, Gly; H, His; I, Ile; K, Lys; L, Leu; M, Met; N, Asn; P, Pro; Q, Gln; R, Arg; S, Ser; T, Thr; V, Val; W, Trp; and Y, Tyr.
7. B. Costa *et al.*, *Endocrinology* **150**, 5438–5445 (2009).
8. D. R. Owen *et al.*, *J. Cereb. Blood Flow Metab.* **32**, 1–5 (2012).
9. A. Colasanti *et al.*, *Psychoneuroendocrinology* **38**, 2826–2829 (2013).
10. K. Nakamura *et al.*, *Am. J. Med. Genet. B. Neuropsychiatr. Genet.* **141B**, 222–226 (2006).
11. B. Costa *et al.*, *Psychiatr. Genet.* **19**, 110–111 (2009).
12. W. C. Kreisl *et al.*, *J. Cereb. Blood Flow Metab.* **33**, 53–58 (2013).
13. A. A. Yeliseev, S. Kaplan, *J. Biol. Chem.* **275**, 5657–5667 (2000).
14. F. Li, Y. Xia, J. Meiler, S. Ferguson-Miller, *Biochemistry* **52**, 5884–5899 (2013).
15. V. M. Korkhov, C. Sachse, J. M. Short, C. G. Tate, *Structure* **18**, 677–687 (2010).
16. S. Zeno *et al.*, *Curr. Mol. Med.* **12**, 494–501 (2012).
17. A. A. Yeliseev, K. E. Krueger, S. Kaplan, *Proc. Natl. Acad. Sci. U.S.A.* **94**, 5101–5106 (1997).
18. A. A. Yeliseev, S. Kaplan, *J. Biol. Chem.* **274**, 21234–21243 (1999).
19. C. Esser, W. Martin, T. Dagan, *Biol. Lett.* **3**, 180–184 (2007).
20. H. Li, V. Papadopoulos, *Endocrinology* **139**, 4991–4997 (1998).
21. D. T. Moore, B. W. Berger, W. F. DeGrado, *Structure* **16**, 991–1001 (2008).
22. L. Jaremko, M. Jaremko, K. Giller, S. Becker, M. Zweckstetter, *Science* **343**, 1363–1366 (2014).
23. R. Farges *et al.*, *Mol. Pharmacol.* **46**, 1160–1167 (1994).
24. Materials and methods are available as supplementary materials on *Science* Online.
25. L. Qin, C. Hiser, A. Mulichak, R. M. Garavito, S. Ferguson-Miller, *Proc. Natl. Acad. Sci. U.S.A.* **103**, 16117–16122 (2006).
26. R. Dutzler, T. Schirmer, M. Karplus, S. Fischer, *Structure* **10**, 1273–1284 (2002).
27. F. Delavoie *et al.*, *Biochemistry* **42**, 4506–4519 (2003).
28. J. J. Lacapère, V. Papadopoulos, *Steroids* **68**, 569–585 (2003).
29. J. Gatliff, M. Campanella, *Curr. Mol. Med.* **12**, 356–368 (2012).
30. A. M. Scarf *et al.*, *Curr. Mol. Med.* **12**, 488–493 (2012).
31. R. Rupprecht *et al.*, *Nat. Rev. Drug Discov.* **9**, 971–988 (2010).
32. K. Morohaku *et al.*, *Endocrinology* **155**, 89–97 (2014).

This is the start of something big.

Science Advances | AAAS

SIGNIFICANT RESEARCH, GLOBAL IMPACT

Introducing _Science Advances_ – the new, online-only, open-access journal from _Science_ and AAAS. Find out how you can be among the first authors published at **scienceadvances.org.**

5 μm Particle Size Column

5 μm particle size Aeris PEPTIDE core-shell columns enable higher efficiencies and higher loading capability for small-scale peptide purification in 10 mm ID semi-prep columns and 21.2 mm ID Axia-packed prep columns. Aeris PEPTIDE is fully scalable over four particle sizes—1.7 μm, 2.6 μm, 3.6 μm, and 5 μm—enabling easy method transfer from analytical high-performance liquid chromatography (HPLC) and UHPLC to preparative applications. Aeris PEPTIDE is ideal for biomolecule separations in pharmaceutical and life science applications. The Phenomenex Axia preparative format delivers longer column lifetime, higher efficiencies, improved performance, and high reproducibility, compared to conventionally packed columns for lab-scale preparative chromatography.

Phenomenex
For info: 310-212-0555
www.phenomenex.com

Multiphoton Excitation Objectives

Dedicated to multiphoton excitation microscopy, Olympus introduces its XLPLN10XSVMP and XLSLPLN25XGMP objective lenses with an 8 mm working distance and support for a large range of refractive indices. The objectives enable super-deep imaging of tissues treated with the latest clearing agents as well as live-cell imaging and light sheet microscopy techniques. Compatible with the industry leading FVMPE-RS and FV1200MPE multiphoton microscopy systems and easily adaptable to home-build light sheet microscopes, the new objectives boast a range of features providing important benefits to researchers. Both objectives offer super-long working distances of 8 mm, providing the capability and space for structural and live-cell imaging deep within large intact samples. A high transmittance range of 400–1,600 nm extending into the infrared spectrum allows deeper imaging with minimal damage to the tissue, and is well-suited to combine conventional multicolor MPE imaging with label-free methods like third- and second-harmonic generation.

Olympus
For info: +49-40-23773-5913
www.olympus-europa.com/microscopy

Cardiomyocyte Measurement Platform

The xCELLigence RTCA CardioECR System combines impedance and Multi Electrode Array (MEA) technology with a pacing function. RTCA CardioECR is the first platform to allow simultaneous cardiomyocyte contractility and field potential measurement. The system is designed to be placed in a standard tissue culture incubator with physiological temperature, CO_2 level, and humidity, allowing better controlled assays with both short-term and long-term measurements in real-time. With the added MEA capabilities and pacing stimuli, the new CardioECR System allows for a deeper assessment of mechanisms of toxicity. Field potential recording provided by MEA electrodes is a measure of the integrated ion channel activity that may be impacted by the tested compound, whereas the pacing function allows for controlling the rate of contractility for a more controlled assay. Furthermore, this combined dual readout system also provides a longer-term measurement of cardiomyocyte viability which can potentially identify those compounds causing longer-term structural damage to cardiomyocytes.

ACEA Biosciences
For info: 866-308-2232
www.aceabio.com/cardioecr

SPE Microplate

The Development Microlute is a Solid Phase Extraction (SPE) microplate which provides a wide assortment of phase chemistries and sorbent loadings in a single plate making it ideally suited for method development. Offering scientists a choice of up to 12 different phases and sorbent loadings (10–100 mg) in a standard format 96-well plate, the Development Microlute allows you to simply and rapidly screen for the optimal retention and selectivity required to achieve your sample preparation objectives. The Development Microlute has been designed to provide all the advantages of automated and high throughput SPE sample preparation in a convenient microplate format capable of rapidly processing 96 samples in one go, repeatedly and precisely. Constructed from a single piece of molded high-quality polypropylene, a Development Microlute plate will not bend or distort because individual SPE cartridges do not have to be repeatedly plugged in and out.

Porvair Sciences
For info: +44-(0)-1978-666239
www.porvair-sciences.com

Gel Electrophoresis Units

The MultiSUB range of horizontal gel electrophoresis units includes a comprehensive choice of optimized units for low and high throughput DNA and RNA applications. Each unit provides an easy-to-use, versatile, and flexible system that can evolve and adapt with the changing needs of today's laboratory researcher. All five units in the Cleaver MultiSUB gel electrophoresis range deliver an unsurpassed combination of economy of gel and buffer volume, with gel size, and sample number versatility. Gel size and sample number requirements can be exactly matched in each unit, with the option of additional gel tray sizes. All units feature removable ultraviolet transparent trays. For optimum value and versatility, systems are available with one, two, or three tray options. Easy-to-use, leak-proof "plug and go" gel casting dams are included as standard to allow gels to be rapidly cast whilst the multiSUB unit is in use for gel running.

Cleaver Scientific
For info: +44-(0)-1788-565300
www.cleverscientific.com

Electronically submit your new product description or product literature information! Go to www.sciencemag.org/products/newproducts.dtl for more information.

Newly offered instrumentation, apparatus, and laboratory materials of interest to researchers in all disciplines in academic, industrial, and governmental organizations are featured in this space. Emphasis is given to purpose, chief characteristics, and availability of products and materials. Endorsement by *Science* or AAAS of any products or materials mentioned is not implied. Additional information may be obtained from the manufacturer or supplier.

Webinar

Now Available for On-Demand Viewing!
Recorded Live On: November 19, 2014

Improving Characterization of Monoclonal Antibodies
Making a Better Biotherapeutic

During the webinar, viewers will:

- Gain a deeper understanding of the factors important in biotherapeutic protein production and characterization

- Learn the fundamentals of microfluidics-based capillary electrophoresis

- Hear how microchip-CE can speed protein analysis, particularly in the drug development pipeline.

Characterization of therapeutic proteins remains labor-intensive and time consuming due to their often complex and heterogeneous structure. This has led to a concerted effort within the biotechnology and biopharmaceutical industry to address these bottlenecks as a means to boost the development of more biotherapeutics. Studies in this vein, such as testing the effect of various cell culture conditions on posttranslational modifications or monitoring the purification process of recombinant proteins, produce large numbers of samples that can easily exceed the capacity of modern analytical laboratories. High throughput analytical platforms with high precision, automation, and ease-of-use are therefore in great demand. To this end, the use of microfluidic analytical platforms such as microchip capillary electrophoresis (CE) have greatly increased the efficiency and reproducibility needed for analyzing proteins intended for therapeutic use. In this webinar, our expert panelists will discuss posttranslational modifications and quality assessment of biotherapeutic proteins for biopharmaceutical development using microfluidic-CE characterization.

View Now! webinar.sciencemag.org

Speakers

Niomi Peckham
Alexion Pharmaceuticals
Cheshire, Connecticut

I-Jane Chen, Ph.D.
PerkinElmer
Hopkinton, MA

Faculty: Making Your Research Count

Managing an academic research group means keeping an eye on the big picture—long-term goals, funding agency priorities, and a publication plan. Faculty members are also charged with training students and postdoctoral fellows. To meet these dual demands, principal investigators must match people to projects in way that gets the group to its goals while encouraging its members to mature as scientists. Faculty members don't usually get formal training in research program management, but that might be changing. **By Chris Tachibana**

When **Robin Wright** was a new professor, her approach to setting up her research group was "kind of organic." She considered how many postdocs, students, and technicians she needed when writing a grant, but once funded, she says, "I just got the best people I could and assumed we were all equals and everyone, including me, would do everything, including the dishes." The strategy worked. Wright is now University of Minnesota associate dean of biological science administration and is starting CourseSource, an online science education journal. But if she launched a new research program again, she says, "I'd be more intentional in thinking about how people would fit into the group, what they'd bring personality-wise and skill-wise. I'd be more proactive about recruiting promising students from my classes."

Traditional research training doesn't cover developing an intentional management strategy. Although we have some excellent science career guides, we don't have extensive formal literature on research planning, says Wright, but we could learn from management studies. "When I was starting as a professor, I never thought of reading the literature on teamwork," she says, "but there's science behind team building that could make people in your lab happier and more productive."

Producing mature scientists—and publications

Biology professor **Malcolm Campbell** has given a lot of thought to strategic research planning. He powers his genomic and synthetic biology projects solely with undergraduates at Davidson College in North Carolina, which has about 2,000 students. Ideally, says Campbell, students work as full-time summer researchers after their first year, after going through an application process that includes recommendations and interviews. Undergraduate researchers are much more productive in the summer than during the school year, when they have to plan experiments around classes and academic breaks, says Campbell. After training in his group, he encourages students to get experience working in large research institutions in subsequent summers.

Campbell uses an American football analogy to describe his approach to project planning. "If you imagine a full project as 100 yards, I might give students 10-yard subprojects that are designed so that even if they only get a few yards, they don't have to punt, they've still accomplished something that could be a poster or presentation." For overall program planning, Campbell, who has bioinformatics collaborations with Davidson Mathematics Professor **Laurie Heyer**, uses a computing analogy: parallel processing. "We never have students competing," he says, "but sometimes they work on something, like cloning a gene, using different methods. Whoever gets it first, we all celebrate together and move on." At the same time, Campbell lets students design, order reagents for, and troubleshoot their own projects, to give them independence. "Sometimes you nurture and sometimes you let them flounder on their own," he says, "for a rich learning experience."

Campbell says filling the lab with students with diverse backgrounds and experiences creates synergy. The bioinformatics projects spur math students to take biology and biology students to take computer science. Paradoxically, having more students in the lab is easier than having a few. "Having eight students is less work than having three," he says, "because the students start relying on and training each other." Having an office within earshot of the lab helps, says Campbell, because he hears students debating questions. As long as they are on the right track, he lets them work out problems on their own.

Of course, funding is the cornerstone of a successful research program that also trains early career scientists. Campbell's strategy of guiding students from laboratory novice to potential graduate student begins with paying students as summer researchers. He suggests that faculty apply to government agencies such as the National Science Foundation Research in Undergraduate Institutions, and private sources such as the Beckman Foundation, the Waksman Foundation for Microbiology, and Sigma Xi.

Funding also affects program planning with Ph.D. students. In many U.S. graduate programs,

Upcoming Features

Postdocs—February 27   ■   *Regional Focus: Japan—March 27*   ■   *Postdocs—August 28*

students rotate through several groups before choosing their thesis advisor. For graduate students in other systems, for example at European universities, funding is for a limited time for a specific project, and deadlines are strict.

Professor **Laura Machesky**, Beatson Institute for Cancer Research in Glasgow, says her students have only a few years of support. Fortunately, they often arrive with undergraduate research experience or possibly a Master's degree. Her clinical fellows, who come in with an M.D., have three years to earn a Ph.D. "I tell them at two years and six months, you have to start writing your thesis now," she says. The funding scheme leaves no time for failure, so Machesky often starts Ph.D. students on several experiments, saying, "Some are safe, so that even if the results are negative, we can probably publish them." An example is changing a gene's expression and asking if a phenotype changes. For a challenge, says Machesky, "I also give them something more open-ended." To develop independence, Machesky likes people in her lab to follow the occasional hunch. "Do an experiment I don't know about," she says. "You can tell me later if it works out."

In distributing projects, Machesky considers the amount of supervision a person will need. Undergraduates or Master's students might be initially paired with a senior scientist. Postdoctoral and especially clinical fellows are treated as colleagues. "I give them credit for their training and let them guide their projects. It's a partnership in which the clinicians see how basic research is done and how it applies to their work, and our senior scientists explain to physicians why their research is relevant." For these more experienced scientists, says Machesky, "the project has to let them to be creative: to think about where it's going and how to get there, to take ownership."

Ownership of projects is what Campbell develops in undergraduates and Machesky promotes in graduate students and senior scientists. It is what **Martin Chalfie**, professor of biological sciences at Columbia University, looks for in his lab personnel. "Especially postdocs," he says, "should come in as a colleague. They should write their own proposal about what the next experiments should be or what new skill they'll bring to the field. People are more excited about and committed to projects they thought of on their own." Even with graduate students, says Chalfie, "I don't assign projects. I ask people what they are interested in." If he wanted a specific experiment done, he says, he'd probably ask a technician to do it rather than assign it to a student or postdoc.

> **"There's science behind team building that could make people in your lab happier and more productive."**
> **— Robin Wright**

Chalfie says his strategy for populating the lab, generating projects, and accomplishing research goals is "flexible." People in his lab work to solve major challenges in the field of nerve cell development rather than ticking off projects listed in a grant proposal. Like Machesky, Chalfie encourages his team to be open to discovery. This is how he came to develop green fluorescent protein as a reporter for gene expression, for which he was coawarded a 2008 Chemistry Nobel Prize. "I never wrote a proposal to do that," he says. "I just got excited about it, and it was in keeping with work we were doing, so I did it. You can't be slavishly tied to a particular plan of work."

Building a strong team

At the University of Minnesota, Robin Wright's colleague **Nathan Springer** has adopted a more structured method for group management—the Strengthsfinder system. Strengthsfinder identifies personal traits such as adaptability, discipline, and responsibility, and is offered to incoming University of Minnesota students. "If people are willing to share their results," says Springer, a biology professor and director of the Microbial and Plant Genomics Institute, "I use the findings to see which parts of a project they might find easy or difficult. For example, some people are strategists and like to plan. Others are more adaptable and might need help planning their project." Springer doesn't use Strengthsfinder results to assign projects or tasks—everyone should be exposed to all aspects of research, he says. But the information might help his group be more efficient. "Sometimes students get stuck on something," he says, "and this just helps me think about what might help them."

Springer also draws on psychosocial studies that have found that "success begets success." He initially puts new students on a fairly mature project before starting their own independent work. "It lets them see what finishing a project and writing a paper looks like," says Springer. "I think learning the habits of success is better than struggling at something for a long time." And since the projects that get new students are led by senior students or postdocs, says Springer, "the other side is that the senior people get experience leading a team."

Although Springer is not convinced he has the optimal program management strategy, it aligns with current trends. Recently, four leading biomedical scientists called for more thoughtful training in their field, including giving students a broader range of skills to prepare for diverse careers, for example in industry, communications, **continued>**

Featured Participants

The Beatson Institute for
Cancer Research
www.beatson.gla.ac.uk

Columbia University
www.columbia.edu

Davidson College
www.davidson.edu

FSC Nettlecombe Court
Field Centre
www.field-studies-council.org/
centres/nettlecombecourt.aspx

Scripps Institution of
Oceanography
scripps.ucsd.edu

University of Minnesota
www.umn.edu

"Having eight students is less work than having three because the students start relying on and training each other."
— Malcolm Campbell

characteristic required for field research, says **Nicholas Lapthorn**, head of center at Field Studies Council (FSC) Nettlecombe Court. The FSC is a nonprofit organization in the United Kingdom that works with secondary schools and universities to promote environmental understanding through fieldwork. The demands of outdoor data collection, says Lapthorn, include "being able to work in rain and the cold, when it's starting to get dark, and when you're tired of walking and carrying equipment. You have to be able to solve problems onsite in a complex environment and communicate and cooperate with others." In this way, a field research team is an intense version of any research group and Lapthorn's recommendations about building an effective team and assigning tasks are universal. Research teams need diversity in skills, says Lapthorn: "Not everyone can be a leader. Dividing up roles is critical to success in teams."

Like Chalfie and Machesky, Lapthorn stresses the importance of project ownership, saying that people are most effective when they are personally invested in their project. "When students have a say over what they are investigating," he says, "they are motivated to collect data and that makes it easier for them to do the analysis later." To cultivate the qualities of resilience and personal investment in a project, Lapthorn says students should be exposed early, before college if possible, to risky, less directed science. This shows them what research is really like—that data will not always confirm expectations and might lead in unexpected directions.

Paradoxically, the best way to cultivate team flexibility, resilience, and adaptability might be careful, advanced planning by the principal investigator. Thinking ahead about how to deal with potential personnel issues, funding ups and downs, and unexpected events such as departmental changes could help a research group hold its course toward long-term goals. A well-managed research team maintains the capacity to recognize and exploit novel results.

Most science faculty members learn by doing when building and managing a research group. However, tools and resources from the management world such as Strengthsfinder and similar programs are finding their way into academic science. Some professional organizations like the American Society for Cell Biology hold workshops on project planning, grant budgeting, and human resource management. The Burroughs Wellcome Fund and Howard Hughes Medical Institute have free online scientific management training manuals (scim.ag/1zVuVQt).

Fricker says she would appreciate training in research program management such as workshops on budgeting with multiple grants. "They would especially benefit new faculty members," she says. "Some people have a natural gift for this, but not me. It would be nice to have training in easy, essential skills for managing grants and projects."

law, or policy (scim.ag/1x2XzNq). Strategies like Springer's might help faculty members think about their advisees' natural skills, to guide conversations about job options.

For some scientists, building research teams and designating projects might be a matter of survival. Professor **Helen Amanda Fricker**, Scripps Institution of Oceanography, does research that includes deep-field sample collection, for example in Antarctica. Fricker says everyone in her group eventually has to sit down at a computer and analyze their data, but they do a bit of self-sorting around the data sources. People who aren't polar explorers at heart can work on projects that use satellite data or computer modeling. When people joining Fricker's team specifically ask to collect glaciology data onsite, she tries to accommodate them. However, she says, "The people who do that work need stamina to endure the tough conditions and the work hours. Because of the long days at the poles in the summer, it's easy to forget what time it is and work past midnight. People have to be able to think on their feet and also be willing to chip in with cooking and cleaning at the campsite."

"Resilience" is the Strengthsfinder-type term for the

Chris Tachibana is a science writer based in Seattle, USA and Copenhagen, Denmark.

UCDAVIS
UNIVERSITY OF CALIFORNIA

Assistant Cooperative Extension Specialist in Rangeland Management
Department of Plant Sciences, College of Agricultural and Environmental Sciences

The Department of Plant Sciences, University of California, Davis, seeks to fill an 11-month, career-track position at the Assistant Specialist in Cooperative Extension rank.

RESPONSIBILITIES: This academic position has 100% Cooperative Extension (CE) responsibilities and will be located in the Department of Plant Sciences in the College of Agricultural and Environmental Sciences (CA&ES) at UC Davis. The candidate will conduct applied research that is closely linked to an extension and outreach program designed to address and solve critical issues and problems associated with rangelands, particularly to optimize management strategies for the dual uses of ranch enterprise economic viability and enhancement of ecosystem services. The successful candidate will exhibit statewide visibility and leadership in research and extension, and interact collaboratively with others within the department and college, as well as those outside the department with expertise in rangeland ecology, water resources, invasive weeds, economics, soils, animal management, animal health, and climate change. Given the importance of the California livestock industry, the diversity of subject matter, and the impacts of rangeland management on millions of acres of land and millions of acre-feet of water, the person in this position needs to be highly interdisciplinary and collaborative. This position fits within the academic plan of the Department of Plant Sciences, CA&ES and UC Division of Agriculture and Natural Resources (ANR), which aims to improve sustainable plant- and animal-based agro-ecosystems for the future.

This position will support relevant UC Agriculture and Natural Resource strategic initiatives and program teams (http://ucanr.edu/About_ANR/). Research and extension activities will be conducted in the laboratories and fields at UC Davis, on diverse stakeholder lands (e.g., commercial ranches, local, state and federal grazing lands), and at UC Research and Extension Centers (RECs) located throughout California.

This CE Specialist is expected to develop a nationally-recognized research program that is directly linked to a statewide extension and outreach program, secure extramural funding, and publish research results in appropriate peer-reviewed journals and extension publications. The Rangeland Management Specialist will be expected to develop an independent but collaborative, mission-oriented integrated research and extension program in rangeland Management. The candidate's interwoven research and extension efforts will focus on developing management strategies to sustain the production of agricultural goods and ecological services on rangelands in the face of challenges such as drought, weed invasion, and the pressing need to increase agricultural productivity. This CE Specialist will bring leadership, visibility, and cohesion to the research and extension efforts of an interdisciplinary team of CE academics and Agricultural

Experiment Station (AES) faculty as well as private and public stakeholders around the state and region. The appointee will also organize, coordinate or participate in meetings/workshops with CE academics and other stakeholders in multiple venues. Meeting these expectations will require extensive in-state travel. The appointee will have the opportunity to support graduate teaching missions of the department and to be a member of graduate programs. In support of affirmative action, CE programs are expected to include outreach to ethnic minorities, women, and other underrepresented clientele.

QUALIFICATIONS: Ph.D. in rangeland management, ecology, or science, applied plant or soil sciences or ecology, weed science, or a closely related field with a demonstrated emphasis on rangeland management. Ability to conduct independent research and outreach in rangeland management must be demonstrated. Of particular interest is a candidate with demonstrated capacity and interest in interdisciplinary rangeland research spanning plant, animal, soil, economic, and environmental sciences. The candidate must be able to meet the experience and academic requirements to become a Certified Range Manager (CA State Board of Forestry) within the first 4 to 6 years following appointment. Applicants must have demonstrated leadership ability and communication skills.

SALARY: Commensurate with qualifications and experience.

TO APPLY: Candidates should begin the application process by registering online at **http://apptrkr.com/564635**

Please include statements of research and extension interests, curriculum vitae, publication list, copies of 3 of your most important research publications, copies of undergraduate and graduate transcripts (if within 5 years of either degree), and the names, e-mail addresses, and telephone numbers of at least five professional references. For administrative questions regarding the application process, please email Ms. Baljit Nijjar (bknijjar@ucdavis.edu). Review of the applications for this position will begin March 6, 2015. The position will remain open until filled.

Dan Putnam, Chair, Search Committee

Department of Plant Sciences

Mail Stop 1, One Shields Ave.

University of California, Davis

Davis, CA 95616

Telephone (530) 752-8982 E-mail: dhputnam@ucdavis.edu

UC Davis is an affirmative action/equal employment opportunity employer and is dedicated to recruiting a diverse faculty community. We welcome all qualified applicants to apply, including women, minorities, veterans, and individuals with disabilities.

POSITIONS OPEN

California State University, Long Beach

ASSOCIATE DEAN FOR RESEARCH

The College of Natural Sciences and Mathematics at California State University, Long Beach (CSULB) invites applications for Associate Dean for Research (Time base: 12 month 0.75 as Administrator III and academic-year 0.25 as tenured, full professor). We seek a visionary leader to use the College's strengths to develop public/private partnerships and research and grant collaborations across STEM disciplines. For more details, visit **website: http://www.csulb.edu/college/cnsm/jobs/AssociateDean.** *CSULB is an Equal Opportunity Employer.*

ASSISTANT/ASSOCIATE/FULL PROFESSOR

The Department of Neural and Behavioral Sciences, Pennsylvania State University College of Medicine invites applications from outstanding candidates for multiple tenure-eligible faculty positions at the Assistant or Associate Professor level. Successful candidates will be expected to have, or to establish, an active research program in neuroscience. Exceptional senior candidates with well-established research programs may also be considered.

The Department of Neural and Behavioral Sciences has developed excellence in a number of areas including central control of visceral organs, vision science, and the neurobiology of addiction. We will consider candidates whose expertise complements that of our existing programs, however, candidates using innovative approaches to study any aspect of neuroscience will be considered. Details of the departmental research interests can be found at our **website: http://www2.med.psu.edu/nbs/.**

The Department of Neural and Behavioral Sciences provides a competitive startup package, remodeled laboratory space, excellent core facilities, and extensive opportunities for collaborative research and participation in graduate training programs.

Candidates should hold a Ph.D., M.D., or equivalent degree, and are asked to submit current curriculum vitae, statement of research interests and goals, and the names of at least three references.

Apply to **job 55231** at **website: http://apptrkr.com/565782.** Campus Security Crime Statistics: For more about safety at Penn State, and to review the Annual Security Report which contains information about crime statistics and other safety and security matters, please go to **website: http://www.police.psu.edu/clery/,** which will also provide you with detail on how to request a hard copy of the Annual Security Report.

Penn State is an Equal Opportunity/Affirmative Action Employer, and is committed to providing employment opportunities to minorities, women, veterans, disabled individuals, and other protected groups.

ONLINE CAREER FAIR
March 4, 2015 │ 10:00 AM – 4 PM EST

Register now for this exciting virtual career fair and engage, screen, and recruit hundreds of targeted candidates.

HOW THE EVENT WILL WORK

Employers receive a fully customized "booth" tailored to meet their recruiting needs. This landing page can include open positions, company information, testimonials and branding videos.

During the live event, candidates browse your booth and then choose to chat one-on-one. The conversations are timed to allow companies to meet as many candidates as possible.

BENEFITS OF EXHIBITING

- Connect with candidates from the comfort of your own desk
- Showcase your employer brand online to your target audience
- No travel or accommodation costs
- Get access to resumes to build your talent community
- Candidate information is displayed during the chat
- Powerful follow up tools to move top candidates through the hiring process
- Screen candidates with pre-qualifying questions to connect with the most relevant candidates

Book your booth today!

For more information, please visit:
ScienceCareers.org/onlinecareerfairemployers

SCIENCECAREERS.ORG

ScienceCareers
FROM THE JOURNAL SCIENCE AAAS

Tenure-Track Faculty Positions in Genomic Medicine

The Jackson Laboratory for Genomic Medicine (JAX-GM) and the University of Connecticut Schools of Medicine and Dental Medicine (UCONN HEALTH) are inviting applications for multiple tenure-track faculty positions at the Assistant, Associate, and Full Professor levels. Successful applicants will have the opportunity to participate in the highly interactive and cooperative culture established by the partnership between JAX-GM and UCONN HEALTH. Faculty appointed to these unique positions will hold a joint faculty appointment at JAX-GM and tenure track/tenured appointment in the appropriate academic Department at UCONN HEALTH, and will work in the new, state-of-the-art JAX-GM facility in Farmington, CT. S/he will also be cross-appointed with the UCONN Institute for Systems Genomics. Successful candidates would be consummate team players in a highly interdisciplinary environment that brings together clinicians, biologists, molecular geneticists, computer scientists, and quantitative scientists. These collaborative research positions are intended to use genetic and genomic strategies to advance precision medicine, understand human biology, identify the complex functional networks underlying health and disease, and develop novel diagnostics and therapeutics. Areas of particular interest include, but are not limited to:

- Translational and Clinical Genomics
- Computational Biology and Bioinformatics
- Functional Genomics and Genomic Technologies
- Genome Editing and Engineering
- Genomics/Genetics of Metabolic and Cardiovascular Diseases
- Genetics of Longevity and Aging
- Microbial Genomics, Microbiome, and Infectious Diseases
- Statistical and Systems Genomics
- Cancer Genomics

Minimum qualifications include a PhD or a terminal degree in the health professions (e.g., MD, DMD, DPharm) with significant research training in an appropriate field, postdoctoral experience, and an outstanding record of research accomplishments. A demonstrated ability to secure external research funding and publication in top peer-reviewed journals is expected.

Applicants should apply at **https://jobs.uchc.edu**, search (2014-1059) with a CV, cover letter and concise statements of research and teaching interests. In addition, applicants should arrange to have at least three letters of reference sent to Dr. Charles Lee or Dr. Marc Lalande at **genomics@uchc.edu** as a PDF document on letterhead with signature. Applications will be continuously reviewed until the positions are filled.

UConn Health and The Jackson Laboratory are both affirmative action employers, in addition to EEO and M/F/V/PWD/PV employers.

ETH *zürich*

Professor of Animal Genetics

→ The Department of Environmental Systems Science (www.usys.ethz.ch) at ETH Zurich invites applications for the above-mentioned position.

→ At the Institute of Agricultural Science, the professorship will be responsible for developing a leading research and teaching program in animal genetics that focuses on an understanding of the genetic basis of important phenotypic traits in livestock. The professorship's main research topics may include, but are not limited to: (i) the use of QTL/association mapping, comparative genomics or other innovative methods to identify key genes or chromosomal regions underlying important traits of livestock species, (ii) the analysis of interactions between genes and the influence of environmental factors on gene activity underlying phenotypic traits; (iii) integrative approaches for matching animal genotype to different environments to improve food security and to allow for a resource efficient land use, and (iv) experimental approaches to understand the underlying causes of quantitative genetic variation.

→ The professorship has with several vacant positions, access to high-throughput genotyping facilities, and access to the currently built novel and excellently equipped field station "Research and Teaching Center Agrovet-Strickhof" suitable for animal phenotyping.

→ The new professor will be expected to teach undergraduate level courses (German or English) and graduate level courses (English) covering both basic and advanced animal genetics.

→ **Please apply online at www.facultyaffairs.ethz.ch**

→ Applications should include a curriculum vitae, a list of publications, and a statement of future research and teaching interests, and the names and contact details of three referees. The letter of application should be addressed **to the President of ETH Zurich. The closing date for applications is 30 April 2015.** ETH Zurich is an equal opportunity and family friendly employer and is further responsive to the needs of dual career couples. We specifically encourage women to apply.

Assistant Professor
Faculty Position
University of Pittsburgh Cancer Institute and University of Pittsburgh Department of Pharmacology and Chemical Biology

Applications are invited for a tenure-stream Assistant Professor-level faculty position at the University of Pittsburgh Cancer Institute (UPCI), specifically a PhD scientist working in the area of breast cancer biology, prevention and/or treatment. The incumbent will have primary appointment in the Department of Pharmacology and Chemical Biology, University of Pittsburgh.

The University of Pittsburgh, School of Medicine ranks among the top 10 NIH-funded academic medical centers, and the department is consistently one of the top 10 NIH-funded Departments of Pharmacology. At UPCI, faculty and lab personnel have access to state-of-the-art shared facilities with animal care, microscopy, mass spectrometry, high throughput drug discovery, translational research and clinical pharmacology analytical capabilities. The UPCI laboratories and shared resources are located in the Hillman Cancer Center and Magee-Womens Research Institute.

Successful candidates should have a track record of extramurally-supported research grant funding, a strong publication record and excellent communications skills. Salary and benefits will be commensurate with experience.

Applicants should provide a one-page statement of research objectives, curriculum vitae, and contact information for three professional references to:

Dr. Maryann Donovan, PhD, MPH
Associate Director for Research Administration, UPCI
C/O Lola Thompson
5150 Centre Avenue, Suite 532
Pittsburgh, PA 15232
Email: thompsonla3@upmc.edu

The University of Pittsburgh is an
Affirmative Action/Equal Opportunity Employer.

SAN DIEGO STATE UNIVERSITY
Leadership Starts Here

TENURE-TRACK POSITION IN ECOSYSTEM AND LAND SURFACE MODELING
DEPARTMENT OF BIOLOGY

The Department of Biology at San Diego State University invites applications for a tenure track Assistant or Associate Professor in **Ecosystem and Land Surface Modeling**, beginning in Fall 2015.

Candidates must have a Ph.D. in Biology, Ecology, Geography, Atmospheric Sciences, or a related field, and demonstrated strength in modeling **ecosystem and/or biosphere-atmosphere interactions**. Demonstrated research potential through a record of publications and funded grants is expected. Demonstrated experience in running dynamic vegetation models (DVM) and land surface models (such as NCAR CLM) to quantity biospheric feedbacks to the climate system is considered strongly beneficial. The successful candidate should be able to teach, or contribute to, undergraduate and graduate courses in ecology, such as: ecology, ecosystems, climate change, sustainability, biosphere-atmosphere interaction and/or numeric modeling. **The successful candidate will join and contribute to the recently established interdisciplinary Area of Excellence: The SDSU Center for Climate and Sustainability Studies (C2S2, http://c2s2.sdsu.edu), interact with new hires in regional climate modeling, climate statistics, and climate and human civilizations** and will participate in the SDSU joint PhD and masters programs in ecology.

Apply via Interfolio at http://apply.interfolio.com/28387.
For more information see: http://www.bio.sdsu.edu/jobs/
Applications received by **February 28, 2015** will be given full consideration.

SDSU is a Title IX, Equal Opportunity Employer.

Cellular, Developmental, or Regulatory Biology Faculty Position

The California Institute of Technology is seeking outstanding candidates for a tenure-track professorial position in the Division of Biology and Biological Engineering. Applicants should have a highly successful record of using molecular, cellular, and/or systems approaches in any area of biology.

The successful applicant is expected to develop an innovative research program and to be committed to high quality teaching. Preference will be given to candidates at the Assistant Professor level; however, well-qualified applicants at the associate or full professor level may also be considered. The term of an initial untenured appointment is for four years and is contingent upon completion of the Ph.D. degree.

Please submit on-line application at **http://bbe.caltech.edu/Positions** and include a brief cover letter, curriculum vitae, relevant publications, and a description of proposed research. Instructions will be given for submission of letters of reference when you apply on-line.

Position will remain open until filled; however, applicants for the assistant professor level should plan on completing an application by **March 2, 2015**, in order to attend a **recruiting symposium at Caltech on March 19-20, 2015**, where they will present their research and future directions.

EOE of Minorities/Females/Protected Vets/Disability.

Bioinformatics Faculty Positions

The **California Institute of Technology** is seeking outstanding candidates for tenure-track or tenured professorial faculty positions in the Division of Biology and Biological Engineering. Applications are invited in any area of bioinformatics research, broadly defined. We are interested in candidates who develop and employ informatics and computational approaches to understand complex biological systems, ranging widely from microbial systems to humans and from molecular level systems to whole organism physiology. Applicants at all professorial levels are encouraged to apply. For untenured positions, initial appointments are for four years, and are contingent upon completion of the Ph.D. degree. For tenured Professor positions, we seek candidates who have developed cutting edge research programs that are having exceptional impact. Candidates with strong commitments to research and teaching excellence are encouraged to apply.

Please submit online application at **http://bbe.caltech.edu/Positions** and include a brief cover letter; curriculum vitae; relevant publications, a description of proposed research; and a statement of teaching interests. Instructions will be given for submission of letters of reference when you apply on-line.

Positions will remain open until filled, however **applications completed by March 2, 2015** will be assured of receiving full consideration.

EOE of Minorities/Females/Protected Vets/Disability.

UNIVERSITY of WASHINGTON

The University of Washington Department of Medicine is recruiting for one (1) full-time faculty position at the Associate Professor, or Professor level in the Division of Medical Genetics, Department of Medicine. This position is offered with state tenure funding.

Successful candidates for this position will have an M.D./Ph.D. or M.D. degree (or foreign equivalent), clinical expertise in genetics, and will be expected to carry out a successful research program. Highly translational PhD (or foreign equivalent) scientists may be considered. Although candidates with productive research programs in translational genetics/genomics and/or precision medicine will be prioritized, investigators engaged in gene therapy research may also be considered.

The University of Washington, including Medical Genetics and Genome Sciences, is at the forefront of modern genomics technology and its applications to human disease. Candidates will have opportunities to collaborate with other internationally recognized members of the faculty who are developing and using cutting-edge technologies and access state-of-the-art research facilities and clinical research programs. Candidates with a strong research background involving the identification and/or characterization of disease genes, or the application of genetic/genomic information toward the diagnosis and/or treatment of human disease, are especially encouraged to apply.

The position will remain open until filled. Send CV and 1-2 page letter of interest to: **Medical Genetics Faculty Search, c/o Sara Carlson, Division of Medical Genetics, Box 357720, University of Washington, Seattle, WA 98195-7430; seisner@u.washington.edu.**

University of Washington faculty engage in teaching, research and service. The University of Washington is an Affirmative Action, Equal Opportunity Employer. The University is building a culturally diverse faculty and staff and strongly encourages applications from women, minorities, individuals with disabilities and protected veterans. In order to be eligible for University sponsorship for an H-1B visa, graduates of foreign (non-U.S.) medical schools must show successful completion of all three steps of the U.S. Medical Licensing Exam (USMLE), or equivalent as determined by the Secretary of Health and Human Services.

MONTANA STATE UNIVERSITY
Mountains & Minds

Biomedical Faculty
Assistant, Associate, or Full Professor Position in Microbiology & Immunology

The Department of Microbiology & Immunology at Montana State University Bozeman invites candidates with a PhD in a biomolecular discipline to apply for a full-time, nine-month, tenure track position beginning August 2015. The successful candidate will have experience using interdisciplinary approaches, including biochemical, cellular, immunological, bioengineering, and/or molecular biology approaches, to investigate human and animal infectious diseases, microbial pathogenesis, and/or host responses to infectious agents. The faculty member will participate in teaching departmental undergraduate and graduate courses in their area of specialization, and will be responsible for providing service to the university and scientific community via integration of research, teaching, and service. Opportunities to participate in the cooperative human medical education program with the University of Washington (WWAMI program) or the Regional Program in Veterinary Medicine (WIMU program) may also be possible. A competitive institutional salary, a generous start-up package, and a renovated state-of-the-art research facility support this position. Full details about the position and application procedure are available at **https://jobs.montana.edu/postings/1196**.

Potential candidates are encouraged to contact the Search Committee Chairpersons, Drs. Mark Quinn or Mark Jutila, (**mquinn@montana.edu**; **uvsmj@montana.edu**) for more details. Screening will begin **January 31st, 2015** and will continue until a suitable applicant is hired.

ADA/EO/AA/Veterans Preference.

ISTFELLOW: Call for Postdoctoral Fellows

Are you a talented, dynamic, and motivated scientist looking for an opportunity to conduct research in the fields of **BIOLOGY**, **COMPUTER SCIENCE**, **MATHEMATICS**, **PHYSICS**, or **NEUROSCIENCE** at a young, thriving institution that fosters scientific excellence and interdisciplinary collaboration?

Apply to the ISTFellow program. Deadlines March 15 and September 15

www.ist.ac.at/istfellow

Co-funded by
the European Union

I|S|T AUSTRIA
Institute of Science and Technology

CAS-JIC Centre of Excellence in Plant and Microbial Sciences (CEPAMS)

John Innes Centre
Unlocking Nature's Diversity

We wish to recruit a **Director** for a flagship research collaboration between two research institutes of the **Chinese Academy of Sciences (CAS)** – the **Institute of Genetics and Developmental Biology in Beijing (IGDB)** and the **Shanghai Institute for Plant Physiology and Ecology (SIPPE)** – and the **John Innes Centre (JIC)** in the UK.

This post offers unique opportunities to shape and lead a new collaboration between three of the world's leading research institutes in plant and microbial sciences. CEPAMS will be based in both Beijing and Shanghai with a core staff of ten project leaders and a research-active Director, and will additionally comprise joint research projects executed by staff in the three research institutes.

The successful candidate will establish and direct the new Centre and conduct an internationally excellent and innovative research programme. They will lead on the recruitment of ten new project leaders, with input from the Directors of IGDB, SIPPE and JIC, manage joint research projects between CAS and JIC project leaders, scope new funding opportunities for the alliance and run their own internationally recognised research programme.

The Director's laboratory will be based in either IGDB or SIPPE, but there will be frequent opportunities to interact with JIC researchers to build on and establish joint collaborative research.

Remuneration is negotiable, and will be compatible with international standards. This post is for a contract of 5 years in the first instance, with the possibility of extension.

For further information and details of how to apply, please visit our web site **http://jobs.jic.ac.uk** or contact **Human Resources, Norwich BioScience Institutes Partnership, Norwich Bioscience Institutes, Norwich, NR4 7UH, UK, 01603 450149**. Informal enquiries about the posts can be directed to Prof Giles Oldroyd (**giles.oldroyd@jic.ac.uk**) or Prof Bin Han (**bhan@ncgr.ac.cn**). As a user of the disability symbol, we guarantee to interview all disabled applicants who meet the minimum essential criteria for this vacancy.

The closing date for applications will be **13th February 2015.**

The John Innes Centre is a registered charity (No. 223852) grant-aided by the Biotechnology and Biological Sciences Research Council and is an Equal Opportunities Employer.

Shandong University of Technology Recruits for High-end Talents Globally

Founded in 1956 and located in the cradle of Ancient Qi Culture-Zibo City of Shandong Province, Shandong University of Technology is a provincially prioritized university with a focus on science and engineering. They cover eight fields of learning, such as engineering, science, economics, management, literature, law, history and pedagogy. It also holds the name of Shandong Provincial Featured University of Applied Talents Cultivation.

I.Disciplines of Recruitment
Mechanical Engineering, Agricultural Engineering, Chemical Engineering and Technology, Mechanics, Materials Science and Engineering, Power Engineering and Engineering Thermophysics, Instruments Science and Technology, Food Science and Engineering, Electric Engineering, Electronic Science and technology, Information and Communication Engineering, Control Science and Engineering, Computer Science and Technology, Civil Engineering, Surveying and Mapping technology, Transportation Engineering, Architecture, Mining Engineering, Textile Engineering, Biology, Economics, Management Science and Engineering, Mathematics, Physics, Law, Literature and other disciplines.

II.Requirements and Treatment
(1). for the leading personnel who holds the post of professor or equivalent position at renowned university from home and abroad, the university will provide a 50,000-1,200,000 RMBs annual salary plus 1,000,000 settling-in allowance and housing of 273m^2. Start-up funding will be offered according to the research work.
(2). for the academic leader who achieved outstanding performance with high academic influence in certain area, the university will provide a 400,000-600,000 RMBs annual salary plus 500,000 settling-in allowance and housing of 248m^2, a reasonable research funds will be offered as well.
(3). for excellent young talents with doctorate, the university will provide 300,000-500,000 RMBs settling-in and housing allowance. Start-up funding will be 50,000-100,000 RMBs for science and engineering, and 30,000-50,000 RMBs for humanities and social science. An associate professor treatment will be offered within 3 years after the talents work in the university.

III.The university will provide support if the talents accord with condition of applying National Thousand Talent Program or Taishan Scholar Program and the applicants will enjoy the same treatment.

IV.Contact Information
Tel:+86-533-2782311/2781219
E-mail: rshch@sdut.edu.cn

西南交通大学 Southwest Jiaotong University, P.R.China
Anticipates Your Working Application

Southwest Jiaotong University (SWJTU), founded in 1896, situates itself in Chengdu, the provincial capital of Sichuan. It is a national key multidisciplinary "211" and "985 Feature" Projects university directly under the jurisdiction of the Ministry of Education, featuring engineering and a comprehensive range of study programs and research disciplines spreading across more than 20 faculties and institutes/centers. Boasting a complete Bachelor-Master-Doctor education system with more than 2,500 members of academic staff, our school also owns 2 first-level national key disciplines, 2 supplementary first-level national key disciplines (in their establishment), 15 first-level doctoral programs, 43 first-level master programs, 75 key undergraduate programs, 10 post-doctoral stations and more than 40 key laboratories at national and provincial levels.
Our university is currently implementing the strategy of "developing and strengthening the university by introducing and cultivating talents". Therefore, we sincerely look forward to your working application.
More information available at http://www.swjtu.edu.cn/

I. Positions and Requirements
A.High-level Leading Talents
It is required that candidates be listed in national top talents programs such as *Program of Global Experts, Top Talents of National Special Support Program, "Chang Jiang Scholars", China National Funds for Distinguished Young Scientists and National Award for Distinguished Teacher.*
Candidates are supposed to be no more than 50 years old. The limitation could be extended in the most-needed areas of disciplinary development.
Candidates who work in high-level universities/institutes and reach the above requirements are supposed to be no more than 45 years old.
B. Young Leading Scholars
Candidates are supposed to be listed in or qualified to apply for the following programs:
• *National Thousand Young Talents Program*
• *The Top Young Talents of National Special Support Program(Program for Supporting Top Young Talents)*
• *Science Foundation for the Excellent Youth Scholars*
Candidates should have good team spirit and leadership, outstanding academic achievements, broad academic vision and international cooperation experience and have the potential of being a leading academic researcher.
C. Excellent Young Academic Backbones
Candidates under 40 years old are expected to graduate from high-level universities/institutes either in China or other countries. Those who are professors, associate professors and other equal talents from high-level universities/institutes overseas could be employed as professors and associate professors as well.
D. Excellent Doctors and Post Doctoral Fellows
Candidates under 35 years old are supposed to be excellent academic researchers from high-level universities either in China or other countries.

II. Treatments
The candidates will be provided with competitive salaries and welfares that include settling-in allowance, subsidy of rental residence, start-up funds of scientific research, assistance in establishing scientific platform and research group as well as international-level training and promotion . As for outstanding returnees, we can offer further or specific treatments that can be discussed personally.

III . Contact us:
Contacts: Ye ZENG & Yinchuan LI   Telephone number: 86-28-66366202   Email: *talent@swjtu.edu.cn*
Address: Human Resources Department of SWJTU, the western park of high-tech zone, Chengdu, Sichuan, P.R.China, 611756

http://www.swjtu.edu.cn/

徐州医学院 徐州市感染与免疫重点实验室
Xuzhou Key Laboratory of Infection and Immunity

Tenure-Track position at the Assistant/Associate/Full Professor level in Laboratory of Infection and Immunity

Xuzhou Key Laboratory of Infection and Immunity at Xuzhou Medical College (http://www.xzmc.edu.cn) is offering tenure-track position at the rank of Assistant/Associate/Full Professor level. Candidates must have a Ph.D. and/or M.D. degree and appropriate postdoctoral experience who have demonstrated the ability to develop a high-quality independent research program distinguished by exceptional originality and productivity.

We are particularly interested in candidates, who have a strong background in the areas of research including, but not limited to, microbiology, parasitology and immunology. The candidates should also have good communication and organization skills, and can also use cutting edge approaches involving genetic, cellular, molecular, biochemistry or behavioral techniques to address key problems related to immunity.

Laboratory of Infection and Immunity, led by Prof. Kuiyang Zheng, was founded at Xuzhou Medical College in 2010, and has the space of 3000 sq. foot. The laboratory has established a series of excellent platforms including biosafety level II laboratory, pathology platform, flow cytometry, magnetic activated cell soring（MACS）, cell culture and protein platform, and molecular platform, etc. Currently, major research areas are being developed, including 1) Pathogen infection and immunity, 2) Immunoregulation and autoimmune disease , and 3) Metabolism and immunity.

The College and laboratory provide a very supportive research environment with excellent resources conductive to developing a successful research program. Qualified candidates will receive a comprehensive package including competitive salary, medical insurance and other benefits.

Interested individuals should submit a detailed letter of expression of interest or research proposal, CV, list of publications, and three reference letters to: rsc@xzmc.edu.cn. For further information, please contact Professor Kuiyang Zheng, Director, Laboratory of Infection and Immunity, at zky02@163.com or Professor Ren-Xian Tang, deputy director, Laboratory of Infection and Immunity, at tangrenxian-t@163.com.

南京工业大学 NANJING UNIVERSITY OF TECHNOLOGY
海外领军人才招聘
Overseas Talents Recruitment

Nanjing Tech University, with a history of more than one hundred years, is a multidisciplinary university with a particular strength in engineering.

Aiming at excellence and innovation, Nanjing Tech University is set to become a first-class research university with a global vision. We are now seeking outstanding academic and research leaders in the following and related fields: Basic disciplines from within the Physical Sciences; Cutting edge disciplines from within the Life Sciences; Applied disciplines from within the Information Sciences; Humanities represented by Management Science.

Applicants should have a Ph.D. with at least 3-years research experience from leading universities or institutes. Candidates should demonstrate an internationally recognized research record and outstanding achievements. Successful candidates are expected to develop vigorous research programs and lead an independent research team. Successful candidates will be provided with a competitive relocation fee and salary package, generous start-up funds and spacious laboratories.

Interested candidates should visit **http://rczyb.njtech.edu.cn** for application details.
Phone: **Ms. Wang +86-25-58139148.**
E-mail: **job@njtech.edu.cn**

By **Jeffrey Mervis**

An education that closed doors

Imagine a penniless immigrant who comes to the United States in pursuit of a world-class education. He works hard and earns a Ph.D. in computational mechanical engineering from one of America's top universities, the California Institute of Technology (Caltech). Then he becomes a founding faculty member at King Abdullah University of Science and Technology (KAUST) in Saudi Arabia, with a generous salary, a hefty startup package for his research, and lots of other perks. ¶ That may sound like an uplifting tale of perseverance and triumph against the odds, but the reality is different: Tamer Elsayed's story also includes prison time and a permanent ban from the United States.

At the age of 39, Elsayed has written a memoir—*Inadmissible*—telling the story of his scientific rise and fall. The memoir's title refers to the fact that Elsayed, an Egyptian citizen, can never again set foot legally in the United States. That's a personal tragedy, because his young daughter lives with his ex-wife in Los Angeles. Also, his academic career is probably over.

The reason he is inadmissible lies at the core of the story. After earning the fifth highest score in the nation on Egypt's annual college admissions test, Elsayed comes to California and overstays his 6-month tourist visa. Needing money to support himself and finance his education, he continues to break a series of federal laws. First, he obtains a fake Social Security card that allows him to work. Later, he obtains a second fake Social Security card that lets him walk away from a poor credit rating based on large, unpaid debts. Much more serious is his decision to lie on his student loan application, telling the government that he is a U.S. citizen.

He qualifies for the loan and uses the money to come within five credits of completing his bachelor's degree in mechanical engineering from California State Polytechnic University, Pomona. But then, acting on a tip from his former girlfriend, federal agents storm his bedroom and arrest him. He winds up serving 15 months in a federal correctional facility in Lompoc, California, for a crime the U.S. government classifies as "involving moral turpitude."

Once released, Elsayed finishes his undergraduate degree and wins a fellowship to Caltech. Michael Ortiz, his adviser there and a member of the U.S. National Academy of Engineering, tells *Science* that Elsayed was "a very hard worker ... one of my best students." Unaware of Elsayed's criminal record, Ortiz found his attitude refreshing: "He

> *"Elsayed, an Egyptian citizen, can never again set foot legally in the United States."*

was respectful, more so than other students, and very deferential."

Ortiz approves Elsayed's dissertation, takes him on as a postdoc, and cheers the job offer from KAUST, a new university with a $20 billion endowment. To Ortiz, it seems like a perfect fit: In addition to his work modeling the behavior of soft materials such as polymers and biological tissue and his admirable work ethic, Elsayed is a devout Muslim who grew up in the Middle East.

But that first-class professional opportunity goes south in a hurry. Despite publishing more than 20 papers on new computational tools for modeling soft materials, his past catches up with him and Elsayed is forced to leave KAUST and Saudi Arabia after 4 years.

Although chastened by all that has happened, Elsayed doesn't apologize. "I was well aware of my fraudulent actions," he writes in his book. "Looking back, there was really no excuse for my deeds. But at that time, I had felt that to play only the cards I'd been dealt—being an Egyptian citizen without the financial means to achieve what I knew I was academically qualified to achieve—would leave me with nothing.

"I could summarize all my shortcomings in one sentence: I was born in the wrong place."

Now living in Budapest with his new wife and their baby girl, Elsayed considers his book a form of confession and self-therapy. "I want to get this load off my chest, to be free of having to live in secrecy and shame. ... [A]nd if you still want to judge me, then there is nothing more I can do." ∎

Jeffrey Mervis is a senior correspondent for Science. *For more on life and careers, visit www.sciencecareers.org. Send your story to SciCareerEditor@aaas.org.*